DEVELOPMENT OF STABLE LIQUID WATER-IN-OIL EMULSIONS BY MODIFYING EMULSIFIER-AQUEOUS PHASE INTERACTIONS

A Thesis Submitted to the College of

Graduate and Postdoctoral Studies

in Partial Fulfillment of the Requirements

for the Degree of Doctor of Philosophy

in the Department of Food and Bioproduct Sciences

University of Saskatchewan

Saskatoon, SK

By

Maria Fernanda Romero-Peña

2021

PERMISSION TO USE

In presenting this thesis in partial fulfilment of the requirements for a Postgraduate degree from the University of Saskatchewan, I agree that the Libraries of this University may make it freely available for inspection. I further agree that permission for copying of this thesis/dissertation in any manner, in whole or in part, for scholarly purposes may be granted by the professor or professors who supervised my thesis work or, in their absence, by the Head of the Department or the Dean of the College in which my thesis work was done. It is understood that any copying or publication or use of this thesis or parts thereof for financial gain shall not be allowed without my written permission. It is also understood that due recognition shall be given to me and to the University of Saskatchewan in any educational use which may be made of any material in my thesis.

Requests for permission to copy or to make other use of the material in this thesis in whole or part should be addressed to:

Dean
College of Graduate and Postdoctoral Studies
University of Saskatchewan
116 Thorvaldson Building, 110 Science Place
Saskatoon, Saskatchewan SK S7N 5C9
Canada

OR

Head of the Department
Food and Bioproduct Sciences
University of Saskatchewan
Room 3E08, Agriculture Building, 51 Campus Drive
Saskatoon, Saskatchewan S7N 5A8
Canada

ABSTRACT

This research investigated the stabilization mechanism of liquid water-in-oil (W/O) emulsions by modifying emulsifiers, aqueous and continuous phase compositions, and interactions. At first, liquid W/O emulsions were developed to resist multiple thermal cycles for their application in droplet digital polymerase chain reaction (ddPCR), which significantly improved the detection limit of conventional PCR. Thermally stable coarse W/O emulsions as DNA microreactors were developed with polyglycerol polyricinoleate (PGPR) and sodium bis(2-ethylhexyl) sulfosuccinate (AOT) as emulsifiers dissolved in a mixture of light and heavy mineral oil, with a range of viscosities. Coarse emulsions, formed by vortex mixing, were subjected to PCR thermal-cycling, after which AOT-stabilized water droplets remained stable; however, PGPR-stabilized water droplets size significantly increased. Higher AOT molecular packing at the interface was proposed as the mechanism of thermal stability.

Next, the (de)-stabilization mechanism of glycerol monooleate (GMO)-stabilized liquid W/O emulsions in mineral (MO) and canola oil (CO) was investigated. It was hypothesized that hydroxyl group donating agents in the aqueous phase would prevent GMO's desorption from the oil-water interface by forming stronger hydrogen bonding. W/O emulsions with 20% aqueous phase were formed by high-pressure homogenizer. Of the three agents, emulsions with low methoxyl pectin (LMP) showed the highest stability in both oils after 7-day storage compared to citric or ascorbic acid with or without sodium chloride. Water and GMO melting behaviour, determined by differential scanning calorimetry, and intermolecular interaction by Fourier transform infrared spectroscopy revealed stronger H-bonding between GMO and LMP, thereby improving emulsion stability.

Finally, the viscoelastic behaviour of GMO-stabilized W/O emulsion was improved such that an elastic gel could be formed by increasing the water content (20 to 50 wt%) and incorporating specific ingredients in the continuous and dispersed phases for application in food-grade low-fat tablespreads. Fully hydrogenated soybean oil was incorporated in CO to create a fat crystal network in the continuous phase. Emulsions with LMP in the aqueous phase exhibited self-supported structure without phase-separation while control emulsions, without LMP, showed flow or water separation. All emulsions exhibited strong gel-like properties; however, control emulsions showed structure breakup after 30-day storage. Overall, the studies in liquid W/O emulsions were the basis to improve our understanding of the molecular assembly and interactions at the W-O interface, which subsequently supported the research to enhance emulsion elasticity.

ACKNOWLEDGEMENTS

I want to thank God and the universe for this exceptional experience. I feel special gratitude for my supervisor, Dr. Supratim Ghosh, for his outstanding efforts in sharing knowledge and expertise. I cannot quantify the knowledge learned during these years, and work with him has been a colossal experience. I want to extend my gratitude to my committee members Dr. Michael Nickerson, Dr. Yongfeng Ai, Dr. Lee Wilson, Dr. Phyllis Shand, and my external Dr. Silvana Martini, for your observations and questions that enhanced the outcomes of this research and motivated me to go beyond. I am also very grateful for the support of Dr. Takuji Tanaka, being my Committee Chair during my comprehensive exam, and admin assistance of Ann Harley and Donna Selby. I want to express gratitude to my former University, Escuela Superior Politecnica del Litoral, for the four years of scholarship which allowed me to start this dream. I extend my appreciation to the Dean, Dr. Angel Ramirez, and coworkers for the support of the MSc. Jorge Duque, Ph.D. Patricio Cáceres, Ph.D. Jonathan Coronel, Ph.D. Fabiola Cornejo, Ph.D. Romulo Salazar, Ph.D. Grace Vásquez ($^{+}$), M.Sc. Maria Fernanda Morales ($^{+}$), and for the tremendous assistance to the admin assistance Maria Moreno and Annabelle Plaza. We received two grants provided by NSERC; without it, the transfer of knowledge with the S.M. Research company (Toronto) would not be possible. My gratitude also goes to Dr. Enders Ng for his support during the study and S.M. Research's teamwork. As well, thanks to NSERC Discovery Grant for giving us funding for the third project. I am also very thankful to Dr. Jason Maley from the Saskatchewan Structural Science Center for the FTIR training. I would also like to thank my coworkers from Dr. Ghosh's lab. I treasured all the experiences shared and the support received, YanRan Tang, Chi Diem, Athira Mohanan, Pravin Gadkari, Kunal Kadiya, Fatemeh Keivaninahr, Saakshi Parolia, Manisha Sharma and Neksha Devaki. I am grateful to have met my classmates, faculty members, administrative staff, laboratory assistants in the Food and Bioproduct Department, with which we shared knowledge, opinions, or planned activities during this delightful journey.

I want to express gratefulness with profound love to my family, my parents, Mariana Peña and Alfonso Romero, my brothers, Byron Romero, Gonzalo Romero, Israel Romero, and my boyfriend Frank Hounjet, for their care and encouragement. I want to thank my friends, Maria Mercedes Jara, Gabriela Orellana, Consuelo Robles, Ana Maldonado, Mike Sibley, Paul Trujillo, Veronica Andrade, Zayda Morales, Rafael Cavassani, Susan Serrano, Ana Jumbo, Seon Hwa Kim, Andrea Fuentes, Evelyn Rodriguez, Mayra Samaniego and Cristian España for their shoulder during challenging times.

TABLE OF CONTENTS

PAGE

PERMISSION TO USE ..... **I**

ABSTRACT ..... **II**

ACKNOWLEDGEMENTS ..... **III**

TABLE OF CONTENTS ..... **IV**

LIST OF TABLES ..... **XIII**

LIST OF FIGURES ..... **XIV**

LIST OF ABBREVIATIONS AND SYMBOLS ..... **XXI**

1. INTRODUCTION **1**

1.1 Summary 1

1.2 Hypotheses 2

1.3 Objectives 3

2. LITERATURE REVIEW **4**

2.1 Emulsions: General Features 4

2.1.1 Definitions and types of emulsions 4

2.1.2 Mechanism of emulsion destabilization 6

2.1.2.1 Gravitational separation 6

2.1.2.2 Flocculation and coagulation 8

2.1.2.3 Coalescence 9
2.1.2.4 Phase inversion 11
2.1.2.5 Ostwald ripening 13
2.2 Water-in-oil emulsions 15
2.2.1 Unique properties of water-in-oil emulsions 15
2.2.2 Ingredients used in water-in-oil emulsion formation and stabilization 16
2.2.3 Application of water-in-oil emulsion in various fields 17
2.2.4 Utilization of water droplets in water-in-oil emulsion as microscale reactors 19
2.2.5 Food application of water-in-oil emulsion and the challenges with their stabilization 20
2.3 Emulsifiers used in water-in-oil emulsions 22
2.3.1 Sorbitan fatty acids esters emulsifiers 23
2.3.3 Glycerol fatty acids esters emulsifiers 24
2.3.4 Ethoxylated emulsifiers 26
2.3.5 Polyglycerol esters of fatty acids and other polymeric emulsifiers 27
2.3.6 Sulfosuccinates 29
2.3.6 Pickering particles 32
2.3.7 Emulsifier characterization techniques 34
2.3.7.1 The solubility concept 34
2.3.7.2 Cloud point 35
2.3.7.3 Phase inversion 35
2.3.7.4 Hydrophilic lipophilic balance 36

2.3.7.5 Interfacial tension 37
2.3.7.6 Interfacial rheology 38
2.4 Structure formation in water-in-oil emulsions 39
2.4.1 Controlling structure formation in the continuous phase 39
2.4.2 Controlling structure formation in the dispersed phase 42
2.4.2.1 Water droplet aggregation 42
2.4.2.2 Water droplet gelation 43
2.4.2.3 Water droplet volume fraction 45
2.5 Characterization of water-in-oil emulsions using different techniques 47
2.5.1 Droplet size determination 47
2.5.1.1 Nuclear magnetic resonance 48
2.5.1.2 Dynamic Light Scattering 49
2.5.1.3 Static light scattering 50
2.5.2 Droplet surface potential 50
2.5.3. Microscopy 51
2.5.3.1 Polarized light microscopy 52
2.5.3.2 Confocal microscopy 53
2.5.4 Rheology of water-in-oil emulsions 55
2.5.4.1 Viscosity of a fluid 55
2.5.4.2 Viscoelasticity of a semi-solid material 58
2.5.5. Differential scanning calorimetry 60

2.5.5.1 Thermal analysis of water-in-oil emulsions....62
2.5.6. Solid fat content....63
2.5.6.1 NMR spectroscopy-based SFC determination....63
2.5.6.2 DSC-based SFC determination....64
2.5.7 Vibrational spectroscopy techniques for water-in-oil emulsion characterization....65
2.5.6.1 FTIR-based analysis of molecular interactions in water-in-oil emulsions....66
2.5.8 Sedimentation analysis in water-in-oil emulsions....68
2.5.8.1 Visual observation of sedimentation....68
2.5.8.2 NMR-based sedimentation analysis....69
2.5.8.3 Light scattering- based sedimentation analysis....69
2.5.9 Spreadability of water-in-oil emulsions....70
3. DEVELOPMENT OF THERMALLY STABLE COARSE WATER-IN-OIL EMULSIONS AS POTENTIAL DNA BIOREACTORS....72
3.1 Abstract....72
3.2 Introduction....73
3.3 Materials and methods....75
3.3.1 Materials....75
3.3.2 Preparation of solutions....75
3.3.3 Preparation of water-in-oil emulsions....75
3.3.4 Experiment design for emulsifier and oil selection....76
3.3.5 Thermal cycles and emulsion stability....76

3.3.6 Determination of emulsion droplet size 76

3.3.7 Determination of interfacial tension 77

3.3.8 Determination of interfacial rheology 78

3.3.9 Viscosity of the oil phase 78

3.3.10 Statistics 78

3.4 Results and Discussion 78

3.4.1 Influence of sorbitan monooleate on water-in-oil emulsion formation and stability 78

3.4.2 Influence of polyglycerol polyricinoleate on coarse water-in-oil emulsion formation, microstructure, and stability after multiple thermal cycles 80

3.4.3 Influence of sodium bis (2-ethylhexyl) sulfosuccinate as an emulsifier for thermally stable water-in-oil emulsions 87

3.4.4 Comparison between PGPR and AOT as potential surfactants for water-in-oil emulsion stabilization for digital PCR 90

3.5 Conclusions 90

3.6 Connection to the Next Study 91

4. STABILIZATION OF FOOD-GRADE LIQUID WATER-IN-VEGETABLE OIL EMULSIONS BY MODIFYING HYDROXYL GROUP DONATING AGENTS' INTERACTIONS AT THE OIL-WATER INTERFACE WITH GLYCEROL MONOOLEATE 93

4.1 Abstract 93

4.2 Introduction 94

4.3. Materials and methods 96

4.3.1 Materials 96

4.3.2 Preparation of solutions 96

4.3.3 Preparation of water-in-oil emulsions 97
4.3.4 Emulsion storage stability 97
4.3.5 Microstructure analysis 97
4.3.5.1 Light microscopy 97
4.3.5.2 Confocal microscopy 98
4.3.6 Determination of emulsion droplet size 98
4.3.7 Accelerated stability analysis 98
4.3.8 Rheological properties of water-in-oil emulsions 99
4.3.9 Determination of interfacial tension 99
4.3.10 Differential Scanning Calorimetry 99
4.3.11 Infra-red spectroscopy analysis 100
4.3.12 Statistics 100
4.4 Results and discussion 100
4.4.1 Emulsion storage stability after seven days 100
4.4.2 Quantification of emulsion kinetic stability against phase separation 102
4.4.3 Microstructure of emulsions 103
4.4.4 Average water droplet size 109
4.4.5 Accelerated sedimentation velocity of emulsions 110
4.4.6 Change in emulsion viscosity with time 112

4.4.7 Emulsion viscoelasticity 113

4.4.7.1 G′ and G″ as a function of strain 113

4.4.7.2 Tan δ 116

4.4.8 The interfacial tension between oil and aqueous phases 118

4.4.9 Emulsion thermal analysis 120

4.4.9.1 Temperatures of ice melting peaks 123

4.4.9.2 Enthalpies of ice melting peaks 123

4.4.9.3 Temperatures and enthalpies of GMO melting peaks 126

4.4.10 Mechanism of interactions among GMO, aqueous phase additives and the continuous oil phase using FTIR spectra 128

4.4.10.1 GMO hydrogen bonding at the oil-water interface (peak at 3400 cm^{-1}) 128

4.4.10.2 GMO carbonyl group stretching at the oil-water interface (peaks 1735 and 1742 cm^{-1}) 131

4.4.10.3 Stretching mode of hydrocarbon chain (CH2 wagging mode from 1330 to 1400 cm^{-1}) 133

4.4.11 Discussion 134

4.5 Conclusions 135

4.6 Connection to the third study 136

5. EFFECT OF PECTIN AND WATER CONTENT ON THE VISCOELASTIC IMPROVEMENT OF WATER-IN-CANOLA OIL EMULSIONS FOR FOOD APPLICATIONS 137

5.1 Abstract 137

5.2 Introduction 140

5.3 Materials and methods 142

5.3.1 Materials 142

5.3.2 Preparation of aqueous and oil phases 142

5.3.3 Preparation of W/O emulsions 143

5.3.4 Emulsion storage stability 143

5.3.5 Microstructure analysis 144

5.3.6 Rheology of W/O emulsions 144

5.3.7 Thermal analysis of emulsions 144

5.3.8 Determination of solid fat content analysis 144

5.3.9 Statistics 145

5.4 Results and discussion 145

5.4.1 Emulsion appearance and storage stability 145

5.4.2 Emulsion viscosity 146

5.4.2.1 Apparent viscosity at a low shear rate 148

5.4.2.2 Apparent viscosity at a high shear rate 149

5.4.3 Emulsion viscoelasticity 150

5.4.3.1 Strain-sweep viscoelasticity 150

5.4.3.2 Comparison of emulsions G' values 152

5.4.3.3 Comparison of emulsion crossover strains 154

5.4.3.4 Emulsion tan δ as a function of strain 154

5.4.4 Microstructure of emulsions 155

5.4.5 Emulsion stability analysis from their thermal behaviour 157

5.4.6 Solid fat content of emulsions 161

5.5 Discussion.....162

5.6 Conclusions 163

6. GENERAL DISCUSSION.....164

6.1 Overview 164

6.2 Emulsion model.....164

6.3 Determination of thermal stability by modifying emulsifier and continuous phase composition 166

6.4 Effect of high energy homogenization and mixing processes 167

6.5 Preventing desorption of glycerol monooleate from water-in-canola oil emulsions 168

6.6 Improvement of viscoelasticity by increasing water content and modifying the interfacial composition 170

6.7 Summary 171

7. GENERAL CONCLUSIONS.....173

8. FUTURE STUDIES 177

9. REFERENCES.....180

10. APPENDICES 201

LIST OF TABLES

PAGE

Table 2.1 Composition of mono-, di- and triesters of fatty acids of Span 40, Span 60, Span 65, Span 80 and Span 85 and HLB. Adopted with modification from Garti et al. (1983), HBL values were compiled from various sources (Croda, 2018; Sigma-Aldrich, 2018). 24

Table 2.2 HLB values of glycerol fatty acids esters. Adopted with modification from various sources (Ash & Ash, 2004; Merianos, 2001; NOSB-TAP, 2001).....25

Table 2.3 Classification of emulsifiers according to HLB numbers. Adopted without modification from Griffin (1949).....36

Table 2.4 HLB group number. Adopted without modification from Davies (1957). 37

Table 2.5 Product types with fat content percentage divided for milk-fat content assigned as butter and vegetable and/or animal fat designated as margarine. Adopted with modification from Council Regulation EC, 1996.....40

Table 5.1 W/O emulsion composition for all water content in 100 g. The last two rows show the composition of control W/O emulsion without LMP in the aqueous phase. LMP: low methoxyl pectin, CO: canola oil, HSO: fully hydrogenated soybean oil, GMO: glycerol monooleate. 143

LIST OF FIGURES

PAGE

Figure 2.1 Mechanism of emulsion breakdown in W/O emulsion (flocculation, coalescence, sedimentation, phase inversion, and Ostwald Ripening). The oil phase is represented in yellow, and the water phase in blue. 6

Figure 2.2 Types of floc formed with droplets characterized by increasing effective size. 9

Figure 2.3 Cyclization and esterification of sorbitol. Adopted without modification from Hasenhuettl (2008).....23

Figure 2.4 Reaction scheme of MAGs and DAGs production via direct esterification and interesterification, R= fatty acid with a carbon number of 8 to 22. Adopted without modification from Hasenhuettl (2008). 25

Figure 2.5 Proposed chemical structure of polyglycerol polyricinoleate. Black dots denote two polyricinoleic acid chains. Adopted without modification from Bastida-Rodríguez (2013). 28

Figure 2.6 Di- and monoesters of sulfosuccinate emulsifier, R represents the alkyl – e.g., fatty alcohol chain. Adopted without modification from Tyagi (2006).....30

Figure 2.7 Diagram of AOT molecule. Adopted without modification from Robinson, Toprakcioglu, Dore, and Chieux (1984).....31

Figure 2.8 Schematic molecular structures of AOT homologues, at the top C6 linear chain and branch chain: (1) to (6) 3,5,5-trimethyl-1-hexyl, through 2-ethyl-1-hexyl (AOT), to 1-ethyl-2-methyl-1-pentyl. Adopted without modification from Nave, Eastoe, and Penfold (2000)...31

Figure 2.9 Representation of a fat crystal at the W-O interface. Adopted without modification from Hodge and Rousseau (2005). 33

Figure 2.10 Fat crystal size effect at the interface, (A) ~1μm, (B) ~5μm, (C) sub-micron. Adopted with modification from Rousseau (2000).....41

Figure 2.11 Photomicrographs in polarized light microscopy (PLM)(A, C) and brightfield (BF)(B, D) of W/O emulsions 10 days aged stabilized with 1 wt% wax. (A, B) pre-crystallized and (C, D) post-crystallized. Adopted without modification from Rousseau and Hodge (2005). 53

Figure 2.12 Micrograph in confocal laser scanning microscope of 5 wt% W/O emulsions with Pickering particles curcumin (red) at different concentrations (a to e, 0.06 to 1.5 wt%), aqueous phase pH 3. Scale bar: 20 μm. Curcumin particles autofluorescence at 488 nm, excited using lasers 488 and 405 nm. Adopted without modification from Zembyla et al. (2018). 54

Figure 2.13 Viscosity of Newtonian and Non-Newtonian: shear thickening and shear thinning. 56

Figure 2.14 Diagram of flocs deformation with the increase of shearing (s^{-1}) and decrease of viscosity (Pa.s) effect. Adopted without modification from McClements (2005). 57
Figure 2.15 Flow curves of ideal Bingham plastic and non-ideal plastic fluids. 58
Figure 2.16 Strain sweep at a constant frequency (1 Hz) of 40 wt% W/O emulsions with low methoxyl pectin in the aqueous phase and GMO and hydrogenated soybean oil in the canola oil in the continuous phase after 30 days of storage. Original data collected by Romero-Pena at the University of Saskatchewan. 60
Figure 2.17 Thermal scans of 20 and 50 wt% W/O emulsions with low methoxyl pectin in the aqueous phase and GMO, hydrogenated soybean oil in canola oil as the continuous phase on day 1, first cooling from 25 to –70 °C, then heating to 70 °C at 5 °C/min. Peaks 1 and 2 belong to water crystallization and peaks 2 and 3 to CO. Original data collected by Romero-Pena at the University of Saskatchewan. 61
Figure 3.1 Mechanism of stability for PGPR and AOT at the W-O interface before and after the thermal cycles. 73
Figure 3.2 Visual observation of W/O emulsions prepared in light mineral oil with Span 80 (2 – 10 % v/v) (A) before and (B) after thermal cycles, and with PGPR (0.2 – 10 % v/v) (C) before and (D) after thermal cycles. All emulsions contained BSA in the aqueous phase. Emulsifier concentration is shown on the image A and C. 79
Figure 3.3 Newtonian viscosity of light (100L) and heavy (100H) mineral oil and their mixtures. Oil mixtures are expressed by their composition. For example, 25H+75L represents 25% L and 75% H mixture. 81
Figure 3.4 Visual observation of W/O emulsion prepared with (A) 0.3 and (B) 0.4% v/v PGPR in different percentages of light mineral oil (L) and heavy mineral oil (H) after thermal cycles with and without the presence of BSA in the aqueous phase. 82
Figure 3.5 Critical micelle concentration (CMC) of PGPR (A, B) and AOT (C, D) with BSA (A, C) and without BSA (B, D) in the aqueous phase, respectively. The emulsifiers were dissolved in two different oil phases containing 50% H + 50% L (○ 50H + 50L) and 75% H + 25% L (▲75H + 25L). Note the difference in the X-axis scale for PGPR and AOT. 83
Figure 3.6 Storage modulus (G') from interfacial rheology with (A) PGPR and (B) AOT, which were absorbed in the interface for 1.5 hours. The aqueous phase was tested with and without BSA. The emulsifiers were dissolved in two different oil phases containing 50% H + 50% L (■ 50H + 50L) and 75% H + 25% L (□75H + 25L). Treatments with the same letter do not differ significantly ($p \geq 0.05$), according to the T-Test. 84

Figure 3.7 Confocal microscopy of W/O emulsions after the thermal cycles with 0.3% PGPR in (A) 50H + 50L, and (C) 75H + 25L oil mixtures, and 0.4% PGPR in (B) 50H + 50L and (D) 75H + 25L oil mixtures. Emulsions were prepared with BSA in the aqueous phase (scale bar: 100 μm). 85

Figure 3.8 The volume means diameter (d_{43}) of water droplets in PGPR (A) and AOT (B) stabilized W/O emulsion before (▦ ■ Fresh) and after thermal treatment (□ ■ Thermal treatment) with and without BSA in the aqueous phase. Emulsifiers concentrations were dissolved in two different oil phases containing 50% H + 50% L (50H + 50L) and 75% H + 25% L (75H + 25L). Treatments with the same letter do not differ significantly ($p \geq 0.05$) according to Tukey's test. 86

Figure 3.9 Visual observation of W/O emulsions prepared with 0.3 – 10 wt% AOT in a continuous oil phase containing 50% heavy and 50% light mineral oil (50H + 50L) (A) before and (B) after the thermal cycles. 88

Figure 3.10 W/O emulsions after the thermal cycles with AOT at 8% in 50H + 50L (A), 10% in 50H + 50L (B), 8% in 75H + 25L (C) and 10% in 75H + 25L with BSA in the aqueous phase (bar: 100 μm). 89

Figure 4.1 Visual observation of emulsions after seven days of storage. Emulsions were prepared with canola oil (CO) or mineral oil (MO). (A) CO emulsions with aqueous phase prepared with no additive, 0.125% salt (sodium chloride, S), 0.125% and 0.5% ascorbic acid (AA), citric acid (CA) and mixtures of salt and acids. (B) MO emulsions with aqueous phase prepared with no additive, 0.125% salt, 0.125% and 0.5% ascorbic acid (AA), citric acid (CA) and mixtures of salt and acids. (C) CO and MO emulsions prepared with aqueous phase with no additive, 0.045% calcium chloride (Ca), 1.5% and 2% low methoxyl pectin (LMP) and mixtures of Ca and LMP. 101

Figure 4.2 The fraction of emulsion height (emulsion layer height after seven days/ total height) containing canola oil (CO, grey bars) or mineral oil (MO, black bars) as the continuous phase. Emulsions prepared with (A) aqueous phase with various levels of salt (S), ascorbic acid (AA), and citric acid (CA); (B) aqueous phase with low methoxyl pectin (LMP) without or with calcium chloride (Ca). The concentration of ingredients is mentioned in the figure. Different letters represent significant differences at $p \leq 0.05$ (Tukey's test). 103

Figure 4.3 The microstructure of water-in-CO emulsions after seven days of storage with various levels of salt (S), ascorbic acid (AA), and citric acid (CA) in the aqueous phase. The concentration

of ingredients is mentioned in the figure. Two images for each sample are shown to demonstrate the variation in the microstructure. Scale bar 100 μm. 105

Figure 4.4 The microstructure of water-in-MO emulsions after seven days of storage with various levels of salt (S), ascorbic acid (AA), and citric acid (CA) in the aqueous phase. The concentration of ingredients is mentioned in the figure. Two images for each sample are shown to demonstrate the variation in the microstructure. Scale bar 100 μm. 106

Figure 4.5 The microstructure of (I) water-in-CO and (II) water-in-MO emulsions after seven days of storage with various levels of low methoxyl pectin (LMP) and calcium chloride (Ca) in the aqueous phase. The concentration of ingredients is mentioned in the figure. Two images for each sample are shown to demonstrate the variation in the microstructure. Scale bar 50 μm. 108

Figure 4.6 Volume means diameter ($d_{4,3}$) of water droplets in emulsions formed with (A) CO and (B) MO taken from confocal microscopy image analysis of with various levels of salt (S), ascorbic acid (AA), and citric acid (CA) in the aqueous phase. The concentration of ingredients is mentioned in the figure. Different letters represent significant differences at $p \leq 0.05$ (Tukey's test). Note the difference in Y-axis between (A) and (B).....109

Figure 4.7 Sedimentation velocity (μm/s) of fresh emulsions in canola (CO) and mineral (MO) oils, centrifuge G-force at 2325xg. (A) Water phase with and without salt (S), S with ascorbic acid (AA), and S with citric acid (CA). (B) Water phase without salt (S), with calcium chloride (Ca), with low methoxyl pectin (LMP) without or with Ca. The concentration of ingredients is mentioned in the figure. Different letters represent significant differences at $p \leq 0.05$ (Tukey's test).....111

Figure 4.8 The viscosity index of emulsions with canola (CO, grey bars) and mineral (MO, black bars) oils. (A) Emulsion aqueous phase without any additive (S0) with salt (S), ascorbic acid (AA), citric acid (CA) and S with AA and CA. (B) Emulsion aqueous without any additive (S0), with calcium chloride (Ca), low methoxyl pectin (LMP) and Ca with LMP. The concentration of ingredients is mentioned in the figure. Different letters represent significant differences at $p \leq 0.05$ (Tukey's test).....112

Figure 4.9 Effect of additives on the storage (G', closed) and loss (G'', open) modulus with a variation of shear strain (0.01 – 1000%) at a constant frequency of 1 Hz. (A) Emulsions prepared with canola oil (CO) - (A1) day 0 and (A2) day 7. (B) Emulsions prepared with mineral oil (MO) – (B1) day 0 and (B2) day 7. The aqueous phases were prepared with and without salt (S), S

with ascorbic acid (AA), and S with citric acid (CA). The concentration of ingredients is mentioned in the figure legends. 114

Figure 4.10 Effect of additives on the storage (G', closed) and loss (G", open) modulus with a variation of shear strain (0.01 – 1000%) at a constant frequency of 1 Hz. (A) Emulsions prepared with canola oil (CO) - (A1) day zero and (A2) day seven. (B) Emulsions prepared with mineral oil (MO) – (B1) day zero and (B2) day seven. The aqueous phases were prepared without salt (S), with calcium chloride (Ca), with low methoxyl pectin (LMP) with or without Ca. The concentration of ingredients is mentioned in the figure legends. 116

Figure 4.11 Tan δ (G"/G') of emulsions with canola (CO, grey bars) and mineral (MO, black bars) oil at 0.01% of strain. (A) Day 0 and (B) day 7 are for emulsions without any additive (S0) with salt (S), ascorbic acid (AA), citric acid (CA) and S with AA and CA. (C) Day zero and (D) day seven are for emulsions without any additive (S0), with calcium chloride (Ca), low methoxyl pectin (LMP) and Ca with LMP. Different letters represent significant differences at $p \leq 0.05$ (Tukey's test). 117

Figure 4.12 Interfacial tension of 4 wt% GMO in CO and MO with different aqueous phase compositions (A) Aqueous phase without any additive (S0) with salt (S), ascorbic acid (AA), citric acid (CA) and S with AA and CA. (B) Aqueous phase without any additive (S0), with calcium chloride (Ca), low methoxyl pectin (LMP), and Ca with LMP. The concentration of ingredients is mentioned in the figure. Different letters represent significant differences at $p \leq 0.05$ (Tukey's test). Note the difference in the Y-axis range between (A) and (B). 120

Figure 4.13 DSC thermograms for ice (A1-D1) and GMO melting (A2-D2) peaks of CO and MO-emulsions prepared with 4 wt% GMO and different aqueous phase compositions. (A, B) Aqueous phase without any additive (S0) with salt (S), ascorbic acid (AA), citric acid (CA) and S with AA and CA. (C, D) Aqueous phase without any additive (S0), with calcium chloride (Ca), low methoxyl pectin (LMP) and Ca with LMP. Note the difference in the Y-axis scale between ice melting (A1 – D1) and GMO melting (A2 – D2). 122

Figure 4.14 (A, B) Ice melting peak temperature (°C) and (C, D) respective ice melting enthalpy ($J.g^{-1}$) of CO and MO-emulsions with different aqueous phases. (A and C) Aqueous phase without any additive (S0) with salt (S), ascorbic acid (AA), citric acid (CA) and S with AA and CA. (B and D) Aqueous phase without any additive (S0), with calcium chloride (Ca), low methoxyl pectin (LMP) and Ca with LMP. The concentration of ingredients is mentioned in the figure. Different letters represent significant differences at $p \leq 0.05$ (Tukey's test). ...125

Figure 4.15 (A, B) GMO melting peak temperatures (°C) and (C, D) respective GMO melting enthalpy ($J.g^{-1}$) of CO and MO-emulsions with different aqueous phases. (A and C) Aqueous phase without any additive (S0) with salt (S), ascorbic acid (AA), citric acid (CA) and S with AA and CA. (B and D) Aqueous phase without any additive (S0), with calcium chloride (Ca), low methoxyl pectin (LMP) and Ca with LMP. The concentration of ingredients is mentioned in the figure. CO s was the subpeak found next to the second peak. Different letters represent significant differences at $p \leq 0.05$ (Tukey's test). 127

Figure 4.16 ATR-FTIR spectra for intermolecular hydrogen bonding (~3400 cm^{-1}) of GMO hydroxyl (OH) groups in (A) CO and (B) MO-emulsions with aqueous phases containing no additive (S0), salt (S), ascorbic acid (AA), S with AA, calcium chloride (Ca), low methoxyl pectin (LMP) and LMP with Ca. (C) The change in intermolecular hydrogen bonding peak frequency in CO and MO-emulsions. (D) Areas under the peaks in both oil emulsions. The concentration of ingredients is mentioned in the figure. Different letters represent significant differences at $p \leq 0.05$ (Tukey's test). 130

Figure 4.17 ATR-FTIR spectra for free C=O at the α position of GMO's head group (1742 cm^{-1}) and hydrogen-bonded C=O (1735 cm^{-1}) with different aqueous phases containing no additive (S0), salt (S), ascorbic acid (AA), S with AA, calcium chloride (Ca), low methoxyl pectin (LMP), and LMP with Ca in (A) CO, and (B) MO emulsions. (C and D) Areas under the peaks in CO and MO emulsions. The concentration of ingredients is mentioned in the figure. Different letters represent significant differences at $p \leq 0.05$ (Tukey's test).....132

Figure 4.18 ATR-FTIR spectra for hydrocarbon chain CH2 stretching mode from 1300 to 1400 cm^{-1} for CO-emulsions with different aqueous phases containing no additive (S0), salt (S), ascorbic acid (AA), S with AA, calcium chloride (Ca), low methoxyl pectin (LMP), and LMP with Ca. (B) The normalized double-gauche (*gg*) CH_2 band at 1354 cm^{-1} and the normalized gauche-trans-gauche (*kink*) at 1367 cm^{-1} with respect to symmetric bending of the end CH_3 vibration at 1378 cm^{-1}. The ingredients and their concentration is mentioned in the figure. Different letters represent significant differences at $p \leq 0.05$ (Tukey's test).....134

Figure 5.1 Proposed mechanism behind the viscoelastic properties of W/O emulsions with 20 and 50 wt% water content without LMP and with LMO. 140

Figure 5.2 Stability of water-in-oil emulsions with different water volume fractions (20, 30, 40 and 50 wt%) prepared with 1.5 wt% LMP or without LMP for control emulsions, GMO and 7 wt% HSO. Petri dish on day 1 (A) and day 30 (B). Glass tube test flipped 90 degrees in parallel with the plane surface on day 30 (C).....145

Figure 5.3 Apparent viscosity of 1.5 wt% LMP solution and 7 wt% HSO in canola oil on day 1 (A). (B and C) Viscosity as a function of shear rate for water-in-oil emulsions with different water content 20, 30, 40 and 50 wt%, prepared without and with LMP, GMO and HSO on day 1 (B) and day 30 (C). (D and E) Apparent viscosity of water-in-oil emulsions with different water content 20, 30, 40 and 50 wt%, prepared without and with LMP, GMO and HSO on day 1 and day 30 at a low (0.1 s^{-1}) shear rate and at high (100 s^{-1}) shear rate (E). Note the difference in y-axis scales due to variation in shear rates. 147

Figure 5.4. Storage (G') and loss moduli (G") as a function of oscillation strain for W/O emulsions with water content from 20 to 50 wt% and 1.5 wt% LMP in the aqueous phase. Control emulsions were made without LMP in the aqueous phase. Data collected on day 1 (A, C, E) and day 30 (B, D, F) are shown for control emulsions (A, B), 20 and 30% water emulsion (C, D) and 40 and 50% water containing emulsions (E, F). The arrow in some figures indicates a peak in G'. 151

Figure 5.5 (A) Storage modulus (G') at 10% of oscillation strain, (B) crossover (% strain) and (C and D) tan δ of water-in-oil emulsions as a function of oscillation strain with different water volume fractions prepared with LMP, GMO and HSO on day 1 (D1) and day 30 (D30). Note difference in y-axis scales due to variation of analysis.....153

Figure 5.6 Polarized light with bright-field micrographs of water-in-canola oil emulsions on day 1 and day 30 for control emulsions without LMP with 20 and 50 wt% water and for LMP emulsions with 20 to 50 wt% water. Scale bar 10 μm. Arrows indicate interfacial fat crystals around the water droplets.....156

Figure 5.7 DSC freeze/thaw thermograms of water-in-oil emulsions under ageing (on day 1 and day 30) for control emulsions with 20 and 50 wt% water without LMP (A and B) and 20, 30, (C, D) 40 and 50 wt% (E, F) water emulsions with LMP. Samples were cooled from 25 °C to –70 °C, and heated to 70 °C, followed by a second cooling to –70 °C, at a rate 5 °C/min. Arrows indicate the direction of the temperature cycle. Important peaks were identified with numbers and discussed in the text.....158

Figure 5.8 The solid fat content of water-in-oil emulsions on day 1 (D1) and day 30 (D30). Control emulsions were prepared without any LMP in the aqueous phase. 162

LIST OF ABBREVIATIONS AND SYMBOLS

θ	Angle
$Å^2$	Angstrom square
A	Absorbance
ADI	Acceptable daily intake
~	Approximately
m	Applied load
AA	Ascorbic acid
AYV	Average yield value
k	Boltzmann's constant
BSA	Bovine serum albumin
BF	Brightfield
CO	Canola oil
Ca	Calcium chloride
Ca^{+2}	Calcium ions
C=O	Carbonyl group
C_{10}	Capric acid
C_8	Caprylic acid
CB-1A	Castor bean allergen
CA	Citric acid
CP	Cloud point
α	Cone angle
c_s	Concentration of solution
CLSM	Confocal laser scanning microscope
p	Contact length of the plate
η_c	Continuous phase viscosity
CNO	Coconut oil
c	Correction factor

HCSO	Cotton stearine
ϕ_{eff}	Critical volume fraction
m^3	Cubic meter
ρ_c	Density of the bulk phase
ρ_d	Density of the dispersed phase
°C	Degree Celsius
DE	Degree of esterification
DNA	Deoxyribonucleic Acid
d_p	Depth of penetration
DLVO	Derjaguin–Landau–Verwey–Overbeek
D_2O	Deuterium oxide
DAGs	Diacylglycerols
d	Diameter
ε	Dielectric constant
DSC	Differential scanning calorimetry
D	Diffusion coefficient of the dispersed phase into the bulk phase
η_d	Dispersed phase viscosity
C_∞	Dispersed phase solubility
E_{disp}	Displacement energy
DLS	Dynamic light scattering
ddPCR	Droplet digital polymerase chain reaction
E	Electrical field
U_E	Electrophoretic mobility
ϕ_{eff}	Effective volume fraction
e_{xy}	Equivalent interfacial shear strain tensor material
EIP	Emulsion inversion point
η_r	Emulsions' relative viscosity
S	Entropy
EDTA	Ethylenediaminetetraacetic acid
EO	Ethylene oxide
e.g.	Example
σ_{EXT}	External stress

T_f	Final melting temperature
ΔG	Free energy
F (d)	Frequency distribution of droplets
FDA	Food and Drug Administration
F	Force
FTIR	Fourier transform infrared or IR spectra
F_m	Fully melted fat
R	Gas constant
GRAS	Generally recognized as safe
σ_g	Geometric standard deviation distribution
g	Grams
F_g	Gravitational force
g (italic)	Gravity force
GMO	Glycerol monooleate
GMS	Glycerol monostearate
HMO	Heavy mineral oil
h	Height
f(κa)	Henry's function
Hz	Hertz
>	Higher than
HO	Hydrocarbon oil
HO/W	Hydrocanbon oil-in-water
HCl	Hydrochloric acid
F_f	Hydrodynamic frictional force
H	Hydrogen
HCO	Hydrogenated canola oil
HSO	Hydrogenated soybean oil
HLB	Hydrophilic-lipophilic balance
HG	Hydrophilic group numbers
OH	Hydroxyl group
I_0	Incident light

H_0	Initial emulsion height
K^s	Interfacial dilatational modulus
k^s	Interfacial dilatational viscosity
ΔA	Interfacial droplet area change
γ	Interfacial tension
τ_i	Interfacial shear stress
G	Interfacial shear elasticity
J	Joule
kg	Kilogram
kPa	Kilopascal
P_L	Laplace pressure
dL	Length deformation
l	Length of the light path
LMO	Light mineral oil
LVR	Linear viscoelastic regime
Lo	Liquid oil fraction
LG	Lipophilic group numbers
G"	Loss modulus
LMP	Low methoxyl pectin
<	Lower than
$MgCl_2$	Magnesium chloride
Φ_m	Maximal packing volume fraction of droplets
MCT	Medium-chain triglycerides
MP	Megapixels
M	Melted mass
CH_2	Methylene
CH_3	Methyl group
m^2	Meter square
µg	Micrograms
µm	Micrometer
µs	Microsecond

mg	Milligram
mL	Millilitre
mM	Millimolar (millimoles per liter)
ms	Millisecond
min	Minute
V_m	Molar volume of the dispersed phase
ε_c	Molar absorptivity coefficient
M	Molarity (moles per liter)
MAG	Monoacylglycerol
nm	Nanometer
N	Newton
NMR	Nuclear magnetic resonance
n	Number of droplets
OSA	Octenyl succinic anhydride
O/W	Oil-in-water
H	Oil separation
P_π	Osmotic pressure
OR	Ostwald ripening
ω	Ostwald ripening rate
O	Oxygen
ppm	Parts per million
Pa	Pascal
%	Percentage
wt%	Percentage by weight
%v/v	Percentage by volume
η_d	Phase dispersed viscosity
PIT	Phase inversion temperature
δ	Phase angle
π	Pi number
PLM	Polarized light microscopy
PEG	Polyethylene glycol

Triton X-100	Polyethylene glycol tert-octylphenyl ether
PGPR	Polyglycerol polyricinoleate
PG	Polyglycerol
PEs	Polyglycerol esters
Tween 20	Polyoxyethylene sorbitan monolaurate
Tween 80	Polyoxyethylene sorbitan monooleate
Tween 60	Polyoxyethylene sorbitan monostearate
Tween 65	Polyoxyethylene sorbitan tristearate
PCR	Polymerase Chain Reaction
KCl	Potassium chloride
pH	Potential of hydrogen
PFG-NMR	Pulse field gradient nuclear magnetic resonance
qPCR	Quantitative polymerase chain reaction
V_{ϕ}	Rate of gravitational separation in emulsion with a finite droplet volume fraction
R^2	R-squared
rad	Radian
r	Radius
s^{-1}	Reciprocal second
cm^{-1}	Reciprocal centimeter
RI	Refractive index
rpm	Revolutions per minute
W	Ring weight
s	Second
SI	Sedimentation index
$\dot{\gamma}$	Shear rate
γ	Shear strain
τ	Shear stress
AOT	Sodium bis(2-ethylhexyl) sulfosuccinate, Aerosol-OT®1, dioctyl sodium sulfosuccinate
S	Sodium chloride
Na^+	Sodium ions

NaOH	Sodium hydroxide
SFC	Solid fat content
SFI	Solid fat index
SWC	Solid wax content
Span 20	Sorbitan monolaurate
Span 80	Sorbitan monooleate
Span 40	Sorbitan monopalmitate
Span 60	Sorbitan monostearate
Span 83	Sorbitan sesquioleate
Span 85	Sorbitan trioleate
STEP	Space and Time resolved Extinction Profiles
C18:0	Stearic acid
G'	Storage modulus
A	Surface area
h	Surface-to-surface separation between the droplets
$d_{3,2}$	Surface-volume mean droplet radius
3D	Three-dimensional
V_{stokes}	Terminal velocity of an isolated rigid spherical particle
T	Temperature
t	Time
N	Total number of water droplets
M	Total sample mass
I	Transmitted light
TAG	Triacylglycerol
VO	Vegetable oil
v	Velocity
η	Viscosity
$d_{4,3}$	Volume average droplet diameter
V	Volume of dispersed droplets
ϕ	Volume fraction of dispersed phase
$d_{3,3}$	Volume-weighted geometric mean diameter

H_2O	Water
W_e	Weber number
W/CO	Water-in-canola oil
W/MO	Water-in-mineral oil
W/HO	Water-in-hydrocarbon oil
W/O	Water-in-oil
W/VO	Water-in-vegetable oil
W-O	Water-oil
WPI	Whey protein isolate
S0	Without additive
ζ	Zeta potential

1. INTRODUCTION

1.1 Summary

Water-in-oil (W/O) emulsions are essential in many different applications, including food, cosmetics, skincare, biotechnology, and petroleum industries. The stabilization of W/O emulsion is due to the lipophilic emulsifiers' presence at the water droplet surface. Most of the lipophilic emulsifiers are structured with a large non-polar chain and a smaller polar head group containing hydroxyl groups, allowing their absorption at the water-oil interface and inverse micelles formation in the oil phase (Bus, Groeneweg, & van Voorst Vader, 1990). Commonly, the emulsifiers used for W/O emulsion formation and stabilization are based on fatty acids esters of sorbitan group (e.g., sorbitan monooleate (Span 80)), monoglycerides (e.g., glycerol monooleate (GMO)), polyglycerol ester of fatty acids (e.g., polyglycerol polyricinoleate (PGPR)). So far, most of the research works have studied various inter-droplet interactions in liquid W/O emulsions with mineral oil (MO), developing different water-in-mineral oil (W/MO) emulsions (Ford & Furmidge, 1966; Opawale & Burgess, 1998; Politova, Tcholakova, Tsibranska, Denkov, & Muelheims, 2017). However, research work on liquid water-in-vegetable oil (W/VO) emulsions faced frequent destabilization and phase separation. Most of the investigations on food-grade W/VO emulsions are performed on margarine-like semi-solid systems, stabilized with a combination of emulsifiers and a saturated fat crystal network that entraps the water droplets (Goubran & Garti, 1988; Scherze, Knoth, & Muschiolik, 2006; Ushikubo & Cunha, 2014). At present, there is a significant lack of knowledge, which can uncover the destabilization mechanism of liquid W/VO emulsions. Such systems are important for the development of margarine-like tablespreads with high health beneficial effects by lowering total fats, saturated fat crystals, replacing synthetic emulsifiers (e.g., PGPR) and delivery of hydrophilic bioactives and aqueous phase ingredients that could modify bulk phase structure.

The project's overall goal was to uncover the mechanism of stabilization of liquid W/O emulsions for broad applications in various fields. To better comprehend the current state of knowledge, a detailed literature review was performed (Chapter 2) on the destabilization mechanisms in W/O emulsions; typical emulsifiers used divided into six different categories, mechanisms of emulsion stability modifying the continuous or aqueous phase and the various new and conventional characterization techniques. The overall hypothesis was that the key to W/O stabilization occurs from the balance of non-covalent interactions between the emulsifier at the water-oil interface and the oil phase versus the aqueous phase.

The research work was divided into three sections. In the first study (Chapter 3) of this project, thermally stable coarse water-in-oil emulsions were developed as potential deoxyribonucleic acid (DNA) bioreactors for biotechnological application. The optimization of polymerase chain reaction (PCR) analysis with W/O emulsions has been used since 2003, where emulsions were destabilized to recover the aqueous phase for DNA detection (Tawfik & Griffiths, 1998). However, the first study proposed a new technique that included DNA detection in stable water droplets' by modifying oil phase viscosity and interfacial interactions, resisting multiple thermal cycles. In the next chapter (Chapter 4) stabilization mechanism of liquid W/VO emulsions was uncovered by modifying interactions of aqueous phase hydroxyl group donating agents at the oil-water interface with a food-grade emulsifier GMO, using W/MO emulsion as a control. GMO is a widely popular food-grade emulsifier; however, its desorption from the water droplet surface towards the vegetable oil (VO) was identified as the main difficulty in improved stabilize of liquid W/VO emulsions (Ghosh, Tran, & Rousseau, 2011). Based on this work's outcome, subsequent research in Chapter 5 focused on providing viscoelasticity to stable liquid W/VO emulsions for food applications by increasing the water content, providing aqueous phase hydroxyl groups donating agents, lowering fat percentage and the addition of a minimum amount of fat crystals.

1.2 Hypotheses

The following hypotheses were assessed in this project:

1) Coarse water-in-oil emulsion stable to multiple thermal cycles could be produced by modifying emulsifier and continuous phase compositions that would form a strong interfacial layer and prevent close contact and sedimentation of water droplets.

2) It would be possible to create stable water-in-oil emulsions by high energy homogenization and vortex mixing processes with the help of ingredient formulation.

3) A stable water-in-vegetable oil emulsion could be developed with food-grade lipophilic emulsifiers by preventing their desorption from the water-vegetable oil interface. Emulsifier desorption from the water droplet surface could be inhibited by forming stronger hydrogen bonds between the emulsifier molecule's hydrophilic portions with specific water-soluble hydroxyl donating agents.

4) Viscoelasticity of water-in-oil emulsion could be significantly improved by increasing water content and the hydrogen bonding at the interface with the help of stabilizing fat crystals in the continuous phase.

1.3 Objectives

This project intended to uncover the mechanism of stabilization of liquid W/O emulsions for broad applications in various fields, such as biotechnology, cosmetics, skincare, and food applications. Initially, the oil phase viscosity and emulsifier type were controlled to provide droplet stability under multiple thermal cycles in a short time, necessary for the specific biotechnological application. Subsequent research on liquid W/O emulsions used mineral oil for cosmetic and skincare applications and canola oil mainly for food applications. Identification of how hydroxyl group donating agents interact with the emulsifier at the interface was the main objective of the second study. The last study was mainly for food applications in low-fat tablespreads by creating an elastic system with previous outcomes by incrementing water content with hydroxyl donating agents interacting with the emulsifier and fat crystals in the continuous phase. The specific objectives of this project were:

1) Develop coarse liquid water-in-mineral oil emulsions stable to multiple thermal cycles by modifying ingredient formulation and implementing vortex mixer processing.

2) Stabilize liquid water-in-oil emulsions by modifying emulsifier interactions at the water-vegetable oil interface using salts and various hydroxyl group donating agents.

3) Improve viscoelastic behaviour of food-grade water-in-canola oil emulsions by increasing water concentration, hydroxyl group donating agent and fat crystals in the continuous phase.

2. LITERATURE REVIEW

2.1 Emulsions: General Features

2.1.1 Definitions and types of emulsions

Aqueous and oil phases are immiscible, but different percentages of these components are intimately mixed in many products. Such liquid dispersed systems are commonly known as emulsions, where one of the phases is dispersed as small spherical droplets in the bulk phase. In these terms, "oil" represents a lipophilic liquid, e.g., vegetable or mineral oils, and "water" represents an aqueous solution containing various hydrophilic ingredients (e.g., water or vinegar) (Walstra, 2005). W/O emulsions stability is essential to understand their stability production, control and to create new products. The aqueous phase's dispersion as fine water droplets in a continuous oil phase is involved in different commercial products, including foods, paints, pharmaceuticals, cosmetics, pesticide formulations, lubricants, and crude petroleum oil (e.g., margarine, butter, lipsticks, and crude oil emulsion) (McClements, 2005). The contact between aqueous and oil phases generates interfacial tension and creates new surfaces, increasing the system's energy, making it thermodynamically unfavourable. An oil-in-water (O/W) emulsion contains oil droplets as dispersed phase in a continuous aqueous phase (e.g., milk, mayonnaise, and vinaigrette). These emulsions are used for the delivery of lipophilic actives (e.g., phytosterols). W/O emulsion contains water droplets as a dispersed phase and oil as the bulk phase. The latter emulsions represent more difficulties forming than O/W emulsions because oils are the bulk phase and possess other mechanisms to stabilize. An actual emulsion used in various food and non-food applications may also contain multiple polar (e.g., water, protein, or polysaccharides) and non-polar (e.g., oil, emulsifiers) ingredients that could significantly affect their formation and stability. Thus, emulsions are complex systems involving different molecular interactions, depending on both phases' physical and chemical properties.

All emulsions required energy input in the system to overcome the free energy (ΔG) needed to increase the interface area because the entropic change is not sufficient (Komaiko & McClements, 2016). In Equation 2.1 is presented free energy calculation where ΔA is the interfacial droplet area change, and γ is the interfacial tension, representing the energy to increment the interface. The temperature is T and S is the entropy, which is the result of all possible organization of droplets and emulsifiers.

$$\Delta G = \Delta A\gamma - T\Delta S \quad (2.1)$$

Different types of equipment give the input energy, allowing reduction of droplet size, such as a high energy homogenization process (e.g., rotor-stator systems, high-pressure homogenizers, ultrasound generators). In those processes, a mechanical force is applied to create small droplets of the dispersed phase in the bulk phase (Hiemenz & Rajagopalan, 1997; McClements, 2005). However, the newly formed emulsion would remain stable only for a few seconds without the presence of any surface-active emulsifiers. Emulsifiers are amphiphilic molecules containing both polar and non-polar parts, enabling them to locate at the water-oil interface and lower the interfacial tension, thereby reducing the energy required to form an emulsion (Dukhin, Kretzschmar, & Miller, 1995; McClements, 2005). The usual emulsifiers utilized in the food industry are small-molecule emulsifiers, proteins, phospholipids, and polysaccharides (McClements, 2005). Some emulsifiers even act over the increment of interfacial strength at the interface (e.g., proteins) (Dalgleish, 2004). The emulsifiers' properties may also determine whether the emulsion will be O/W or W/O type and the inversion between both phases. An emulsifier's effectivity in emulsion formation depends on the mobility and the ability to adsorb at the interface and the capacity to decrease the water-oil interfacial tension (Tadros, 2013). Solid particles can also act as emulsifiers at the water-oil interface and stabilize the matrix by Pickering or networking stabilization (e.g., solid fat, wax, or plat base particles) (Ghosh & Rousseau, 2012). Emulsions can also be formed using a low energy process (e.g., stirring rod or microchannels), where depending on emulsifier types and concentrations, the dispersed phase droplets can be formed spontaneously under a simple mixing of phases or change in temperature (McClements, 2005; Pinnamaneni, Das, & Das, 2003).

Based on droplet size and thermodynamic stability, emulsions are classified as conventional, nanoemulsions, and microemulsions (Komaiko & McClements, 2016). Conventional emulsions are the most widely used, with a general opaque appearance and droplets diameters ranging from 200 nm to 100 μm and emulsifier: oil ratio from 0.2 – 1: 10 (McClements, 2010; Ray, Gupta, & Rousseau, 2015). Nanoemulsions and conventional emulsions showed metastable systems, implicating that these emulsions can be become kinetically stable for a long time but will always separate given enough time (Komaiko & McClements, 2016). Nanoemulsions have droplet diameters less than 200 nm, contributing to more kinetic stability against gravitational force and droplet aggregation. Depending on droplet volume fraction and size, nanoemulsions may appear optically translucent to opaque and requires almost the same weight proportion of oil and emulsifier concentration (Ray et al., 2015; Weder & Mütsch, 1992). These emulsions have potential applications for the encapsulation of bioactives and functional compounds for their higher bioavailability than conventional emulsions (McClements, 2012). Microemulsions are thermodynamically stable emulsions with a smaller droplet size than nanoemulsions. These emulsions are developed with a very

high emulsifier concentration where the droplets formed spontaneously, leading to transparent dispersions with droplets size ranging from less than 10 nm to 100 nm. These emulsions are often created with co-surfactants, which make their application limited to the food industry.

2.1.2 Mechanism of emulsion destabilization

Apart from microemulsions, all emulsions eventually destabilize. Depending on the application, emulsion destabilization may be the desired phenomenon (e.g., crude oil separation) or an undesirable effect that must be stopped for product performance. Therefore, it is essential to understand the various mechanisms of emulsion destabilization (Figure 2.1).

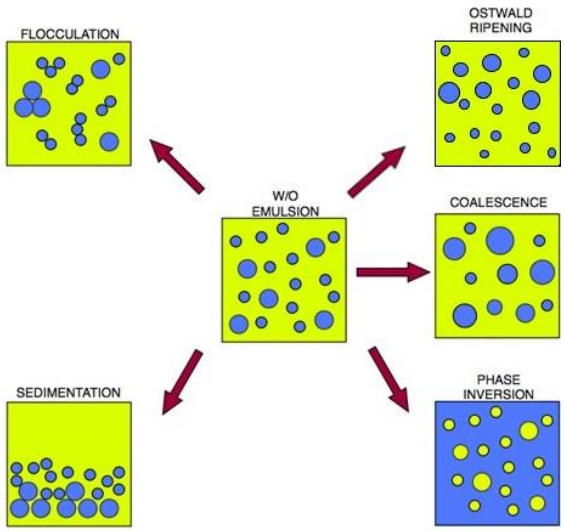

Figure 2.1 Mechanism of emulsion breakdown in W/O emulsion (flocculation, coalescence, sedimentation, phase inversion, and Ostwald Ripening). The oil phase is represented in yellow, and the water phase in blue.

2.1.2.1 Gravitational separation

Gravitational force acts on any mass in the Earth. This force may induce sedimentation or creaming of the dispersed droplets based on the density difference between the continuous and dispersed phases. Sedimentation occurs in systems where the dispersed phase has a higher density than the bulk phase in W/O emulsions. The droplets sink and sediment at the base of the container. Conversely, creaming can occur in O/W emulsions, forming a cream layer at the top of the emulsion (Coupland, 2014). As the final result, a phase break can be observed, and it is even faster with a highly dispersed volume fraction of droplets (ϕ)

(Walstra, 2005). During the gravitational separation, the emulsion droplets do not lose their shape, and the only agitation is required to redistribute them in the continuous phase (Dalgleish, 2006). The gravitational separation in food products is usually considered as an unfavourable effect on product quality. For instance, the separation of an emulsion (e.g., milk) into a visible opaque layer at the top and a turbid bottom layer is unwanted by consumers. Textural attributes of a product are also affected by gravitational separation because the visible opaque layer has the characteristic of being more viscous than normally expected. In contrast, the less opaque layer tends to have low viscosity. An equation to calculate the terminal velocity (V_{stokes}) of an isolated rigid spherical particle under gravitational force (F_g) and hydrodynamic frictional force ($F_f = F_g$) in an ideal liquid of infinite dilution was presented by Stokes' law (Equation 2.2) (McClements, 2005).

$$V_{stokes} = \frac{g(\rho_d - \rho_c)d^2}{18\eta_c} \quad (2.2)$$

Where η_c is the viscosity of the continuous phase, ρ_d is the density of the dispersed phase, the density of the bulk phase is ρ_c, g is acceleration by cause of the gravity, and d is the particle's diameter (Ghosh & Rousseau, 2010). The sign of V_{stokes} determines whether the droplets ascend against gravity (−) or descend towards gravity (+). If ρ_d is higher than ρ_c the droplets will sediment (in case of W/O emulsion), and if the ρ_d is lower than ρ_c the droplets will cream (O/W emulsion situation). As well, the smaller size of droplets reduces the gravitational velocity. A correction is needed to estimate droplets' velocity in real emulsions with a given dispersed phase volume fraction (equation 2.3). Thus, the rate of gravitational separation (V_ϕ) in emulsion with a finite droplet volume fraction is calculated from Equation 2.3 (Hunter, 1989):

$$V_\phi = V_{stokes}(1 - \phi)^{\eta_c} \quad (2.3)$$

Where the exponent $\eta_c = 6.55$ for a monodisperse emulsion (Hunter, 1989). For $\phi = 0.1$, the rate of gravitational separation would decrease by a factor of 2. In real food emulsions, with polydispersity droplet size distribution, the η_c value could even reach up to 9, further reducing the gravitational separation rate (Walstra, 2003). Another significant limitation of Stokes' law equation is the Brownian motion effect's omission to evaluate emulsion droplets' creaming velocity (Walstra, 1996). Brownian motion is the random distribution of droplets through the entire emulsion, which may prevent partially gravitational separation, and it is more applicable for small droplet sizes (e.g., nanoemulsions). Other strategies to avoid gravitational separation are: 1) lowering the density difference between the continuous and water phase, for instance,

using fat crystals or Pickering particles in the bulk phase in W/O emulsions (Rousseau, 2000), or employing brominated vegetable oil in O/W emulsions or reducing solids in the aqueous phase (Coupland, 2014). 2) Increasing the bulk phase viscosity can support more stability. W/O emulsions can establish higher stability by adding heavy mineral oil to light mineral oil, and the mixture increases the viscosity. However, this strategy also depends on the emulsification methodology (Romero-Pena, Kaion Ng, & Ghosh, 2020). O/W emulsions stability can be obtained by incorporating viscous water-soluble polysaccharides (e.g., ester gum or xanthan gum) (Coupland, 2014).

2.1.2.2 Flocculation and coagulation

Droplets are in constant movement in emulsion systems due to different forces (e.g., gravity, thermal, mechanical, or Brownian motion), and many collide. According to the energy barrier, the droplets can move away without aggregation due to a high energy barrier or coagulate with strong flocculation caused by a low energy barrier. Flocculation occurs when two or more droplets move toward each other and form an aggregate keeping their shape (McClements, 2005). Generally, the close approach of droplets is caused by the absence or reduction of repulsive forces. In systems without repulsive forces, attractive Van der Waals forces acting between droplets play an essential role in flocculation. Indeed, Van der Waals force is inversely proportional to the droplet-droplet distance of separation (Israelachvili, 2011; Tadros, 2013). Droplet flocculation may be either advantageous or unwanted in emulsions depending on the final product's purpose and functionality. Flocculation is essential to create desirable rheological behaviour, appearance, and texture (Walstra, 2003).

The cluster of droplets increases emulsions' viscosity due to the significant increase of effective size than the sum of individual droplets. The forces holding them together are more significant than the shear forces that may separate them (Coupland, 2014). In diluted emulsions, flocculation can cause creaming for the increased droplet effective diameter; however, flocs in higher volume fractions can prevent separation by forming a three-dimensional (3D) network. Two floc effective sizes have been shown in Figure 2.2. Fast flocculation is associated with greater attractive forces and lower dispersed phase volume fraction forming an open packing of flocs (e.g., branch network), which entrap large quantities of the continuous phase (McClements, 2005). However, in slow flocculation, lower attractive forces are presented, and the packing of flocs formed is compact, thus, not entrapping enough continuous phase.

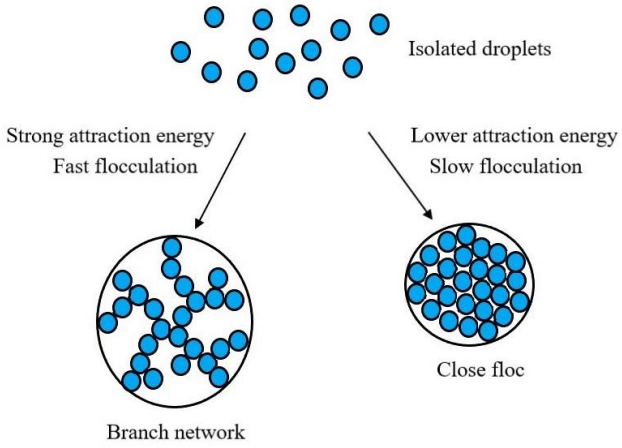

Figure 2.2 Types of floc formed with droplets characterized by increasing effective size.

Two steps could influence the rate of droplet aggregation between the droplets. First, the movement of droplets toward each other, and second is the consequence contact. When two droplets encounter by droplet-droplet forces (e.g., Brownian motion or diffusion) is known as perikinetic coagulation. If droplets' movement is due to the velocity gradient, it is identified as orthokinetic coagulation (e.g., stirring) (Hiemenz & Rajagopalan, 1997). Electrostatic repulsion can reduce flocculation in O/W emulsions. Using ionic emulsifiers, proteins, or polysaccharides, the electrostatic charge increases on the droplets, thereby improving repulsive interactions among them (McClements, 2005; Tadros, 2013). However, in W/O, proteins or polysaccharides can strengthen the interface layer of dispersed water droplets, developing a physical barrier. This barrier can prevent flocs formation in the food matrix. Emulsifiers' bulky structure can also form a thicker interfacial layer to prevent water droplets' coagulation (McClements, 2005). W/O emulsions have also been developed with solid fat. Hodge and Rousseau (2003) demonstrated that wax crystals' rapid crystallization gave more resistance to the system to prevent coalescence and flocculation.

2.1.2.3 Coalescence

Coalescence is caused by the thin film's rupture between two or more droplets into one large droplet in a floc or creamed layer (Hiemenz & Rajagopalan, 1997; Tadros, 2013). It is essential to differentiate the aggregation process, flocculation, from coalescence. During coalescence, the droplet number decrease,

droplet size increase, and droplet effective volume remains constant (Coupland, 2014). The coalescence process involves four consecutive steps: (1) two drops encounter each other via Brownian motion, flow-induced collisions, or impacts during gravitational separation. (2) A thin film of the bulk phase is created due to the droplets' attraction forces. (3) The bulk phase film becomes thinner, and molecules' motion will lead to a small pore at the interface allowing the ruptured. (4) The pore will spontaneously grow, and the two droplets merged as a single large droplet (van Aken, 2004). Specific conditions like larger diameter, significant internal stress, and low interfacial tension can support droplets' deformation as they approach each other when the film separating the droplets is thin (McClements, 2005). The surfaces of the droplets become flat due to a significant increase of external forces than internal forces, which are the ones that keep the spherical shape in droplets. Laplace pressure (P_L) (Equation 2.4) is strictly related to the inner strengths and the interfacial membrane resistance to deformation (Walstra, 2003).

$$P_L = \frac{2\gamma}{r} \tag{2.4}$$

where γ is the interfacial tension and r is the droplet radius. This equation shows the inside pressure is associated with the droplet size and the opposite external force exerted by the surface tension (Walstra, 2003). The smaller the water droplet, the highest resistance to the external forces. The lower the value of Laplace pressure, the lower energy required to break these droplets.

The deformation of droplets due to the balance of external and internal forces can be explained by Weber number (W_e) – Equation 2.5, which is the ratio of the external disruptive force to the interfacial tension at the interface of a droplet (Ghosh & Rousseau, 2010; Walstra, 2003):

$$W_e = \frac{\sigma_{EXT}\, r^2}{2\gamma h} \tag{2.5}$$

where σ_{EXT} is the external stress, and h is the surface-to-surface separation between the droplets. For We < 1, the droplets incline to stay spherical. For We > 1, the droplets tend to be deformed, and a flat film is created between them when they closely approach one another (van Aken, 2004). It is preferred a We < 1 to prevent coalescence associated with a low droplet radius; however, We critical range is between 0.1 and 1 because too low or too high will deform the droplet breaking up the droplet eventually (Walstra, 1996). The droplet size is a significant factor influencing the droplets' rate of coalescence. The smaller droplet sizes in an emulsion, the more stable it would be (Rosen, 2004). The increase of interfacial tension and rigidity of the interfacial layers protect the droplets, decreasing the coalescence rate (McClements, 2005). It will depend on the surface-active molecules used at the interface. The emulsifier geometry and

structure are also essential to decrease the coalescence rate, increasing the h. For instance, in W/O emulsions, more separation between the droplets can be performed with bulk lipid tail emulsifiers (e.g., PGPR) (Christiansen, 2014). Friberg, Larsson, and Sjoblom (2003) suggested that some emulsifiers may also promote the formation of a multilayered interface (e.g., monoacylglycerides), thereby developing a shield against droplets coalescence. Besides, the use of mixed emulsifiers (e.g., anionic and nonionic) along with appropriate co-emulsifiers (e.g., long-chain alcohols) could promote the reduction of coalescence due to an increase of interfacial elasticity (Tadros, 2013). Coalescence enables emulsion droplets to cream or sediment more quickly due to increased droplet diameter. A layer of oil at the top is noted due to this process in O/W emulsions; conversely, in W/O, the water layer appeared at the bottom (McClements, 2005; Walstra, 2005).

One curious counter pattern is observed in the partial coalescence of semi-crystalline oil droplets in O/W emulsions. The crystals located at the surface of one droplet penetrate the second droplet developing a pore formation. The solid fat network precludes changing the droplets' shape and complete merging, causing a matrix to be formed by big aggregates of partially-coalesced lipid droplets (Coupland, 2014). These fat clusters are the initial step for the butter process developed during the cream churning; the same occurred in ice cream and whipped cream.

2.1.2.4 Phase inversion

Phase inversion is the inter-conversion among W/O and O/W emulsions. It is indispensable to produce butter as a product of aggregation (e.g., phase inversion of creams by churning) (Amer, 1981; Ghosh & Rousseau, 2010). Some studies investigated phase inversion to control drug delivery (Izquierdo et al., 2002; Solans, Izquierdo, Nolla, Azemar, & Garcia-Celma, 2005). Other studies also researched phase inversion in the petroleum industry related to reducing frictional pressure and increasing fluid flow in pipes (Ioannou, Nydal, & Angeli, 2005; Xu, Li, Guo, & Wu, 2010).

Phase inversion caused by small emulsifiers can be divided into catastrophic and transitional (McClements, 2005). The catastrophic phase inversion arises with the increment of the dispersed phase volume fraction over a critical concentration compared to the bulk phase known as the emulsion inversion point (EIP). In W/O emulsions, critical ϕ is around 0.7 (Binks & Lumsdon, 2000). The EIP relies upon the formulation, emulsification conditions (e.g., intense agitation, stirrer type, dispersed phase rate of addition), and interfacial tension (Kumar, Li, Cheng, & Lee, 2015). The order of addition is also an essential factor; adding the water to the oil bulk phase with an emulsifier will form a W/O emulsion; whereas, the addition

of the same oil phase into the aqueous phase may generate an O/W emulsion (Forgiarini, Esquena, González, & Solans, 2001). All these changes are typically irreversible. The incorporation of electrolytes or other additives can also lead to a catastrophic phase inversion. The addition of a strong electrolyte in an O/W emulsion stabilized by ionic surfactants may invert it into a W/O due to ions screening of the emulsifier head groups (McClements, 2005). Phase inversion by fat crystallization has a root cause in the partial droplet coalescence. When a fully liquid O/W emulsion is cooled to a temperature where the droplets are semi-crystalline, posterior sheared, it can experience a phase inversion to a W/O emulsion. It conducts a continuous fat crystal network formation that can entrap water inside it, which is the primary step in producing butter (McClements, 2005). Phase inversion can also be promoted by colloidal particles at the interface and is more applicable in the cosmetic and pharmaceutical industries.

Transitional phase inversion of emulsions is induced by geometry variations in the emulsifier molecules caused by changes in the formulation (e.g., mixing emulsifiers or altering emulsifier affinity) and processing parameters (e.g., temperature, ionic strength) and is usually reversible (Bouchama, van Aken, Autin, & Koper, 2003; Thakur, Villette, Aubry, & Delaplace, 2008). Change in the emulsion formation has been demonstrated using a nonionic emulsifier and altering the system's temperature. For example, when the temperature of an O/W emulsion stabilized with a nonionic surfactant is increased, progressive dehydration of hydrophilic groups of the surfactant make them more hydrophobic, thereby inverting it into a W/O emulsion at a critical point known as a phase inversion temperature (PIT) (Usón, Garcia, & Solans, 2004). At intermediate temperature, nonionic emulsifiers can develop flat monolayers, favouring a bicontinuous system. PIT depends on concentration and emulsifier type, system composition, carbon atoms of the oil phase, and water: oil ratio (Kumar et al., 2015). The critical factor is the emulsifier concentration via PIT, which can be challenging because the emulsifier's high concentration can lead to Ostwal ripening via oil diffusion from smaller to larger droplets. Incorporating long-chain alcohols or fatty acids may turn an O/W emulsion into a W/O emulsion by becoming the emulsifiers mixture acting more lipophilic (Rosen, 2004). Anton, Mojzisova, Porcher, Benoit, and Saulnier (2010) developed a model to encapsulate hydrophilic molecules in W/O nanoemulsions by phase-inversion temperature using polyethoxylated emulsifier at two concentrations, 5.6 and 13 wt%, in medium-chain triglycerides. The encapsulation yields were between 81.1 and 90%, respectively. This model with 70% water has the potential for drug delivery and controlled release of hydrophilic and lipophilic bioactives in the respective soluble phase.

Solid particles of ~100 nm size can also be used to stabilize droplets with micrometres size (Chevalier & Bolzinger, 2013). One phase will wet more the particle than the other phase, the more poorly

wetting phase becoming the dispersed one. The wettability at the interface is quantified by the contact angle (θ). An $\theta > 90°$, the particles stabilize W/O emulsions, and for $\theta < 90°$, it stabilizes O/W emulsions (Binks & Lumsdon, 2000). The particles can change their wettability caused by pH, temperature, or emulsifiers and invert the phase (Kumar et al., 2015).

2.1.2.5 Ostwald ripening

Ostwald ripening (OR) occurs by the diffusion of the dispersed phase from small droplets to form large ones. In W/O emulsions, water's chemical potential is higher in little droplets, creating a water transport gradient from the smaller to the larger droplets. Thus, the larger droplets grow, and smaller droplets are reduced in size, and polydispersity decreases (Kizling & Kronberg, 1990). OR is an irreversible destabilization mechanism. OR can be prevented by (1) reducing the partial solubility between oil and water. (2) narrow droplet size distribution. The initial OR rate also rises as the droplet size distribution's width grows (McClements, 2005). (3) The reduction to smaller droplets could reduce the OR rate. Thus, it is critical to identify an effective droplet size range, considering other instability mechanisms related to large droplets (e.g., flocculation). (4) The incorporation of additives in the dispersed droplets can prevent OR. In W/O emulsions, water-soluble components with a lower solubility to the lipid bulk phase (e.g., salts) can significantly inhibit OR (Walstra, 2003). (5) Forming a thick and cohesive interfacial layer (e.g., proteins or polysaccharides) can develop a resistance to deform the droplet interface (Tcholakova et al., 2011). (6) Reducing interfacial tension using a much effective emulsifier can also diminish the OR rate (e.g., PGPR) (Choudhary et al., 2018).

In W/O emulsions, electrolytes' addition in the aqueous phase can increase the ionic strength and decrease the solubility. Kizling and Kronberg (1990) studied the addition of salts to stop OR and reduce the attractive forces among the water droplets. They used hydrocarbon oils (HO), polyoxyethylene dodecyl ether and high salt concentration in the aqueous phase. OR was not reported in the system with dodecane and hexadecane bulk oils. They pointed out that high salt concentration in tiny water droplets, when moved toward big droplets, the salt concentration will decrease in big droplets driven by the chemical potential. Thus, the water remained in smaller droplets due to this force driving. They also measured the refractive index associated with the attractive forces. The refractive index of water with salt increased, approaching the refracting index of HO. Thus, the attractive forces decreased with the increment of salt concentration. Those two effects by salt concentration inhibited the OR of water droplets. However, disperse droplets' deformation with salt concentration can also be identified with the forces acting over the surface area.

The droplet deformation can be identified with changes in the osmotic pressure (P_π) of water droplets, Equation 2.6, which considers the ϕ, the surface area of droplets (A), and the volume of dispersed droplets (V). If the ϕ is equal to 0.7405 in a monodisperse system, the droplets are no longer spherical and $P_\pi = 0$ (Princen, 1986).

$$P_\pi = \gamma\phi^2 \frac{d(A/V)}{d\phi} \tag{2.6}$$

Koroleva and Yurtov (2003) studied the difference in the osmotic and Laplace pressures in different droplet sizes as a function of S concentration in W/O emulsions with ϕ = 0.65. The oil was a HO, and as emulsifiers, 0.13 M Span 80. The water diffused partially from smaller to larger droplets. They calculated the difference between osmotic pressure and Laplace pressure. If the value was < 0, Laplace pressure was higher than osmotic pressure. Hence, there was no OR. If the difference was > 0, the osmotic pressure was dominant, and water diffuses from smaller to bigger droplets and OR occurred. Thus, the electrolyte concentration was more significant in tiny droplets, showing an increase in the osmotic pressure. Conversely, larger droplets had a lower concentration of electrolytes, indicating a decrease in osmotic pressure. Three different mechanisms were characterized it. Electrolyte concentration < 0.012 M exhibited an increase in water droplet size. Electrolyte concentrations between 0.012 to 0.188 M showed a constant number of water droplets but a redistribution of droplet size and salt concentration. Electrolyte concentration > 0.188 M caused a change in water droplet size in < 1%.

Different studies had characterized O/W emulsions with the mathematical model of Lifshitz and Slyozov (1961) and Wagner (1961) – Equation 2.7, which assume a solid matrix that contained solid spherical grains.

$$\omega = \frac{dr^3}{dt} = \frac{8DC_\infty V_m^2 \gamma}{9RT} \tag{2.7}$$

where ω is the OR rate, D is the diffusion coefficient of the dispersed phase into the bulk phase, C_∞ is the dispersed phase solubility at the planar interface, V_m is the molar volume of the dispersed phase, R is the gas constant, and T is the absolute temperature.

Jiao and Burgess (2003) used Equation 2.7 to compare experimental results and OR calculations in W/O emulsions. Various HOs were utilized – n-heptane, n-decane, n-dodecane, n-tetradecane, and light mineral oil with sorbitan sesquioleate (Span 83, 1.8 x 10^{-1} to 1.8x10^{-2} M). The water volume fraction was 0.005. The results were correlated, and the OR rates of water droplets (1 – 2 hours) were from higher to

lower in m^3/s, heptane (3.0×10^{-24}), decane (2.3×10^{-24}), dodecane (1.8×10^{-24}), tetradecane (5.8×10^{-25}) and light mineral oil did not show an increase of droplet size. OR rates in W/HO emulsions are around four times less than in HO/W emulsions. The diffusion of water in alkane oils is indifferent to the carbon number length, decreasing slightly with carbon chain length increment.

Overall, emulsion with greater droplet polydispersity would show a more significant difference in diffusion of dispersed phase from smaller to larger droplets, leading to a higher driving force for OR (Tadros, 2013). In O/W emulsions, the molecular diffusion is higher for oil molecules in a lower viscosity bulk phase. In W/O emulsion, water droplet diffusion is lower in a higher viscosity bulk phase. OR occurs in foams with wide bubble size distribution and smaller droplet size. As well in matrixes with fat crystals, OR drives the diffusion growth from small to large crystals, caused by the thermodynamic stress to decrease the contact area between the fat crystals and the dispersed phase (Coupland, 2014).

2.2 Water-in-oil emulsions

2.2.1 Unique properties of water-in-oil emulsions

W/O emulsions are unique systems that are quite different from O/W emulsions. W/O emulsions commonly exhibit lower stability than O/W emulsions on behalf of the bulk oil phase composition and density, which causes various mechanisms to separate the phases (Colucci et al., 2020). The oils possess a low dielectric constant; thus, stability cannot merely be explained with the DLVO theory (Scherze, Knoth, & Muschiolik, 2006). Hence, stabilization due to electrostatic repulsion would be insignificant in W/O emulsion. However, salt added into the water phase can cause ionic interactions in isolated conditions surrounded by oil. According to the emulsifier's structure, electrolyte interactions can be located at the interface or core of water droplets. It does not mean that salts are highly efficient in increasing the stability of all W/O emulsions. Studies with W/MO exhibited stability; however, to avoid the opposite effect, the salt concentration should not increase too high (0.012 to 0.188 M) (Koroleva & Yurtov, 2003). It has been reported that using PGPR in sunflower oil and different calcium salts in the aqueous phase formed 10 wt% W/O emulsions with different stability. For instance, calcium chloride (Ca) produced more stable emulsions than calcium lactate or calcium carbonate. Ca decreased the attractive force between the water droplets due to a higher electrolyte concentration, allowing superior stability (Márquez, Medrano, Panizzolo, & Wagner, 2010).

The main factors that dictate the water droplet stability in the oil bulk phase are droplet size, aqueous phase volume, oil viscosity (Goubran & Garti 1988), and compatibility of the lipidic chain between the

emulsifier with the continuous oil phase (Garti & Remon, 1984). The latter factor affects more when vegetable oils are used in the formulation. For example, in W/VO emulsion, it has been reported that an emulsifier with unsaturated fatty acid would be more suitable for vegetable oils with a high degree of unsaturation (Garti & Remon, 1984). Other essential factors are the emulsifier kind, considering the charge in the polar head and diverse lipidic composition, and the ability to reduce interfacial tension (Kovalchuk & Masalova, 2012). The emulsifier should be lipophilic; therefore, the hydrophilic-lipophilic balance (HLB) should generally be between 3 – 6. Thus, many parameters of stability W/O emulsions are different than for O/W emulsions.

2.2.2 Ingredients used in water-in-oil emulsion formation and stabilization

There are three major parts in a W/O emulsion: a dispersed aqueous phase, the continuous oil phase, and the emulsifiers. The aqueous phase may contain various salts, such as S, Ca, magnesium chloride, potassium chloride, ferrous sulphate, calcium lactate and calcium carbonate (Gaiti, Aserin, & Cohen, 1994; Márquez et al., 2010; Scherze et al., 2006). In the production of chocolates with heat resistance, W/O emulsions have been used with icing sugars (Norton, Fryer, Parkinson, & Cox, 2009), grape sugar, malt sugar and sugar alcohols in the aqueous phase (Takemori, Tsurumi, & Takagi, 1992). Some W/O emulsions used water-soluble additives to prevent bacteria growth (e.g., EDTA, tricalcium phosphate (E341)) (Nishimi & Miller, 2001). A critical factor is the control of pH with buffers (e.g., phosphate buffer, sodium hydroxide, hydrochloric acid) (Yi, Zhu, McClements, & Decker, 2014). Proteins in the aqueous phase have also been added for partial replacement of lipophilic emulsifiers (e.g., β-lactoglobulin, sodium caseinate) (Gülseren & Corredig, 2012). In the production of margarine and low-fat spreads, which are also W/O emulsions, fat crystals are used to crystallize at cold conditions and form the viscoelastic structure (e.g., hydrogenated sunflower oils) (Young & Wassell, 2019).

The oil phase could consist of a wide range of lipidic compositions with low or high polarity. The triacylglyceride (TAG) from vegetable oil (e.g., canola oil, sunflower oil, soybean oil, castor oil, olive oil, walnut oil) has higher polarity for the glycerol backbone at the polar head and more viscosity than most hydrocarbon oils (Yi et al., 2014). Hydrocarbon oils can be pure alkane hydrocarbons (e.g., decane, n-hexadecane, squalene, etc.) and a mixture of alkanes (e.g., light and heavy mineral oil) (Huston & Larson, 2015; Peng, Liu, Kwan, & Huang, 2010). The oil phase can also consist of edible fat mixtures. For instance, W/O emulsions in some chocolate applications used milk fats and cocoa butter as the continuous phase (Norton et al., 2009).

The emulsifiers used for water droplet formation and stabilization have a wide range of categories, considering structure and functional properties. Section 2.3 details the common W/O emulsifiers used in food, biotechnology, cosmetic and skincare applications. The emulsifiers were divided into six groups: (1) sorbitan fatty acids esters, (2) glycerol fatty acids esters, (3) ethoxylated, (4) polyglycerol ester of fatty acid and other polymeric emulsifiers, (5) sulfosuccinates and (6) Pickering particles.

2.2.3 Application of water-in-oil emulsion in various fields

W/O emulsions are used in multiple industrial areas and life science applications, such as food, personal care and cosmetics products, biotechnology, pharmaceuticals, petrochemical, and agriculture industries. The demand for W/O emulsion is due to the flexibility to modify the fat composition, delivery of hydrophilic bioactives and product price reduction with the increase of water volume fraction. In food, margarine, spreads, and butter (prepared by phase inversion of cream by churning) are W/O emulsions and should include a fat content from 10 to 90% (Young & Wassell, 2019). These emulsions can stabilize the water droplets by surface-active fat crystals, high-melting emulsifiers or particles located at the interface. The mechanism of particle stabilization is known as Pickering stabilization, which establishes a physical barrier around the water droplets (Ghosh & Rousseau, 2011; Zembyla, Murray, & Sarkar, 2018). Another stability mechanism is a network of fat crystals in the continuous oil phase. The crystal performs Van der Waals interaction, which restricts droplet movement and provides a semi-solid or solid texture (Brooker, 1993; Goff, 1997). Both mechanisms can act simultaneously, selecting a suitable emulsifier that cooperates with heterogeneous nucleation (Ghosh et al., 2011).

W/O nanoemulsions are utilized as lotions or moisturizing creams in the personal care and cosmetic industry, in which the water droplets' primary function is to deliver hydrophilic bioactive molecules. For instance, Shakeel and Ramadan (2010) created 20 wt% W/O nanoemulsions with a transdermal application of 1 wt% caffeine in the dispersed phase to treat skin cancer caused by sunlight. The *in vitro* study exhibited high permeability in nanoemulsions containing caffeine than the caffeine solution. The emulsion with the best permeability contained diethylene glycol monoethyl ether, isopropyl alcohol, propylene glycol mono- in diester lauric acid oil. Wu, Ramachandran, Weiner, and Roessler (2001) also created W/O nanoemulsions for transfollicular absorption in topical insulin delivery (5 μg/ mL), a non-metabolized polysaccharide water-soluble used to assess filtering kidney function. The *in vitro* study used a mixture of emulsifiers, Span 80 and polyoxyethylene sorbitan monooleate (Tween 80). Olive oil was tested between 66.6 to 72.8 %v/v and aqueous phase 2.3 to 3.2 %v/v at pH 7.4. The inulin transportation across the skin was proportional to the HLB of emulsifier mixtures, showing higher inulin permeation (0.4 to 0.6 %/ hour) around 1.5 to 2.5

HLB. It was reported that a minimal concentration of co-emulsifier Tween 80 was necessary to increase the water content in the emulsions. They found factors that did not affect the skin absorption, like hydrophilic bio-active molecular size and animal skin characteristics (Wu et al., 2001). Lipstick is a standard cosmetic product that consists primarily of hydrophobic compounds (e.g., oils, waxes, and colourants). The high percentage of these compounds can cause dryness on lips blocking natural lubrication (Beri, Norton, & Norton, 2013). W/O emulsion can provide moisture to the lips. Another application is lipsticks, developed with base material up to 40 wt% of water content, dispersed in a continuous wax-based matrix (Dunphy, 1992; Le Révérend, Taylor, & Norton, 2011).

In the pharmaceutical industry, W/O emulsions are used to deliver hydrophilic bio-actives for various functions (e.g., antidiarrhoeic, gastrointestinal protector, dermatological protector, anti-inflammatory, local anesthetic or mineral supplements) (Carretero & Pozo, 2010). For instance, W/O microemulsions were developed to deliver acyclovir through the skin to treat herpetic mucocutaneous – herpes 1, herpes 2, Epstein-Barr, and varicella-zoster (Shishu, Rajan, & Kamalpreet, 2009). The aqueous phase contained polyoxyethylene sorbitan monolaurate (Tween 20), sorbitan monolaurate (Span 20) and dimethylsulfoxide (to increase the water solubility of acyclovir), and the oil phase isopropyl myristate, glycerol caprylate caprate and caprylic/ capric triglycerides. The formulation was studied *in vivo* and *in vitro*, showing total inhibition after 24 hours of herpes lacerations' development (Shishu et al., 2009). Chatzidaki et al. (2016) also studied *in vitro* digestion using pancreatic and gastric lipases, comparing W/O emulsions and microemulsion bioavailability. The hydrophilic bio-active was hydroxytyrosol, a natural antioxidant in a small percentage of olive oil, which acts as a cardioprotective anti-ageing and anti-inflammatory agent. The 2 wt% W/O microemulsions were prepared with propylene glycol, medium-chain triglycerides (MCT), lecithins and monoglycerides. The 5 wt% W/O emulsions contained sucrose solution, MCT, PGPR/monoglycerides. W/O microemulsion exhibited lower gastric and pancreatic lipase activity due to emulsifiers' high concentration than the conventional emulsion (Chatzidaki, Mateos-Diaz, Leal-Calderon, Xenakis, & Carriere, 2016). Constantinides et al. (1995) investigated W/O microemulsions absorption via the duodenum. The study was *in vivo*, and the aqueous phase carried an antiplatelet and antithrombotic molecule – fibrinogen receptor with low oral bioavailability. The highest absorption (29%) was developed with 5.3 wt% W/O microemulsions using caprylic acid and capric acid (C_8/C_{10}) diesters of propylene glycol oil, C_8/C_{10} mono-/di-glycerides, lecithins, polyoxyethylene glycerol triricinoleate. They reported that medium-chain acids, C_8/C_{10} mono and di-glycerides, substantially improve bioavailability via duodenum without significant modification in the gastrointestinal mucosa, showing the potential of these emulsions in human tissue.

W/O emulsions are formed in the petroleum industry during crude oil extraction from the seabed and fracking processes. These emulsions are often stabilized by asphaltenes and wax crystals (Bi et al., 2015). The aqueous phase of crude petroleum emulsions may contain various salts and acidic compounds, which can cause severe corrosion problems in pipelines and plant equipment, promoting operational safety issues and extra operation costs (Bi et al., 2015). Before the crude petroleum oil can be further processed, it must be separated from the water phase; therefore, efficient destabilization of water-in-crude oil emulsion is a significant focus of the petroleum industry (Bi et al., 2015; Etchepare, Oliveira, Azevedo, & Rubio, 2017; Yang et al., 2014).

2.2.4 Utilization of water droplets in water-in-oil emulsion as microscale reactors

The aqueous phase of W/O emulsions is also an essential carrier of biological reactions, like DNA replication by DNA polymerase. The study of DNA sequence variation or somatic mutations is executed to detect presymptomatic cancers and disease stages (Dressman, Yan, Traverso, Kinzler, & Vogelstein, 2003). In W/O microemulsions, the aqueous droplets are confined, giving a unique way of controlling many chemicals, physical and biological reactions. Quantitative polymerase chain reaction (qPCR) uses an aqueous phase mixture with buffers to amplify DNA for gene quantification. Higuchi, Fockler, Dollinger, and Watson (1993) recorded a PCR assay using buffers and DNA templates to analyze the kinetics during the thermo-cycles. They found that qPCR is sensitive to the initial amount of template DNA, being the minimum limit 10^3 templates. The data point belonging to 10^2 initial DNA templates has a significant statistical deviation for the regression fitted line for 10^3 to 10^8 initial templates, indicating limitations at low concentrations.

Recently, W/O emulsion-based PCR has been reported to allow millions of non-interacting amplifications within water droplets in millilitres to microliters scale volume, acting as DNA micro-reactors (Shendure et al., 2005). It raises the concentration of initial template DNA inside each droplet and significantly improves DNA amplification efficiency and allows detection of low DNA concentration. In studies, this new molecular biology technique is called droplet digital polymerase chain reaction (ddPCR), which offers complete quantification of target nucleic acids with no requirement of an external calibrator. ddPCR reported a smaller variation coefficient, especially at low DNA concentration than qPCR (Zhao, Xia, Yin, & Wang, 2016). For instance, in qPCR, the *Escherichia coli* colonies must be selected individually to perform the amplification. However, in ddPCR, the amplification can be multiple, remaining the water droplet dispersion (Shendure et al., 2005).

Shendure et al. (2005) used ddPCR to obtain nonelectrophoretic sequence automation to replicate *Escherichia coli* MG1655, ~30.1 million bases 99.7% accuracy. A million droplets were restrained in a polyacrylamide gel. They used an epifluorescence microscope, and the droplets were ligated to four-colour (gold, red, light blue, and purple) for image analysis. They found three unique mutations in the evolved strain. This rapid-technology cost was one-ninth of qPCR (Shendure et al., 2005), indicating that W/O emulsions allowed a more accurate PCR and reduced cost. Dressman et al. (2003) implemented a technology known as BEAMing that relies on magnetic beads, in which W/O microemulsions are also used for DNA replication. The aqueous phase with primers and templates was stirred with mineral oil as the oil phase (Span 80, Tween 80, polyethylene glycol tert-octylphenyl ether (Triton X-100)) and form W/O microemulsions. The emulsions were exposed to thermal cycles in PCR and broken with vortex and centrifugation. In this technology, the DNA templates can be replicated in millions of copies to identify infinitesimal sequence variations.

2.2.5 Food application of water-in-oil emulsion and the challenges with their stabilization

Food-grade W/O emulsions are complicated systems to stabilize. They require a high concentration of food-grade lipophilic emulsifiers in the continuous phase. Also, it has been reported that in the case of unsaturated vegetable oil, an emulsifier with an unsaturated hydrocarbon group would have a higher affinity (Garti & Remon, 1984). Indeed, liquid W/O emulsions are not very common in food for their stabilization difficulties (Colucci et al., 2020). For instance, butter and margarine are not simple W/O emulsions. In addition to emulsifiers, the continuous oil phase contains triglyceride crystals to promote Pickering and network stabilization. The fat crystal structure is a space-filling network that immobilizes the droplets. For the Pickering stabilization of W/O emulsion, solid particles must have a contact angle > 90 ºC at the water-oil interface. The particle size should be several orders of magnitude smaller than the oil droplets. The particles must also be densely packed, covering the droplet surface, otherwise bridging the droplets or coalescence can occur between them (Ghosh et al., 2011; Walstra, 2003). Many low-fat spreads contain high water content and not enough crystals to keep efficient Pickering stabilization and network formation. In this kind of system, stability can be achieved by gelling the water droplets with an ingredient that could form fast gelation upon cooling (e.g., gelatin), and their coalescence becomes impossible (Walstra, 2003).

So far, the only emulsifier that showed stabilization of liquid W/VO emulsion is a synthetic polyester of polyglycerol, PGPR, that could bind to the water droplet interface due to its structure with multiple hydroxyl groups and carbonyl groups in the polar head, which enhanced the viscous interfacial

rheology. Even then, a very high concentration of 10 wt% PGPR is needed for optimal stabilization of 30 wt% W/O emulsions (Benichou, Aserin, & Garti, 2001). Liquid food-grade W/VO oil emulsions without any saturated fat crystal network are complicated systems to stabilize. It has been commonly used lipophilic emulsifiers with low HLB (e.g., Spans and lecithin), which failed to stay at the water droplet interface, and W/VO emulsion destabilizes in a few hours after their preparation using a rotor-stator. Scherze et al. (2006) investigated different emulsifying devices to obtain stable 30 wt% W/O emulsions. It was tested in the aqueous phase, S with gelatin or whey protein isolate, and in the bulk phase, sunflower oil with lecithin or PGPR. The rotor-stator device and S addition did not form stable lecithin-emulsions. However, in PGPR-emulsions were essential S incorporation to develop stability.

Water droplet formation by microchannels has been researched as a methodology to obtain stable liquid W/O emulsions. Ito, Uehara, Wakui, Shiota, and Kuroiwa (2017) investigated W/O formation in microchannel emulsification using vegetable oil and mineral oils as bulk oils due to unclear operational aspects to obtain stability with high energy homogenization. Different oils were investigated olive oil, ethyl oleate, oleic acid, tetradecane with different emulsifiers such as decaglyceryl penta oleic acid, sorbitan trioleate (Span 85) or PGPR. The aqueous phase contained 0.2 M S to simulate butter or margarine salt concentration. Homogeneous droplet size was performed in all oils. Still, droplet diameter relied on the viscosity ratio (Equation 2.8).

$$\text{Viscosity ratio} = \frac{\eta d}{\eta c} \tag{2.8}$$

Where the dispersed phase viscosity is (η_d), the authors found that the average droplet diameter was higher with a reduced viscosity ratio. Olive oil has the lowest viscosity ratio, and the average droplet size attained 1.8 times that of tetradecane oil, which had the highest viscosity ratio. It indicates that incrementing the viscosity of the bulk phase caused a larger water droplet size. They reported production of monodisperse droplets size from 24 to 90 μm with a variation lower than 7%. Skimmed milk and whey powder affected the droplet creation at the end of the microchannel due to the change of interfacial tension. Nonetheless, the use of high-pressure devices is essential to form W/O emulsions commercially.

Ghosh et al. (2011) proposed a hydrogen bond-based destabilization mechanism for the water-VO interface's emulsifiers. In VO, the carbonyl group (C=O) of fatty acid esters form hydrogen bonds with the hydroxyl group (OH) of the emulsifiers, which is stronger than the hydrogen bond with water molecules (Bus et al., 1990). This process is described as VO's capacity to attract the emulsifier towards itself, thereby promoting emulsifier desorption from the interface, hindering the stability of W/VO emulsions. In contrast,

due to the polar group's lack, many other oils, such as mineral oil, do not interact with the polar head of emulsifiers. Hence, their interaction with the OH of water molecules dominates, leading to emulsion stabilization (Ghosh et al., 2011). Nevertheless, not much research has been done on the stability mechanism of liquid W/VO emulsions using natural lipophilic emulsifiers and unsaturated oils. Modern consumers have shown interest in innovative food products with a low percentage of saturated fat, unsaturated oil, the presence of bioactives, and the use of natural ingredients. A better understanding of the destabilization mechanism of W/VO emulsion and the development of a suitable stable product containing minerals and vitamins encapsulated in the water droplets will be of great benefit.

2.3 Emulsifiers used in water-in-oil emulsions

Emulsifiers used to prepare W/O emulsions are mostly nonionic and have an extensive non-polar part (long-chain alkyl) and a smaller polar region with several hydroxyl groups attached to it, with HLB between 3 – 6 (Kralova & Sjöblom, 2009). Due to the presence of a sizeable non-polar group, these emulsifiers are mostly oil soluble. Most of the emulsifiers produced worldwide are synthetic (Belitz, Grosch, & Schieberle, 2009). Based on the nature of the polar group, they can be divided into several different classes: (1) sorbitan fatty acid esters: e.g., Span 20, sorbitan monopalmitate (Span 40), sorbitan monostearate (Span 60), Span 80, sorbitan sesquioleate (Span 83), sorbitan trioleate (Span 85) (Garti, Wellner, Aserin, & Sarig, 1983); (2) glycerol fatty acids esters (small molecule emulsifier): e.g., GMO, glycerol monostearate (GMS), diglycerol monooleate etc. (Holstborg, Pedersen, Krog, & Olesen, 1999); (3) ethoxylated ester: e.g., ethoxylated laurylalcohol, poly bis-(2-hydroxyethyl) oxyethylene cocoalkyloxypropylamine, poly (15) oxyethylene tallow amine, etc. (Cox & Weerasooriya, 1997; Maag, 1984); (4) polyester of polyglycerol: e.g., PGPR, polyglycerol iso-stearate, etc. (Ciriminna, Katryniok, Paul, Dumeignil, & Pagliaro, 2015); (5) sulfosuccinates: e.g., sodium bis(2-ethylhexyl) sulfosuccinate (AOT); (6) Pickering particles: e.g., hydrophobic silica, polyphenol crystals, fat crystals. These emulsifiers can be considered as small molecules, except PGPR, which is a polymeric emulsifier. Small emulsifiers absorb rapidly at the W-O interface (Dalgleish, 2004). These emulsifiers may not form a viscoelastic interfacial layer but create a compact interfacial layer. Only sorbitan fatty acid esters, monoglycerides and diglycerides, and PGPR are generally recognized as safe (GRAS) and can be used as food-grade emulsifiers. On the other hand, for W/MO emulsion with bulk phase hydrocarbon chain used in biotechnology and skincare, all the classes of emulsifiers mentioned above can also be used. All the emulsifiers mentioned in this section have been used in cosmetics or pharmaceuticals (Kralova & Sjöblom, 2009).

2.3.1 Sorbitan fatty acids esters emulsifiers

These emulsifiers are partial esters formed from several natural fatty acids (e.g., palmitic, stearic, oleic, isostearic acids, etc.) and sorbitol (Garti, 1983) also known as "Spans". Reactions of cyclization or dehydration generate a mixture of sorbitol, sorbitan, and isosorbide (Figure 2.3). The esterification reaction yields a random allocation of monostearate through hexastearate. The mixture of fatty acids and sorbitol is reacted with sodium hydroxide or zinc stearate under heat in an inert atmosphere to cause simultaneous esterification and cyclization reactions (Hasenhuettl, 2008).

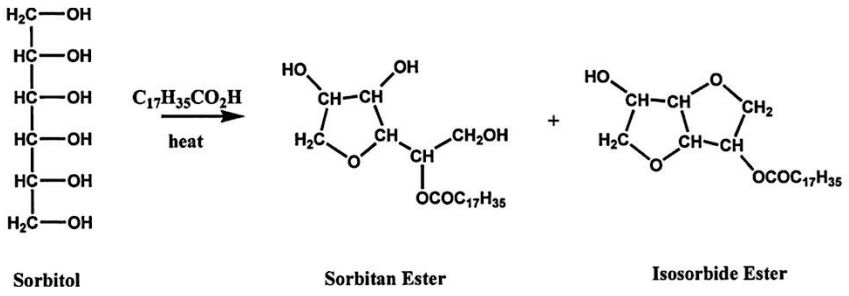

Figure 2.3 Cyclization and esterification of sorbitol. Adopted without modification from Hasenhuettl (2008).

A sorbitan monoester structure is shown in Figure 2.3 (Korhonen, Lehtonen, Hellen, Hirvonen, & Yliruusi, 2002b). Depending on the number of carbons in the fatty acid chain, the names were designated. The emulsifiers are called based on the lipid tail chain, sorbitan monolaurate (Span 20) when C_{12} fatty acid, sorbitan monopalmitate (Span 40) when C_{14} fatty acid, sorbitan monostearate (Span 60) when C_{18} fatty acid and Span 80 when $C_{18:1}$ oleic acid. According to Garti (1983), sorbitan fatty acid esters contain a mixture of monoester, diesters, and triesters (Table 2.1), although the exact composition depends on the manufacturer (Wu, Iglauer, Shuler, Tang, & Goddard, 2010). The HLB of Span emulsifiers ranges between 1 and 8 (Table 2.1) based on the attached fatty acids. Hence, they are mainly used for W/O emulsion formation. Peltonen, Hirvonen, and Yliruusi (2001) analyzed Spans (20, 40, 60 and 80) in different hydrocarbons oils (pentane, hexane, heptane, octane, nonane, decane and dodecane). They found an increase in interfacial tension with a larger oil's alkyl chain related to the bulk phase (14.4 to 22.4 mN/m). Span 40 performed the lowest interfacial tension in all hydrocarbon oils, followed by Span 60. Span 20 and Span 80 performed high interfacial tension, related to the short and unsaturated lipidic chain, which represent difficulties to pack at the interface.

Table 2.1 Composition of mono-, di- and triesters of fatty acids of Span 40, Span 60, Span 65, Span 80 and Span 85 and HLB. Adopted with modification from Garti et al. (1983), HBL values were compiled from various sources (Croda, 2018; Sigma-Aldrich, 2018).

Sorbitan fatty acid esters	% monoesters	% diesters	% triesters	HBL
Span 40 (palmitic acid)	52	39	9	6.7
Span 60 (stearic acid)	48	34	18	4.7
Span 65 (stearic acid)	38	31	31	2.1
Span 80 (oleic acid)	52	34	14	4.3
Span 85 (oleic acid)	35	33	32	1.8

2.3.3 Glycerol fatty acids esters emulsifiers

These compounds are commonly found in natural fats and oils. Industrially, glycerol fatty acids esters are obtained via direct esterification of glycerol with a fatty acid or by glycerolysis of natural or hydrogenated fats and oils (Figure 2.4), which results in the similar yield of monoacylglycerols (MAGs), and diacylglycerols (DAGs) (Krog & Vang Sparsø, 2004). MAGs and DAGs are frequently utilized as food additives or emulsifiers (e.g., margarine, bakery products, frozen desserts etc.) (Pagliaro, 2017). The glycerolysis procedure is more cost-effective than direct esterification because fats are inexpensive than fatty acids, and less glycerol is needed. Fatty acids and fats have minimal solubility in glycerol, so elevated temperatures are essential to force the reaction to continue (Hasenhuettl, 2008). Glycerolysis also raises the crystallization temperature of vegetable oils without altering the fatty acid percentages (Nicholson & Marangoni, 2020). Direct esterification can be catalyzed with acids or bases (e.g., pyridine). The concentration of glycerol over fatty acid defines MAGs and DAGs; more glycerol yields higher MAGs concentrations (Hasenhuettl, 2008).

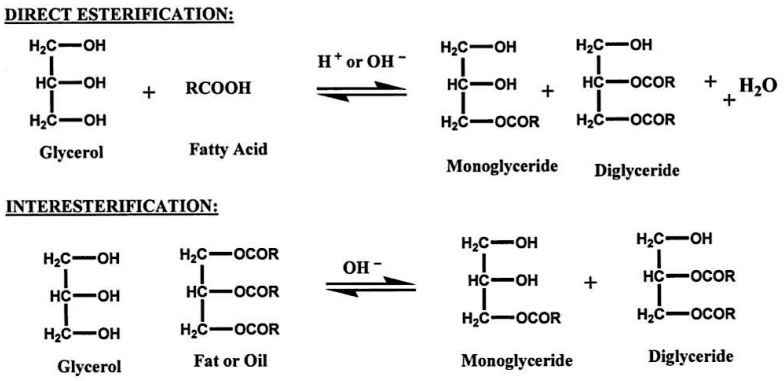

Figure 2.4 Reaction scheme of MAGs and DAGs production via direct esterification and interesterification, R= fatty acid with a carbon number of 8 to 22. Adopted without modification from Hasenhuettl (2008).

MAGs and DAGs are lipophilic eco-friendly renewable emulsifiers and are mainly used as mixtures. The production of glycerol fatty acid esters and by-products represents 75% worldwide (Belitz et al., 2009). MAGs molecules have only one fatty acid chain attached to a glycerol backbone (Wang, Peyronel, & Marangoni, 2016). For instance, GMO is a glycerol ester of oleic acid with a *cis* double bond at ninth carbon (C9). GMS is a glycerol ester of stearic acid with a saturated eighteen-carbon tail. The HLB of different glycerol fatty acids ester emulsifiers is shown in Table 2.2.

Table 2.2 HLB values of glycerol fatty acids esters. Adopted with modification from various sources (Ash & Ash, 2004; Merianos, 2001; NOSB-TAP, 2001).

Glycerol fatty acid esters	HLB
Glycerol monooleate	3.8
Glycerol monostearate	3.8
Glycerol monolaurate	5.2
Glyceryl monohydroxystearate	3.4
Diglycerol monooleate	4.5
Diglycerol monostearate	5.5

The HLB values are within 3 to 5, indicating their ability to form W/O emulsions. Commercially available MAGs may be obtained in two forms, a mixed glyceride form referred to only as monoacylglycerols and distilled monoacylglycerols. Mixed glycerides generally include 42 to 46% MAGs.

Distilled MAGs are primarily pure, typically containing > 90% MAGs and < 5% DAGs (Boyle, German, & Whelan, 1996). The melting point of MAGs gave specific characteristics that depend on the fatty acids' composition. Ghosh et al. (2011) used commercial GMO (Dimodan MO with 92% purity monoacylglycerols, source: sunflower oil) and reported that it melted at 12 °C, being in a liquid state at room temperature. However, GMS (Pationic 901, 95% purity monoacylglycerols) melted at 61 °C, being in a solid state at room temperature. They also showed GMS micrographs acting as Pickering particles at the water droplets interface at lower temperatures than its melting point. GMO mechanism of stability is by increasing fat crystals polarity, allowing Pickering at the interface and crystal network stabilization. Verstringe, Danthine, Blecker, and Dewettinck (2014) used commercial Myverol 18 04-PK (95% purity monoacylglycerols), containing palmitic and stearic acid. This emulsifier showed two melting peaks at 60 °C and 5 °C, α and sub-α1 polymorphism. Thus, even that commercial MAGs showed high purity, thermal analysis should be performed to identify the mechanism of stability in W/O emulsions. The high melting temperature gives high solifidy and functionality to MAGs and DAGs.

Glycerol fatty acids esters emulsifiers disperse quickly in oils and swell in water to form lyotropic liquid crystalline structures (Qiu & Caffrey, 2000). Chemists and enzymologists have made enormous attempts to create MAGs, treating fats with fatty acids at low cost without distillation (Kralova & Sjöblom, 2009). Nicholson and Marangoni (2020) investigated an enzymatic glycerolysis from liquid vegetable oils to produce MAGs and DAGs. In this way, the solid fat increased in the vegetable oils. For instance, cottonseed and peanut oils, at 5 °C, the solid fat reached 29% from 8% and 30% from 9%, respectively.

2.3.4 Ethoxylated emulsifiers

Ethoxylation is a method to increase the hydrophilicity of nonionic emulsifiers (Raith, Schmelzer, & Neubert, 2006) by the addition of hydrophilic molecules, such as ethylene oxide (EO) or polyethylene glycol (PEG). EO is a molecule with three oxygen atoms forming a ring, and it is the most reactive member of the family of cyclic ethers (van Os, 1998). As the ring strain is relatively high, the molecule can freely undergo an exothermic ring-opening reaction. The opened ring can then condense with EO second molecule to initiate a polymerization chain reaction creating PEG (Hasenhuettl, 2008). PEGs are polymers of EO with molecular weight from 200 to over 10.000, where the molecules with 200 – 600 molecular weight are proper for W/O emulsions (Fruijtier-Pölloth, 2005). The degree of ethoxylation means the number or length of EO or PEG in the polar side chains or the two-terminal called PEG derivatives (Raith et al., 2006). PEGs and PEGs derivatives described the degree of ethoxylation with the polymer chain molecular weight, indicated in the generic name (e.g., PEG-400) (Fruijtier-Pölloth, 2005). PEG esterified with ethers (e.g., oleths,

laureths) and fatty acid esters (e.g., stearates, laurates) are widely used in cosmetics and skincare (Fruijtier-Pölloth, 2005).

Esterifying fatty acids with PEG can develop different ethoxylated emulsifiers (e.g., PEG-2 laurate, PEG-2 stearate), sorbitan fatty acid esters (e.g., PEG-2 sorbitan isostearate, PEG-3 sorbitan oleate), fatty alcohols with ether structure (e.g., Steareth-2, Laureth-1), glycerides (e.g., PEG-7 glyceryl cocoate from fatty acids of coconut oil, PEG-7 glycerol monoricinolate) and fatty amides (e.g., PEG cocamides), vegetable oils (e.g., PEG-2 castor oil), PEG sorbitan beeswax (e.g., PEG-6 sorbitan beeswax), PEG soy sterols (e.g., PEG-5 soy sterol) (Fruijtier-Pölloth, 2005; Raith et al., 2006). Most ethoxylated monoesters have shown higher solubility compared to di-esters. Garti, Schlichter, and Sarig (1986) identified that mixtures of Spans with Tween were useful to accelerate the crystals' polymorphic transition in cocoa butter. The most effective combinations were Span 60 with polyoxyethylene sorbitan monostearate (Tween 60) and Span 60 with polyoxyethylene sorbitan tristearate (Tween 65). Ford and Furmidge (1966) reported suitable W/O ethoxylated emulsifiers. The amides of long-chain acid-ethoxylated, in which anion and cation were absorbed to the interface, without disturbing the net charge. For instance, PEG-2 coconut-amide was surface-active and formed stable W/O emulsions with myristic or oleic acid.

2.3.5 Polyglycerol esters of fatty acids and other polymeric emulsifiers

Polyglycerol esters (PEs) have been used as emulsifiers in cosmetics and food as dough strengtheners, crystal modifiers, beverage clouding agents or fat substitutes (McIntyre, 1979). In margarine production, PEs enhance functional properties like organoleptic profile, stabilizing or aerating (Norn, 2014). The synthesis of PEs initiates with the polyglycerol (PG) formation (Bastida-Rodríguez, 2013). The polymerization of glycerol starts heating the glycerol during a basic or acidic catalyst in an inert atmosphere (Ciriminna et al., 2015). Ether linkages are formed with the condensation of free hydroxyl groups to discard water. Intramolecular condensation yields linear oligomer, and intramolecular condensation produce cyclic groups, giving the polar head size. The condensation of glycerol increases the size of the hydrophilic head group of the emulsifiers (Hasenhuettl, 2008). The esterification is made between the hydroxyl groups of the polyglycerol molecule and the carboxylic acids of fatty acids (e.g., edible fats or oils). Various ratios of PG: carboxylic acids can be yielded, getting different polyglycerol esters (Ciriminna et al., 2015). PEs have high viscosity even at high temperatures, which is an advantage to develop stable W/O emulsions (Ciriminna et al., 2015).

PGPR is an essential emulsifier in the food industry. It is found in most chocolate labels due to the highly surface-active, preventing fat bloom and increasing viscosity, as well used in baking and low-fat

spreads (Bastida-Rodríguez, 2013). This emulsifier is formed by the esterification of polyglycerol with poly-ricinoleic acid. The HLB value of PGPR is in the range from 1 to 5 (Christiansen, 2014). PGPR has an unknown molecular structure; however, researchers have proposed several different schematic diagrams (Figure 2.5). Ricinoleic acid (12-hydroxy-9-cis-octadecenoic acid) is monounsaturated oleic acid with a hydroxyl group attached. It is derived from castor oil – plant origin *Ricinus Communis L.* (Bastida-Rodríguez, 2013).

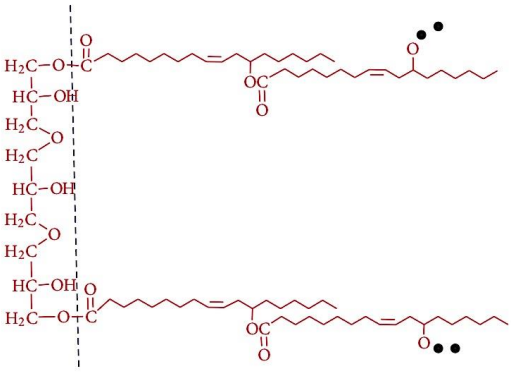

Figure 2.5 Proposed chemical structure of polyglycerol polyricinoleate. Black dots denote two polyricinoleic acid chains. Adopted without modification from Bastida-Rodríguez (2013).

Castor seeds contain ricin, ricinine, and castor bean allergen molecules that are toxins and potentially hazardous to workers during the oil extraction (Burdock, Carabin, & Griffiths, 2006). For this reason, between 1950 and 1960, toxicology studies were conducted to investigate PGPR effects in humans and animals. The study in humans did not show any health or toxicology impact related to PGPR (Wilson & Smith, 1998). The study with rats and mice reported the same results as the study in humans, with no toxicity effects. However, liver and kidney organ weight increased associated with an adaptive hypertrophy transient (Smith, Wilson, & Hepburn, 1998). After that, each country or continent has set different laws applicable to food products. In Canada, PGPR can be used in chocolate products or unstandardized chocolate confectionery at 0.5% (Health Canada, 2012). The Food and Drug Administration (FDA) accepts PEs, including decaglycerol esters prepared with corn, palm, peanut, cottonseed oils, lard, or a mixture of stearic, coconut and oleic fatty acids (U.S. Food and Drug Administration, 2021). In Europe, the Scientific Committee for Food set an acceptable daily intake (ADI) of 7.5 mg/ kg body weight per day for PGPR (EFSA Panel, 2017). In low-fat spreads and dressing, PGPR concentration was set at 4 g/ kg, and in chocolate or cocoa-based confectionery was established at 5 g/ kg (European Parliamnet and Council

Directive, 1995).

The concentration required to form stable 30 wt% W/O emulsions is 10 wt% PGPR using a rotor-stator in soybean oil (Benichou et al., 2001). Ghosh and Rousseau (2011) reported that the combination of PGPR with coconut oil did not form stable W/O emulsions under freeze-thaw conditions. However, the mixture of hydrogenated canola oil, canola oil and PGPR in even low percentage (0.125 wt%) increased the fat crystals adhesion to the W-O interface, promoting emulsion stability. PGPR concentration of 0.1 wt% up to 1 wt% is declared to mask or prevent off-flavours and off-tastes in edible W/O emulsions consisting of 15 – 85 wt% of fat (Unilever, 2008). In cosmetic or medical applications, the dosage of PGPR is usually 1.5 – 3 wt% (Christiansen, 2014).

Other PEs emulsifiers such as polyglyceryl-6 ricinolate (HLB 6.0), polyglyceryl-4 isostearate (HLB 5.0), polyglyceryl-3 diisostearate (HLB 5.0), polyglyceryl-4 diisostearate, polyhydroxystearate, polyhydroxysebacate (HLB 5.0), polyglyceryl-2 diisostearate (HLB 4.0), polyglyceryl-2 dipolyhydroxystearate (HLB 3.5) were used to stabilize W/O emulsion for cosmetic applications (Kim, Lee, & Lee, 2012). The challenges of PEs are mainly in the purification of PG. Other processes to produce PG uses reactive petrochemical molecules like epichlorohydrine, which is a hazardous material. This molecule reacts with glycerol during the etherification process (Norn, 2014). A second disadvantage is that some chemicals used in the polymerization that make it a non-competitive process, such as glycidol, a derivative of glycerol and can react with glycerol or epichlorohydrin (Norn, 2014). Also, the methods to manufacture PGPR require long-time reactions and high temperatures, which caused problems of coloration and odours not recommended in food products (Bastida-Rodríguez, 2013).

2.3.6 Sulfosuccinates

Sulfosuccinates anionic emulsifiers are the sodium salts of alkyl esters of sulfosuccinic acid – monoester or diester (Tyagi, 2006). They are synthesized through the reaction of the maleic acid anhydride with hydroxyl groups of molecules (e.g., fatty alcohol), followed by sulfonation with sodium bisulphite (de Guertechin, 2009). These emulsifiers have mainly been utilized in the cosmetic industry to develop gentle formulas for shampoos and other personal care products (Maxon, 1988). Diesters have fewer variations made in fatty alcohol chains (e.g., linear, branch or cyclic) (Figure 2.6). Diesters are utilized as a wetting agent and dispersant. It is soluble in vegetable and hydrocarbon oils above 75 °C, and the solubility depends on the hydrophobic chain and branch. As the molecular weight increases, polar solubility decreases and non-polar solubility increases. However, sulfosuccinates monoesters can have more variants by modifying

chain length, saturation grade of the carbon chain and degree of ethoxylation (Tyagi, 2006). These derivatives included fatty alcohol, fatty alcohol ethoxylates, fatty acid alkanolamides, fatty acid alkanolamides ethoxylates (de Guertechin, 2009; Tyagi, 2006).

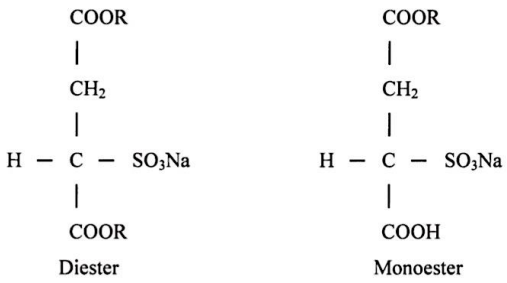

Figure 2.6 Di- and monoesters of sulfosuccinate emulsifier, R represents the alkyl – e.g., fatty alcohol chain. Adopted without modification from Tyagi (2006).

In general, sulfosuccinates have good biodegradability and sensitive to strong pH acids or basic (Tyagi, 2006). Sulfosuccinate emulsifiers derived from silicone-based monoesters have low HBL (e.g., dimethiocone copolyol sulfosuccinate, HBL 4). They are used in personal care formulas to enhance softness and foam characteristics (Maxon, 1988). A widely used di-ester sulfosuccinate emulsifier is sodium bis(2-ethylhexyl) sulfosuccinate or also found in publications as dioctyl sodium sulfosuccinate, which is commonly known as Aerosol-OT®1 (AOT) (Figure 2.7). The synthesis of this emulsifier starts with a maleic anhydride reaction with isooctyl alcohol catalyzed by p-toluenesulfonic acid to obtain maleic acid diisooctyl, then by sulfonation with sodium bisulphite (Meng-Juguang, 2014).

Dioctyl sodium sulfosuccinate is approved to be used in cosmetics up to 0.42% (Andersen, 1998). It is accepted as a food additive, as a wetting agent at 10 ppm and like a solubilizing agent on gums at 0.5 wt% or emulsifying agent up to 25 ppm (U.S. Food and Drug Administration, 2021). AOT has been studied extensively for their exceptional efficiency in forming W/O microemulsions without any co-emulsifier and is the most soluble sulfosuccinate emulsifier in polar and non-polar solutions (Nave, Eastoe, Heenan, Steytler, & Grillo, 2000; Tyagi, 2006). Engel and Riggi (1969) reported an *in vitro* study of heparin, an anticoagulant, in which dioctyl sodium sulfosuccinate increased intestinal absorption of heparin after 30 min of administration.

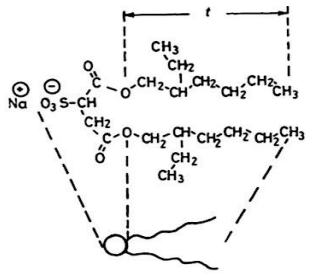

Figure 2.7 Diagram of AOT molecule. Adopted without modification from Robinson, Toprakcioglu, Dore, and Chieux (1984).

These emulsifiers can possess bulk branching, from 3,5,5-trimethyl-1-hexyl, through 2-ethyl-1-hexyl (AOT), to 1-ethyl-2- methyl-1-pentyl (Figure 2.8).

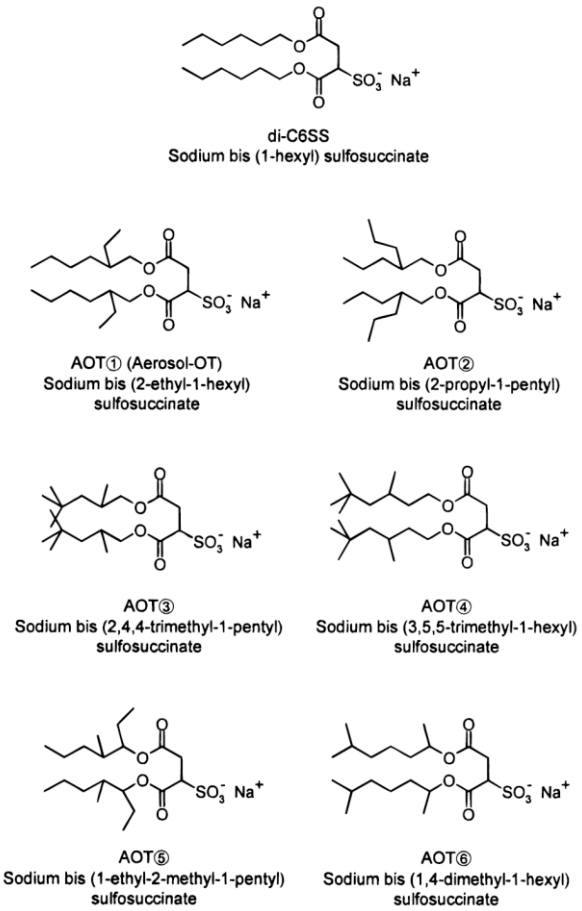

Figure 2.8 Schematic molecular structures of AOT homologues, at the top C6 linear chain and branch chain: (1) to (6) 3,5,5-trimethyl-1-hexyl, through 2-ethyl-1-hexyl (AOT), to 1-ethyl-2-methyl-1-pentyl. Adopted without modification from Nave, Eastoe, and Penfold (2000).

To study the unique structural characteristics of AOT molecules at the air-water interface, Nave et al. (2000) compared 11 similar AOT structures in Figure 2.8 with 4, 5, 6, 7, 8 linear chains, and 6 branched-chain included AOT. As a result of this investigation, it was concluded that AOT is not a special emulsifier and follows the pattern of sulfosuccinates. All the emulsifiers were analyzed at the air-water interface. The branch chain's emulsifiers exhibited a significant rise in surface area at the critical micelle concentration from 10 to 20 $Å^2$, compared to the linear homologues. The packing behaviour was similar among all the sulfosuccinates. In a second study reported by the same research group, all AOT molecules were evaluated at the interface. They compared packing at the two different interfaces, air-water and W-O, and no remarkable differences were reported. They did not find an explanation for its efficient stability in W/O microemulsion, which is believed to be related to the conelike shape, that even at temperature exposure did not change its surface-active capacity (Nave, Eastoe, Heenan, et al., 2000).

2.3.6 Pickering particles

Pickering is the kinetic stabilization of emulsions by absorbing colloidal particles at the droplet interface (Binks, Clint, & Whitby, 2005). The study of Pickering particles to stabilize O/W emulsions started 114 years ago for insecticidal application. Pickering (1907) presented comprehensive research with paraffin oil, and the O/W emulsions were formed by churning or shaking. The stability mechanism was obtained by coating the oil droplets with solid particles inhibiting droplets' coalescence. He reported that the better soluble emulsifying properties were performed with sulphates iron and sulphates copper in the aqueous phase, showing 81% of emulsion stability after 3 months. Other soluble particles that achieved good stability were starch and glue; however, saponin and quillaia were effective in low oil percentages. Additional particles with good performance were nickel sulphate, ferrous hydroxide, calcium arsenate, ferrous hydrosulphide, and basic ferrous sulphate.

Hodge and Rousseau (2005) clarified essential factors in the Pickering mechanism performed by fat crystals in W/O emulsions: (1) wettability by the continuous or disperse phase, (2) interfacial film viscoelastic behaviour of wetted fat crystals, and (3) fat crystal morphology, size, and composition. These factors impact the particle contact angle at the W-O interface, measured by the aqueous phase (Figure 2.9).

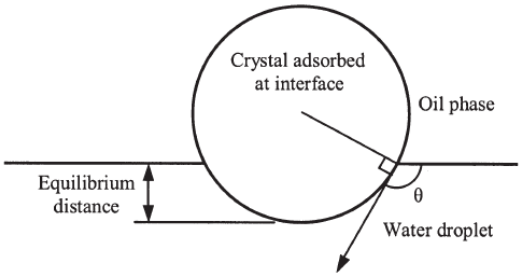

Figure 2.9 Representation of a fat crystal at the W-O interface. Adopted without modification from Hodge and Rousseau (2005).

If the contact angle is less than 90°, it will form O/W emulsions, but if the angle is higher than 90°, W/O emulsions will be developed. It is not favourable that particles get thoroughly wetted for either phase because that will not allow the crystals to behave as surface-active. They reported that rapid crystallization of W/O emulsions after homogenization favours forming a small crystals network.

Binks et al. (2005) used hydrophobic bentonite clay to develop W/O emulsions with different water volume fractions (0.1 to 0.6) in isopropyl myristate and toluene oils. Emulsions with isopropyl myristate exhibited large particles of bentonite clay, which promoted flocculation that increased with more water volume fraction, showing sedimentation. However, W/O emulsions in toluene showed micrometre clay particles suspended due to the network formation. It indicated that particles could have different re-organization according to the continuous phase used. Zembyla et al. (2018) reported the first study using curcumin and quercetin particles - naturally occurring polyphenols (0.06 to 1.5 wt%). It was formed 5 wt% W/O emulsions in soybean oil. They highlighted that the particle's average droplet size should be one order of magnitude less than the emulsion droplet size to obtain effective Pickering. Water droplet size did not showed change at concentrations > 0.14 wt% and < 0.25 wt% with both particles. The increase of pH from 3 to 7, develop coarse emulsions maybe due to the increase of negative charge in the particle. They pointed out the particles' shape differences. Curcumin had a polyhedral form and quercetin a rod shape and larger size. These characteristics were related to the interfacial shear viscosity, quercetin particles showed stronger interface than curcumin.

Murray (2019) explained that solid particles with non-deformable behaviour and insoluble in both phases could perform shear modulus > 0.1 MPa (e.g., organic crystals, pure polymer, or mineral particles). Particles that anchor at the interface with a defined surface displace energy (E_{disp}) that can be calculated in Equation 2.9.

$$E_{disp} = -\pi r^2 \gamma (1 - |\cos \theta|)^2 \quad (2.9)$$

Where is assumed a spherical particle, θ is the particle contact angle. If particle absorption occurs, higher E_{disp} will result (Ghosh & Rousseau, 2011). If the θ is closer to 90°, r is larger or γ higher, indicating stronger particle absorption (Murray, 2019). Different particles have been used in food-grade products. For instance, octenyl succinic anhydride (OSA)-starch materials can increase the hydrophobic character of any polysaccharide material (Murray, 2019). Sarkar and Dickinson (2020) reported potential types of particles for W/O emulsions, such as particles polysaccharides (e.g., cellulose, zein particles, chitin), proteins (e.g., lignin, oleosomes) and polyphenol particles (e.g., rutin, naringin). Pickering emulsions restricted OR and coalescence. However, the application of shear can break the structure formed. Most natural particles are also not monodisperse or homogeneous in shape, so it is challenging to develop orderly packing (Murray, 2019).

2.3.7 Emulsifier characterization techniques

2.3.7.1 The solubility concept

According to Bancroft's empirical rule, the greater concentration emulsifier's solubility defines the type of emulsion to be created (Bancroft, 1912). Oil-soluble emulsifiers naturally produce oil-continuous emulsions, while water-soluble emulsifiers form water-continuous emulsions. The Bancroft rule postulates a very general instruction that mainly depends on the emulsifiers' structure. However, advanced applications need to evaluate emulsifier properties because partial solubility in oil or water is also possible, leading to different results.

Binks (1993) tested this theory with a nonionic emulsifier, pentamethylene glycol monododecyl ether, in heptane and 0.01 M S in a 1:1 water to oil ratio. The focus was on the emulsifier concentration and the impact over the microemulsion type formed based on temperature variation. He found contraventions of the Bancroft rule when the emulsifier concentration was beyond the CMC. The transition from O/W to W/O emulsions was possible at concentrations over the CMC at any temperature. The same inversion occurred with the increment of both factors, temperature over the phase inversion temperature and the emulsifier concentration. In summary, it was determined that Bancroft's empirical rule and HLB include when emulsifier aggregates forming micelles instead of the total presence of emulsifiers, including monomers and micelles.

2.3.7.2 Cloud point

Cloud point (CP) is a unique characteristic of nonionic emulsifiers (Holmberg, Jönsson, Kronberg, & Lindman, 2002). This phenomenon implies instability (e.g., separation of phases, turbidity) when the emulsion with nonionic emulsifiers is over a limited temperature range. The CP is essential in suspensions, emulsions, lotions, and foams stabilized with nonionic emulsifiers. These systems become unstable when their temperature is close to the emulsifier cloud point. Different additives impact the nonionic emulsifier solution's clouding state (Hoque, Mitu, Patoary, & Islam, 2016). For instance, anionic emulsifiers (e.g., sodium alkyl sulfate) increase the CP of nonionic emulsifiers (e.g., Triton X-100). The effect was pronounced with a lower concentration of nonionic emulsifiers. The ionic emulsifier promoted the formation of charged micelles with the nonionic emulsifier (Panchal, Desai, & Nagar, 2006). However, the addition of sodium salts in the aqueous phase (e.g., S, sodium sulfate, and sodium nitrate) decreased nonionic emulsifiers' cloud point (e.g., Tween 80) (Hoque et al., 2016). Two mechanisms were described for the salting effect of nonionic emulsifiers by anions salts. First, some ions (e.g., sulphate ion) are water structure makers, which prevent water molecules' movement. Other ions (e.g., chloride ion, nitrate ion) are water structure breakers due to high polarity, allowing water molecules to release. These water molecules can form bonds with ether groups of the nonionic emulsifiers. The second mechanism is based on the direct interaction of ions over nonionic emulsifiers. These mechanisms were evident because the clouding reaction was exothermic and was identified by the change of enthalpy (Hoque et al., 2016). The cloud point relies on both the hydrophobic chain length and the number of oxyethylene units in the emulsifier molecule. For surfactants with long polyoxyethylene chains, the cloud point may exceed 100 ^{o}C (Holmberg et al., 2002).

2.3.7.3 Phase inversion

Some nonionic emulsifiers tend to decrease hydrophilicity with increasing temperature. It promotes a conversion from water solubility at low temperatures to oil solubility at higher temperatures (Bergenståhl, 2008). Based on the Bancroft rule, such changes may convert a water-continuous emulsion to an oil-continuous emulsion. The temperature of such change in the system is known as the phase inversion temperature (Rosen, 2004), mentioned in section 2.1.2.4 as the mechanism of instability and section 2.3.7.1 is related to the solubility concept. An emulsifier's strength against such phase-inversion can be determined from its temperature difference from the breakeven point to the PIT (Bergenståhl, 2008). Shinoda and Saito (1968) reported that the best temperature stability of an O/W emulsion is obtained at 30 °C under the PIT and for a W/O emulsion at about 20 °C above the PIT.

2.3.7.4 Hydrophilic lipophilic balance

The properties of emulsifiers depend on their structures and type of functional groups. The type of emulsion that can be formed is related to the balance between the hydrophobic and hydrophilic groups of an emulsifier molecule. HLB theory is also associated with the solubility concept (section 2.3.7.4, paragraph 1). For instance, a hydrophobic emulsifier will form W/O emulsions, and a hydrophilic will form O/W emulsions. It is essential to consider Binks (1993) proposal in which it is expressed that HLB just considers emulsifiers as aggregates, not as monomeric. The HLB number of an emulsifier represents the balance between their hydrophilic and lipophilic groups. The emulsifiers were classified numerically on the HLB scale, which indicates the HLB of an emulsifier related to their oil and water solubilities (Table 2.3) (Griffin, 1949).

Table 2.3 Classification of emulsifiers according to HLB numbers. Adopted without modification from Griffin (1949).

HLB Range	Application
4-6	W/O emulsifier
7-9	Wetting agent
8-18	O/W emulsifier
13-15	Detergents
15-18	Solubilizing

It must be highlighted that the HLB value does not predict the emulsion stabilization capability of an emulsifier. HLB is associated with the emulsifier structure, related to the emulsion type to form (Davies, 1957). The HLB numbers were calculated through an empirical Equation 2.10, considering their chemical structure, using hydrophilic group numbers (HG) and lipophilic group numbers (LG) (Table 2.4) (Davies, 1957).

$$HLB = \Sigma (HG) - \Sigma (LG) + 7 \qquad (2.10)$$

Table 2.4 HLB group number. Adopted without modification from Davies (1957).

Hydrophilic groups	Group number
$-SO_4Na^+$	38.7
$-COO^-K^+$	21.1
$-COO^-Na^+$	19.1
N (tertiary amine)	9.4
Ester (sorbitan ring)	6.8
Ester (free)	2.4
-COOH	2.1
Hydroxyl (free)	1.9
-O-	1.3
Hydroxyl (sorbitan ring)	0.5
Lipophilic groups	
-CH- $-CH_2-$ CH_3- =CH-	-0.475
Derived groups	
$-(CH_2-CH_2-O)-$	0.33
$-(CH_2-CH_2-CH_2-O)-$	-0.15

2.3.7.5 Interfacial tension

Interfacial tension is determined by the magnitude of the imbalance of molecular interactions across an interface. The greater the inequality of interactions between the water and oil phases is greater the interfacial tension (Evans and Wennerström, 1994; Israelachvili, 2011). As a concept, interfacial tension can be deduced as a contractile force, as any oil-water mixed system tends to minimize the contact area between two phases. Interfacial tension can be expressed as the energy required to create an interface per unit of interfacial area (J/m^2) or force per unit of an interface length (N/m) (McClements, 2005). Interfacial tension at a fluid-fluid interface is measured using a tensiometer. Various kinds of tensiometer are available, which differs according to the physical principles of operation, mechanical design, static or dynamic measurements, and whether they can measure surface tension, interfacial tension, or both.

For instance, the Du Nouy ring method is used to measure static surface and interfacial tensions. The apparatus consists of a vessel containing the liquid to be analyzed and a ring attached to a sensitive force measuring device (McClements, 2005). Initially, the ring diameter is kept at the interface, and the force applied under the ring to remove from the interface is recorded. The force exerted (F) on the ring weight (W) at detachment from the interface is approximately equal to the surface tension multiplied by the length of the ring perimeter (Equation 2.11) (Tadros, 2014; McClements, 2005).

$$F = W + 4\pi d\gamma \quad (2.11)$$

The Wilhelmy plate works with a plate (e.g., platinum foil) removed from the interface. The entire force is provided by the weight of the plate, the interfacial tension force, and the contact length (p) of the plate through the liquid, which is the plate perimeter (Equation 2.12) (Tadros, 2014).

$$F= W + \gamma p \quad (2.12)$$

Both methods required a complete cleaning procedure before and after each measurement to avoid reading mistakes. The Wilhelmy plate requires some seconds before starting the measure to reach an equilibrium between the phases.

2.3.7.6 Interfacial rheology

Interfacial rheology studies the mechanical and flow properties of molecules adsorbed at the fluid interfaces and the subsequent interface deformation (Murray & Dickinson, 1996). When an emulsion undergoes mechanical agitation, the droplets' surface experiences different deformations due to their stresses (Walstra, 2003). Therefore, the interfacial rheology is strongly governed by the factors that alter the nature and strength of the interactions between the molecules adsorbed to the interface (e.g., emulsifier concentration, temperature, pH, and ionic strength).

Two types of interfacial rheology measurements are generally used for deformations in the two-dimensional plane – x and y (Murray, 2002). In the interfacial shear rheology, a bi-cone disk or a Du Nouy ring is placed at the interface, similar to interfacial tension measurement. The force required to oscillate or rotate the disk or the ring is measured with a rheometer, which converted into interfacial viscoelasticity, being interfacial shear elasticity (G) (Equations 2.13 and 2.14) (Brooks, Fuller, Frank, & Robertson, 1999; Murray, 2002).

$$\tau_i = Ge_{xy} \quad (2.13)$$

$$\tau_i = \eta_c \frac{de_{xy}}{dt} \quad (2.14)$$

Where τ_i is the interfacial shear stress performing in the y-direction (tangential) on a material parallel to the x-direction, e_{xy} is the equivalent interfacial shear strain tensor material, t is time (Murray, 2002). All the intramolecular and intermolecular bonds in macromolecules impact the shear rheology, increasing G and η_c. However, it can proceed the opposite if the same interactions inhibit the interface's emulsifier action (Martin, Bos, & Van Vliet, 2002).

In the interfacial dilatational rheology test, a droplet is formed in the air or the continuous phase, the interface oscillates at a determined frequency and strain. The force recorded is the surface stress against the area increased, and the interfacial tension is transformed into dilatational modulus (K^s) and dilatational viscosity (k^s) (Equations 2.15 and 2.16) (Freer, Svitova, & Radke, 2003; Murray, 2002).

$$K^s = \frac{d\gamma}{d\ln A} \quad (2.15)$$

$$k^s = \frac{d\gamma}{\frac{d\ln A}{dt}} \quad (2.16)$$

Interfacial dilatational rheology has an advantage. In a short time of operation, can obtain constant interfacial stress. To have the same information with the oscillatory technique used in interfacial shear rheology, a more extended time is needed due to the low frequencies required to reduce stress relaxation (Freer, Yim, Fuller, & Radke, 2004).

2.4 Structure formation in water-in-oil emulsions

In general, structures in W/O emulsions can be formed by interactions between the molecules in the continuous phase, dispersed phase or among the phases and modifying temperature to develop a microstructure.

2.4.1 Controlling structure formation in the continuous phase

Structure formation in the continuous phase is aimed to give support to all the dispersed elements in the food matrix, generally below 100 μm (Aguilera, 2005). In W/O emulsion, the highest weight percentage is in the bulk phase formed by TAGs or alkaline chains. Different research groups have controlled the continuous or disperse phase to develop a microstructure without flow to satisfy consumers' demands with spreads that mimic commercial products. The spreadable fats are described as semi-solid, but

the structure formed should be a plastic emulsion. The desired behaviour at 20 and 4 °C should be semi-solid and spreadable (Young & Wassell, 2019).

The most utilized W/O emulsions in the food industry are stabilized by partially or wholly crystalline fats, called spreadable fats with 10 – 90 wt% oils and fats. Over a century, margarine and butter have had a minimum fat content of 80 wt%, maximum of 16 wt% water, and 4 wt% is a complex mixture of salt, emulsifier, protein, flavour, colour, and vitamins. Any product under 80 wt% fat has to be called spread or low-fat, with a minimum of 10 wt% fat (Table 2.5) (Young & Wassell, 2019).

Table 2.5 Product types with fat content percentage divided for milk-fat content assigned as butter and vegetable and/or animal fat designated as margarine. Adopted with modification from Council Regulation EC (1996).

Product type	**Fat content (%)**	**Product type**	**Fat content (%)**
Butter	80-90	Margarine	80-90
Dairy spread	62-80	Three-quarter fat margarine	39 to >41
Half-fat	41-60	Half-fat margarine	<39 to 41-60
Three-quarter fat butter	39-41	Fat spreads	>62 to <80
	Product type	**Fat content (%)**	
	Reduced-fat	41-62	
	Low-fat or light	≤41	

An essential aspect of margarine and spreads stabilization relies on the triglycerides crystallization based on the unique fatty acid composition, which impacts the texture in the whole system (Young & Wassell, 2019). Heterogeneous nucleation is the mechanism that food emulsions follow due to the system's impurities (Ghosh & Rousseau, 2011). Fat crystals can be interfacial active and are known as Pickering fat crystals, saturated MAGs (e.g., glycerol monostearate), and cover the water droplets surface, forming a physical barrier (Rousseau, 2000). The fat crystals can also be surface-inactive, fully saturated fats (e.g., palm stearin) that merged through Van der Waals interactions and formed a 3D network in the continuous phase, entrapping water droplets (Johansson, Bergenståhl, & Lundgren, 1995). Both mechanisms can occur in W/O emulsions using small emulsifiers (e.g., GMO) and surface-inactive fat crystals. Fat crystal size is essential for the stability of W/O emulsions for long-term stability. Figure 2.10 showed the three different ranges of size. Smaller fat crystals in A exhibited better coverage at the interface than crystals in B. The

best mechanism of interfacial crystallization is presented in C, where the crystallization is directly at the interface with tiny size crystals covering the entire water droplet surface.

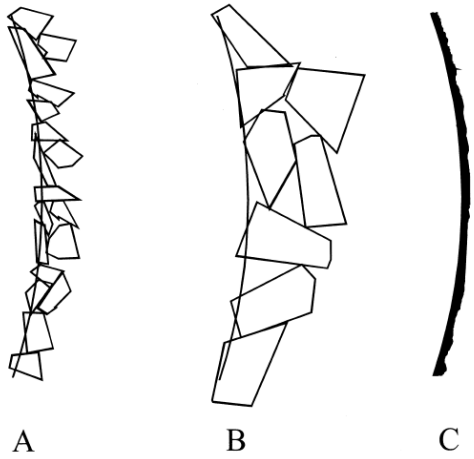

Figure 2.10 Fat crystal size effect at the interface, (A) ~1μm, (B) ~5μm, (C) sub-micron. Adopted with modification from Rousseau (2000).

Ghosh et al. (2011) reported that 10 wt% hydrogenated canola oil (HCO) and 4 wt% GMO with similar alkyl chain lengths formed interfacial Pickering crystallization. GMO provided a surface polarity to HCO surface-inactive crystals, supported by higher E_{disp} of HCO with GMO, leading to Pickering integration and network-type stabilization. Nadin, Rousseau, and Ghosh (2014) identified network stability with 2 wt% PGPR combined with 10 wt% HCO in 20 wt% W/O emulsions with canola oil which formed a crystals network. The group also experiment with S in the aqueous phase (2.5, 5 and 10 wt%), and the network structure allowed a salt diffusion according to the salt concentration. The emulsions were stable after 30 days of storage at room temperature. Prichapan, McClements, and Klinkesom (2017) stabilized 20 wt% W/O emulsions comprising a crystal network with 15, 30 and 45 wt% rice bran stearin in rice bran oil mixed with 1 to 4 wt% PGPR. The aqueous phase contained ferrous sulphate, which was effectively encapsulated and released. After 6 days of storage, the most stable emulsions with 45 wt% rice bran stearin revealed oil phase separation of less than 1% with all three different PGPR levels, indicating that an increase of rice bran stearin was more effective than PGPR. Ghosh, Pradhan, Patel, Haj-shafiei, and Rousseau (2015) developed 20 wt% W/O emulsions in light mineral oil with 5 wt% paraffin wax and 0.05 wt% GMO. The aqueous phase contained 3.5 wt% S. Different cooling methods such as slow-static, slow-stirred, quenched-static and quenched-stirred were compared. Under stirring and quenching, crystallized wax (surface-inactive) with

GMO performed Pickering and network crystallization; the first lead to the second structure formation. GMO was essential to give wax adhesion at the water droplet surface, forming a thin physical barrier. These emulsions were visible stable for 1 year and 6 months.

Haj-shafiei, Ghosh, and Rousseau (2013) experimented with the increment of water content (10 to 50 wt%) and the addition of paraffin wax (2.5 to 4.5g in 5 wt% of oil phase) in light mineral oil to create a structure with both mechanisms. Waxes are alkanes and surface-inactive, but with GMO (0.025 to 0.125 wt%) presence and cool temperature, waxes can crystallize at the water droplet surface. Fresh emulsions exhibited a proportional increase of viscosity with the rise of water content. After 28 days of ageing, viscosity showed a relation with wax content. For instance, emulsions with 10 wt% water content (higher %wax) reported viscosity expanded 4-fold, and with 50 wt% water was 2-fold at low shear. Creep compliance and recovery test at 0.3 Pa in the linear viscosity region exhibited that emulsions with 50 wt% water distorted in smaller magnitude due to water droplets' internal flexibility. Conversely, at 10 wt% water (more wax crystals), the structure was more breakable and irreversible deformation. Storage modulus in fresh emulsions was equivalent to the increase of water cuts. However, the increment of wax content increased storage modulus (G') only at 50 wt% water entailing a synergetic effect with water increase over ageing due to the wax network formation.

2.4.2 Controlling structure formation in the dispersed phase

2.4.2.1 Water droplet aggregation

The aggregation of water droplets affects emulsion stability, rheological properties and may lead to structure formation in emulsions. Emulsions with flocculated droplets have a greater viscosity than an emulsion with the same concentration of non-flocculated droplets. It is due to a higher effective volume fraction (ϕ_{eff}) of flocs (droplet clusters) than the sum of volume fractions of individual droplets where the continuous phase is entrapped by the flocs (Quemada & Berli, 2002). The types of flocs were described in section 2.1.2.2 (paragraphs 1 and 2). The ϕ_{eff} is the volume occupied by the particles divided by the volume of the suspension. At low droplet concentrations or when the inter-cluster attraction is weak, clusters are not interconnected, and the suspension remains liquid-like. Dispersed droplets can penetrate closer to other droplets when the attraction is weak, forming a pack floc, entrapping less continuous phase with ϕ ~0.63, approaching the random packing value in monodisperse particles (Dickinson, 1992). In contrast, above a critical droplet concentration or when the inter-cluster attractive interactions are strong, clusters are interlinked. The extended flocs integrated a 3D network throughout the material, forming a microstructure

that maintains the matrix's stability. The whole emulsion may become a solid-like gel (Quemada & Berli, 2002). Flocs structure and formation rate in W/O emulsions vary according to the water percentage (Koroleva, Tokarev, & Yurtov, 2015). The presence of flocs manifests into a complex rheological behaviour of the emulsions. Emulsions with flocculated droplets usually exhibit pronounced shear-thinning behaviour, so the viscosity decreases as the shear rate or time of shear increases. Shear-thinning exits for two principal causes: (1) The flocs are distorted and become aligned with the shear application, which diminishes their resistance to flow. (2) The flocs are broken down by the shearing forces, which reduces their effective volume fraction (Buján-Núñez & Dickinson, 1994).

Koroleva et al. (2015) studied the increase of water volume fraction related to flocs development in W/O emulsions. The research compared experimental data and simulation based on the Langevin model for the dynamic's method, which makes it feasible to predict W/O emulsions stability to flocculation and successive sedimentation. Mineral oil with 0.08 wt% Span 80 was used as the continuous phase. The aqueous phase contained 1 wt% S, with a water volume fraction from 0.05 to 0.6. A cubic simulation box of 10 μm side length was used in the study where a certain number of droplets were randomly formed with ϕ range from 0.05 to 0.5. Based on the experimental design and model, emulsions with ϕ less than 0.15 did not form clusters. The aggregates were found to be at a significant distance between them, and sedimentation was reported in these emulsions. With ϕ from 0.15 to 0.4 showed branched aggregates creating a network but with slow rate aggregation, above $\phi = 0.2$, no visible separation was exhibited. Concentrations over $\phi = 0.4$ water developed a compact network in fractions of a second. The model concluded similar results. In $\phi = 0.5$ water, the water droplets flocculation started nearly immediately.

2.4.2.2 Water droplet gelation

Water droplet gelation is a useful structure formation method in W/O emulsion, with a reduced saturated fat concentration. The stability of strongly aggregated water droplets could be achieved by restricting the aqueous phase's flow by inducing gelation of the internal water droplets. Different gel induction methods have been studied with the addition of proteins or polysaccharides to the aqueous phase with or without pH modification before emulsification, followed by post-emulsification thermal treatment (Alexa, Mounsey, O'Kennedy, & Jacquier, 2010; Surh, Vladisavljevic, Mun, & McClements, 2007). The added compound in the water droplets should have the capacity to form a gel on cooling or under modified ambient conditions.

McClements group did advance research in this mechanism. Iqbal, Hameed, Baloch, and McClements (2012) reported controlled aggregation of gelled-dispersed phase in W/O emulsions using 10 wt% whey protein isolate (WPI) in the aqueous phase. Thermal denaturation of WPI was produced under pH 7 and 100 mM S. Those conditions induced protein aggregation and consequent gelation at high protein concentrations to form a 3D network. Soybean oil and 8 wt% PGPR composed the bulk phase. The aqueous phase content was tested from 10 to 40 wt% to increase the floc size with the aggregation of water droplets in soybean oil from 90 to 60 wt%. After emulsification, the liquid water droplets were transformed into gelled-dispersed phase micro-particles by thermally denaturing WPI at 90 ºC (beyond the WPI thermal denaturation temperature) for 30 min. When the dispersed phase droplets were between 20 and 40 wt%, the viscosity increased significantly but decreased considerably over shear rate. At high water content, 30 and 40 wt%, behave like solid-like at a low shear rate, exhibited shear-thinning at an intermediate shear rate and were broken at the high shear rate. Complex shear modulus also showed similarly high values related to solid-like properties. Those rheological behaviours were associated with the protein aggregation and 3D network formation of gelled dispersed water droplets in the W/O emulsions.

Then, Iqbal, Hameed, Baloch, and McClements (2013a) used a similar methodology to investigate acidic conditions in the previous study to identify the controlled aggregation of aqueous phases containing WPI. The aqueous phase contained 10 wt% WPI and 10 mM citrate, 100 mM S, pH 3.5. Over 70 ºC, the above denaturation temperature of WPI, the gelation appeared, which could be for β-lactoglobulin, the major globular protein in WPI that unfolds around that temperature. G' exhibited similar values between unheated and heated W/O emulsions. All emulsions showed shear-thinning; however, heated emulsions reported increased viscosity in parallel with water increment (20 to 30 wt%). They described those rheological results with paste-like materials, which keep their shape at low shear stress but are likely to flow at high shear stress. The gelation in W/O emulsions with 40 wt% water was identified with the decrease in the phase angle < 45°, around 70 °C. Storage modulus was higher than loss modulus, indicating a solid-like material; however, these gels were weaker than those developed at pH 7.

Consequent work, Iqbal, Hameed, Baloch, and McClements (2013b) developed 40 wt% W/O emulsions to test the aggregation-gelation of oppositely charged proteins in water droplets. The aqueous phase incorporated 10 wt% lactoferrin (positive charge) or β-lactoglobulin (negative charge) with 10 mM phosphate, 100 mM S at pH 7.0. Soybean oil with 8 wt% PGPR was the bulk phase. Proteins were mixed or separated in a 1:1 ratio of 40 wt% W/O emulsions. W/O emulsions with just protein showed similar thermal behaviour as the mixture of both proteins. The complex shear modulus was low from 30 – 76 °C,

increased from 78 – 90 ºC, and even further during the holding at 90 ºC and cooling at 30 ºC. The gel formation occurred from 78 – 81 ºC, observed with the decrease sharp of the phase angle ~23° for the mixture, ~27° in lactoferrin and ~35° in β-lactoglobulin, which remained constant low during the holding and cooling. The emulsions with the mixture of proteins showed the minor phase angle and the higher shear modulus, which indicates that the network developed was more robust. The effect can be associated with hetero-aggregation due to the reversed charged proteins. β-lactoglobulin and mixed proteins emulsions exhibited higher viscosity and complex shear modulus under heated conditions. The aggregation of globular proteins produced gelation inside the water droplets that were already in close-packing for the increase in water content, forming a more stable 3D network in the oil phase.

Recently, Iqbal, Xu, Huang, and Chen (2019) explored three polysaccharides with different water affinity in the aqueous phase of 40 wt% W/O emulsions. In the aqueous phase was utilized 2 wt% high methoxy pectin, kappa-carrageenan, and starch, independently, with 10 mM citrate, 100 mM S at pH 3.5. Soybean oil with 8 wt% PGPR was the bulk phase. The emulsions were heated or unheated at 90 ºC. All heated emulsions showed higher yield stress, shear viscosities and complex shear moduli than no-heated emulsions. The heated induced gelation of polysaccharides caused by the changes in the random organization of polysaccharides molecules. During heating inside the dispersed droplets, junction zones were formed by hydrogen and hydrophobic interactions in the polysaccharide's solutions, which impacted the 3D network development in W/O emulsions. Kappa-carrageenan emulsions exhibited more significant shear stress and shear viscosity than other emulsions with polymers, which could be for the more extended junction zones to form a firmer gel. After heating, test tube-inverted showed pectin and carrageenan emulsions remained at the top of the tube related to semi-solid characteristics, and starch-emulsions moved to the bottom associated with viscous-like properties.

2.4.2.3 Water droplet volume fraction

The volume of a dispersed phase in a continuous phase can be measured in volume fraction or percentage. The increment in ϕ can increase water droplets' packing, showing different rheological behaviour and reducing gravitational separation (McClements, 2015). When the ϕ is, ~0.13 open flocs can be formed, retaining large amounts of the continuous phase, influenced by strong inter-droplet interaction and dispersed droplet size (Dickinson, 1992). When the ϕ is smaller than the maximum packing volume fraction of droplets (ϕ_m), the droplets are close to the other and can pack in different ways. It has been reported maximum packing volume according to the packing performed by the volume fraction of droplets or particles. For uniform spheres, the ϕ_m of random close packing is 0.637, glass transition ϕ_m is 0.58, and

for hexagonal close-packing, ϕ_m is 0.7404 (Pal, 2020).

A different approach was analyzed for higher water dispersed concentrations (ϕ, 0.74 to 1). These emulsions were believed impossible to develop. This type of W/O emulsions presented polyhedral droplets instead of spheres and can be formulated with low emulsifier concentration (0.5 wt%) and high water content (99 wt%) (Ponton, Clément, & Grossiord, 2001). In that emulsions, the concentration of droplets is above the limit of maximum packing volume fraction, in which the droplets started to deform due to the nearest droplet's pressure avoiding the flow (Masalova & Malkin, 2007). The increase in dispersed volume fraction was also investigated with a further decrease in the oil droplet size to enhance the emulsions' rheological properties. The size reduction would decrease the surface-to-surface distance between the droplets, enhancing the hydrodynamic interaction, enabling droplets packing and increasing the elastic properties (Mason, 1999; Pal, 2000; Quemada & Berli, 2002).

Princen and Kiss (1986) presented a model with that characteristic for a polydisperse system, which involved the elastic shear modulus, interfacial tension, surface-volume mean droplet radius ($d_{3,2}$) to identify the critical volume fraction (ϕ_c) of 0.712 (Equation 2.17).

$$G' = 1.77\left(\frac{\gamma}{d_{3,2}}\right)\phi^{\frac{1}{3}}(\phi - \phi_c) \qquad (2.17)$$

This kind of random jammed-emulsion system has the advantage of liquid to solid-like gel transformation without any saturated or trans fat presence. W/O emulsions with high water volume fractions have been developed for cosmetic and skincare applications. Ponton et al. (2001) formulated W/O emulsions and corroborated Princen's theory. Cetyl dimethicone copolyol was the emulsifier used at a constant concentration in the isohexadecane oil. The aqueous phase contained glycerin, magnesium sulfate, methylparaben and sorbic acid. Water concentrations increased from 69.5 to 82.5% in the oil phase from 22 to 9% by stirring. The water mass fraction was from 74 to 85%. All emulsions were stable after 6 months, except for the emulsions with mass fractions 74 and 75%, which had larger droplet sizes, on average 3.2 μm; thus, a thin layer of water was observed at the bottom. The water phase mass fraction increased from 76 to 85% were stable due to smaller droplet size (2.85 to 1.69 μm, $d_{3,2}$). Emulsions with mass fraction > 75%, the G' > loss modulus (G"), forming a gel. They calculated the ϕ_c from their emulsions, which was equal to 0.714. This value was close to 0.712, which was the one used in Princen's model.

Similar structure formation in high-internal phase W/O emulsion was also observed by many researchers. Malkin, Masalova, Slatter, and Wilson (2004) formulated highly concentrated W/O emulsions

in hydrocarbon oils, with a concentration ~91 wt% of water saturated with nitrate salts, with poly(isobutylene) succinic anhydride as an emulsifier in the oil phase. The addition of water in the oil phase was at super-cooled temperature, 20 °C under the water crystallization temperature. The emulsions were stable for over a month and behaved as non-Newtonian liquids. Four different water droplet size ranges were created with one decimal order gap. A plateau G' was observed with the frequency increase in all emulsions, behaving as elastic materials. Viscosity at a low shear rate exhibited Newtonian domains in all emulsions. The prolonged shearing force increased the viscosity significantly in the low shear rate domain, indicating rheopexy behaviour. The smaller droplet size (8.2 μm) in emulsions showed evidence of closer packing, reporting the highest G' and viscosity. In food-grade W/O emulsions, not much research has been done with a significant increase of water ϕ, primarily due to the inability to prevent emulsion destabilization without forming a crystal network or Pickering stabilization, which was explained in section 2.4.1.1.

2.5 Characterization of water-in-oil emulsions using different techniques

2.5.1 Droplet size determination

Water droplet size distribution analysis is essential to understand the formation and stability of every emulsion. The number can be represented in droplet size distribution, volume or intensity weighted distribution versus diameter (Walstra, 2003). For a straightforward interpretation of droplet size distribution data, a range of statistical parameters can be applied, such as (a) average size of droplets population, (b) median or 50% of the data, (c) mode or the value with the highest repetition. Besides, three different means can be determined depending on how the data was collected and analyzed. The number mean diameter ($d_{1,0}$) is the arithmetic mean of the number of droplets in the sample. The surface-volume means diameter ($d_{3,2}$) or Sauter mean diameter is used to know the droplet size above and below, in which the specific surface areas of all the droplets are equal. It is most sensitive to the presence of small droplets in the size distribution. The volume-weighted means diameter ($d_{4,3}$) or De Brouckere mean diameter is used to reflect the average size based on all the droplets' volume. It is most sensitive to the presence of larger droplets (Malvern, 2012).

The main challenge in analyzing droplet size in W/O emulsions is the immediate floc formation of water-dispersed droplets due to physical barrier is the principal mechanism of stability (Colucci et al., 2020). The droplets can show a range of polydispersity and nonspherical shapes. When W/O emulsions are not entirely aggregated, it is recommendable to use a confocal microscope, dye in the oil or dispersed phase and software for image analysis to diminish mistakes in the droplet size lecture (Romero-Pena et al., 2020). This technique requires a high volume of images and abilities in image analysis that can be time-consuming but

close to an accurate scenario. Thus, the best technique for short-time analysis is nuclear magnetic resonance (NMR). There are three most used techniques to determine water droplet size in W/O emulsions:

2.5.1.1 Nuclear magnetic resonance

The nuclear magnetic resonance (NMR) self-diffusion technique can be used to determine the size of emulsion droplets and has been extensively used in butter, margarine and low-fat spreads (Balinov, Söderman, & Wärnheim, 1994). NMR techniques based on the restricted diffusion of molecules within emulsion have been established to measure emulsion's droplet size distribution, allowing unimodal characterization (Balinov, Mariette, & Söderman, 2004). Pulsed field gradient nuclear magnetic resonance (PFG-NMR) calculates the molecule's mean translational movement during the time between the pulsed field gradients' exposure (Balinov et al., 1994). The pulses cause high excitation of some hydrogen nuclei, which produces a measurable NMR signal. The higher motion of the nuclei in the sample caused lower signal amplitude, measured at different times can identify restrictions on the emulsion and estimate the droplet size (McClements, 2015).

Self-diffusion calculation of hydrogen nuclei requires applying two equal field gradients inside a standard spin-echo pulse series. The effect of molecular diffusion diminishes the intensity of the observed echo. In emulsions, droplet diffusion is limited by droplet interfaces (Ghosh & Rousseau, 2009). Once this boundary is attained, the echo intensity stops decreasing. Signal attenuation is logged as a function of gradient strength. A volume-weighted log-normal droplet size distribution function is mathematically adapted to the measured data by the mean droplet diameter and geometric standard deviation distribution (σ_g) (Ghosh & Rousseau, 2009) (Equation 2.18).

$$F(d) = \frac{1}{d\ln\sigma_g\sqrt{2\pi}} \exp\left(-\frac{(\ln d - \ln d_{3,3})^2}{2(\ln\sigma_g)^2}\right) \quad (2.18)$$

The frequency distribution of droplets F(d) is characterized by the number of droplets (n) of diameter and the volume-weighted geometric mean diameter ($d_{3,3}$) and σ_g, which is calculated in Equations 2.19 and 2.20, respectively.

$$d_{3,3} = \exp\frac{\sum nd^3 \ln d}{\sum nd^3} \quad (2.19)$$

$$\sigma_g = \exp\left(\sqrt{\frac{\sum n[\ln (d/d_{0,0})]^2}{N-1}}\right) \quad (2.20)$$

Where N is the total number of water droplets and $d_{0,0}$ is the number-weighted geometric mean diameter and is related to $d_{3,3}$ according to Equation 2.21 (Ghosh & Rousseau, 2009).

$$d_{0,0} = \frac{d_{3,3}}{n^{3\sigma_g^2}} \quad (2.21)$$

Water droplet size can be expressed as $d_{3,3}$, $d_{0,0}$ with the respective σ_g. The technique was based on water molecules' movement between droplets, which allows identifying the size increase (e.g., coalescence and OR) instead of the clustering of droplets (e.g., flocculation and coagulation) (Ghosh & Rousseau, 2009). Balinov et al. (1994) experimented with PFG-NMR and reported advantages over conventional sizing methods and complications. The benefits were (1) independent of emulsion viscosity or physical sample type, (2) non-invasive, (3) small sample requirement and (4) fast analysis. As disadvantages were (1) predictions in the method just for spherical droplets and (2) diffusion is measured in one dimension.

2.5.1.2 Dynamic Light Scattering

Dynamic light scattering (DLS) analyzes the small particle translational diffusivity that experiences Brownian motion by the interaction between polarized laser light and the emulsion (Goldburg, 1999). The photons that collide with the droplets are scattered with an angular location that depends on the droplets' particle size (Alexander & Dalgleish, 2006). This technique measures particles' size and the surface charge of nanoparticles from 1 nm to 1 μm, and requires a small sample size and offers some advantages as quick analysis (Malvern, 2012). In a diluted emulsion with spherical particles and no particle-particle interaction, droplets' size radius can be measured by applying the Stokes-Einstein – Equation 2.22 (McClements, 2015).

$$r = \frac{kT}{6\pi\eta_c D} \quad (2.22)$$

Where D is the diffusion coefficient of the dispersed phase, k is the Boltzmann constant. For non-spherical particles, the sphere radius with the same D is measured. A collective diffusion coefficient of the scatterers is obtained, which involves the particles' motion in their dispersing medium, including a layer of solvent surrounding the particle with a rough surface or protruding parts. DLS calculated the scatterers' apparent hydrodynamic radius, which permits the thickness determination of emulsifiers' adsorbed layers (Alexander & Dalgleish, 2006). The collective diffusion allows the monitoring aggregation of particles due to the slow-motion (Dalgleish & Hallett, 1995).

The intensity of scattered light is based on the difference between the refractive index (RI) of the oil medium and the water droplet for W/O emulsions (Eastoe, Young, Robinson, & Steytler, 1990). The

scattering angles commonly used are 90 or 173°. At large angles, less scatter was produced for dust particles, which means reduced false data (Fischer & Schmidt, 2016). DLS analysis depends on different variables, including solvent's viscosity, temperature, the RI of the material (Naiim et al., 2015). Series of light scattering instruments (e.g., Malvern Zetasizer® series), Brookhaven (NanoDLS® series) have emerged in recent years. A major limitation of DLS is the assumption of Newtonian viscosity in the aqueous phase, which is not when it contains biopolymers (McClements, 2015). DLS also requires that the colloids' concentration be sufficiently dilute, so the dilution should reach almost optically clear, which could allow a photon to scattered the sample at once (Dalgleish & Hallett, 1995). The use of DLS for the analysis of droplet size is not quite common in W/O emulsions. Most of the studies in W/O emulsions that reported droplet size with DLS technique were in microemulsions or nanoemulsions, with minimal difference between the refractive index of oil and aqueous phase or small droplet size, produced transparent emulsions (Blochowicz, Gögelein, Spehr, Müller, & Stühn, 2007; Porras, Solans, Gonzalez, & Gutierrez, 2008).

2.5.1.3 Static light scattering

Static laser diffraction is a commonly used technique for determining droplets' size distribution based on the light scattering total intensity calculated as a function of scattering angle (Hiemenz & Rajagopalan, 1997). Droplet size can be measured from 0.1 to 1000 μm by static light scattering (McClements, 2015). The results are generated in less than a minute, and a larger number of particles could be analyzed for each measurement (Walstra, 2003). According to the scattered light intensity, the angular variation occurs when a laser is passed through a sample inside a glass chamber. Large particles scatter light at small angles, while small particles scatter light at large angles. The equipment analyzes the angular scattering intensity data by comparing with an equivalent light scattering data generated using Mie theory with the relative refractive index (ratio of the RI of the dispersed and the continuous phase), assuming an equivalent sphere volume diameter model (Malvern, 2012). The Mie theory assumes that light waves just scattered a single particle, rigorously applicable to dilute emulsions (McClements, 2015). Each commercial instrument has its specific characteristic and design so that the same emulsion can show different droplet size distributions. Coupland and McClements (2001) reported significant differences in particle size distributions on emulsions using two different static light scattering equipment. It is recommendable just to monitoring qualitative changes than absolute values.

2.5.2 Droplet surface potential

Surface potential is an analysis of the electrostatic charge on droplets in a liquid suspension. It is one of the fundamental parameters to identify the driving force in electrostatic interactions. The quantity of

electrical charge for the unit interfacial area is the surface charge density. The surface potential is the quantity of free energy needed to raise the surface change density from zero to the altered surface charge density (McClements, 2015). The surface charge density change due to the type and concentration of surface-active molecules absorbed at the interface, temperature, pH, salt addition and is more applicable for O/W emulsions (Duffus, Norton, Smith, Norton, & Spyropoulos, 2016). There are different types of ionic species that can influence the interface's electrical properties. (1) Potential determining ions are responsible for the association or dissociation of charged groups (e.g., hydrogen ions and hydroxyl ions) and the degree of ionization in the acidic or basic groups domain. (2) Indifferent electrolyte ions accumulate around charged groups due to attractive electrostatic interactions (e.g., sodium ions) and can reduce the electrical field strength causing electrostatic screening. (3) Absorbed ions to the interface alter the surface charge density (e.g., ionic emulsifiers or polyvalent ions) (McClements, 2015).

The electrical potential measurement helps with detailed insight into the causes of dispersion aggregation or flocculation. It can be measured via electrophoresis mobility (Israelachvili, 2011). The emulsion is exposed to a static electrical field (E) between a pair of electrodes, which leads to any charge droplet moving toward the oppositely charged electrode until the reach of a constant velocity (v). The movement direction can deduce the sign of the charge. Zeta potential is measured by the movement of droplets based on the size, charge, thickness of the Debye layer, viscosity surrounding the liquid and the applied electric field's strength, expressed in Henry's Equation 2.23 (McClements, 2015). It is usually lower than surface potential.

$$U_E = \frac{2\,\varepsilon\,\zeta\,f(\kappa a)}{3\eta_c} \qquad (2.23)$$

Where U_E is the electrophoretic mobility (v/ E), ζ is the zeta potential (mV), ε is the dielectric constant of water and $f(\kappa a)$ is the Henry's function (dimensionless). The $f(\kappa a)$ value varies between 1 and 3/2 according to the particle size ratio to the Debye length, $1/\kappa$ (Lowry et al., 2016). W/O emulsions cannot get ζ-potential in the lipid bulk systems due to the lack of electrostatic stability. However, it can give some insight into crystals' behaviour when they are partially wetted by water at the W-O interface (Zembyla et al., 2018).

2.5.3. Microscopy

Microscopy is a useful technique to characterize W/O emulsion microstructure, which reveals droplet aggregation, coalescence, and many other structural changes. In light microscopy, light is

transmitted from a source located on the opposite side of the sample. The light passed by a condenser to focus it on the sample and attains maximum illumination. After the light passes through the sample, it goes through the objective lens to magnify the image. In the regular light microscope, out-of-focus light passing through the objective lens promotes a diminution in image contrast and reduces resolution (John-Innes-Center).

2.5.3.1 Polarized light microscopy

Polarized light microscopy (PLM) investigates the local anisotropy of a sample's optical characteristics, which is the property of crystalline structure exhibiting different values when measured with axes in different directions (e.g., refraction and absorption) (Oldenbourg & Mei, 1994). Birefringence is the anisotropy in the RI or double RI, and dichroism is the anisotropy of the absorption coefficient. Samples exhibit a characteristic variation of intensity as they rotated between crossed linear polarizing filters (Oldenbourg, 2013). Polarization refers to restrictions on the path of wave oscillation. A polarizer is a filter that allows passing only light oscillating in one orientation (Carlton, 2011).

Crystals possess molecular order in which absorption, refraction and scattering of light rely on the material orientation to the light's polarization (Oldenbourg, 2013). A few crystals also have double refraction, and the incoming light is divided into different optical axes where the speed of light varies. When those lights are recombined in a polarizing light microscope, it receives inference, and with PLM, a visual interferogram is observed at the back focal plane of the objective (Carlton, 2011). Generally, the polarizer and analyzer are in a cross direction, so the analyzer obstructs most, or all the light passed through the sample. Thus, the sample's image looks dark, except for birefringent or optically anisotropic structures, which appear bright against the dark background. When the optical axes rotated full 360°, the birefringent parts shift brightness, shifting four times, from dark to bright and bright to dark. A birefringent sample appears darkest when its optical axes are 90° to polarizer and analyzer called the extinction position. The rotation by 45° from the extinction position causes more brightest in the birefringent part (Oldenbourg, 2013).

In W/O emulsions, this technique has been used to observe the microstructure formed between water droplets' and fat wax crystals in the continuous phase in brightfield and completed polarized optical axes (Figure 2.11) (Rousseau & Hodge, 2005). Temperature, sample amount and correct coverslip placement are critical factors to observe the clear morphology images.

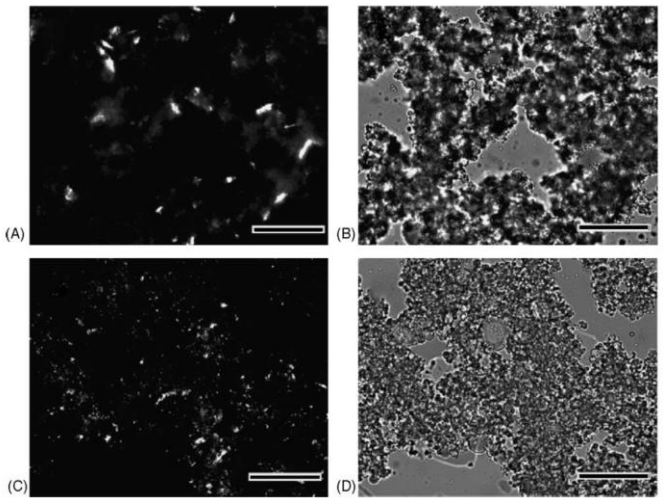

Figure 2.11 Photomicrographs in polarized light microscopy (PLM)(A, C) and brightfield (BF)(B, D) of W/O emulsions 10 days aged stabilized with 1 wt% wax. (A, B) pre-crystallized and (C, D) post-crystallized. Adopted without modification from Rousseau and Hodge (2005).

2.5.3.2 Confocal microscopy

A confocal laser scanning microscope (CLSM) is one of the most significant advances in light microscopy because it allows (1) the high contrast fluorescence of different phases and compounds, (2) the confocal effect due to the pinhole, which focuses on a small area of analysis, and (3) the 3D visualization of thick samples and very high-quality images (Wilson, 1994). The confocal microscope can utilize fluorescent or reflected light as a source. The CLSM used a laser beam of external light (the excitation beam with photons) focused through the microscope objective on a tiny place in the sample. The CLSM produces optical sections by scanning the sample point-by-point using the laser beam focuser over the sample and using a spatial filter, a pinhole, to eliminate unwanted fluorescence from over and below the focal plane of analysis (Paddock, 1999). The laser beam has a size as wavelength of light about 0.5 μm (Nwaneshiudu et al., 2012). The characteristic of CLSM is the use of a pinhole to inhibit out-of-focus light coming out of the droplet, which limits a small part to capture in high resolution. The wavelength of light, the aperture of the

objective and the alignment between the field diaphragm and the eyepiece field affect the focal plane's depth. For obtaining a full image, the point of light is moved across the sample by scanning mirrors.

In a CLSM, multiple lasers are employed to excite hydrophobic and hydrophilic fluorophore reference dye solutions incorporated into an emulsion's oil and, in the aqueous phase, to identify the spatial organization phases. Several fluorescent label images are collected using a system equipped with a single krypton argon laser. It can be combined with three separate lasers with a fibre optic connection. For instance, the 488 nm argon laser is used for the fluorescein channel, a green helium-neon laser (543nm) for the rhodamine channel and a red diode laser (635 nm) the cyanine 5 channel (Paddock, 1999). The excited dye molecules emit fluorescence at a particular wavelength, then collected using a range of filters, which only allows photons of a specific wavelength. For instance, the fast green fluorescent dye (excitation 488 nm and emission 500 – 550 nm) has been utilized to stain hydrophilic molecules as proteins (e.g., β-lactoglobulin), and red fluorescent dye Nile red (excitation 543 nm and emission 573 – 613 nm) to stain lipid molecules or phase (e.g., lactoferrin) (Iqbal et al., 2013a). However, some particles also caused autofluorescence to a specific wavelength without a dye requirement (e.g., curcumin at 488 nm and quercetin at 405 nm) (Figure 2.12) (Zembyla et al., 2018).

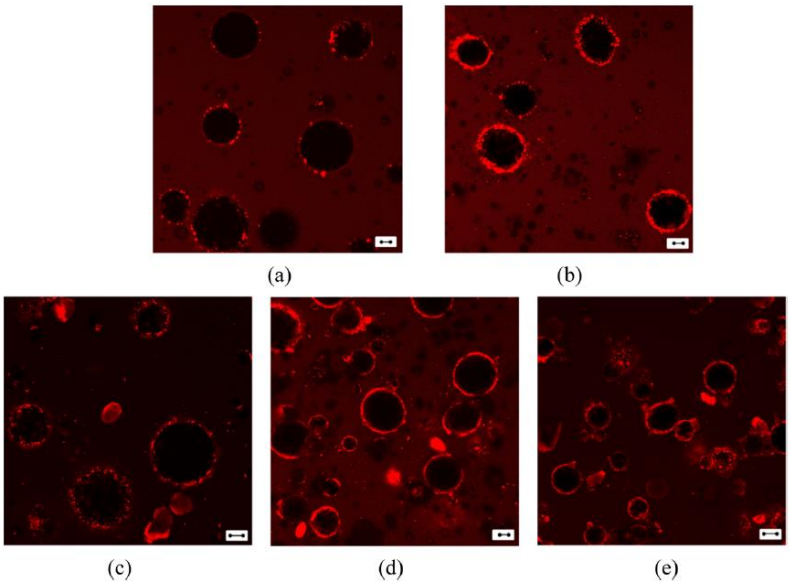

Figure 2.12 Micrograph in confocal laser scanning microscope of 5 wt% W/O emulsions with Pickering particles curcumin (red) at different concentrations (a to e, 0.06 to 1.5 wt%), aqueous phase pH 3. Scale bar: 20 μm. Curcumin particles autofluorescence at 488 nm, excited using lasers 488 and 405 nm. Adopted without modification from Zembyla et al. (2018).

The emitted/reflected light passing through the pinhole is transformed into electrical signs by a photomultiplier and displayed on a computer monitor (John-Innes-Center). As the scanning continues, the detector's signal supplied to the computer accumulates all the "point images" of the sample and successively composes the image one pixel at a time (Nwaneshiudu et al., 2012). Photobleaching is a common mistake due to the extensive exposure to light, limiting the number of photos taken by location in the sample.

2.5.4 Rheology of water-in-oil emulsions

Rheology is the study of the flow and deformation of materials. Ideal solids deform elastically, and the energy needed for deformation is all recovered when the stress is removed. Ideal fluids deform irreversibly due to the flow, and the deformation energy is dissipated within the fluid in the form of heat, and the energy is not easily recovered (Schramm, 1994). W/O emulsions are neither ideal solids nor ideal fluids but are in the region between elastic and viscous called "visco-elastic".

Different forces can act in a material. (1) Stress (τ) defines the forces acting on a material per unit of area (Equation 2.24). (2) Strains refer to relative deformations (e.g., size and shape) in a material exposed to stress (Equation 2.25) (Bourne, 2002). Ideal solids exposed to stress respond with a proportional strain (Schramm, 1994).

$$\text{Stress} = \frac{F}{A} \tag{2.24}$$

$$\text{Strain} = \frac{dL}{h} \tag{2.25}$$

Where dL is the length deformation due to shear stress and h is the height, and γ is a dimensionless strain (Schramm, 1994). Non-ideal solid exposed to stress react proportionally with strain only inside an elastic limit, and beyond that, the material break (McClements, 2015).

2.5.4.1 Viscosity of a fluid

Viscosity is described as the internal frictional forces of fluids or its tendency to resist movement (Bourne, 2002). It can be evaluated using a rheometer or viscometer (TA-Instruments, 2018). A rheometer measures the viscosity of materials by analyzing the resistance against the controlled flow of a material confined between a stationary and a moving plate. A viscometer is limited to measure the viscous flow behaviour of Newtonian fluids in a limited shear rate range. Sir Issac Newton was the first to express the fundamental law of viscosity, describing an ideal liquid's flow behaviour (Schramm, 1994). An ideal liquid, such as water and vegetable oil, exposed to stress responds with a proportional rate of strain (shear rate, $\dot{\gamma}$)

due to flow. The slope is known as the viscosity (η, Pa.s), and it remains constant for Newtonian fluid (Equations 2.26 and 2.27) (Bourne, 2002).

$$\tau = \eta * \dot{\gamma} \tag{2.26}$$

$$\dot{\gamma} = \frac{dv}{dh} \tag{2.27}$$

Where dv is dL/dt, the rate of the flow, dh is the deformation, and $\dot{\gamma}$ is in s^{-1} (Schramm, 1994). Stress is applied tangentially to a material. It is a force vector that has magnitude and direction. Shear rate is the velocity gradient in a fluid due to the applied stress.

Materials such as emulsions, dispersions, gels and polymer solutions frequently demonstrate flow properties remarkably different from Newtonian behaviour (Willenbacher & Georgieva, 2013). Non-Newtonian fluids viscosity is not constant with shear rate, and stress is not proportional to shear rate. Here, viscosity is termed as apparent viscosity, which is the ratio of stress to shear rate (McClements, 2015). A material whose viscosity increase related to the shear rate is a shear thickening fluid (e.g., emulsions stabilized with hydrophilic silica particles) (Rajagopal, 1993). For materials that viscosity decreases concerning shear rate are shear-thinning fluids (e.g., cosmetic emulsions) (Figure 2.13). A significant degree of shear-thinning is essential to ensure good pour and spreadability of materials (Willenbacher & Georgieva, 2013).

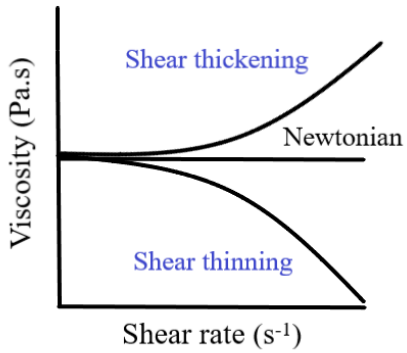

Figure 2.13 Viscosity of Newtonian and Non-Newtonian: shear thickening and shear thinning.

Emulsions with flocculated droplets often exhibit shear-thinning behaviour, meaning that viscosity diminishes as the shear rate or shear time rises (Figure 2.14) (Buján-Núñez & Dickinson, 1994).

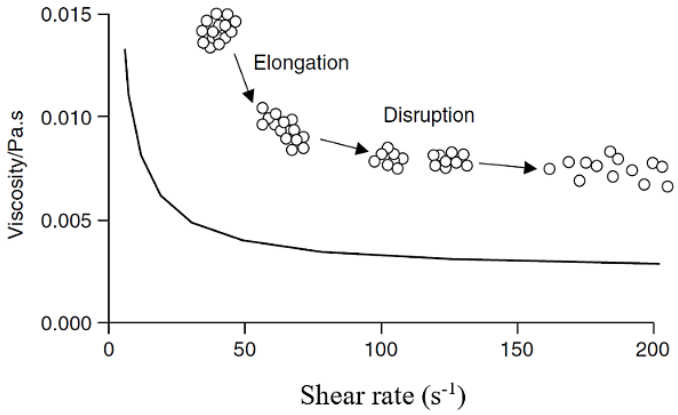

Figure 2.14 Diagram of flocs deformation with the increase of shearing (s^{-1}) and decrease of viscosity (Pa.s) effect. Adopted without modification from McClements (2005).

The main reasons for shear-thinning under shear rate or shear time are (1) alignment with the shear field, causing a reduction in the flow resistance and (2) shear forces, decreasing their ϕ_{eff}. Einstein elaborated the first theory to model small solid sphere suspension, where the emulsions' relative viscosity (η_r) was calculated with Equation 2.28 (Masalova & Malkin, 2007).

$$\eta_r = 1+2.5\ \phi \qquad (2.28)$$

Later a modification was presented to consider elongation or flattened changes in dispersed droplets. Taylor (1932) proposed the first theory of emulsions viscosity, considering η_d and η_c (Equation 2.29).

$$\eta_r = 1+\frac{n_c+2.5n_d}{n_c+n_d}\phi \qquad (2.29)$$

Another important type of fluid is Bingham plastic, in which minimum shear stress, known as "yield stress" must be applied before the flow starts (e.g., melted chocolate, tomato puree). Beyond the yield stress, it behaves like a Newtonian fluid. However, non-ideal plastics, after yield stress, also acts as non-Newtonian (e.g., mayonnaise, concentrated emulsions) (Figure 2.15) (Bourne, 2002).

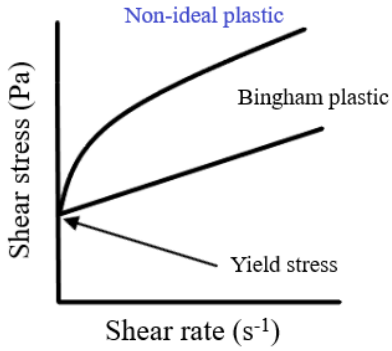

Figure 2.15 Flow curves of ideal Bingham plastic and non-ideal plastic fluids.

The viscosity of an emulsion is higher than the specific viscosities of the dispersed and continuous phases. It is difficult for the droplets to move due to friction and drag force from the continuous phase and other droplets. This difficulty increased in the presence of a velocity gradient (Walstra, 2003). Emulsion viscosity generally is higher with an increase in the dispersed phase volume fraction. There are many theories on how the viscosity (η) of an emulsion depends on the volume fraction of the dispersed phase and the viscosity of the bulk phase (η_c) (McClements, 2005). More details are discussed in section 2.4.4 (paragraph 1). Two critical phenomena associated with the time-dependent flow conduct are thixotropy and rheopexy. The viscosity progressively reduces with time under constant shear rate or shear stress, followed by a gradual structural recovery when the stress is removed, known as thixotropic behaviour. The behaviour can be detected by measuring the shear stress by progressively increasing and decreasing the shear rate (e.g., ketchup and concentrated emulsions). Rheopexy behaviour is defined as the increase of viscosity under an imposed shearing action; when the stress is removed, the fluid return to its original low viscosity (e.g., highly concentrated W/O emulsions) (Willenbacher & Georgieva, 2013).

2.5.4.2 Viscoelasticity of a semi-solid material

Hooke's law of elasticity can describe solids' ideal elastic behaviour. The displacement or deformation is directly proportional to the force applied; under these conditions, the material recovers its original size and shape upon removing the pressure and energy is released (Willenbacher & Georgieva, 2013). However, few materials are entirely elastic. Most emulsions possess elastic behaviour of an ideal solid and flow behaviour of an ideal liquid, for example, viscoelastic liquids (e.g., salad dressing) and viscoelastic solids (e.g., margarine) (Bourne, 2002). In viscoelastic materials, part of the applied energy is stored within the material's molecular structure, being the elastic behaviour. The other energy part is lost due to partial flow, showing viscous properties (Schramm, 1994). Emulsions can form different structures

due to attractive interactions that increase the individual droplet volume fraction creating 3D networks in the matrix, leading to weak or strong gels (McClements, 2015).

Dynamic rheology tests produce data on viscosity and elasticity related to the frequency or amplitude of the applied strain. This test mode is associated with the designated angular velocity or frequency to the resultant oscillating stress or strain. In a rotational rheometer, the rotor deflects with a sinusoidal time-function alternatively for a small angle (e.g., 1°) to the left and right; the sample placed between the shearing gap is pushed to strain in a similar sinusoidal function (Schramm, 1994). This test is also known as small deformation rheology. The experiments can have two methods (1) at a constant frequency with a variable amplitude of oscillation (strain) and (2) at constant amplitude (strain) with variation in frequency (McClements, 2015).

The rheological graphs can be analyzed by observing the storage modulus (G') and loss modulus (G") for elastic and viscous properties. The term storage implies that the stress is temporarily stored through the test but that it can be recovered subsequently. The term loss suggests that the energy applied to initiate flow is irreversible lost and converted into shear heat or dissipated in the material structure. The tan δ (G" / G') is used to identify the gel breakdown point or yield point (G" = G') and the phase angle (δ). Viscoelastic fluids presented a phase angle within the limits of $0 < \delta < 90°$. The liquid-like structure showed G" > G', tan $\delta > 1$ and $\delta \sim 90°$. The elastic materials exhibited G' > G", tan $\delta < 1$ and $\delta \sim 0°$ (McClements, 2015). While the stress relaxation is proportional to the strain, a linear viscoelastic regime (LVR) can be observed where the modulus does not change with the applied strain. Beyond a critical strain, the apparent shear modulus turns into strain-dependent, called the non-LVR (Willenbacher & Georgieva, 2013). Dispersions and gelts present a yield point, which is initiated by a reduction in the intermolecular interactions that hold the structure together. At a higher strain, beyond the yield point, the structure breakdown leading to gel to solution transition and the flow of the material.

Figure 2.16 shows the strain sweep of a gelled 40 wt% W/O emulsion formulated with GMO and hydrogenated soybean oil in the canola oil and low methoxyl pectin in the aqueous phase. A short LVR region can be observed. Strain from 0.01 to 30 % strain exhibited G' > G" reporting a weak gel-like character. The increase of strain reduced the G' and G" until the gel breakdown at ~30% of strain, after that point G" > G'. In this case, the water droplets networks with fat crystals were broken for the increase of strain.

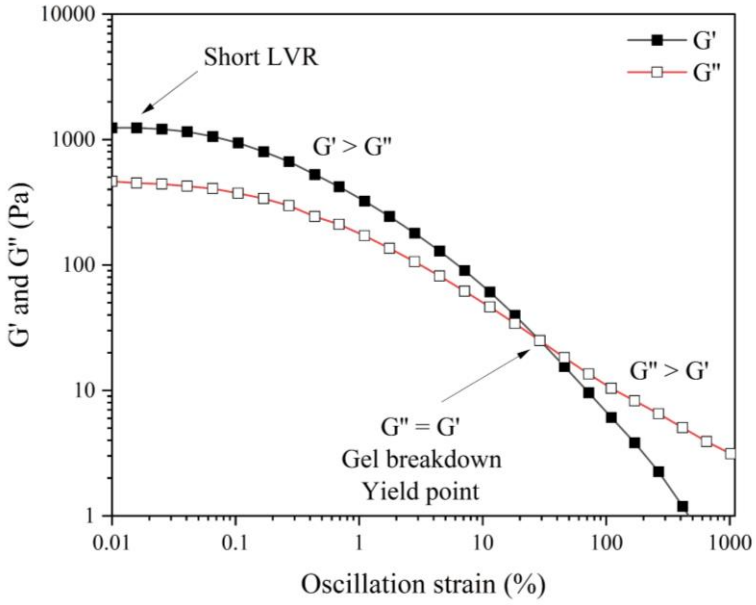

Figure 2.16 Strain sweep at a constant frequency (1 Hz) of 40 wt% W/O emulsions with low methoxyl pectin in the aqueous phase and GMO and hydrogenated soybean oil in the canola oil in the continuous phase after 30 days of storage. Original data collected by Romero-Pena at the University of Saskatchewan.

In viscoelastic materials, G' and G" and δ are frequency dependent. A frequency sweep includes the strain frequency is stepwise increased at a constant strain and at any frequency step G', G" and δ are measured (Schramm, 1994). Frequency sweeps are useful to investigate the time-dependent behaviour of material within the LVR region and to simulates short-term behaviour on short timescales, and high angular frequency; however, to simulate the slow-motion in long-term storage to analyze structural strength or consistency at rest, low angular frequency is selected (Willenbacher and Georgieva, 2013). The only condition is that strain or stress selected must be within the LVR region (Willenbacher and Georgieva, 2013). The frequency sweeps are presented with G' and G" in the y-axis and the angular frequency in the x-axis.

2.5.5. Differential scanning calorimetry

Differential scanning calorimetry (DSC) is a remarkable experimental technique for researching biomolecules' thermodynamic properties. It can examine lipid associations, proteins unfolding or phase transitions, polysaccharides and DNA by analyzing thermodynamic stability, intermediate states, melting and crystallization temperatures (Spink, 2008). This technique is based on a controlled temperature program, which measures the heat released or absorbed by a sample (in a sealed pan) against a reference (empty pan).

When crystallized, a material releases heat (exothermic) and, when it melts, absorbs heat (endothermic) (Höhne, Hemminger, & Flammersheim, 2003). A zero-temperature variation between the reference material and the sample must be determined during the test. DSC documents the energy required to keep no variation of temperature by supplying energy to either the sample or the reference during cooling or heating cycles, so the energy absorption rate is plotted as a function of temperature (McClements, 2015). Every phase transition absorbs or releases heat so that peaks can be visually identified in the thermal graph. The controlled temperature program can be modified to a different range of temperatures that will depend on the sample type (solid or liquid state) and the reference material.

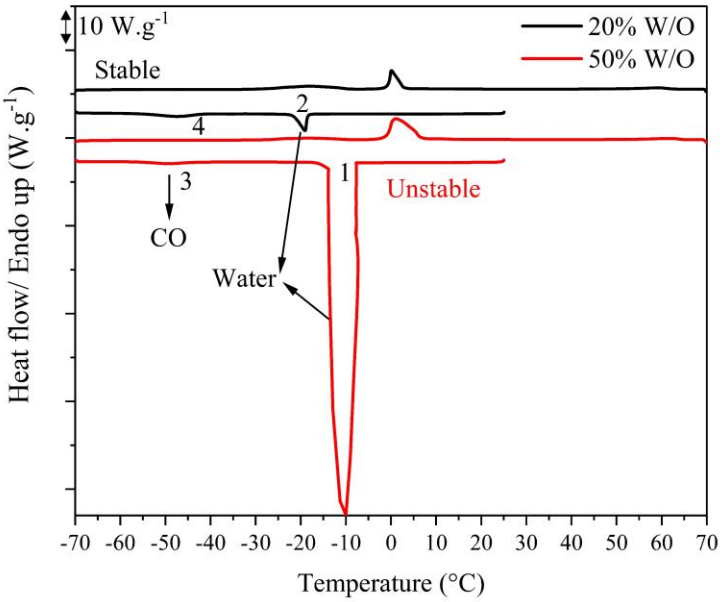

Figure 2.17 Thermal scans of 20 and 50 wt% W/O emulsions with low methoxyl pectin in the aqueous phase and GMO, hydrogenated soybean oil in canola oil as the continuous phase on day 1, first cooling from 25 to –70 °C, then heating to 70 °C at 5 °C/min. Peaks 1 and 2 belong to water crystallization and peaks 2 and 3 to CO. Original data collected by Romero-Pena at the University of Saskatchewan.

Figure 2.17 presents an example that simulates freeze-thaw conditions, this can be multiple cycles, but just two were subjected in this specific case to identify the water droplet instability. Peaks 1 and 2 belong to the water droplets crystallization for 50 and 20 wt% W/O emulsions, respectively. In 50 wt% W/O emulsions indicated that most water droplets crystallized in bulk. However, 20 wt% W/O emulsions showed a small peak related to polydisperse water droplets and thermally stable emulsion. It can indicate partial

thermal stability in some water droplets due to the emulsifier's high mobility and fat crystals at the interface. Peaks 3 and 4 showed the canola oil crystallization, which similar for both emulsions.

2.5.5.1 Thermal analysis of water-in-oil emulsions

DSC is also used for thermal behaviour and phase transition of pure or mixed compounds, including protocols during freeze-thaw analysis. Ghosh and Rousseau (2009) used DSC for analysis of crystallization peak related to demulsified water. The 20 wt% W/O emulsions were prepared with 2 wt% PGPR or 4 wt% GMS in CO or coconut oil (CNO). The DSC cycles were initiated from 40 to –70 °C at 5 °C/min, held for 5 min, followed by heating at 40 °C with the same rate. The freeze-thaw cycles were repeated 20 times for pure, mixed compound and W/O emulsions. They reported that pure water crystallized at –13 °C under the specific cooling rate and thawed at 0 °C. GMS induced fast heterogeneous nucleation at a higher temperature due to its co-crystallization with various triglycerides fractions. Freeze-thaw cycles demonstrated in both oils formed with PGPR; the droplet water crystallization was at –40 °C, associated with the homogeneous nucleation caused by the impurities separation. GMS stabilized water droplets crystallized at -38 °C, linked to the polydispersity of water droplet size. The crystallization enthalpy data was used to determine the bulk phase water separation (%) as a freeze/thaw cycle function. The water bulk separation increased in the order: GMS-CNO, GMS-CO, PGPR-CO and PGPR-CNO.

Zaidel, Sahat, Jusoh, and Muhamad (2014) utilized DSC to identify the thermal transitions of margarine-type W/O emulsions with water-to-oil ratios 25:75, 20:80, 15:85, using a blend of palm stearin and palm oil as the oil phase (40: 60). The aqueous phase contained 47.5 wt% anthocyanins (from 2 sources: roselle and red cabbage) encapsulated with maltodextrin or non-encapsulated and 5 wt% S. The thermal protocol started at 70 °C for 15 min, then cooled to –30 °C for 15 min, and last final heating cycle to 70 °C at 5 °C/min. The best margarine thermal behaviour is defined with the highest melting temperature and the lowest onset crystallization temperature. It indicates rapid melting at body temperature in the mouth with the lowest gumminess. All the emulsions exhibited continuous phase melting around 47 °C and crystallization around 23 °C. The 25 wt% W/O emulsions with encapsulated red cabbage exhibited the highest melting of 47.4 °C, and the 25 wt% W/O emulsions with encapsulated roselle showed the lowest crystallization temperature 22 °C. DSC supported identifying the thermal properties of these margarine-type W/O emulsions to select the best formulations.

Frasch-Melnik, Norton, and Spyropoulos (2010) analyzed 60 wt% W/O emulsions with DSC to identify fat crystals' melting points. The W/O emulsions contained in the 1 wt% S in the aqueous phase. Sunflower oil was the bulk phase with 0.5, 1 and 2 wt% tripalmitin. The DSC protocol started from 0 to 80

°C at 1°C/min. A proportional increment in temperature melting peak was exhibited with increased tripalmitin content from 24 to 30 °C. Similarly, the melting peak temperature increased from 48 to 53 °C. All emulsions showed a broad melting peak, indicating that the crystals were more soluble in the oil phase with the increment of temperature. Hence, the crystals at the interphase and in the continuous phase were weakened at high temperatures. Melting of the crystals shells created imperfections at the interface; thus, water can migrate between multiple water droplets or into the bulk phase and release salt. Different protocols and analyses are possible with this technique to linked results with droplet size or emulsifiers' mobility through freeze-thaw cycles.

2.5.6. Solid fat content

Most food-grade W/O emulsions contain solid fat to provide stability and plasticity to the materials. Hence, it is important to detect the amount of solid fat content (SFC) in the emulsion; there are two major methods.

2.5.6.1 NMR spectroscopy-based SFC determination

Nuclear magnetic resonance spectroscopy relies on the fact that some nuclei possess a permanent atomic magnetic moment. Those nuclei acquire a specific, distinct state in an external magnetic field that belongs to different energy levels (Balinov et al., 2004). It was discussed in section 2.5.1.1 the restrictive diffusion for the measurement of droplet size. Still, NMR in food emulsions' first use was in analyzing SFC. The SFC analysis contends with pulsed NMR is based on 90° pulse magnetization of solid fat (μs), which diminishes much faster than oil (ms). For instance, the signal's contribution is < 0.1% for solid fat than for liquid oil < 1%. The signal intensity is proportional to the number of protons in the liquid. The direct method analyzes the SFC from the signals, associating the total amount of solid fat and liquid oil at time zero and the amount of liquid oil at a final time. The indirect method compares the signal from the liquid oil fraction (L_o) with the signal from fully melted fat (F_m) (Equation 2.30) (Balinov et al., 2004).

$$SFC = \frac{cF_m - L_o}{cF_m} \text{ x } 100\ \% \qquad (2.30)$$

Where c is the correction factor of a reference liquid sample considering the signal at the measuring temperature divided by the same reference liquid signal at the melting temperature, the indirect method is usually used as a previous reference for the direct method, while the liquid oil and solid fat signals are monitored. Also, the indirect method's error range is 1 – 2%, and for the direct method is 0.4% (Balinov et al., 2004). Commercial spectrometers transform the NMR signal into a percentage of SFC using the direct method.

Rousseau's research group has used NMR extensively for SFC. Rafanan and Rousseau (2017) analyzed the SFC of W/O emulsions comparing GMO and PGPR with HSO at 4 °C. The SFC was analyzed from 5 to 20 wt% W/O emulsions without statistical difference between GMO and PGPR (10.7 – 9%); though, a slight reduction was observed after 7 days of storage (10.6 – 8.6%). Ghosh et al. (2011) investigated the SFC in W/O emulsions with GMS, GMO-HCO, and GMS-HCO at 25 °C after 7 days of ageing. GMS was increased from 1 to 8 wt%, and the SFC was from 0.5 to 4.7%. GMO was set at 4 wt%, and HCO risen from 2 to 10 wt% reported SFC range from 1.6 to 6%. GMS (1 – 4 wt%) was mixed with HCO from 2.5 to 10 wt% showing SFC range from 2.7 to 7.8%. All the SFC measured in NMR were lower than the total fat in formula, they reported this could be due to lipid solubilization in the oil phase. The mixed GMO-HCO produced higher SFC from the three mixtures than the counterparts, indicating that HCO crystallization was prevented with GMS. They reported that this mechanism could be due to stearic acids in GMS may interact with the crystal lattices in HCO, decreasing the SFC. Ghosh et al. (2015) analyzed solid wax content (SWC) in W/O emulsions at 4 and 25 °C. The emulsions used 0.05 wt% GMO and 5 wt% paraffin wax. SWC was significantly higher after ageing of 78 weeks, at 4 °C (~20%) and 25 °C (~60%) due to the wax solidification.

2.5.6.2 DSC-based SFC determination

Most W/O emulsion contains mixtures of crystalline fat with oils, and DSC melting scans are used to measure solid-state fat in percentage or fraction under different conditions. Prichapan et al. (2017) used melting scans of 20 wt% W/O emulsions to calculate the fraction of liquid oil presented. They integrated the partial area of the melting peaks to obtain the enthalpy, and the liquid fraction percentage was used to calculate the solid fat index (SFI) of rice bran stearin (0 – 45 wt%) at 25 °C. The samples were heated from 25 to 80 °C and hold for 30 min, then cooling to –30 °C and final heating to 80 °C, both last cycles at 10 °C/min. The SFI is the fraction of solid fat compared to the overall lipid in the emulsion, solid plus liquid. The increase of PGPR concentration (1 to 4 wt%) did not significantly change the SFI. No solid fat was identified with 0 and 15 wt% rice bran stearin in W/O emulsions due to solubility. Despite higher concentrations (30 and 45 wt%) of rice bran stearin showed SFI of 2 to 5 wt%, correspondingly.

Pérez, Wagner, and Márquez (2016) calculated the SFC of 20 wt% W/O emulsions applying a method tested for their research group using DSC (equation 2.31) melting energy is converted into melted mass by a linear association between melting enthalpy and various triglycerides melting point. The continuous phase of emulsions was low trans vegetable fat, bovine fat, or hydrogenated soybean oil (HSO) and 0.5 – 4 wt% PGPR. The samples were sealed for 1 day in a pan and lid at 7 °C. The cycle started with

cooling to 1 °C at 10 °C/min, with a hold for 10 min, followed by heating to 70 °C at 5 °C/min. The melting scans were used to integrate the enthalpy energy to transform it into melted mass (m) and applied the Equation 2.31, where (T_f) is the final melting temperature and (M) is the total sample mass.

$$SFC = \frac{\int_{T}^{T_f} m dT}{M} \times 100 \quad (2.31)$$

The results showed that SFC was related to the fat nature selected as the continuous phase. At lower temperatures (10 to 20 °C), the order from higher to lower was HSO, bovine fat and low trans vegetable fat. However, at higher temperatures (30 to 40 °C), HSO presented the smallest SFC due to its lower melting point. Low trans vegetable fat and bovine fat exhibited related higher values. The addition or absence of 1 wt% PGPR showed the same SFC trend with the fats. Indeed, the PGPR concentration increase the SFC in LT and BF compared to without PGPR, which can be affected by the fat nature. SFC content in fats with PGPR variation from 0.5 to 4 wt% did not show a difference between the fat samples (except 4 wt% PGPR at 10 °C), which was associated with the PGPR adsorption at the interface, dropping the concentration of emulsifier accessible to affect crystallization in the lipidic continuous phase. Analysis of low trans vegetable fat without water showed that PGPR increment caused an increase in SFC, which was also observed in the rise of enthalpy between 25 to 40 °C in DSC scan. The authors reported that it could be that PGPR with low trans vegetable fat leads to the formation of more stable crystals.

2.5.7 Vibrational spectroscopy techniques for water-in-oil emulsion characterization

Vibrational spectroscopy implicates the study of radiation interaction with molecular vibrations but varies in how photon energy is transferred to the molecule by shifting the vibrational state (Larkin, 2017). The demand for molecular interaction techniques with high chemical selectivity and specificity has increased based on the commercial availability of appropriate high-performance multi-channel sensors and the growth of efficient evaluation and interpretation software (Salzer & Siesler, 2014). FTIR (Fourier transform infrared or IR) is specific for analysis that involved heteronuclear diatomic molecules (e.g., carbon monoxide, hydrochloric acid, nitrogen oxide) because those molecules possess dipole moments being IR active (Larkin, 2017). In W/O emulsions, IR can provide information about various functional groups, which have specific vibration wavenumber. It is also possible to recognize between intramolecular or intermolecular interactions, shifts, and areas under the peak to know more about the bonding interactions at the water-oil interface and in the continuous phase.

2.5.6.1 FTIR-based analysis of molecular interactions in water-in-oil emulsions

The average IR spectrometer broad-band source radiates each IR frequencies of interest, selected according to the functional groups and corresponding vibrations. The IR bands are divided into three groups of wavenumber range: (1) near-IR region between 14000 – 4000 cm^{-1}, (2) the mid-IR zone from 4000 to 400 cm^{-1}, and (3) far-IR band among 400 – 10 cm^{-1}. The IR spectrum is acquired by plotting the intensity (e.g., absorbance or transmittance) against the wavenumber. The IR absorption process is based on the molecules' absorption of energy if the vibration produces a change in the dipole moment, causing a modification in the vibrational level, and each group has its unique vibration wavenumber (Larkin, 2017). A lot of information about molecular interactions can be obtained in the complex system formed in W/O emulsions; however, not many studies have been done.

Bus et al. (1990) investigated the mechanism of interaction of emulsifiers' hydroxyl polar heads during micelle formation in W/O emulsions. The oil solutions were subjected to IR-spectra. The creation of hydrogen bonds caused a significant change in bending vibration that its strength is presented at a specific wavenumber in the spectra. Intramolecular hydrogen bonds occur due to interaction within the molecule. Intermolecular hydrogen bonds proceed when the interaction is between other molecules. Both bonds change according to the concentration of the OH-involving molecules and can be detected by IR spectra. In GMO, one OH group is esterified, and the two OH have various options of state: (1) free-no interaction, (2) form an intramolecular bond the next OH group or with the carbonyl in the same molecule and (3) create an intermolecular bond with the OH or C=O of a neighbour molecule. The OH stretch band can present a shift in the spectrum that depends on the H-bond's strength. The experiment was conducted with two concentrations of GMO (0.002 and 0.009 M) in heptane. Three bands were analyzed, free OH (3630 cm^{-1}), intramolecular H-bond (3600 cm^{-1}) and intermolecular H-bond (3400 cm^{-1}).

At low GMO concentration, the peaks were more visible for each band with a broader band at the intermolecular wavelength; however, the peak shift was mostly to the intermolecular band at high GMO concentration. The interactions were corroborated with critical micelle formation, a transition between 3 to 4 mM was identified, at that point, free and intramolecular H-bond decrease, and intramolecular H-bond increased 3-fold. However, CMC showed a lower concentration (2.1 mM), which may be that water presence promoted better packing of GMO at the interface. They found that H-bonding between OH-groups of the emulsifiers can characterize the micelle formation with OH-involving emulsifiers in a hydrocarbon oil. They also did IR spectra of GMO (0.002 to 0.06 M) in glycerol trioleate (3 units of oleic acid). The IR spectra change slightly in the whole concentration range but showed a significant peak at 3541 cm^{-1}, H-bond's vibration with carbonyl groups. There was no effect on GMO concentration, which indicates that

glycerol trioleate provides a surplus of carbonyl groups that almost all the OH groups form an intermolecular bond with CO groups.

Ghosh et al. (2011) theorized that in W/O emulsions, GMO prefers to interact with the bulk oil than the water interface, developing a desorption mechanism from the interface visible in emulsion droplets coalescence previously exposed by Bus et al. (1990). The IR spectra analysis was with 4 wt% GMO in canola oil or mineral oil. Pure GMO showed a significant intermolecular H-bonding peak (3400 cm^{-1}). GMO in mineral oil showed a similar peak for intermolecular H-bond between GMOs' molecules, showing no H-bonding evidence with alkanes structure. GMO in canola oil exhibited a significant intermolecular peak at 3476 cm^{-1} between carbonyl groups of TAGs in canola oil with OH-groups in GMO and a free OH small peak at 3620 cm^{-1}. They reported that GMO was not freely available for emulsion formation due to the extensive H-bonding with carbonyl groups in canola oil. This interaction was corroborated with the CMC in both oils with GMO. The CMC in mineral oil was 0.15 wt% and in canola oil was 4 wt%. The CMC increase can be promoted for the same mechanism that GMO interacted with canola oil which prevented the diffusion toward the W-O interface.

Besides, Kiefer, Frank, and Schuchmann (2011) analyzed with IR spectroscopy samples of 30 wt% W/O emulsions to understand the stability mechanism. The aqueous phase contained 0.05 wt% anthocyanin from bilberry extract added in medium-chain triglyceride oil with 3 wt% PGPR. The bilberry extract solutions showed OH-stretch peaks between 3045 to 3535 cm^{-1}. Higher wavenumber implies that water was not completed ordered, thus presenting stronger covalent bonds in water. PGPR has a few ether groups with a permanent dipole that can interact with water droplets and weaken the intramolecular H-bonding between the water molecules. The W/O emulsion spectrum exhibited a wider band from 3060 to 3664 cm^{-1}. All the deconvoluted peaks in the wavelength range indicated that intermolecular H-bonding was between water and PGPR. Water in bilberry solutions showed a fully H-bonded of 12.2%, and in bilberry W/O emulsions decreased to 9.7%. These results probed structural changes in the water caused by the emulsifier, which promotes the stability of W/O emulsions.

Jorgensen, Van De Weert, Vermehren, Bjerregaard, and Frokjaer (2004) utilized IR in the secondary structure of insulin and growth hormone dissolved in W/O emulsions to identify processing changes in stability or availability. The water phased represented the 60 wt% and 20 mg/mL of protein – insulin or growth hormone. Fractionated coconut oil was the bulk phase with 3.5 wt% PGPR and 1 wt% Span 80 as emulsifiers. The protein spectrum was selected from 2000 to 1700 cm^{-1} to eliminate the phosphate buffer and oil-emulsifier spectra. The amide band in the region 1595 to 1705 cm^{-1} was

deconvoluted to identify the protein secondary structure. In both proteins, α-helix and β-sheet decreased during W/O emulsions manufacturing. However, more impact was exhibited with the growth hormone than insulin. However, the variation on manufacturing parameters, like temperature or homogenization time, did not represent a further decrease in the peak area than the protein solutions. It was suggested that proteins change when interacting at the interface; however, emulsifiers act as the protectors of the proteins in water droplets during emulsification. IR can give insights into the mechanism and interactions in W/O emulsions, and with other techniques, it can be completed the whole picture of what is happening in those complex systems. Nevertheless, further research should be done to discover unexplained stability or instability mechanism in various W/O emulsions.

2.5.8 Sedimentation analysis in water-in-oil emulsions

The sedimentation is measured by obtaining the velocity at which droplets sediment in a gravitational or centrifugal field (McClements, 2015). In section 2.1.2.1 (paragraph 1), the details of gravitational separation and how to prevent it are discussed. The measurement of absolute sedimentation value is difficult due to the broad size distribution of the emulsions droplets (Balinov et al., 2004). The most common visual observation method is taking images on day 0 and after storage time from a cylindrical glass tube controlling temperature. The sedimentation index (SI) is obtained by measuring the heights and using the Equation 2.32. Where H_0 is the initial emulsion height on day 0, and H is the upper oil separation after storage (Ushikubo & Cunha, 2014).

$$SI\ (\%) = \frac{H}{H_0} \tag{2.32}$$

2.5.8.1 Visual observation of sedimentation

Hodge and Rousseau (2005) used tubes for sedimentation analysis in 20 wt% W/O emulsions. The storage time was 10 days at 5 °C with post- or pre-crystallized HCO or cotton stearin (HCSO). The tubes' white phase constituted emulsified water droplets with random solid fat crystals, and the clear region is the free oil. The higher white volume means that the emulsion is more stable to sedimentation. At lower fat crystals concentration, post- and pre-crystallized emulsions prepared with HCO were slightly more stable to sedimentation than HCSO emulsions showing a similar trend. No sample was fully resistant to sedimentation. At high HCSO concentrations, emulsions exhibited sedimentation and creaming, maybe for air bubbles in the system ~68%. Control emulsions without fat crystals showed ~45% sedimentation volume. A high percentage of HCO exhibited a sedimentation volume of ~52%. HCO in post-crystallized

conditions in low concentrations (0.25, 0.5 wt%) and HCSO (0.5 wt%) were the emulsion with the lowest sedimentation.

2.5.8.2 NMR-based sedimentation analysis

Two NMR methods can give valuable information related to the sedimentation rate of emulsions. The first relies on the quantitative analysis of the dispersed water phase amount. Normally larger droplets gradually reorganize in a test tube. Sedimentation can be analyzed by identifying the amount of droplet dispersed phase suspended in the W/O emulsion at a fixed position as a function of time. It can be measured in a tube used in NMR or by the phase's withdrawal during different time intervals. Further centrifugation and the posterior NMR comparison of the lower and upper portions have been used to measure more stable emulsions (Balinov et al., 2004). The second method is PFG-NMR, which is sensitive to flow rates, reporting micrometres per second along the magnetic field's gradient direction (Balinov et al., 2004). As explained before, in section 2.5.1.1 (paragraph 1), the PFG-NMR signal for self-diffusion analysis also gives data on the droplet size and its progress in droplet size distribution over time (Balinov et al., 1994). This method easily differentiates the continuous and the dispersed phased based on its molecules' transport properties. For instance, molecules restricted in the dispersed water droplets have an apparent diffusion coefficient much lower than the corresponding value in the continuous phase. Conversely, molecules in the continuous phase have an apparent diffusion coefficient related to the value in the bulk phase. Both facts are used to identify the type of continuous phase and the mechanism of instability that promoted sedimentation (Balinov et al., 2004).

Marques, Sørland, Less, and Vilagines (2018) used PFG-NMR to monitor the separation efficiency in water-in-crude oil emulsions. The sedimentation and coalescence of emulsions were analyzed through simultaneous measurements of the evolution of the brine and droplet size distribution. They improved the signal-to-noise ratio because, for low oil viscosities, it was not possible to distinguish from water droplets signals. The system applied magnetic field gradients to suppress the bulk signals and only detect emulsified water. This method used the fact that the phase with the lowest apparent diffusion coefficient at long observation times corresponds to the water molecules restricted by the droplet sizes. This suppression method is called the root of mean square displacement, which calculates the droplet size distribution from the apparent diffusion coefficient.

2.5.8.3 Light scattering- based sedimentation analysis

Light transmitted across the sample is also used to analyze sedimentation, combined with centrifugation to accelerate the phase separation. The equipment is an analytical centrifuge (LUMiSizer®)

that used STEP-technology® (Space and Time-resolved Extinction Profiles), which combines sedimentation principles with a specific optical detection system for transmission and absorbance analysis. The sample is exposed between the light source, and a charged-coupled device sensor detects the transmitted light during centrifugation. This design allows the data collection of space and time-resolved extinction and transmission profiles at any point and time during the experiment. In the beginning, the droplets are homogeneously dispersed in the whole sample. The sensor detects the intensity of the transmitted light over the complete sample, and the first extension profile is taken. The centrifugation forces the water droplets' motion from the meniscus to the cuvette's bottom based on their shape, mass, and size characteristics. The Beer-Lambert law defines the method (Equation 2.33), which is associated with the attenuation of light to the material properties where the light is crossing (Gross-Rother et al., 2018).

$$\text{Absorbance} = -\log\frac{I}{I_0} = \varepsilon_c c_s l \qquad (2.33)$$

Where I is the transmitted light, I_0 is the incident light, ε_c is the molar absorptivity coefficient, c_s is the solution's concentration, and l is the light path's length. The sedimentation velocity relies on captured extinction profiles over time (Gross-Rother et al., 2018).

Tian, Xiang, Wang, Zhang, and Li (2021) analyzed sedimentation velocity in 20 wt% W/O emulsions with PGPR (0.3 to 2 wt%) at 25 °C for 9 hours. The emulsions contained xanthan gum and locust bean gum (6: 4) in the aqueous phase and were stored for 30 days. All the control emulsions without xanthan gum and locust bean gum showed higher sedimentation velocity than the mixture of PGPR-polysaccharides from 0.7 to 0.2 μm/s. However, W/O emulsions with PGPR-polysaccharides reported lower sedimentation with PGPR increment from 0.5 to 0.17 μm/s. It indicates that the polysaccharides mixture enhanced the stability of the W/O emulsions with PGPR. The higher PGPR concentrations reduced the sedimentation velocity due to a reduction in droplet size, which influenced the lower sedimentation velocity.

2.5.9 Spreadability of water-in-oil emulsions

Spreadability is the second attribute in margarine highly regarded. SFC between 10 to 20 has been reported as the optimal range to obtain acceptable fat-spreadable in a consumer panel. The standard evaluation of fatty materials utilizes a cone penetrometer (Deman, 1983), in which the penetration is the distance that the cone does in 5 seconds after its discharge on the sample surface. The result is reported in hardness index or yield value. Some margarine cannot associate SFC with hardness due to the fat crystal network (Chrysan & Hwang, 2020). The average yield value (AYV) is calculated from the displacement experiments using the following Equation 2.34.

$$AYV = \frac{mg}{\pi \tan^2\left(\frac{\alpha}{2}\right) d_p^2} \quad (2.34)$$

Where m is the applied load (kg), g is the gravity, α is the cone angle, and d_p is the depth of penetration. Margarine, butter and spreads have hedonic spreadability preferences with yield values between 30 to 60 kPa and an AYV of ~0.28 related to temperature (Rohm, Strobl, & Jaros, 1997).

Rohm et al. (1997) analyzed two commercial butter samples, and the cone penetration method was compared with sensorial panellists under day and red light. The samples were analyzed at 18 °C and 16.5 °C, the AYV was ~41 kPa. When the temperature increased to 19.3 °C, the samples reported 27.1 kPa. However, when the temperature was reduced to 17.1 °C, the AYV increased to 54.6 KPa. Further reduction of temperature at 15.6 °C, higher AYB of 54.8 KPa was demonstrated. It indicates as the temperature was reduced, the AYB increased. In the sensorial panel daylight, the samples were determined as easy to spread. The results were completely different on daylight than red light; a significant bias was identified in the butter sample with a more intense yellowish colour. During daylight, the panellist did not have a problem determining the easy-to-spread sample; however, over red light was impossible to achieve. It was evident a bias due to colour intensity and spreadability even with well-trained panellists in the department.

A modern methodology to measure spreadability used a texture analyzer for gels or plastics fats. The spreadability test probe is fitted with a conical geometry. The method of compression mode sets penetration depth, speed, and post-test speed. The sample is compressed between two cones and returned to the initial position. The collected data of force against distance, firmness can be analyzed. High firmness indicated lower spreadability, being lower firmness the opposite (Mohanan, Tang, Nickerson, & Ghosh, 2020).

3. DEVELOPMENT OF THERMALLY STABLE COARSE WATER-IN-OIL EMULSIONS AS POTENTIAL DNA BIOREACTORS[1]

3.1 Abstract

Conventional polymerase chain reaction (PCR) performed in a continuous aqueous phase often shows an inability to detect ultra-low DNA concentration. Droplet digital PCR, where DNA polymerization happens in isolated water droplets of water-in-oil (W/O) emulsions, could significantly improve the detection limit. However, water droplet breakups under multiple thermal cycles necessary for DNA polymerization is preventing the wide-spread application of such technology. The present research aims to develop thermally stable coarse W/O emulsions that could act as DNA microreactors. Span 80, polyglycerol polyricinoleate, or sodium bis(2-ethylhexyl) sulfosuccinate (AOT) were dissolved in mixtures of light and heavy mineral oils at different concentrations. The aqueous phase was selected based on PCR protocol, without the presence of enzymes and DNA. Emulsions prepared without bovine serum albumin (BSA) in the aqueous phase was used as a control to understand its effect on stability. Emulsions were formed using a vortex mixer for 2 minutes at 3200 rpm. Only the emulsions without visible aqueous phase separation were exposed to PCR thermal cycling. The volume means diameters of water droplets were calculated by image analysis. Span 80-stabilized emulsions destabilized upon thermal cycling, while PGPR emulsions remained stable with an increase in water droplet size.

[1]Published manuscript of an article published in the Journal of Dispersion Science and Technology on June 21, 2020. The present chapter is a copy of this publication.
Romero-Peña, M., Ng, E. K., & Ghosh, S. (2020). Development of thermally stable coarse water-in-oil emulsions as potential DNA bioreactors. *Journal of Dispersion Science and Technology*, 1-10. https://doi.org/10.1080/01932691.2020.1794886.
Author role: Romero-Peña, M. carried out the experiments and wrote the first draft. M., Ng, E. K. was a collaborator from S.M. Research Inc., ON, Canada, who reviewed the manuscript. Ghosh, S. supervised, reviewed, and edited the manuscript.

AOT was able to form thermally stable emulsions, with an average droplet size around 119 μm without any significant change. The influence of emulsifiers concentration, surface saturation, molecular interaction with BSA at the interface, and continuous oil phase viscosity was considered to explain the mechanism of emulsion formation and thermal stability. Figure 3.1 shows the mechanism of stability for PGPR and AOT before and after thermal cycles.

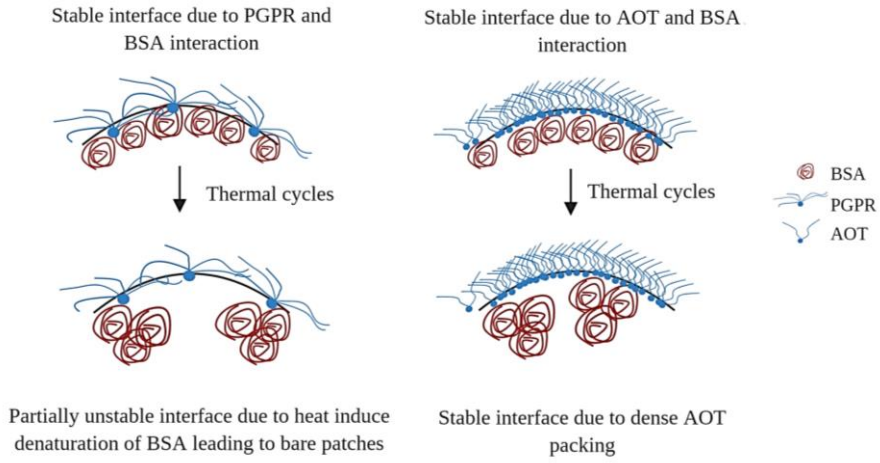

Figure 3.1 Mechanism of stability for PGPR and AOT at the W-O interface before and after the thermal cycles.

3.2 Introduction

Polymerase chain reaction (PCR) is extensively utilized in molecular biology and applied microbiology to create copies of specific deoxyribonucleic acid (DNA) segments and subsequent detection of a gene sequence (Musyanovych, Mailänder, & Landfester, 2005). In PCR, multiple thermal cycles are used for denaturation, hybridization, and polymerase extension of DNA segments from a small amount to a factor of 10^6 (Mullis et al., 1986). Conventional single-molecule PCR amplifies several DNA molecules in a vial simultaneously to replicate and increase the DNA percentage (Hori, Fukano, & Suzuki, 2007). Because the DNA amplification is done in a continuous aqueous phase, DNA quantification becomes extremely difficult at extremely low detection levels (Kanagawa, 2003).

The use of water-in-oil (W/O) emulsions as a DNA bioreactor is a novel technique used in droplet digital PCR (ddPCR), which reduces the problems of conventional PCR and allows effective detection of DNA even from minimal initial concentrations (Hori et al., 2007). ddPCR could have a significant impact on cancer treatment allowing the identification of minimal genetic alteration at an early stage concerning location, progression and response to treatment (Perkins, Lu, Garlan, & Taly, 2017). Water droplets as DNA

bioreactors have been developed with various lipophilic emulsifiers, different types of oils and with diverse thermal cycle procedures since 1998 (Tawfik & Griffiths, 1998). Nakano et al. (2003) experimented with silicone oil (viscosity 98 mPa.s) as the continuous phase and a mixture of non-ionic emulsifier polyethylene glycol tert-octylphenyl ether (Triton X-100 at 0.1% v/v) and bovine serum albumin (0.1 mg ml^{-1}) in the dispersed aqueous phase. The W/O emulsion with a droplet size ranged from 2 – 10 μm was formed by magnetic stirring in cold conditions. After the thermal cycles for DNA polymerization, the emulsions were broken by centrifugation (9000 x g for 3 min). The researchers reported that silicone oil (viscosity 98 mPa.s) was a suitable continuous phase, compared to mineral oil (viscosity 15 mPa.s) with lower viscosity which was used in a previous study by Tawfik & Griffiths (1998). Baier et al. (2011) used Span 80 (5.6 wt% in oil) and Tween 80 (0.8 wt% in oil) to form W/O nanoemulsions (water droplets as a nanoreactor for one molecule of DNA) using three different types of oils – mineral oil (viscosity 15 mPa.s), soya oil (viscosity 80 mPa.s) and castor oil (viscosity 1.5 mPa.s), and an aqueous phase containing PCR buffer and gelatin. The emulsions were formed by stirring under ice-cooling for 30 minutes and homogenized with an ultrasonicator. Stable nanoemulsions with water droplets from 250 – 320 nm were developed; however, only the mineral oil with the highest viscosity did not show any phase separation. After DNA polymerization via thermal cycling, the emulsions were centrifuged to separate the aqueous phase for further detection. Musyanovych et al. (2005) utilized a C12–C14 isoparaffinic mixture (viscosity 1.9 mPa.s) and light mineral oil (viscosity 24.1 mPa.s) as continuous phase with a mixture of Tween 80 (0.4% v/v), Span 80 (4.5% v/v), and TritonX-100 (0.05% v/v) as emulsifiers.

The emulsions were formed by mechanical stirring at 1400 rpm for 30 minutes, then exposed to thermal cycling followed by breaking the water droplets using ultrasonification. The researchers reported that emulsions with light mineral oil were thermally stable with a water droplet size range from 100 – 300 nm, due to its higher viscosity compared to the isoparaffinic mixture. In most of these studies, the aim was to create highly stable emulsions and sub-micrometre size water droplets that would be stable during thermal cycling, but posterior needs to be destabilized after DNA polymerization for extraction and detection. In the present research, the aim was to keep the water droplets stables even after the thermal cycles, so that DNA can be optically detected *in situ* inside the water droplets for better identification and quantification effectivity. However, to achieve that level of optical detection and to allow uninterrupted DNA polymerization inside the droplets, the water droplets size needs to be between 80 – 100 μm. Therefore, experiments were designed with the aim to develop thermally stable W/O emulsions with water droplet sizes between 50 – 100 μm by modifying the emulsifiers and viscosity of the continuous phase. In this work,

we focused on the development of the W/O emulsions that could be suitable for ddPCR, not the actual application with DNA polymerization.

3.3 Materials and methods

3.3.1 Materials

Light mineral oil (L, code O121-4) and heavy mineral oil (H, code O122-4) were purchased from Fisher Scientific (Toronto, ON, Canada). Polyglycerol polyricinoleate (PGPR, IMWITOR 600) was provided by SASOL North America (Houston, USA). Non-ion emulsifier Span 80 (sorbitan monooleate), anionic emulsifier sodium bis (2-ethylhexyl) sulfosuccinate (Aerosol-OT, AOT, molecular weight: 444.56 g/mol., purity 97%), bovine serum albumin (BSA, code A2058, lyophilized powder, isoelectric point (IEP) at pH 4.7-4.9) and Nile red were obtained from Sigma-Aldrich (Oakville, ON, Canada). Purified water by Milli-Q^{TM} (Millipore Corporation, MA, USA) was used for the dispersed phase. Tris hydrochloride (Tris HCl, ultra-pure grade > 99.5%) was purchased from G-Biosciences (Edmonton, AB, Canada). Potassium chloride (KCl) and magnesium chloride ($MgCl_2$, $6H_2O$) were purchased from VWR (Edmonton, AB, Canada). Sodium hydroxide (NaOH) was purchased from BDH (Toronto, ON, Canada).

3.3.2 Preparation of solutions

The aqueous phase contained 10 mM Tris HCl, 50 mM KCl, 5 mM $MgCl_2$, 0.5 mg/ml BSA, and the pH was adjusted at 8.3 ± 0.02 with 1M NaOH to simulate the condition for DNA polymerization. The pH is optimized between 8 – 8.6 to obtain high DNA yield (Kovárová & Dráber, 2000). BSA is used as an additive in the PCR buffer to limit any inhibitors and increase amplification yields of DNA (Farell & Alexandre, 2012). An aqueous control phase consisting of everything except BSA was also used in emulsion preparation to understand the effect of BSA's surface activity on emulsion formation and stability. The oil phase with light mineral oil, heavy mineral oil or their mixtures was prepared with the emulsifier. Different concentrations of PGPR (0.2 – 10%) and Span 80 (2 – 10%) were mixed with the oil via magnetic stirring for 2 hours at 400 rpm at room temperature. For AOT (0.3 – 10%), the emulsifier and the oil were heated for 15 minutes at 60 °C at the same stirring conditions followed by cooling down at room temperature for 2 hours. Both oils and aqueous phases were stores at 4 °C before emulsification.

3.3.3 Preparation of water-in-oil emulsions

Coarse W/O emulsions were prepared with 80% v/v (80 μL) oil phase and 20% v/v (20 μL) aqueous phase in 0.2 mL thin-walled vials with flat caps (Thermofisher, Toronto, ON, Canada). The oil phase was

added into the vial, and the aqueous phase was added dropwise using a micropipette (VWR, Edmonton, AB, Canada). The vials were placed in an accessory holder for 8 vials fixed to an analog vortex mixer (VWR, Edmonton, AB, Canada), and the emulsification speed was set at 10 (3200 rpm) for 2 minutes. Fresh emulsions were placed immediately into the thermal cycler.

3.3.4 Experiment design for emulsifier and oil selection

The influence of emulsifiers on emulsion stability and water droplet size distribution was determined as a function of types and concentrations. Each emulsifier was tested in a range of concentrations, as mentioned before, to form coarse emulsions. Each emulsifier had a different concentration range due to their different emulsification ability. After emulsifier selection, the effect of bulk oil viscosity on the formation and stability of coarse water droplets was investigated. To test the effect of continuous phase viscosity, various mixtures of L and H were used as emulsifier continuous phase: 100% L (100L), 25% H with 75% L (25H + 75L), 50% of H and L (50H + 50L), 75% H with 25%L (75H + 25L), and 100% H (100H).

3.3.5 Thermal cycles and emulsion stability

All fresh W/O emulsions were visually checked for uniformity and stability before they were exposed to thermal cycles. If an emulsion had a visually separated layer of free water at the bottom of the vial, it was discarded. Freshly prepared stable emulsions in 0.2 mL vials were placed in a PCR thermocycler with 16 wells (model MA 1620Q, Suzhou Molarray Co. Ltd., Suzhou City, China). The thermal treatment started at 95 °C for 30 seconds, then 40 cycles at 60 °C for 30 seconds, followed by one cycle at 95 °C for 30 seconds and finally at 60 °C for 1 minute. The samples were then moved into a refrigerator for 15 minutes to cool down at 4 °C for image analysis. The emulsions were considered thermally stable when emulsions did not show any aqueous phase separation at the bottom of the vial. Photographs of fresh and after thermal treatment emulsions were recorded with an iPhone 8's camera (12 MP) to identify emulsion stability.

3.3.6 Determination of emulsion droplet size

The droplet size distribution of stable W/O emulsions was determined by image analysis of emulsion microstructure. Nile red (0.1 wt%) was dispersed in the light mineral oil and stirred overnight at 400 rpm. Nile red helps to identify the water droplets in the W/O emulsion, where they appear dark against the bright oil phase in a confocal microscope. The images were taken by exciting the sample with a 543 nm laser and collecting the emission spectra with 573 – 613 nm filter using a confocal microscope (Nikon Eclipse E400, Nikon Canada, Mississauga, ON, Canada). Fresh and thermally stable emulsions (200 μL)

were mixed with 5 μL of the Nile red solution (0.0025 wt% Nile red in the final emulsion). A drop of the sample was added over a glass microscope slide (VWR, Edmonton, AB, Canada), and a coverslip was placed over the sample. About 15 to 20 images were taken for every emulsion with the confocal microscope with both 10x and 20x objectives lens. The images were analyzed with ImageJ (v1.5 2i – Fiji project) (Schindelin et al., 2012). A scale was set according to the image bar, and the image type was modified to 8 bits, and the threshold was changed to black and white. The parameters chosen for image analysis were a droplet size range from 0 to infinity, droplets circularity was selected from 0.7 – 1, and the droplets on the image's edges were excluded. The droplets' area data were exported to an Excel spreadsheet (Microsoft, Office 365), and further calculation was done to obtain droplet diameters. Data from all the replicates were combined for droplet size distribution in Excel spreadsheets. Also, the volume means diameter (De Brouckere mean, $d_{4,3}$) was calculated based on Equation 3.1, where n is the number of droplets. For each emulsion prepared with PGPR n ranged from 1000 – 2000 and while for the ones prepared with AOT, n was between 300 – 800.

$$d_{4,3} = \frac{\sum_1^n d^4}{\sum_1^n d^3} \tag{3.1}$$

3.3.7 Determination of interfacial tension

A force tensiometer (K20 by Krüss GmbH, Hamburg, Germany) with a Wilhelmy plate (20 x 10 mm) was used to determine oil/water interfacial tension. A sample of oil (65 mL) with PGPR or AOT was added to a wide-mouth glass beaker (130 mL). The Wilhelmy plate was moved down to be completely immersed in the oil phase, and the position was tared. The plate was then moved up, cleaned with acetone (A18-4, Fisher, US) and flamed with a butane torch (Bernzomatic, OH, USA). A sample of the aqueous phase (22 mL) was added to another similar glass beaker and placed over the stage. The plate was moved to reach the Wilhelmy plate, and the system was set at zero position. Then, the previously used oil phase was added with a pipette (VWR, Edmonton, AB, Canada) to fill at the tare. Finally, at zero position, interfacial tension measurements were performed until a standard deviation of 0.1 mN/m could be reached between subsequent measurements. For the determination of critical micelle concentration (CMC), different concentrations of emulsifiers were dissolved in the oil phase, and the interfacial tension measured against an aqueous phase was plotted against emulsifier concentration. The intersection point from the slope of the two distinct portions of the graph was used to find the CMC beyond which no changes in interfacial tension was observed.

3.3.8 Determination of interfacial rheology

The interfacial strength between the oil and aqueous phase was measured using an AR-G2 rheometer (TA Instruments, Montreal, QC, Canada) at 25 °C using a Du Nouy ring (10 mm diameter). A wide-mouth glass beaker (70 mm diameter) was placed onto the stationary plate of the rheometer, then the aqueous phase (40 mL) with or without BSA was gently added into the cup. The geometry was moved down to the surface of the aqueous phase. An equal volume of oil with PGPR or AOT was gently added with a pipette (VWR, Edmonton, AB, Canada) to form the W-O interface. The step time was set up to allow the interface formation for 1.5 hours while the interfacial storage (G') and loss moduli (G") were recorded at a constant oscillation strain (0.01 to 1000%) and frequency (0.1 rad/s).

3.3.9 Viscosity of the oil phase

The viscosity of mineral oils and its mixtures were measured using the AR-G2 rheometer (TA Instruments, Montreal, QC, Canada) at 25 °C as a function of shear rate from 0.01 to 100 s^{-1} and loading gap of 500 μm using an acrylic parallel plate (60 mm diameter).

3.3.10 Statistics

Emulsions were prepared in triplicates, and the image analysis of water droplets was done on each replicate to calculate the $d_{4,3}$. Interfacial tension was also measured in triplicate. The three means were analyzed with one-way Anova to determine the statistical significance. The viscosity of oils and the interfacial rheology was measured in duplicate and analyzed with T-Test to determine the statistical significance using IBM SPSS Statistics 20.

3.4 Results and Discussion

3.4.1 Influence of sorbitan monooleate on water-in-oil emulsion formation and stability

Span 80 is a small molecule lipophilic emulsifier widely used to develop W/O emulsions (Koneva et al., 2017). It is an unsaturated sorbitan monoester with double-bond in the oleic acid (18:1 *cis*-9) as the hydrophobic tail (Korhonen, Lehtonen, Hellen, Hirvonen, & Yliruusi, 2002a). Span 80 was selected for its large molecular area (37 – 46 $Å^2$) at the interface compared to other Spans and for its liquid state at 25 °C compared to Span 40 (sorbitan monopalmitate) or Span 60 (sorbitan monostearate) (Peltonen et al., 2001). Emulsifier liquid-state was necessary for ease of detection of DNA post-PCR. At first, W/O emulsions were prepared with 2, 5, 7.5 and 10 %v/v Span 80 in light mineral oil (Figure 3.2A). Initially, all emulsions were

stable without any visible phase separation; however, after the thermal cycles, all of them were destabilized with extensive aqueous phase separation (Figure 3.2B). The free water layer appeared at the bottom of the vials along with a top clear oil layer, and a thin middle emulsion layer indicates emulsion destabilization by thermal cycles (Figure 3.2B). Yoshioka, Sternberg, and Florence (1994) hypothesized that the unsaturated branch of Span 80 at the oil-water interface creates open space and allows permeability at the interface leading to water movement between the self-assembled molecules and promotion of coalescence of water droplets which could be enhanced at high temperature leading to water droplet destabilization. The presence of surface-active BSA in the water droplets could also influence Span 80 interfacial film. Gaiti et al. (1994) reported that Span 80 and BSA absorbed together at the interface, forming a complex film by hydrogen bonding and hydrophobic interactions. Holm et al. (2007) showed that an increase in temperature of BSA solution reduced α-helix content while the β-structure increase in the form of BSA unfolding. These conformational changes were reported to be irreversible at 70 ºC and above.

Figure 3.2 Visual observation of W/O emulsions prepared in light mineral oil with Span 80 (2 – 10 % v/v) (A) before and (B) after thermal cycles, and with PGPR (0.2 – 10 % v/v) (C) before and (D) after thermal cycles. All emulsions contained BSA in the aqueous phase. Emulsifier concentration is shown on the image A and C.

In the present case, during thermal cycling, emulsions were heated up to 95 ºC, leading to the irreversible unfolding of BSA, which could reduce hydrogen bonding and hydrophobic interaction with Span 80, thereby destabilizing the O-W interface. Therefore, Span 80's emulsification ability was deemed unsuitable for forming thermally stable emulsions and was discarded from further research.

3.4.2 Influence of polyglycerol polyricinoleate on coarse water-in-oil emulsion formation, microstructure, and stability after multiple thermal cycles

PGPR is an effective emulsifier for W/O emulsion and is widely used in the food industry due to its thermal stability, high surface-activity, ability to form stable water droplets in oil and retain high viscosity even at a higher temperature (Ciriminna et al., 2015). PGPR is a large polymeric molecule – a combination of partial esters of polyglycerol with polyricinoleic acids (Ghosh & Rousseau, 2012). During the initial screening, emulsions were prepared with 0.2 to 10 %v/v PGPR in light mineral oil with BSA in the aqueous phase (Figure 3.2C). All W/O emulsions were thermally stable, except the one with 0.2% PGPR, which demonstrated aqueous phase separation at the bottom of the vial (Figure 3.2D). The vials with a white emulsion phase at the bottom and a transparent oil layer at the top indicate that the water droplets have sedimented without any visual aqueous phase separation; hence, these emulsions were considered thermally stable. From 1 to 10 %v/v PGPR in light mineral oil, the average volume droplet diameter ($d_{4,3}$) was 7 – 9 μm, while with 0.3 – 0.8% PGPR in light mineral oil, $d_{4,3}$ ranged from 19.4 – 45.2 μm (data are not shown). As mentioned before, a critical requirement in the development of thermally stable water droplets as a DNA bioreactor for digital PCR is that the minimum size of water droplets should be 80 – 100 μm, for subsequent optical detection of DNA from each droplet. As shown in Figure 3.2D, PGPR could form a thermally stable emulsion, but the droplet size was too small.

Lower PGPR concentration in the oil phase could increase the water droplet size, but it would be difficult to keep the droplets stable and suspended in the oil phase. Hence, the oil phase viscosity was increased by mixing different concentrations of high viscosity heavy mineral oil (H) with low viscosity light mineral oil (L), while keeping the PGPR concentration in the lowest possible range. The viscosity of H and L mixtures is shown in Figure 3.3. The viscosity of 100% L (100L) was 44.8 ± 0.73m Pa.s, while the viscosity of 100% H (100H) was 143.8 ± 0.83 mPa.s. The viscosity of the oil mixtures increased with the increase in H concentration. W/O emulsions were prepared with all of these oil mixtures using 0.2 to 0.4 %v/v PGPR. To understand BSA's influence on PGPR's interfacial interaction and emulsion stability, the emulsions were prepared with and without the presence of BSA in the water droplets. All the treatments with 0.2 %v/v PGPR were thermally unstable (data are not shown).

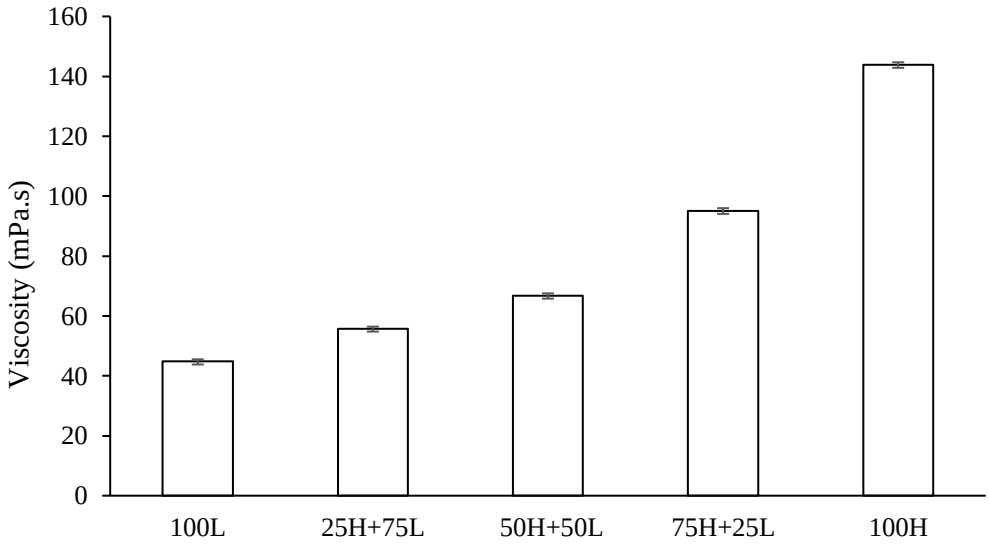

Figure 3.3 Newtonian viscosity of light (100L) and heavy (100H) mineral oil and their mixtures. Oil mixtures are expressed by their composition. For example, 25H+75L represents 25% L and 75% H mixture.

Emulsions formed with 0.3 and 0.4 %v/v PGPR were stable after the thermal cycles only with the oil mixtures 50H + 50L (viscosity 66.8 ± 0.75 mPa.s) and 75H + 25L (viscosity 95.1 ± 0.91 mPa.s) (Figure 3.3A, B). However, with the oil phases 100L, 25H + 75L or 100H, the emulsions destabilized after the thermal cycles with visible aqueous phase separation at the bottom of the vials (Figure 3.4A, B). Sengupta, Walker, and Khair (2018) analyzed the absorption-desorption behaviour of emulsifiers from the interface to the bulk phase based on convection and diffusion mechanism. The authors proposed that in the presence of an external flow field (such as temperature fluctuation-induced flow), surfactant transport from the bulk phase to the interface is driven by convection in addition to diffusion-controlled mass transport. When surfactant molecules are very close to the interface, they adsorbed and set up an adsorption-desorption equilibrium. The adsorbed surfactants also undergo lateral re-distribution at the interface due to external convective movement, leading to Marangoni flow, which along with their movement towards the interface, tends to create a uniform molecular distribution at the water droplet surface. An increase in bulk oil phase viscosity beyond a critical value could prevent Marangoni flow leading to a non-uniform surfactant distribution and the formation of bare-patches devoid of any surfactant at the interface (Sengupta et al., 2018). In the present case, such bare-patches on the interface could be the reason for droplet coalescence for emulsions with high viscosity oil phase (100H) under intense temperature fluctuation. Therefore, the two opposing factors of increasing continuous phase viscosity (improved stability due to restricted droplet

movement and increased droplet coalescence due to reduced movement of surfactant at the interface) could establish a critical range of viscosity where optimization of both factors could lead to a stable emulsion. We propose that such optimization happened in the present case when the oil phase viscosity was more than 60 mPa.s and less than 100 mPa.s (for the oil mixtures 50H + 50L and 75H + 25L), thereby forming thermally stable emulsions.

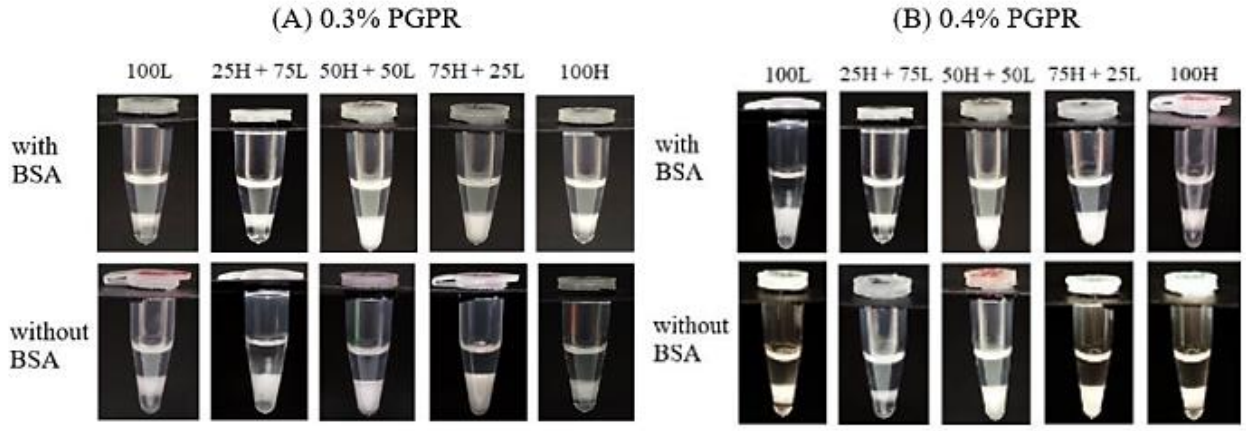

Figure 3.4 Visual observation of W/O emulsion prepared with (A) 0.3 and (B) 0.4% v/v PGPR in different percentages of light mineral oil (L) and heavy mineral oil (H) after thermal cycles with and without the presence of BSA in the aqueous phase.

PGPR is known to interact at the interface with proteins. Gülseren and Corredig (2012) showed that a constant concentration of PGPR (0.008 wt%) at the soybean oil-water interface produced different interfacial tensions with β-lactoglobulin (7.3 mN m^{-1}) and sodium caseinate (3.1 mN m^{-1}). In this case, we have BSA in the aqueous phase, which might interact with PGPR at the interface. Therefore, PGPR CMC was determined to understand how the oil phase viscosity and the presence of BSA in the water droplets influence PGPR interfacial adsorption with (Figure 3.5A) and without BSA (Figure 3.5B). The two mixtures of mineral oils (50H + 50L and 75H + 25L), exhibiting thermal stability, were used for these experiments. CMC of PGPR with BSA in the aqueous phase (Figure 3.5A) decreased from 0.33 ± 0.02 wt% to 0.23 ± 0.01 wt% when the viscosity of the oil phase increased. However, the interfacial tension at CMC was not significantly different (4.20 ± 0.4 mN m^{-1}). Without BSA in the aqueous phase, PGPR CMC further decreased to 0.22 ± 0.01 wt% against both oil mixtures. The interfacial tension at CMC was 5.05 ± 0.03 mN m^{-1} for 50H + 50L and 4.31 ± 0.86 mN m^{-1} for 75H + 25L, higher than that with BSA.

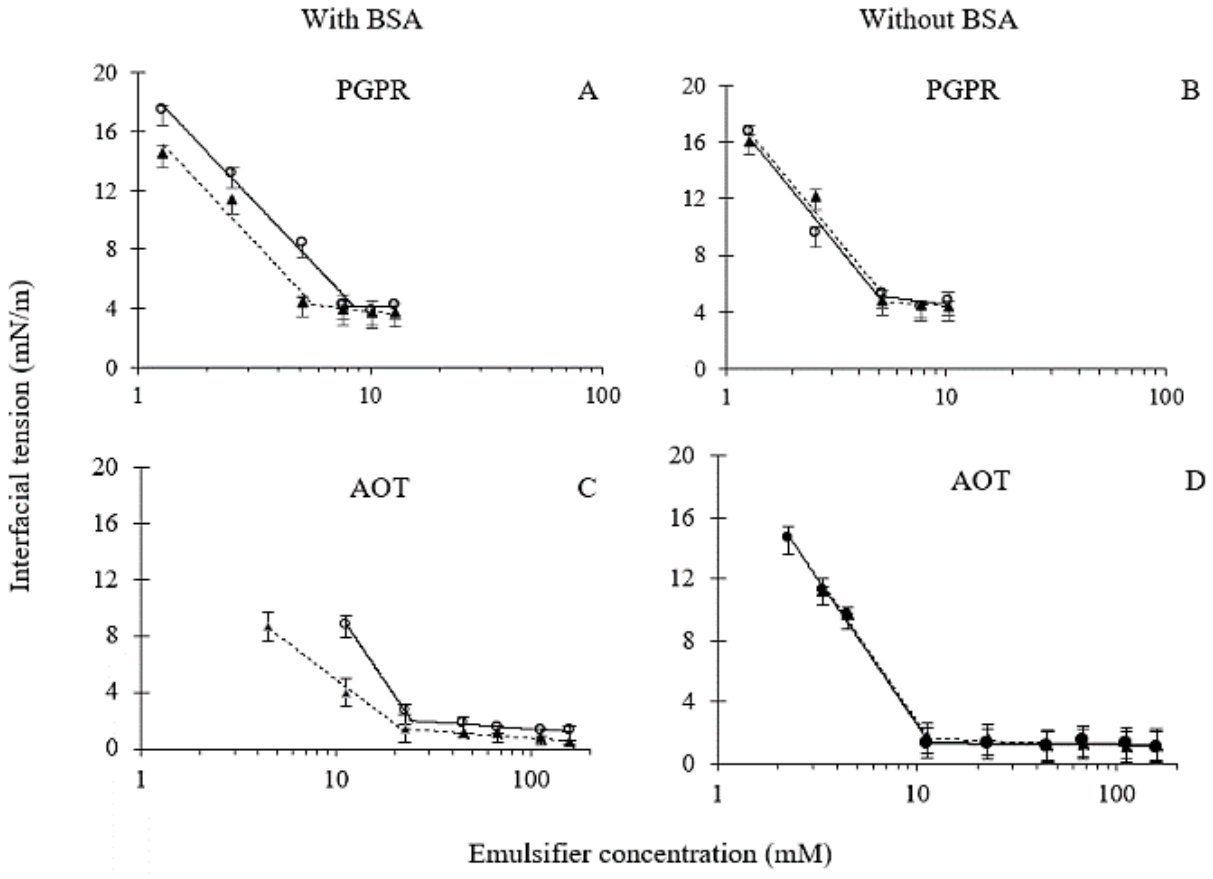

Figure 3.5 Critical micelle concentration (CMC) of PGPR (A, B) and AOT (C, D) with BSA (A, C) and without BSA (B, D) in the aqueous phase, respectively. The emulsifiers were dissolved in two different oil phases containing 50% H + 50% L (○ 50H + 50L) and 75% H + 25% L (▲75H + 25L). Note the difference in the X-axis scale for PGPR and AOT.

From the CMC data, it can be said that in the presence of BSA, a lower concentration of PGPR was required to saturate the interface for the oil with higher viscosity, while without BSA in the aqueous phase, no significant effect of oil viscosity was observed. If we consider just the 50H + 50L oil mixture, PGPR with BSA had higher CMC than without BSA, which means that in the presence of BSA, PGPR's interaction with the protein forces them in a more compact structure such that more PGPR can be accommodated to saturate the interface. However, when the viscosity of the continuous phase increased (75H + 25L), PGPR's CMC with BSA became similar to that without BSA. The higher viscosity might impact reducing the emulsifier mobility at the interface. Restricted mobility could lead to a more stretched conformation of individual PGPR molecules at the interface and surface saturation at a lower concentration.

PGPR's adsorption at the interface can also be estimated from interfacial strength. The interfacial storage modulus (G') for PGPR with and without BSA is shown in Figure 3.6. In the presence of BSA and 0.3 %v/v PGPR, interfacial G' was 0.30 ± 0.05 and 0.35 ± 0.05 N/m for 50H + 50L and 75H + 25L, respectively. However, without BSA, G' decreased significantly to 0.21 ± 0.01 N/m. In the presence of BSA with 0.4 %v/v PGPR, interfacial G' was 0.26 ± 0.07 and 0.15 ± 0.01 N/m for 50H + 50L and 75H + 25L, respectively, which again decreased significantly when BSA was absent (0.09 ± 0.01 N/m). These values indicate that higher interfacial strength can be developed by the presence of both BSA and PGPR at the interface and their interactions.

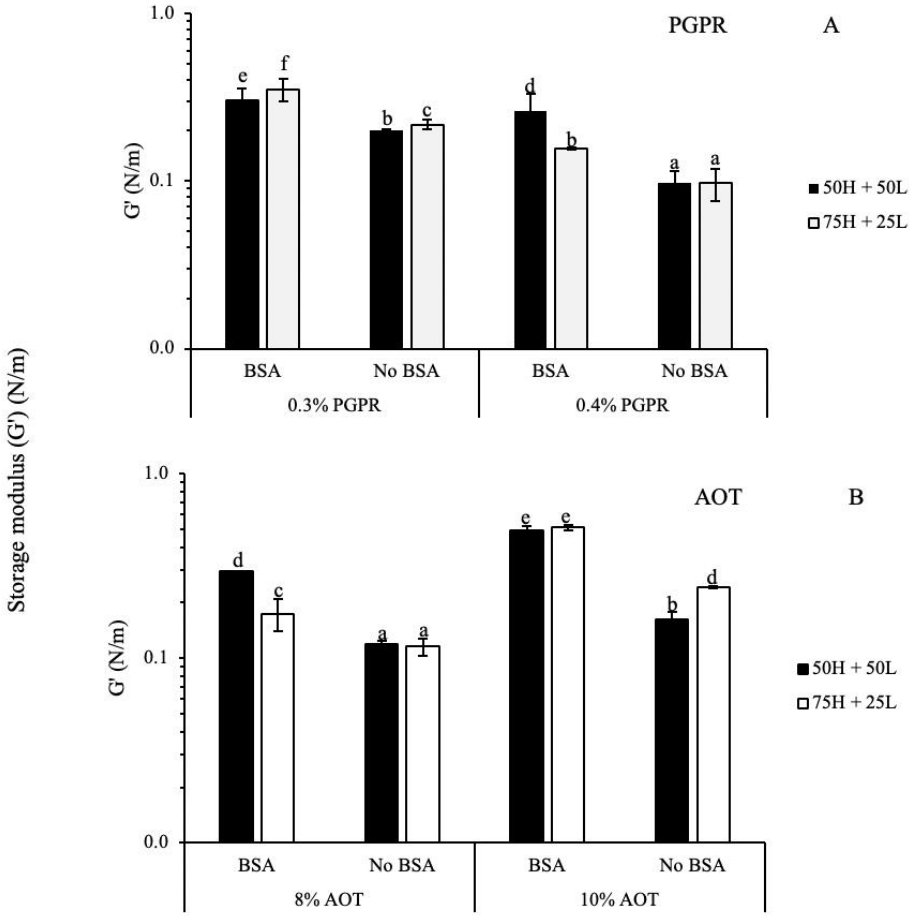

Figure 3.6 Storage modulus (G') from interfacial rheology with (A) PGPR and (B) AOT, which were absorbed in the interface for 1.5 hours. The aqueous phase was tested with and without BSA. The emulsifiers were dissolved in two different oil phases containing 50% H + 50% L (■ 50H + 50L) and 75% H + 25% L (□75H + 25L). Treatments with the same letter do not differ significantly ($p \geq 0.05$), according to the T-Test.

The microstructure of the thermally stable W/O emulsions with 0.3 and 0.4 %v/v PGPR in 50H + 50L and 75H + 25L oil mixtures were captured using a confocal microscope before and after the thermal cycles. In Figure 3.7, microscopy results of emulsions after thermal cycles are shown. In all micrographs, dark water droplets (no fluorescent dye added) of various sizes were dispersed in the bright bulk oil phase (stained with Nile red).

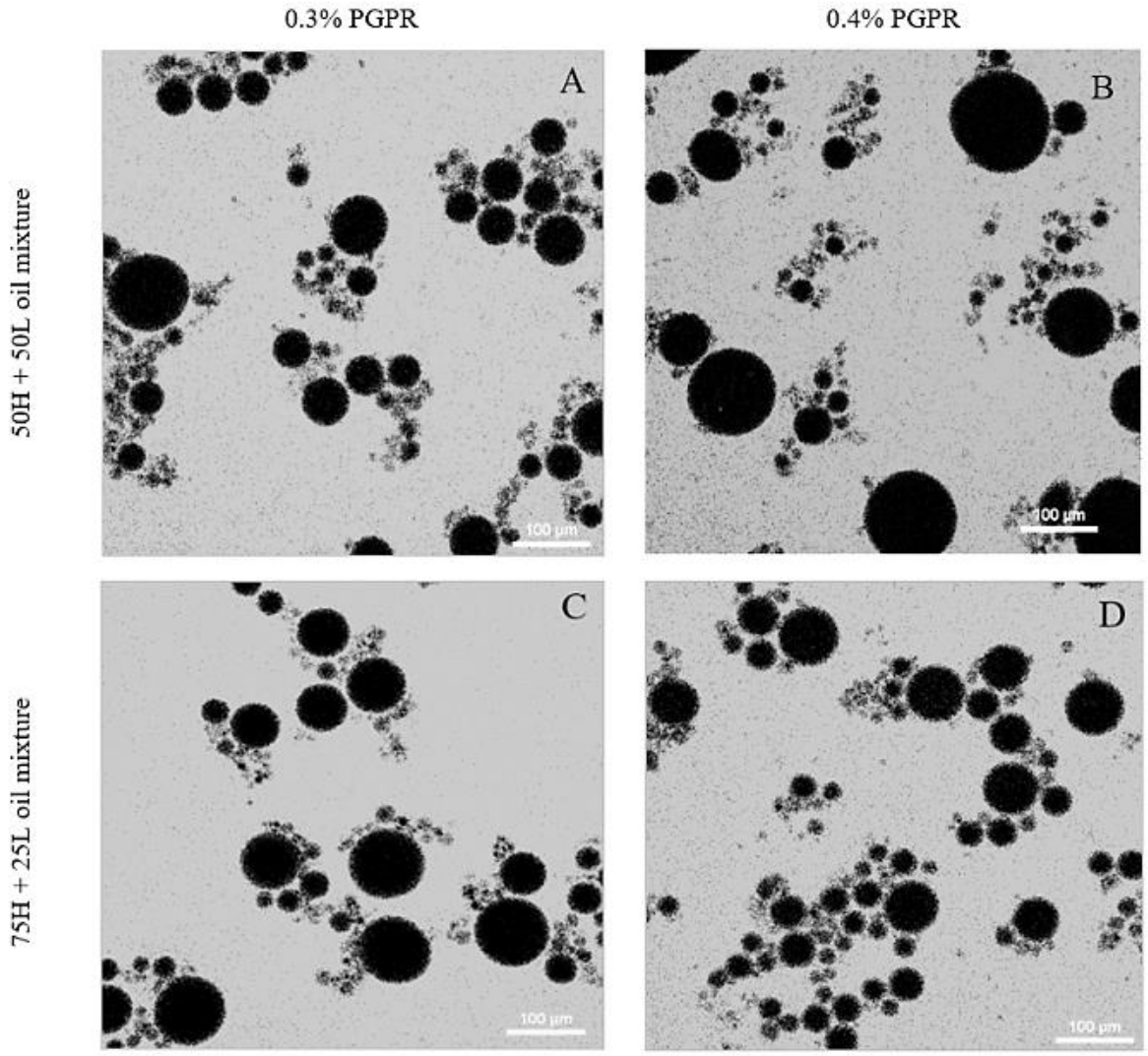

Figure 3.7 Confocal microscopy of W/O emulsions after the thermal cycles with 0.3% PGPR in (A) 50H + 50L, and (C) 75H + 25L oil mixtures, and 0.4% PGPR in (B) 50H + 50L and (D) 75H + 25L oil mixtures. Emulsions were prepared with BSA in the aqueous phase (scale bar: 100 µm).

The presence of both large and small water droplets are visible, and no apparent difference in droplet size could be observed from the various micrographs. The volume average droplet diameters ($d_{4,3}$) were calculated using image analysis to get a quantitative estimation of average droplet size before and after thermal cycles (Figure 3.8).

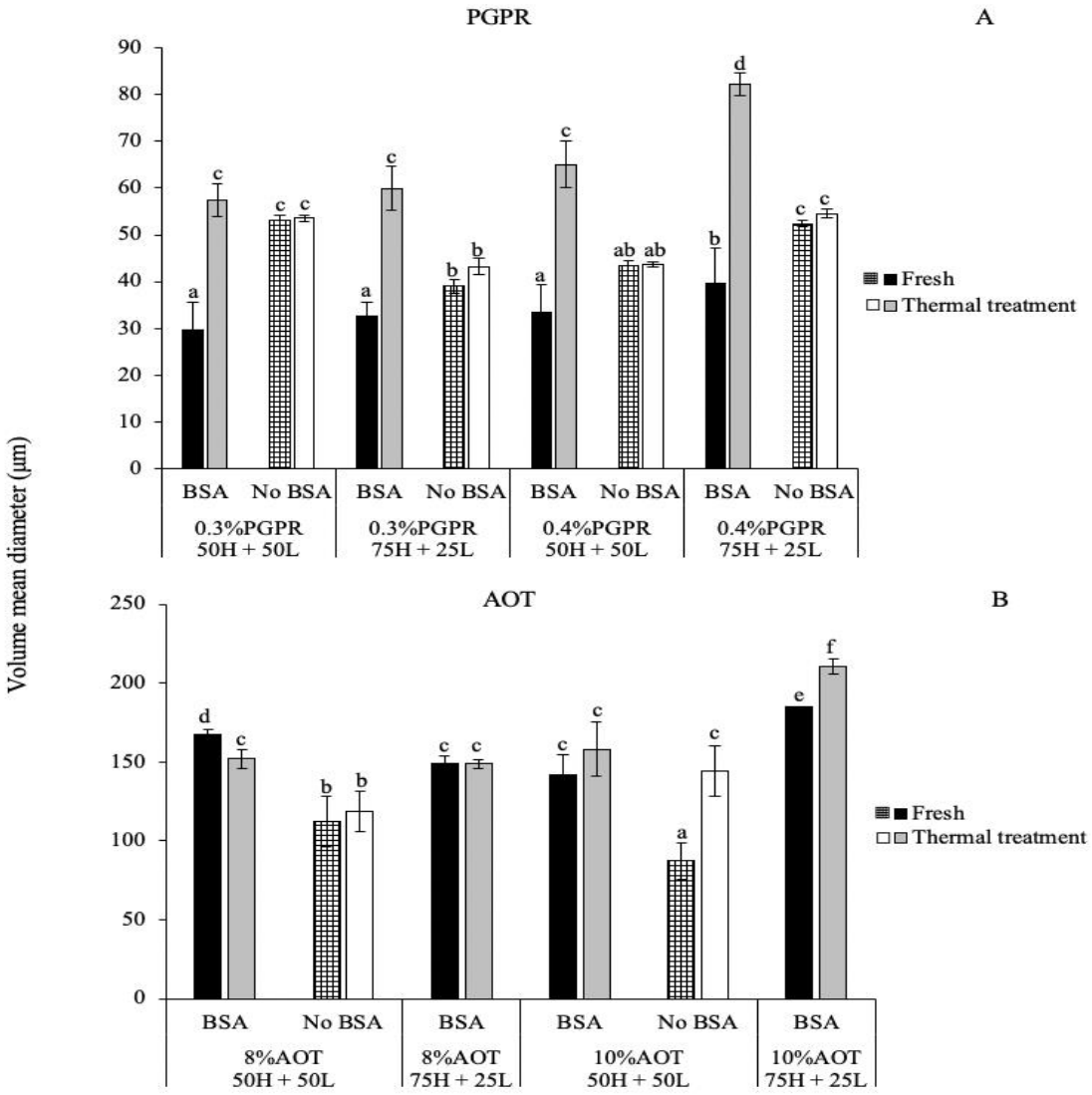

Figure 3.8 The volume means diameter (d_{43}) of water droplets in PGPR (A) and AOT (B) stabilized W/O emulsion before (▦ ■ Fresh) and after thermal treatment (□ ■ Thermal treatment) with and without BSA in the aqueous phase. Emulsifiers concentrations were dissolved in two different oil phases containing 50% H + 50% L (50H + 50L) and 75% H + 25% L (75H + 25L). Treatments with the same letter do not differ significantly ($p \geq 0.05$) according to Tukey's test.

For all fresh emulsions prepared with BSA, no significant effect of PGPR concentration or continuous phase viscosity on droplet size was observed. All of them showed an average droplet diameter in the range of 30 – 40 μm. When BSA was not present in the aqueous phase, a significant increase in water droplet size was found for all fresh emulsions compared to the ones with BSA. For example, for the emulsions stabilized with 0.3 %v/v PGPR in 50H + 50L oil mixtures, the average droplet size increased from 29.7 ± 6 μm with BSA to 53.1 ± 1 μm without BSA. Hence, higher CMC and the ability to pack a higher number of PGPR molecules at the interface with BSA (Figure 3.5A) was helpful in lowering the interfacial tension and creating smaller droplet sizes compared to the emulsions without BSA.

Smaller droplet size for emulsions and the presence of BSA at the interface could not prevent some water droplet coalescence during thermal cycles. All emulsions with BSA showed a large increase in $d_{4,3}$ after the thermal cycles. However, for the emulsions without BSA, although with larger droplet sizes than the ones with BSA, no significant change in $d_{4,3}$ was observed after thermal cycles (Figure 3.8A). For example, average droplet size increased from 29.7 ± 6 μm to 57.4 ± 3.6 μm upon thermal cycling of the emulsions with BSA stabilized with 0.3 % v/v PGPR in 50H + 50L oil mixtures ($p < 0.05$). In contrast, the average droplet size of similar emulsions without BSA changes from 53.1 ± 1 μm to 53.6 ± 0.7 μm upon thermal cycling ($p > 0.05$) (Figure 3.8A). During thermal cycles, the BSA suffers heat-induced denaturation and forms irreversible aggregates (Green, Hopkinson, & Jones, 1999), possibly damaging the interfacial adsorption of PGPR and coalescence of water droplets. Nevertheless, although there was an increase in droplet size after thermal cycles, the emulsions (with BSA) remained stable without any visible aqueous phase separation (Figure 3.2A, B), indicating their potential successful application in ddPCR.

3.4.3 Influence of sodium bis (2-ethylhexyl) sulfosuccinate as an emulsifier for thermally stable water-in-oil emulsions

AOT is a branched anionic oil-soluble emulsifier. It has two ethyl-hexyl non-polar hydrocarbon chains attached to a sulphosuccinate group. AOT was selected for its non-polar branched chains, ionic nature, thermal stability and efficacy to stabilize W/O emulsions (Nave, Eastoe, Heenan, et al., 2000). AOT can form a flexible lamella structure in a wide range of concentrations and temperatures (Poghosyan, Adamyan, & Shahinyan, 2019) and has been used for drug encapsulation in W/O emulsions with chitosan in the aqueous phase (Grenha, 2012). W/O emulsions (containing BSA in the aqueous phase) were formed with 0.3 to 10 wt% AOT in 50H + 50L oil mixture to screen the range of concentration needed for thermal stability (Figure 3.9). Only the emulsions with 8 and 10% AOT were thermally stable. Therefore, further experiments were carried out with 8 and 10 wt% AOT-stabilized W/O emulsions.

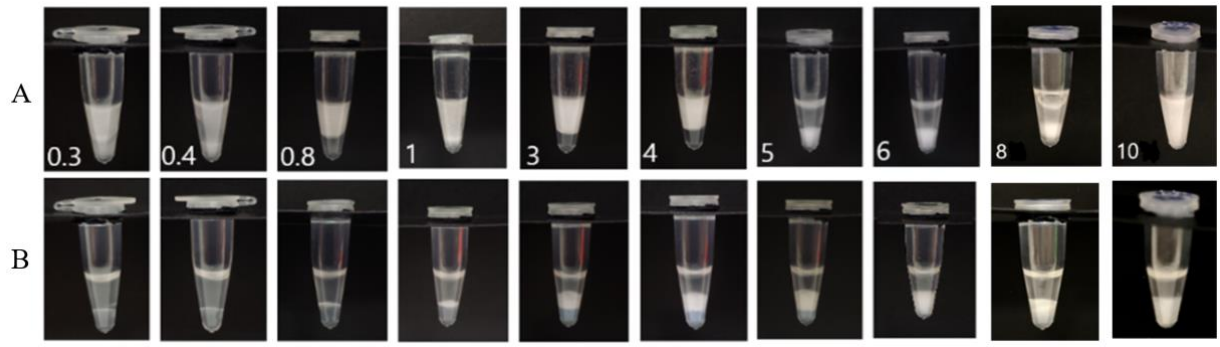

Figure 3.9 Visual observation of W/O emulsions prepared with 0.3 – 10 wt% AOT in a continuous oil phase containing 50% heavy and 50% light mineral oil (50H + 50L) (A) before and (B) after the thermal cycles.

CMC of AOT was measured in 50H + 50L and 75H + 25L oil mixtures with and without BSA in the aqueous phase to understand whether the protein could influence the interfacial absorption of AOT (Figure 3.5C, D). The CMC with BSA in the aqueous phase was 1.05 ± 0.08 wt% and 0.95 ± 0.02 wt% for 50H + 50L and 75H + 25L, respectively ($p > 0.05$), while the interfacial tension at the CMC was 1.98 ± 0.29 mN m^{-1} and 1.29 ± 0.23 mN m^{-1} for for 50H + 50L and 75H + 25L, respectively ($p < 0.05$) (Figure 3.4C). The CMC and the interfacial tension at the CMC without BSA in the aqueous phase were not significantly different for the two oil phases (11.3 ± 0.01, Figure 3.4D). The presence of BSA in the aqueous phase showed a significant increase in AOT CMC, which indicates that BSA allowed better packing and self-assembly of AOT at the interface, perhaps forming a bilayer structure (Stocker et al., 2014). It is possible that interfacial complexation between BSA and AOT led to the compaction of molecular conformation and packing of more AOT at the interface before surface saturation can be reached. Interfacial strength was also analyzed for AOT by measuring interfacial G' with and without BSA in the aqueous phase (Figure 3.6B). Overall, the presence of BSA increased the interfacial strength for both oil mixtures and both AOT concentrations, suggesting BSA's presence at the interface along with AOT.

W/O emulsions with 8 and 10 wt%. AOT in 50H + 50L and 75H + 25L oil mixtures with and without BSA in the aqueous phase were prepared for thermal stability analysis. Emulsions with 75H + 25L at 8% and 10% AOT without BSA were thermally unstable (data not shown), which could be due to lower interfacial adsorption of AOT in the absence of BSA as shown in Figure 3.5D. Micrographs of thermally stable emulsions were collected before and after thermal cycles (Figure 3.10).

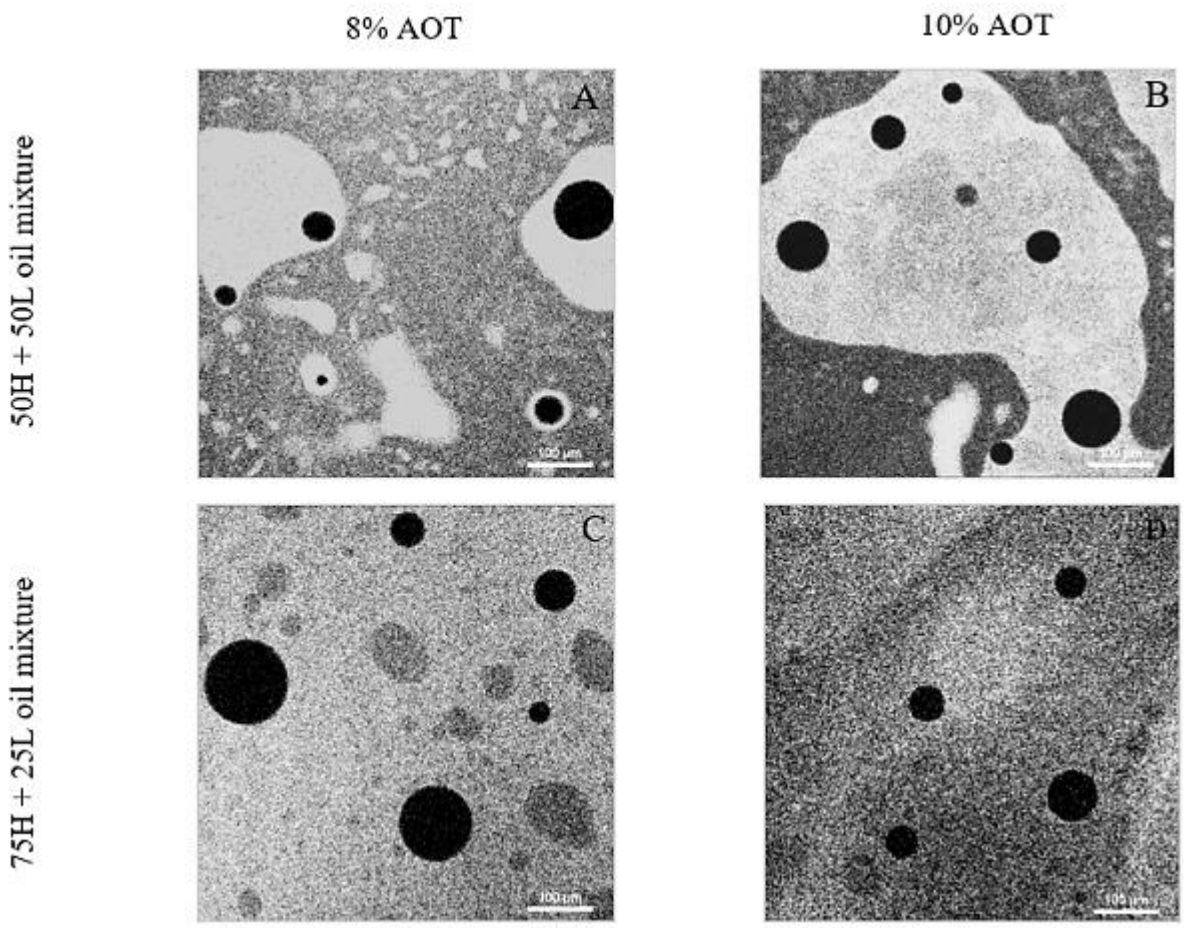

Figure 3.10 W/O emulsions after the thermal cycles with AOT at 8% in 50H + 50L (A), 10% in 50H + 50L (B), 8% in 75H + 25L (C) and 10% in 75H + 25L with BSA in the aqueous phase (bar: 100 μm).

A few large water droplets and the lamella structure dispersed in the bulk phase can be observed in the micrographs. According to Stocker et al. (2014), AOT coexists in both micelles and lamellar phases at ~10 times the CMC. In the present case, thermally stables emulsions were at 8 and 10 wt% in the bulk phase, which is nearly 10 times its CMC, which indicates that AOT was thermally stable using these two-phase regimes and when BSA was present to improve its interfacial packing. The volume average droplet size ($d_{4,3}$) of the emulsions was calculated from image analysis and plotted in Figure 3.8. Fresh emulsions with BSA in the aqueous phase showed average droplet sizes ranging from 142 – 185 μm with both oil mixtures. Upon thermal cycling, no significant change in water droplet size was observed for 8 and 10 wt% AOT in 75H + 25L and 50H + 50L oil mixtures (149 – 152 μm), except for 10 wt% AOT in 75H + 25L, which was

slightly higher (210 ± 5 μm). In the absence of BSA, a significant drop in water droplet size was observed compared to the emulsions with BSA (87 – 112 μm) at both concentrations in 50H + 50L oil mixture, which remained stable after thermal cycling for 8 wt% AOT (119 ± 13 μm); however, with 10 wt% AOT, a significant increase in droplet size was observed (144 ± 16 μm). The presence of BSA in the aqueous phase could lead to interfacial interactions between the positive patches on the protein with negatively charged sulphonate groups of AOT, leading to a complex formation and better interfacial packing (as observed from their higher CMC). The interfacial elasticity of such packing could prevent further droplet breakup during the mild emulsification process, leading to a larger average droplet size for the emulsions with BSA compared to those without BSA. Overall, the droplet sizes for the thermally stable emulsions with AOT were large enough for DNA polymerization and subsequent detection; therefore, they could be used for ddPCR.

3.4.4 Comparison between PGPR and AOT as potential surfactants for water-in-oil emulsion stabilization for digital PCR

The interaction between BSA and PGPR formed stable W/O emulsions with average droplet size in the range of 30 – 40 μm when the continuous phase viscosity was within a critical range. However, during thermal cycling, BSA was affected, and so was its interaction with PGPR, thereby destabilizing the self-assembled interactions at the interface leading to a significant increase in the water droplets size (Figure 3.8A). With AOT, average droplet sizes were much larger compared to PGPR; however, the emulsions with BSA in the aqueous phase were stable against thermal cycling with a minor change in average droplet size (Figure 3.8B). The CMC of AOT in all the treatments was significantly higher (11.3 – 24.1 mM) compared to PGPR (4.9 – 8.5 mM), which means that more molecules of AOT could self-assemble at the interface that could withstand the thermal cycling. This could be due to the larger molecular size of polymeric PGPR in contrast to the smaller size of the AOT molecule. Due to this large size, a much lower concentration of PGPR (0.3 – 0.4 % v/v, which is equivalent to 0.2 – 0.3 wt%) was required to form thermally stable W/O emulsions compared to AOT, which requires 8 – 10 wt% for improved thermal stability.

3.5 Conclusions

Different oil-soluble emulsifiers (Span 80, PGPR and AOT) were used to develop coarse W/MO emulsions, and their stability against multiple thermal cycles was tested for their potential application in ddPCR. All emulsions prepared with Span 80 destabilized upon thermal cycles, while both PGPR (0.2 – 0.3 wt% in oil) and AOT (8 – 10 wt% in oil) formed emulsions with better thermal stability and required average

droplet size (50 – 100 μm). The viscosity of the continuous oil phase was varied by mixing heavy and light mineral oil such that a critical viscosity range was found (66 – 95 mPa.s) where thermally stable emulsions could be formed. The water droplets stabilized with PGPR (average droplet diameter 30 – 40 μm) showed a significant increase after thermal cycles, irrespective of PGPR concentration and oil viscosity. In contrast, the water droplets stabilized with AOT showed minimal disruption after the thermal cycles. However, an excess AOT in the continuous phase was required to form thermally stable emulsions. CMC of AOT was almost five times larger than PGPR, indicating more molecular packing at the interface, which could be responsible for its increased stability against multiple thermal cycles. Further research would be required to test the performance of the two W/O emulsion systems with DNA for ddPCR.

3.6 Connection to the Next Study

In Chapter 3, W/O emulsions were developed with a water solution containing BSA and buffers and a combination of light and heavy mineral oil with PGPR and AOT emulsifiers for biotechnological application in emulsion-PCR to optimize the identification of cancer or other gene mutations. All the conditions were established to permit the aqueous phase to act as bioreactors in microvolume. Thus, the water droplets' sizes had to be large size (50 – 100 μm) for subsequent quantification and identification of polymerized DNA under a microscope. The emulsification was done with a vortex mixer because a high-pressure homogenizer would not be able to form the desired range of large water droplets. Visual analysis of emulsions was performed to identify destabilization. An image analysis procedure was developed for the determination of water droplet size. Interfacial tension and interfacial rheology were measured for each emulsifier and oil viscosity to identify their interaction at the interface.

Chapter 4 was about developing liquid W/O emulsions using a high-pressure homogenizer for cosmetic, skincare, and food applications. The main research question was to address why it is more challenging to stabilize liquid W/O emulsions in vegetable oils than mineral oils. Therefore, the emulsion stability mechanisms in both canola oil and mineral oil-based liquid emulsions were investigated. A food-grade emulsifier was needed for emulsion formation with both vegetable oil and mineral oil. AOT used in the previous study is not frequently used for human consumption, and is restricted only as a wetting agent in dry beverages bases and in sausages casings in parts per million level (Health Canada, 2012); hence it was not considered. PGPR, although food grade, has several restrictions on its use, and there is a greater need to replace PGPR from food products. Therefore, in the second study, food-grade GMO was used as an emulsifier. Although GMO is a very common emulsifier in food, it is known to be quite poor in stabilizing liquid W/VO emulsion due to its stronger interaction with vegetable oil leading to desorption from the water-

vegetable oil interface and emulsion destabilization. Hence, the study's objective was to introduce in the aqueous phase hydroxyl group donating agents, which could form interaction with GMO at the interface and provide improved emulsion stability. Different techniques were used to understand the molecular-level interactions between the emulsifier, water, oils, and the hydroxyl groups donating agents. In this context, differential scanning calorimetry was used to identify the changes in melting enthalpies and temperatures influenced by the additives and the oil type to understand the interfacial interaction. Infrared spectra analysis was done with deuterium oxide to determine the interactions without the confounding effect of water molecules' hydrogen bonding. The wavenumber of GMO polar head groups, carbonyl and lipidic tail was analyzed to reveal the role of interfacial interactions on improving emulsion stability.

4. STABILIZATION OF FOOD-GRADE LIQUID WATER-IN-VEGETABLE OIL EMULSIONS BY MODIFYING HYDROXYL GROUP DONATING AGENTS' INTERACTIONS AT THE OIL-WATER INTERFACE WITH GLYCEROL MONOOLEATE[2]

4.1 Abstract

Liquid water-in-vegetable oil emulsions are difficult to stabilize due to the emulsifier's desorption from the W-O interface owing to their interaction with VO fatty acid carboxylic groups. It was investigated the destabilization mechanism in liquid water-in-canola oil emulsions stabilized with glycerol monooleate and improved emulsion stability by modifying the dispersed aqueous phase composition with hydroxyl group donating agents. As a control, water-in-mineral oil emulsions were also utilized. Different concentrations of agents were added (e.g., citric acid (CA), ascorbic acid (AA), low methoxyl pectin (LMP)) with and without S or Ca to the aqueous phase before emulsification, which enhanced emulsifier binding to the W-O interface. The emulsions were formed by coarse emulsification followed by high-pressure homogenization. Emulsions phase separation, stability against accelerated gravitation, microstructure and viscoelasticity were determined in all samples on day zero and day seven. LMP was able to provide the highest emulsion stability in both oils compared to AA and CA. Mineral oil emulsions exhibited better stability compared to canola oil emulsions. Differential scanning calorimetry and mid-IR spectroscopy were used to understand the mechanism of interfacial interaction and emulsion stability. Water and GMO melting peaks from DSC were analyzed to identify H-bonding strength. Water melting peaks exhibited more H-bonding in MO-emulsions prepared with salts, AA, and Ca than CO. However, LMP emulsions reported a stronger H-bonding with CO than MO. GMO melting peaks with the agents demonstrated significant interaction in CO than MO. IR spectra revealed that LMP formed stronger intermolecular H-bonding than AA, and its molecular structure allowed more order GMO packing at the interface. Overall, the hydroxyl group donating agents interacted with GMO forming H-bonding, mainly depending on the molecular structure, and liquid W/O emulsions improved stability with this research.

[2]Romero-Peña, M. carried out the experiments and wrote the first draft. Ghosh, S. conceptualized, supervised, reviewed, and edited. This manuscript is under preparation for submission to a journal.

4.2 Introduction

Products containing W/O emulsions are widely used in the pharmaceutical, cosmetic, petroleum and food industries. In food, almost all W/VO emulsions have been in a solid or semisolid state (Ushikubo & Cunha, 2014). Their stabilization mechanism has been mainly with fat crystallization as Pickering and network stabilizers (Ghosh & Rousseau, 2011). The emulsifiers used to form W/O emulsions are nonionic lipophilic emulsifiers (e.g., PGPR, Spans, monoglycerides) or hydrophobic solid particles (e.g., silica particles, fat crystals). The selection of emulsifiers is also based on their HLB, which must be low (3 – 6) for efficient stabilization of W/O emulsion. Although stable semi-solid food-grade W/VO emulsions have been successfully developed in margarine, fluid W/O emulsions are difficult systems to stabilize due to sedimentation, coalescence, and emulsifiers desorption from the water droplet interface (Ghosh & Rousseau, 2011; Ushikubo & Cunha, 2014).

Various research groups have worked with different combinations of oil, emulsifiers and aqueous phase ingredients to obtain stable liquid W/O emulsions. Opawale and Burgess (1998) investigated concentrated 50 wt% water-in-light mineral oil emulsions with Span 20, 80, 83 and 85 (1 – 5 %v/v) in the oil and S (0 – 1 M) in the aqueous phase. The addition of S enhanced the stability of the emulsion. However, a decrease in interfacial elasticities was reported with an increase in S. Therefore, a range of S concentration was established for Spans (0.03 – 0.05 M) to obtain an optimum packing of the emulsifier at the W-O interface (Opawale & Burgess, 1998). Scherze et al. (2006) investigated stabilization of 30 wt% water-in-MCT oil emulsion with PGPR (4 wt%) and soy lecithin (2.5 wt%) in the presence of 0.6 % S in the aqueous phase. Interestingly, based on the type of emulsifier, the influence of S was different. For lecithin, S favoured the coalescence of water droplets. However, for PGPR, the incorporation of S was necessary to obtain a stable W/O emulsion (Scherze et al., 2006). Lindenstruth and Muller (2004) investigated 30 wt% W/O emulsions prepared with a 1:1 mixture of olive oil and MCT with 20% soya lecithin. They found that the *cis* double bond of oleic acid needed more space at the W-O interface, which prevented efficient packing of lecithin at the interface (Lindenstruth & Muller, 2004). In another research, Márquez et al. (2010) prepared W/O emulsion (20 – 40 wt% water) using sunflower oil with PGPR (0.2, 0.5 and 1 wt%), an aqueous phase containing various concentrations of Ca and other salts (calcium lactate or carbonate; sodium, magnesium or potassium chloride). The incorporation of any salt allowed emulsion stabilization with higher water content. The stabilization effect of calcium salt was associated with a reduced attractive force between the water droplets and a higher PGPR adsorption density at the water droplets surface. The salts and PGPR stabilizing effect were not associated with rheological properties because emulsions viscoelastic values were reduced by increasing calcium and PGPR concentrations.

Prichapan et al. (2017) prepared 20 wt% W/O emulsions with rice bran oil and stabilized them by rice bran stearin and PGPR. Emulsions without rice bran stearin were highly unstable to phase separation after one day. Phase separation was decreased by incrementing the PGPR concentration (2 to 4 wt%) due to the reduction in water droplet size. The most stable emulsion was prepared with an oil phase containing 45 wt% rice bran stearins, which indicates that the incorporation of rice bran stearin was more efficient than increasing the PGPR level to enhance emulsion stability.

PGPR is one of the most commonly used emulsifiers to develop food-grade W/O emulsions for its ability to stabilize water droplets by physical barrier (Mettu, Wu, & Dagastine, 2018). It is classified as GRAS. In 1979, the Scientific Committee for Food of the European Community determined an acceptable daily intake of 7.5 mg/kg body weight. In 1980, the Canadian Regulations reduced the maximum concentration of PGPR to 0.25% in chocolate products (Wilson, van Schie, & Howes, 1998). However, in 2017, PGPR was limited just for chocolate products with a maximum of 0.5% (Health Canada, 2017). For this reason, different groups investigated various combinations of PGPR with other ingredients to optimize a lower concentration for W/O emulsion (Ghosh & Rousseau, 2009; Rafanan & Rousseau, 2017).

The present study investigated the complete replacement of PGPR by GMO in the development of stable liquid food-grade W/VO emulsions without the use of any stabilizing fat crystals. Due to the adverse health effect, there is a high demand to reduce saturated fat in our food. However, to our knowledge, no research so far has looked into stabilizing liquid W/VO emulsions without using PGPR and fat crystals. GMO is a widely studied low HLB (3 – 4) emulsifier that is non-toxic, biodegradable, and classified as GRAS. However, despite their excellent emulsification ability, liquid W/VO emulsions prepared solely with GMO are impossible to stabilize due to GMO's desorption from the water droplet interface towards the VO. Ghosh and Rousseau (2011) observed that GMO desorption from the W-O interface strongly relies on hydrogen bonding interactions with the VO's fatty acid carboxylic groups being stronger than the hydrogen bonding interaction with water hydroxyl groups. The authors also showed that, in the presence of a hydrocarbon oil (such as mineral oil), GMO could very well remain at the water droplet surface due to the lack of interaction with the oil, thereby improving emulsion stability. Therefore, we hypothesized that by providing molecules in the dispersed aqueous phase that could form stronger hydrogen bonds at the W-O interface than the continuous VO, we would be able to increase GMO's interaction at the interface, thereby improving the stability of the W/VO emulsions. Three different hydroxyl group donating agents (two small molecules with multiple carboxylic groups, AA, and CA and one biopolymer, LMP, with or without the presence of salts, S or Ca were investigated to enhance the interaction of GMO at the water-oil interface and improve the stability of W/CO emulsions. As a control, light mineral oil (made of saturated

hydrocarbon) was also used to form W/MO emulsions, and their effect was compared to the effect of the presence of carboxylic groups in canola oil on emulsion destabilization. Emulsion droplet size, stability against gravitational separation, and rheology were determined as a function of time. Mechanism of interaction of GMO molecules with oil, water and the hydroxyl group donating agents at the water-oil interface was also investigated with infrared spectroscopy and thermal analysis and by determining their interfacial tension.

4.3. Materials and methods

4.3.1 Materials

Canola oil (CO) was purchase from a local grocery store and stored at 4 °C. Distilled monoglycerides DMG 0298 (90 – 95% monoglycerides, 75 – 91% oleic, 2 – 17% linoleic, 3 – 6% stearic, 3 – 5% palmitic, 0.5 – 2% behenic, 0.1 – 0.5% eicosenoic, 0.2 – 0.5% arachidic, 0 – 0.3% linolenic, <0.5%myristic acid, <0.5% palmitoleic) was donated by Palsgaard® (Juelsminde, Denmark). L-ascorbic acid (AA) and Nile red were purchased from Sigma Aldrich (Oakville, ON, Canada). Citric acid anhydrous (CA), light mineral oil (MO, code O121-4), deuterium oxide (99.8%) and hydrochloric acid (HCl) (1 N) were purchased from Fisher Scientific (Toronto, ON, Canada). Sodium chloride (S) and calcium chloride (Ca) were obtained from BDH (VWR International, Edmonton, AB, Canada). Low methoxyl pectin amidated, Genu® pectin type LM-101 AS (LMP, degree of esterification 36% and degree of amidation 14%, carbohydrate 83%, moisture 12%, protein 3% and ash 2%) was provided by CP Kelco (Lille Skensved, Denmark). Purified water by Milli-Q^{TM} (Millipore Corporation, MA, USA) was used for the dispersed phase.

4.3.2 Preparation of solutions

Three different aqueous phases were prepared for the W/O emulsions. AA and CA aqueous solutions were dissolved at 0.125, 0.5, 2 and 4 wt% with S at 0, 0.125, 0.5 and 1 wt% at room temperature with stirring at 400 rpm. LMP solutions at pH 3.0 ± 0.2 with 1N HCl were prepared at 1, 1.5 and 2 wt% LMP with or without Ca at 0.045 wt% at 90 ± 0.5 °C, stirred at 200 rpm for 20 min. The final LMP solutions were cooled down to room temperature before the W/O emulsions preparations. The zeta potential of LMP, measured at pH 3.0 using a zeta potential analyzer (Litesizer500, Anton Paar, Montreal, QC, Canada), was -18.68 ± 0.2 mV. Control solutions with just S at 0.125, 0.5 and 1 wt% and Ca at 0.045 wt% were also prepared using similar methods. All the solutions were prepared the same day as emulsions. The pH and conductivity of the aqueous solutions were determined with a pH/ conductivity meter (Orion Star A215,

Thermo Scientific, MA, USA) at room temperature. The oil phase was prepared by dissolving 4 wt% of GMO in canola oil (CO) or mineral oil (MO) under stirring (400 rpm) at 60°C for 25 min.

4.3.3 Preparation of water-in-oil emulsions

The aqueous and oil solutions were warmed at 40 ± 2 °C before weighting. The oil phase (70 g, 80 wt%) was weighed in a glass beaker (100 mL), and the aqueous phase (17.5 g, 20 wt%) was added dropwise while stirring at 400 rpm. The same weight of each phase and glass beaker was used for all emulsion batches. Coarse emulsification was done with a rotor-stator blender (Polytron, Brinkman, ON, Canada) at level 10 for 1 minute. The blender was pre-heated with the bulk oil phase (CO or MO) kept at 50 ± 2 °C. The coarse emulsions were then further homogenized in a high-pressure homogenizer (Emulsiflex C3, Avestin Inc., Ottawa, ON, Canada) at 20,000 psi for three cycles. The homogenizer was pre-heated by-passing hot oil (CO or MO, 50 ± 2 °C) at 20,000 psi to reach 70 °C. Preliminary experiments showed that three cycles were enough to reduce the droplet size, and after that, not further decrease was observed. The final emulsions were collected in 250 mL beakers and cooled down at room temperature while stirring with a magnetic stirrer (size 3.5 x 0.7 cm) at 290 rpm for 20 minutes.

4.3.4 Emulsion storage stability

Fresh sample emulsions (25 ± 0.5 mL) were transferred to 40 mL clear glass vials (VWR International, Edmonton, AB, Canada) and stored at room temperature for seven days. The images were taken with an iPhone 8's camera (12 MP). The images of the vials were used to measure the height of the emulsion layer on day 0 and after seven days with ImageJ (v1.5 2i – Fiji project) (Schindelin et al., 2012) to calculate the fraction of emulsion height (Equation 4.1).

$$\text{Fraction of emulsion height} = \frac{\text{Emulsion height after seven days}}{\text{Total emulsion height on day 0}} \qquad (4.1)$$

4.3.5 Microstructure analysis

4.3.5.1 Light microscopy

The emulsion microstructure was capture after seven days of storage. A sample was taken with a disposable pipette of 3 mL capacity (VWR International, Edmonton, AB, Canada), a drop was placed over a glass depression microscope slide with 1 – 1.2 mm thickness (VWR International, Edmonton, AB, Canada), and covered with a coverslip (VWR International, Edmonton, AB, Canada). A light microscope

(Eclipse E400, Nikon Mississauga, ON, Canada) was used to observe the emulsions samples. The images of the microstructure were captured at magnifications 10x and 100x.

4.3.5.2 Confocal microscopy

Emulsions microstructure was also captured with a confocal microscope (Nikon Eclipse E400, Nikon Canada, Mississauga, ON, Canada). One drop of 0.1 wt% Nile red solution in mineral oil was mixed with nine drops of fresh emulsion, and a drop of this mixture was placed over a glass depression microscope slide (VWR International, Edmonton, AB, Canada) covered with coverslip and place under the microscope. The sample was excited using a 543 nm laser, and the emission spectra were collected from 573 to 613 nm using a 40x and 60x objectives lens.

4.3.6 Determination of emulsion droplet size

The water droplet size of the emulsions was determined by analyzing the images taken with the confocal microscope. It was essential to select three to four images of each sample where the number of water droplets quantified was between 3,000 – 18,000. The image analysis methodology developed in the previous chapter (section 3.3.6, paragraph 1) was used to quantify the water droplet size using ImageJ software (v1.5 2i – Fiji project) (Schindelin et al., 2012). The image analysis data (area of each droplet) was exported to an Excel spreadsheet (Microsoft Office 365), and further calculation was done to obtain the volume-weighted means droplet diameter ($d_{4,3}$) using Equation 3.1, where d is the diameter of each droplet obtained from the image analysis.

4.3.7 Accelerated stability analysis

The accelerated storage stability of fresh emulsion was analyzed using an analytical photocentrifuge LUMiSizer® LS650 (LUM GmbH, Berlin, Germany) using the methodology used by Erramreddy, Tu, and Ghosh (2017). The emulsion (400 μL) was added with a syringe into a rectangular polycarbonate cuvette (8 mm x 2 mm) (LUM GmbH, Berlin, Germany) and centrifuged at 4000 rpm (2325xg). The equipment transmits an 865 nm wavelength laser through the cuvette each 60 s (1000 profiles in 16 h 40 min) during the centrifugation. The light intensity transmitted through the emulsion depends on droplet movement under the centrifugal force. Data analysis and calculation of sedimentation velocity (μm/s) from the final transmission profile were processed using the SEPView® software 4.1 (LUM GmbH, Berlin, Germany). All cuvettes were also photographed before and after centrifugation.

4.3.8 Rheological properties of water-in-oil emulsions

The apparent viscosity and viscoelasticity of fresh and 7 days stored emulsions were measured using an AR-G2 rheometer (TA Instruments, Montreal, QC, Canada) at 25 °C with an acrylic parallel plate (60 mm diameter). The rotational mode for viscosity measurement used a shear rate from 0.01 to 100 s^{-1} and a loading gap of 1000 μm. The oscillatory mode was used at strain ranged from 0.01 to 1000% to measure storage (G') and loss moduli (G") at a constant frequency of 1 Hz. (6.18 rad/s). The values G' and G" were used to calculated tan δ (G"/G'). The apparent viscosity values of emulsions at a shear rate of 0.1 s^{-1} on day 0 and after 7 days of storage were used to calculate the viscosity index (Equation 4.2) to determine the viscosity change with time.

$$\text{Viscosity index} = \frac{\text{Apparent viscosity of emulsion after seven days of storage}}{\text{Apparent viscosity of fresh emulsion}} \qquad (4.2)$$

4.3.9 Determination of interfacial tension

A force tensiometer (K20 by Krüss GmbH, Hamburg, Germany) with a Wilhelmy plate (20 x 10 mm) was used to determine oil/water interfacial tension at room temperature. The oil phase (65 mL) with 4 wt% GMO was added in a wide-mouth glass beaker (130 mL). The Wilhelmy plate was immersed entirely in the oil phase, set as the zero-immersion depth. The plate was then removed and cleaned with acetone (A18-4, Fisher, US) and flamed with a butane torch (Bernzomatic, OH, USA). The aqueous solution (22 mL) was added to another similar glass beaker and placed over the stage. The plate was placed very close to the liquid-air interface for surface detection. Then, the oil phase was gently added on top of the aqueous solution with a pipette (VWR International, Edmonton, AB, Canada) to fill to the zero-immersion depth. The interfacial tension measurements were performed until a standard deviation of 0.1 mN/m could be reached between readings.

4.3.10 Differential Scanning Calorimetry

A differential scanning calorimeter Q2000 (TA Instruments, Montreal, QC, Canada) was used to measure melting and crystallization temperatures and enthalpies of different components of emulsions. Samples of fresh and stored emulsions (8 –10 mg) were sealed using aluminum T- Zero hermetic lids (T-170915) and pans (T-171030) and temperature-cycled from 25 °C to −70 °C and reheated to 70 °C at a rate of 5 °C/min. An empty T-Zero pan was used as a reference. The software TA Universal Analysis 2000 was used to integrate the peak areas to obtain the enthalpies (J/g) of each phase transition process.

4.3.11 Infra-red spectroscopy analysis

Infrared spectral analysis was performed with an IlluminatIR FTIR microscope II with a 36X Diamond ATR objective and an MTC detector (4000 to 650 cm^{-1} range) manufactured by Smiths Detection (Danbury, USA). Each sample was collected with 512 scans at room temperature with SynchronizIR Basic software (Olympus Soft Imaging Solutions, Munster, Germany). All the emulsions were prepared with deuterium oxide (D_2O) to exclude the hydrogen bonding from water (H_2O). Data analysis was done with the software OriginPro 2020b (OriginLab, Massachusetts, USA) using the peak deconvolution App. The method of 2^{nd} derivative analysis was used for the search of hidden peaks (Appendix section 10.9, page 209). The peak finding results reported the area, center, and width at half-height for each peak.

4.3.12 Statistics

All the emulsions were prepared in triplicate, and each of them was analyzed on day 0 and day 7. The statistical analysis was performed using the software IBM SPSS Statistics 20, in which Tukey's test was performed to compare the data replicates with a significance level of 0.05. Significant differences in the standard deviations among the samples were detected ($p \leq 0.05$).

4.4 Results and discussion

4.4.1 Emulsion storage stability after seven days

The W/O emulsions instability was visually observed as the separation of the oil phase from the whole emulsion phase due to water droplet sedimentation. Higher emulsion height or lower oil phase separation indicates better emulsion stability. Figure 4.1 showed the vials' images with emulsions using two different bulk oils, CO, and MO, after 7 days. The control emulsions were indicated with no-additive (S0), S0.125 (0.125% sodium chloride) and Ca0.045 (0.045% calcium chloride). CO and MO emulsions with AA and CA, with or without S, are shown in Figure 4.1A, B, respectively. Figure 4.1C showed both CO and MO emulsions with LMP, with or without Ca. The addition of S0.125 showed a significant increase in emulsions height compared to S0 in both bulk oils. The emulsions with a combination of S0.125 and AA and CA demonstrated higher emulsion height and lower oil separation for both oil phases than the emulsions with only AA or CA. The addition of Ca also increased emulsion height compared to S0 in both oils (Figure 4.1C). The emulsions with only LMP reported a higher emulsion height than the emulsions with LMP and Ca, indicating Ca was not that critical for storage stability when LMP was present. Besides, LMP emulsions (Figure 4.1C) seem to be more stable with lower phase separation for both CO and MO than the emulsions formed with S-AA and S-CA (Figure 4.1A, B). For most emulsions, lower phase separation was observed

with MO than CO, indicating higher emulsion stability with the MO, which followed the observation by Ghosh and Rousseau (2011).

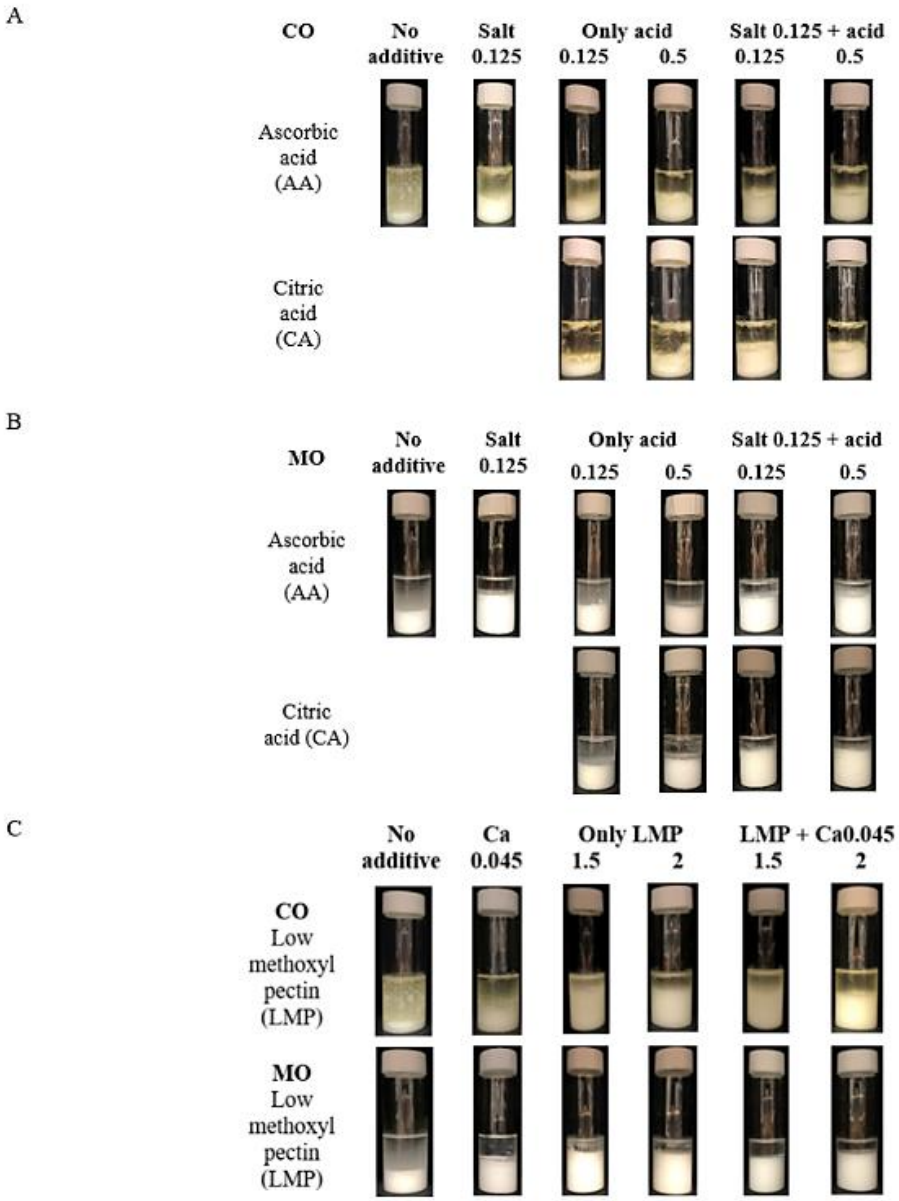

Figure 4.1 Visual observation of emulsions after seven days of storage. Emulsions were prepared with canola oil (CO) or mineral oil (MO). (A) CO emulsions with aqueous phase prepared with no additive, 0.125% salt (sodium chloride, S), 0.125% and 0.5% ascorbic acid (AA), citric acid (CA) and mixtures of salt and acids. (B) MO emulsions with aqueous phase prepared with no additive, 0.125% salt, 0.125% and 0.5% ascorbic acid (AA), citric acid (CA) and mixtures of salt and acids. (C) CO and MO emulsions prepared with aqueous phase with no additive, 0.045% calcium chloride (Ca), 1.5% and 2% low methoxyl pectin (LMP) and mixtures of Ca and LMP.

4.4.2 Quantification of emulsion kinetic stability against phase separation

The emulsion layer height reported in the visual observation (Figure 4.1) was measured and presented as a fraction of the total emulsion height. A value of one represents 100% of the emulsion phase and no phase separation (Figure 4.2). A higher value of emulsion height signifies emulsions with higher stability against phase separation. CO-emulsions height showed a significant increase from S0 (0.16 ± 0.01) to S0.125 (0.54 ± 0.02) (Figure 4.2A). Similarly, in MO emulsions, the height significantly increased from S0 to S0.125 (0.39 ± 0.01 to 0.72 ± 0.01). For both CO and MO emulsions, the incorporation of only AA and CA (both AA0.125 and AA0.5) did not improve the emulsion height further than the S0.125, which indicates that AA and CA added to the aqueous phase were not as effective as salt in improving emulsion stability.

Interestingly, when both salt and organic acids were present, the CO-emulsions height significantly increased compared to only salt-added emulsions. In contrast, for MO-emulsion, no significant difference was observed when both salt and organic acids were present compared to only salt (Figure 4.2A). The CO emulsions with S0.125 and either AA or CA had a non-significant difference in the emulsion height fraction, which was, on average, 0.62 ± 0.02. Similarly, for MO emulsions, S0.125 with AA or CA concentrations showed no difference in emulsion height fraction (average 0.75 ± 0.02) (Figure 4.2A).

With the addition of LMP (both 1.5 and 2%) (Figure 4.2B), a significant improvement in both CO and MO emulsion stability was observed. It indicates that aqueous conditions (pH 3) induced some pectin depolymerization through β-elimination, which is the separation of galacturonic acids units from the chain (Schmidt, Schmidt, Kurz, Endreß, & Schuchmann, 2015). It suggests that the structure opening allows the interaction at the interface with GMO polar head groups. The emulsion height reached the highest in CO-emulsions with LMP (both 1.5 and 2%) (0.72 ± 0.02). Although the height of MO-emulsions with LMP1.5 (0.77 ± 0.03) and LMP2 (0.75 ± 0.00) reported still higher values than CO-emulsions with LMP, the difference was not significant. However, as soon as Ca was added to the CO-emulsions, the height decreased to 0.67 ± 0.02 and 0.61 ± 0.02 for LMP1.5 and LMP2, respectively. It could be possible that Ca formed ionic linkages between the carboxylic groups from two LMP chains, which decreased LMP interaction with GMO at the interface (Flutto, 2003). In MO-emulsions, a lower concentration of LMP with Ca demonstrated reduced emulsions height (0.66 ± 0.02). Conversely, LMP higher level with Ca did not significantly diminish emulsions height (0.75 ± 0.02) than only LMP-added MO-emulsions. It might suggest that LMP2-Ca reached a balance and LMP excess unreacted was available to stabilize the interfacial GMO leading to better emulsion stability. Between CO and MO emulsions, it can be said that the effectiveness of LMP in improving liquid W/O emulsion stability was hindered by Ca addition, more extensively in CO than MO.

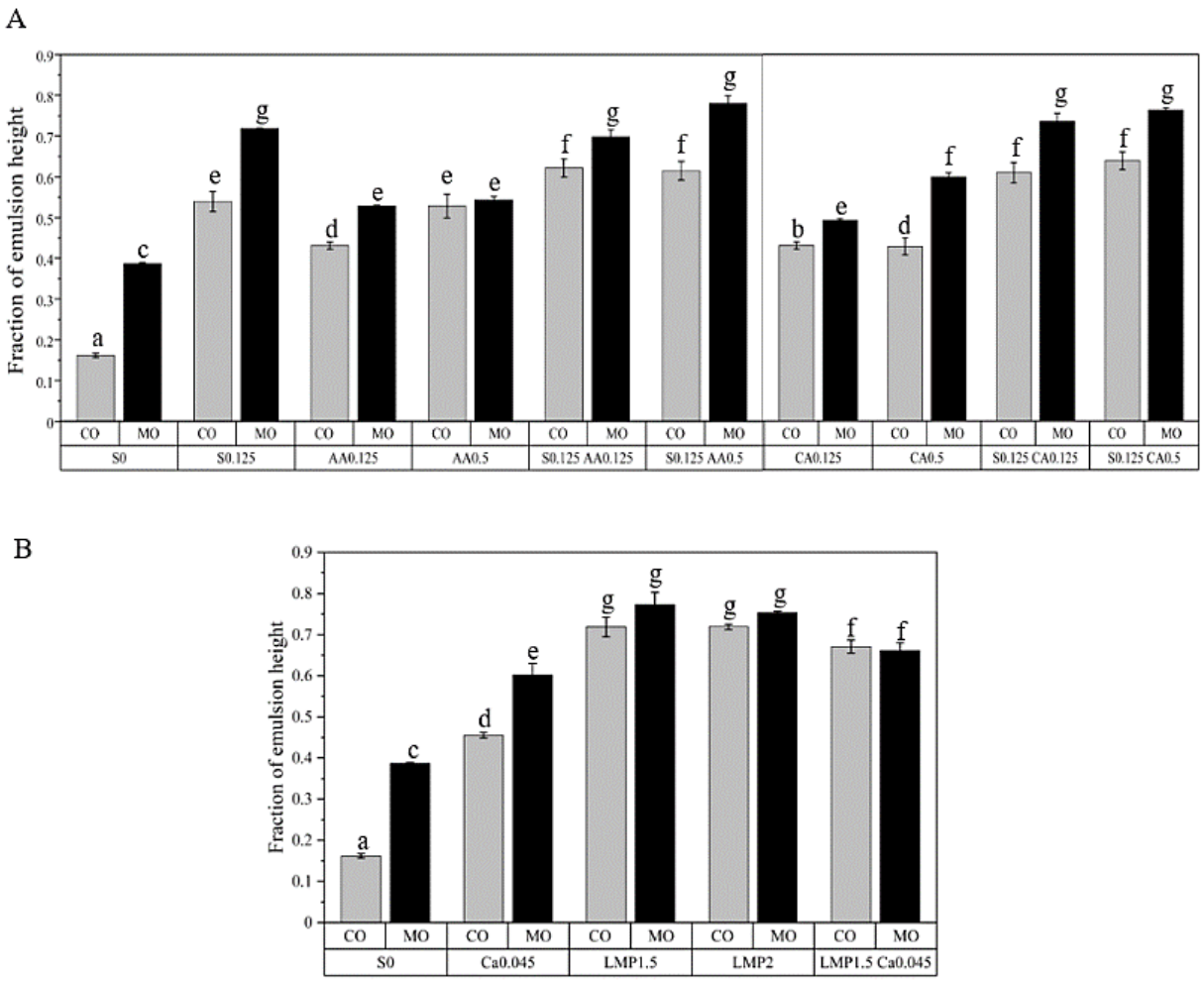

Figure 4.2 The fraction of emulsion height (emulsion layer height after seven days/ total height) containing canola oil (CO, grey bars) or mineral oil (MO, black bars) as the continuous phase. Emulsions prepared with (A) aqueous phase with various levels of salt (S), ascorbic acid (AA), and citric acid (CA); (B) aqueous phase with low methoxyl pectin (LMP) without or with calcium chloride (Ca). The concentration of ingredients is mentioned in the figure. Different letters represent significant differences at $p \leq 0.05$ (Tukey's test).

4.4.3 Microstructure of emulsions

The microstructure of CO-emulsions taken with an optical microscope after seven days of storage is reported in Figure 4.3. To better understand the variation in emulsion microstructure, two images of each sample are shown. All emulsions formed water droplets dispersed in the continuous oil phase as free and aggregated networks. The control emulsions without any additive (S0) had larger droplets with some aggregation showing apparent coalescence signs (Figure 4.3A). The incorporation of S0.125 reported some

coalescence and the initial appearance of extensive water droplet network formation (dark irregular-shape matter in the image) (Figure 4.3B). Such droplet aggregation also appeared with AA or CA (both concentrations) addition into the aqueous phase (Figure 4.3C, D, G and H). When S0.125% was incorporated with AA (Figure 4.3E, F) and CA (Figure 4.3I, J), a more extensive water droplet network structure was identified, where free droplets were hard to identify in the continuous phase. Perhaps the water droplet network's extension was responsible for the higher emulsion height of salt and AA, or CA-added CO-emulsions (Figures 4.1 and 4.2).

The microstructure of MO-emulsions with S, AA and CA captured after seven days of storage with an optical microscope is presented in Figure 4.4. Emulsions without any aqueous phase additive (S0) showed water droplets well distributed in the continuous MO phase without coalescence sign (Figure 4.4A). Comparable to CO emulsion, the incorporation of S0.125% in MO-emulsion reported water droplet network development (Figure 4.4B). The microstructure of MO-emulsions with AA (Figure 4.4C, D) or CA (Figure 4.4G, H) also demonstrated water droplet network formation, which appeared broader than CO emulsions. The addition of S0.125% with AA or CA in MO-emulsions developed an extensive water droplets network structure related to CO-emulsions. Overall, the water droplets in these emulsions appeared smaller than the emulsions without additives and with only S or organic acids.

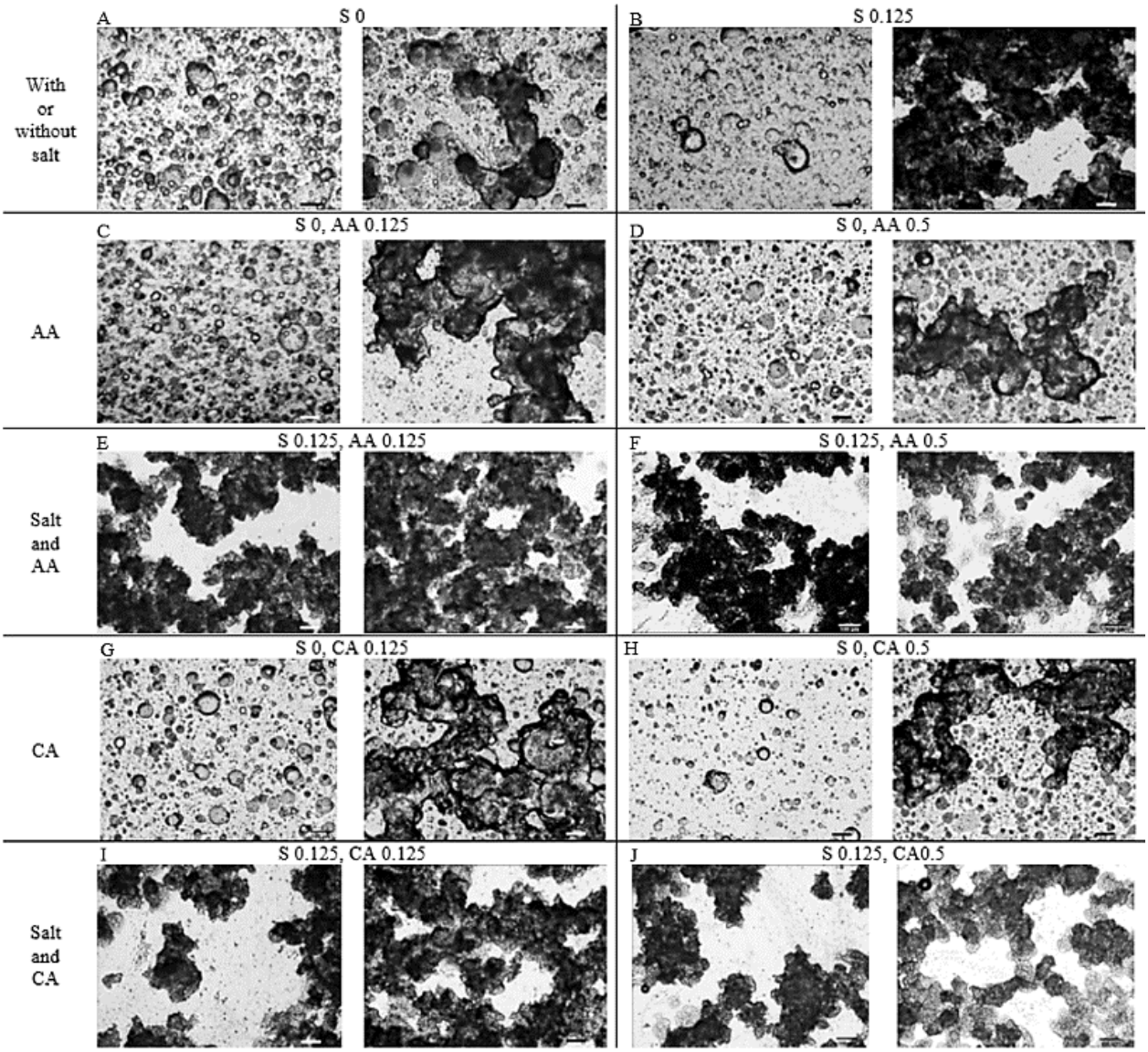

Figure 4.3 The microstructure of water-in-CO emulsions after seven days of storage with various levels of salt (S), ascorbic acid (AA), and citric acid (CA) in the aqueous phase. The concentration of ingredients is mentioned in the figure. Two images for each sample are shown to demonstrate the variation in the microstructure. Scale bar 100 μm.

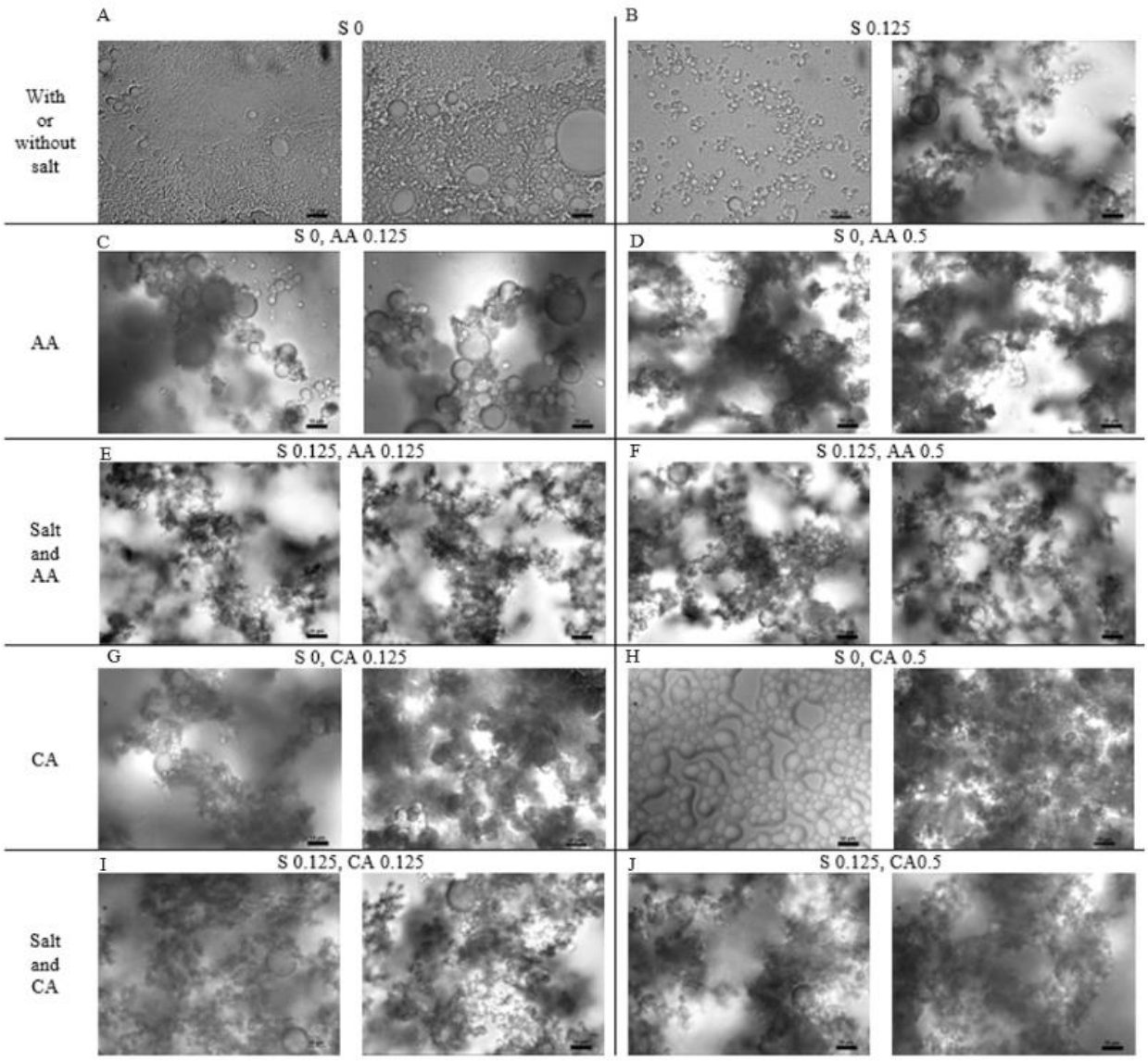

Figure 4.4 The microstructure of water-in-MO emulsions after seven days of storage with various levels of salt (S), ascorbic acid (AA), and citric acid (CA) in the aqueous phase. The concentration of ingredients is mentioned in the figure. Two images for each sample are shown to demonstrate the variation in the microstructure. Scale bar 100 μm.

The microstructure of emulsions formed with LMP and Ca after seven days of storage are presented in Figure 4.5). CO-emulsions without Ca (S0, Figure 4.5 I-A) and with Ca (Figure 4.5 I-B) showed dispersed water droplets with some degree of droplet coalescence. The incorporation of LMP formed an extensive water droplets network throughout the emulsion, making it difficult to capture the emulsion's clear images (Figure 4.5 I-C, I-D). However, the mixture LMP and Ca illustrated another structure related to gel-formation due to Ca^{2+}. Divalent ions can induce gelation by promoting strong interaction between calcium ions and dissociated carboxyl groups in pectin molecules (Yuliarti & Othman, 2018). Also, low methoxyl pectins amidated require low calcium ions concentrations (15 to 37 mg) compared to conventional low methoxyl pectins (20 to 85 mg) (Flutto, 2003). Our LMP possesses 14% of amidation and required 0.045wt% of Ca in the formula. The structure formed by LMP-Ca can coexist with the water droplet formation (Figure 4.5 I-E, I-F). All MO-emulsions showed droplet network formation even with or without Ca (Figure 4.5 II-B, II-A). In the presence of LMP, MO-emulsions formed an even broader water droplets network (Figure 4.5 II-C, II-D). Emulsion with LMP-Ca (Figure 4.5 II-E, II-F) reported similar behaviour. Comparing the CO and MO-emulsions with LMP, it can be said that the presence of MO led to a finer droplet network that was better able to provide emulsion stability against phase separation. Overall, CO and MO-emulsions with LMP (Figure 4.5) showed a more expanded water droplets network than the emulsions with S, AA or CA, S-AA, and S-CA (Figures 4.3 and 4.4). Such droplet networks could be responsible for increasing emulsion stability against phase separation reported in Figures 4.1 and 4.2.

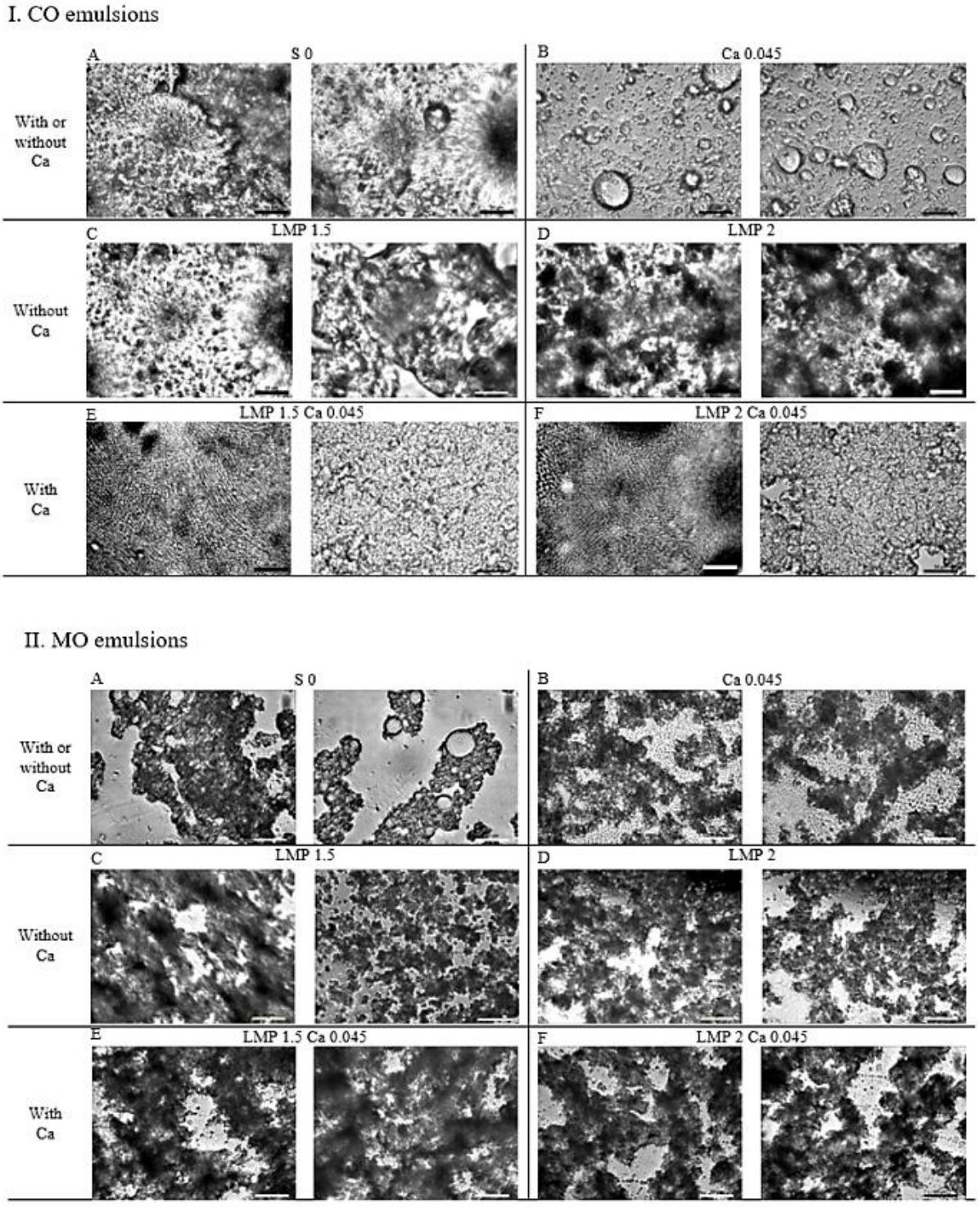

Figure 4.5 The microstructure of (I) water-in-CO and (II) water-in-MO emulsions after seven days of storage with various levels of low methoxyl pectin (LMP) and calcium chloride (Ca) in the aqueous phase. The concentration of ingredients is mentioned in the figure. Two images for each sample are shown to demonstrate the variation in the microstructure. Scale bar 50 μm.

4.4.4 Average water droplet size

The water droplet size was calculated from the microstructure taken with a confocal microscope using image analysis and reported as volume mean diameter ($d_{4,3}$) in Figures 4.6A and 4.6B. For this calculation, only the water droplets outside the network structure were analyzed. Thus, emulsions with LMP and Ca in CO and MO were not reported because the water droplets were all aggregated, forming a network spanning the whole microstructure. It was assumed that the free water droplet size would represent the entire emulsions for comparison purposes. The control CO emulsions (S0) showed a high $d_{4,3}$ (9.2 ± 0.1 µm), which was similar to CA0.5, followed by CA0.125 (8.2 ± 0.0 µm) and S0.125 (7.9 ± 0.0 µm) (Figure 6A). The emulsions formed with AA showed considerably low $d_{4,3}$ (6.0 ± 0.1 µm) at both concentrations. The addition of S to AA0.125 and CA0.5 exhibited the lowest $d_{4,3}$ (4.6 ± 0.2 µm). CO emulsions with S0.125 AA0.5 and S0.125 CA0.125 also presented a smaller $d_{4,3}$ (5.5 ± 0.1 µm).

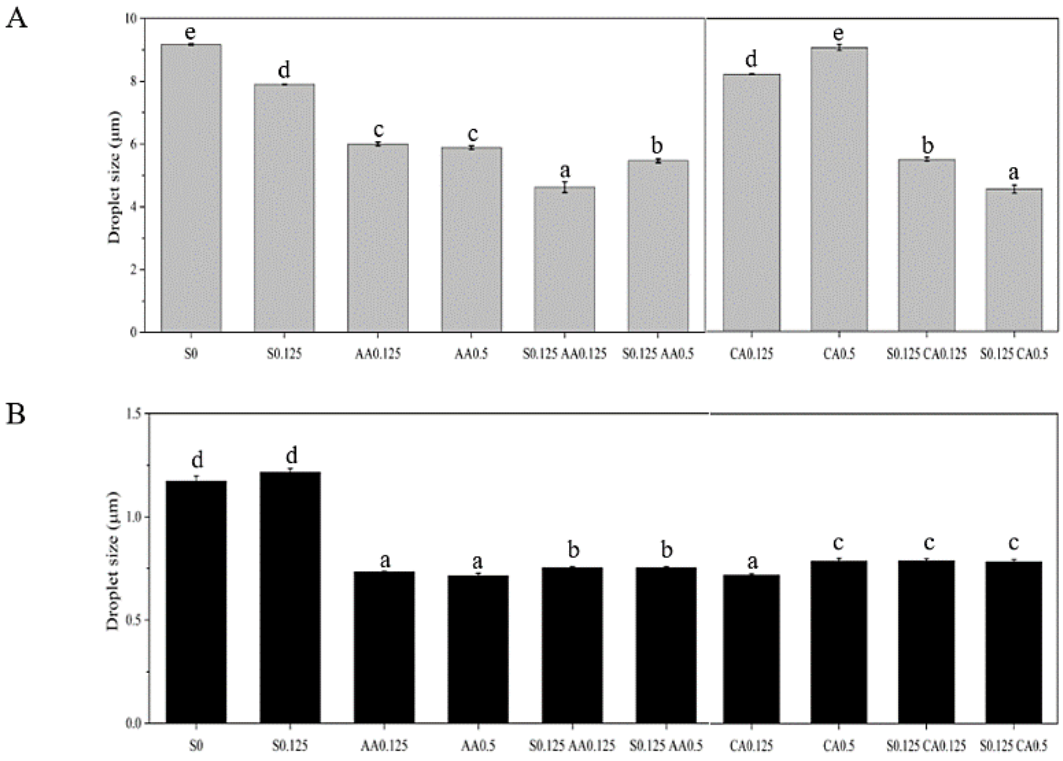

Figure 4.6 Volume means diameter ($d_{4,3}$) of water droplets in emulsions formed with (A) CO and (B) MO taken from confocal microscopy image analysis of with various levels of salt (S), ascorbic acid (AA), and citric acid (CA) in the aqueous phase. The concentration of ingredients is mentioned in the figure. Different letters represent significant differences at $p \leq 0.05$ (Tukey's test). Note the difference in Y-axis between (A) and (B).

The smaller droplet size of the emulsions with both S and AA or CA can be related to their higher emulsion height fraction reported in Figure 4.2. All MO emulsions reported a smaller droplet size (about 7 times) than CO emulsions (Figure 4.6B). The emulsions prepared with S0 and S0.125 showed a non-significant difference in $d_{4,3}$ (1.2 ± 0.03 µm), indicating that water droplet size did not decrease with S0.125 incorporation in MO emulsions. The incorporation of AA and CA reported a significant reduction of droplet size (0.72 ± 0.01 µm). The combinations of S0.125 with AA or CA also diminished the droplet size. The smaller droplet size obtained in MO emulsions can be a factor for higher emulsion stability against phase separation observed previously (Figure 4.1 and 4.2).

4.4.5 Accelerated sedimentation velocity of emulsions

Water droplets' sedimentation velocity under accelerated gravitation (2325xg) was used to identify how fast the emulsions would separate phases (Figure 4.7). The higher sedimentation velocity signifies that the water droplets moved quickly to the bottom of the vial and could be used as an indicator of long-term emulsion stability. The CO emulsions with S0 and S0.125 had high sedimentation velocity under accelerated gravitation, on average, 9.8 ± 0.2 µm/s. It could be due to the larger water droplets and coalescence under centrifugal force (Figure 4.7A). There was a sharp decrease in sedimentation velocity with AA in the aqueous phase (6.0 ± 0.2 µm/s), which can be associated with the combined presence of smaller water droplets with the water droplet network formation. Then, with the addition of S0.125 along with AA, there was a slight increase in sedimentation velocity. Still, the values remained significantly lower than S0 (7.4 ± 0.1 µm/s), which can be related to the broad extension of the water droplets network. The CO emulsions with CA at both concentrations slightly increased the sedimentation value (6.7 ± 0.1 µm/s) compared to emulsions with AA (5.9 ± 0.2 µm/s). However, S-CA (both concentrations) incorporation reported the lowest sedimentation velocity (5.7 ± 0.1 µm/s), associated with higher emulsions height presented in Figure 4.2.

The sedimentation velocity in MO-emulsions significantly decreased with S0 (6.8 ± 0.2 µm/s) and S0.125 (7.3 ± 0.1 µm/s) compared to CO-emulsions, which could be due to the smaller droplet size of the former (Figure 4.7A). However, the sedimentation velocity of all other MO emulsions with AA, CA, S-AA, or S-CA demonstrated higher values (8.3 – 9.8 µm/s) than CO-emulsions, despite their visually higher emulsion height, under earth gravitation after seven days (Figure 4.1 and 4.2). The microstructure analysis shows that MO-emulsions showed extensive water droplets network formation (Figure 4.4) compared to CO-emulsions (Figure 4.3). It can be said that the water droplet network was able to provide better emulsion kinetic stability against earth gravity. However, accelerated gravitational force probably broke the network

structure, leading to a faster separation of large water droplet aggregates in MO-emulsions. Erramreddy et al. (2017) reported a correlation between gel yield point and centrifugal separation. The minimum relative centrifugal force required for the creaming of oil droplets increased with gel strength. In the present case, the higher sedimentation velocity of MO-emulsions could be due to their lower-yielding behaviour compared to CO emulsions, which will be discussed under the viscoelasticity section.

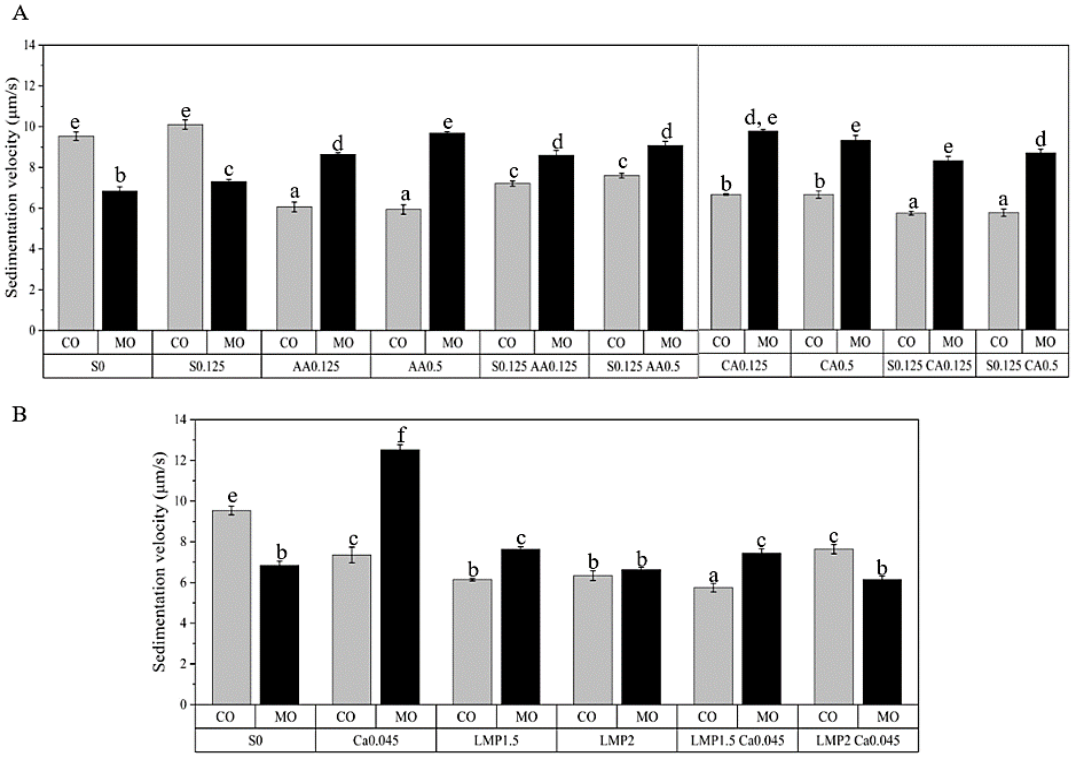

Figure 4.7 Sedimentation velocity (μm/s) of fresh emulsions in canola (CO) and mineral (MO) oils, centrifuge G-force at 2325xg. (A) Water phase with and without salt (S), S with ascorbic acid (AA), and S with citric acid (CA). (B) Water phase without salt (S), with calcium chloride (Ca), with low methoxyl pectin (LMP) without or with Ca. The concentration of ingredients is mentioned in the figure. Different letters represent significant differences at $p \leq 0.05$ (Tukey's test).

The CO-emulsions formed with Ca0.045 and LMP2-Ca reported sedimentation velocities, 7.4 ± 0.4 and 7.6 ± 0.2 μm/s, respectively (Figure 4.7B). Emulsions with LMP1.5 (6.1 ± 0.1 μm/s) and LMP2 (6.3 ± 0.2 μm/s) exhibited a reduced velocity ($p > 0.05$). However, the Ca addition to LMP1.5 emulsions showed the lowest sedimentation velocity (5.8 ± 0.2 μm/s), which was the same value as the S-CA emulsion. The sedimentation rate of MO emulsions significantly increased with Ca0.045 (12.5 ± 0.25 μm/s) compared to CO-emulsions (Figure 4.7B). The incorporation of LMP1.5 reported a decrease (7.6 ± 0.12 μm/s) compared

to Ca0.045. However, the increment to LMP2 further decreased the sedimentation rate (6.6 ± 0.10 µm/s) compared to LMP1.5. The combination of Ca with LMP slightly decreased the sedimentation rate to 7.4 ± 0.21 µm/s (LMP1.5-Ca), and 6.1 ± 0.17 µm/s (LMP2-Ca) compared to only LMP. Overall, CO-emulsions with AA, CA and their S-mixtures exhibited lower sedimentation velocity than MO-emulsions. A similar trend was observed for Ca, LMP1.5 with and without Ca, indicating that the presence of aqueous phase ingredients could help to improve long-term emulsion stability.

4.4.6 Change in emulsion viscosity with time

The emulsion viscosity changes were calculated using the viscosity index, which is a ratio of apparent emulsion viscosity on day 7 to day 0 (Figure 4.8).

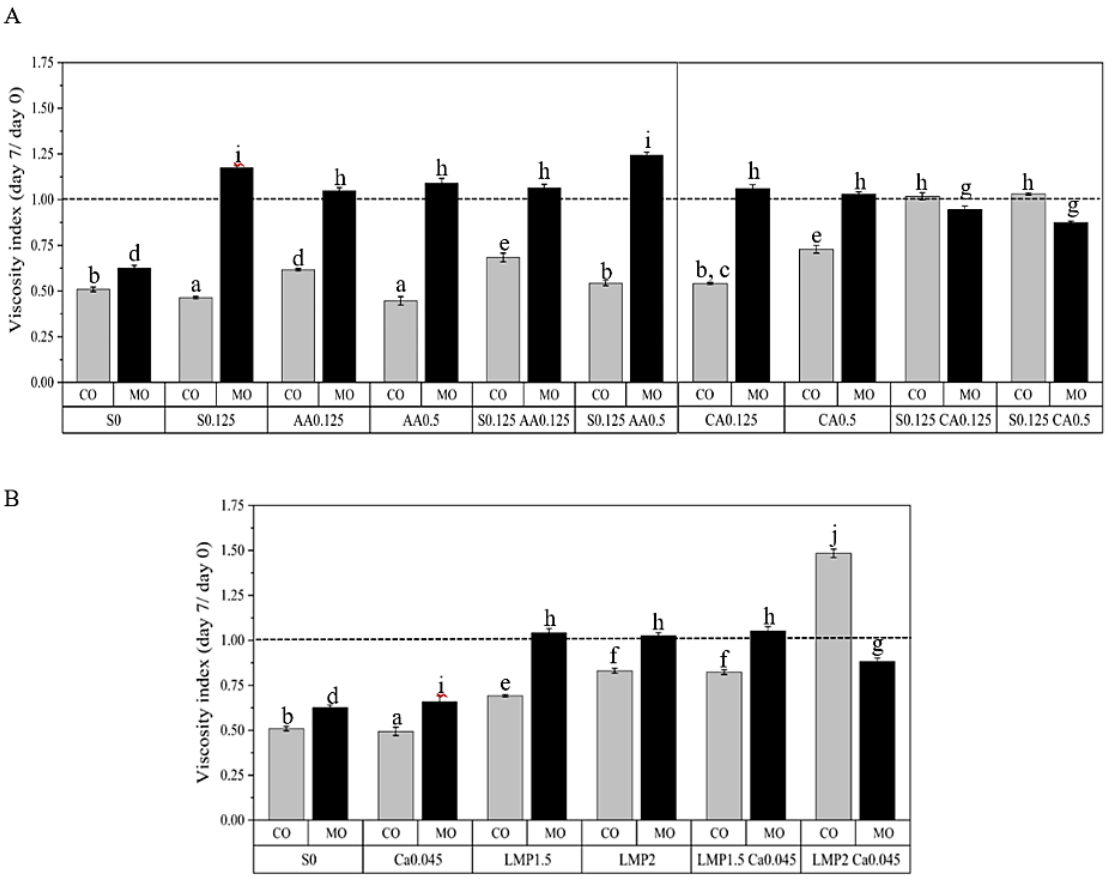

Figure 4.8 The viscosity index of emulsions with canola (CO, grey bars) and mineral (MO, black bars) oils. (A) Emulsion aqueous phase without any additive (S0) with salt (S), ascorbic acid (AA), citric acid (CA) and S with AA and CA. (B) Emulsion aqueous without any additive (S0), with calcium chloride (Ca), low methoxyl pectin (LMP) and Ca with LMP. The concentration of ingredients is mentioned in the figure. Different letters represent significant differences at $p \leq 0.05$ (Tukey's test).

Viscosity index can be related to the strength modification of the network structure and emulsion stability after seven days. A value of viscosity index less than one indicates that the viscosity decreased upon storage, which could be due to the water droplet network breakdown and lowering of emulsion stability. However, if the index is more than one, it indicates that the viscosity increased upon storage, which could be due to strengthening the water droplet network structure with time. All CO-emulsions reported viscosity indexes less than one, except the emulsions with S-CA (both concentrations, $p > 0.05$) (1.02 ± 0.02) (Figure 4.8A). Conversely, all MO-emulsions with additives in the aqueous phase reported a viscosity index above one, except the S-CA emulsions (0.95 ± 0.02 and 0.87 ± 0.01, for S0.125 CA0.125 and S0.125 CA0.5, respectively), which can be related to the higher stability of MO-emulsions.

With LMP, all CO-emulsions showed viscosity indexes lower than one, except by LMP2-Ca0.045, which had the highest viscosity index (1.48 ± 0.02), associated with the strongest network formation after storage (Figure 4.8B). On the contrary, all MO emulsions with LMP demonstrated a viscosity index above one (1.04 ± 0.02), except for LMP2-Ca, which showed an intermediate-high value (0.88 ± 0.02) (Figure 4.8B). Overall, the MO bulk phase might allow more interaction of aqueous phase additives due to the hydrocarbon structure. In this way, a stronger network could be developed during storage, leading to better emulsion viscosity than CO-emulsions.

4.4.7 Emulsion viscoelasticity

4.4.7.1 G′ and G″ as a function of strain

The emulsions' viscoelasticity was measured as a function of strain at a constant frequency (1 Hz) (Figure 4.9 and 4.10). In a low-strain regime, higher G' than G" demonstrates a gel structure between weak and strong gelation behaviour. A linear viscoelastic region (LVR) in the low-strain regime also indicates strong gelation. All the emulsions reported higher G' than G" in the low-strain regime. No emulsions showed true LVR except fresh S0 and S0.125 (Figures 4.10 A1 day 0), indicating most were weak gels.

For comparison purposes, G' values at 0.1% strain were categorized in low (< 15 Pa), medium (≥ 15 – 30 Pa), and high (> 30 Pa) gel strength. The CO-emulsions without additive (S0), S0.125, AA0.125, CA (both concentrations) and S-CA (both concentrations) reported low-range G', although CO-emulsions with AA0.5, S-AA (both concentrations) showed medium-range G' (Figure 4.9, A1). After storage, all CO-emulsions reported G' in the lower range (Figure 4.9, A2), implying that the initial structure on day 0 has diminished in strength. The G" of S0.125 exhibited two yield points before and after the gel breakpoint (G' = G"). It indicates two structure breakdowns.

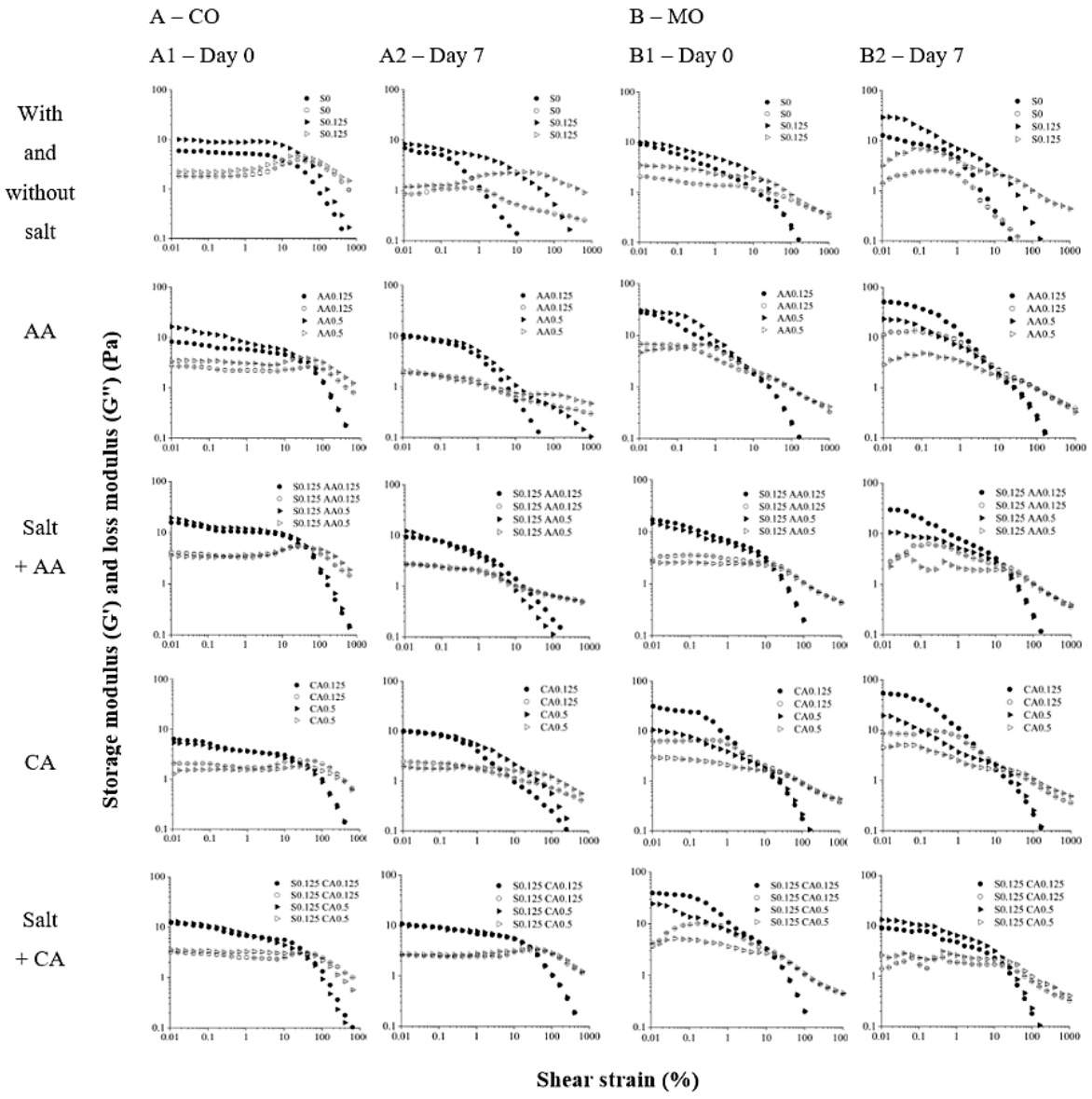

Figure 4.9 Effect of additives on the storage (G', closed) and loss (G", open) modulus with a variation of shear strain (0.01 – 1000%) at a constant frequency of 1 Hz. (A) Emulsions prepared with canola oil (CO) - (A1) day 0 and (A2) day 7. (B) Emulsions prepared with mineral oil (MO) – (B1) day 0 and (B2) day 7. The aqueous phases were prepared with and without salt (S), S with ascorbic acid (AA), and S with citric acid (CA). The concentration of ingredients is mentioned in the figure legends.

A similar phenomenon has been reported by Tang and Ghosh (2021) in oil-in-water emulsions formed with canola protein. They related the first yield to the breakdown of inter-cluster, and the second yield was associated with the cage opening allowing the free movement of droplets. G" of AA (both

concentrations) and S-AA (both concentrations) also exhibited one yield before the breakpoint, indicating cluster disruption.

All MO-emulsions exhibited G' yield points at lower strain than CO-emulsions, which could explain their higher sedimentation velocity under accelerated gravitation (Figure 4.7). Fresh MO-emulsions without additive (S0), S0.125, S-AA0.5 and CA0.5 demonstrated low-range G' (Figure 4.10, B1). In contrast, medium-range G' was showed by emulsions with AA0.125, S-AA0.125 and S-CA0.5, suggesting a soft intermediate gel. MO-emulsions with AA0.5, CA0.125 and S-CA0.125 reported higher range G'. After 7 days, MO-emulsions without additives, S0.125, CA0.5, S-CA (both concentrations), demonstrated low-range G' similar to CO-emulsions after storage. MO-emulsions with AA0.5, S0.125-AA0.125 reported medium-range G', comparable to CO emulsions. G" of AA0.5, S-AA0.125 and S-AA0.5 exhibited two-yield points. However, emulsions with AA0.125 and CA0.125 showed higher G' (Figure 4.9, B2), which indicates an increment after storage. All MO-emulsions G" showed evidence of structural breakdown with one or two yield points.

CO-emulsions with Ca reported medium-range G' (15 – 30 Pa) (Figure 4.10, A1). Emulsions with only LMP (both concentrations) reported low-range G' (< 15 Pa). Emulsions formed with LMP1.5-Ca reported medium-range G' (15 – 30 Pa), but LMP2-Ca displayed a low-range G'. Emulsions with Ca, LMP's and LMP's-Ca showed two yield points in G" before the gel point. After 7 days, all CO-emulsions showed mostly unchanged viscoelastic behaviour, except the emulsion with Ca, which shows increased G' (> 30 Pa) (Figure 4.10, A2). As well, G" behaviour was similar for Ca, LMP-Ca (both concentrations). Conversely, LMP1.5 did not show yield. It indicates that LMP1.5 emulsions exhibited a stronger structure after storage than LMP2.

Fresh MO-emulsions with Ca, LMP 1.5 and LMP1.5-Ca, demonstrated low-range G' (Figure 4.10, B1). All emulsions showed two yields in G". After storage, MO-emulsions formed with Ca demonstrated an increase in G' (Figure 4.10, B2). MO-emulsions with LMP1.5 showed higher G' than LMP 2, indicating that gel strength raised in LMP1.5 compared to day 0. Comparable to day 0, G" exhibited similar behaviour. Overall, CO and MO emulsions viscoelastic behaviour showed different strength levels in weak to medium gels strength with one or two structural breaks before the gel point performed by the molecules S, AA, CA, Ca and LMP in both oils. However, in CO, LMP1.5 with and without Ca showed only one break at the gel point showed stronger gel strength after 7 days.

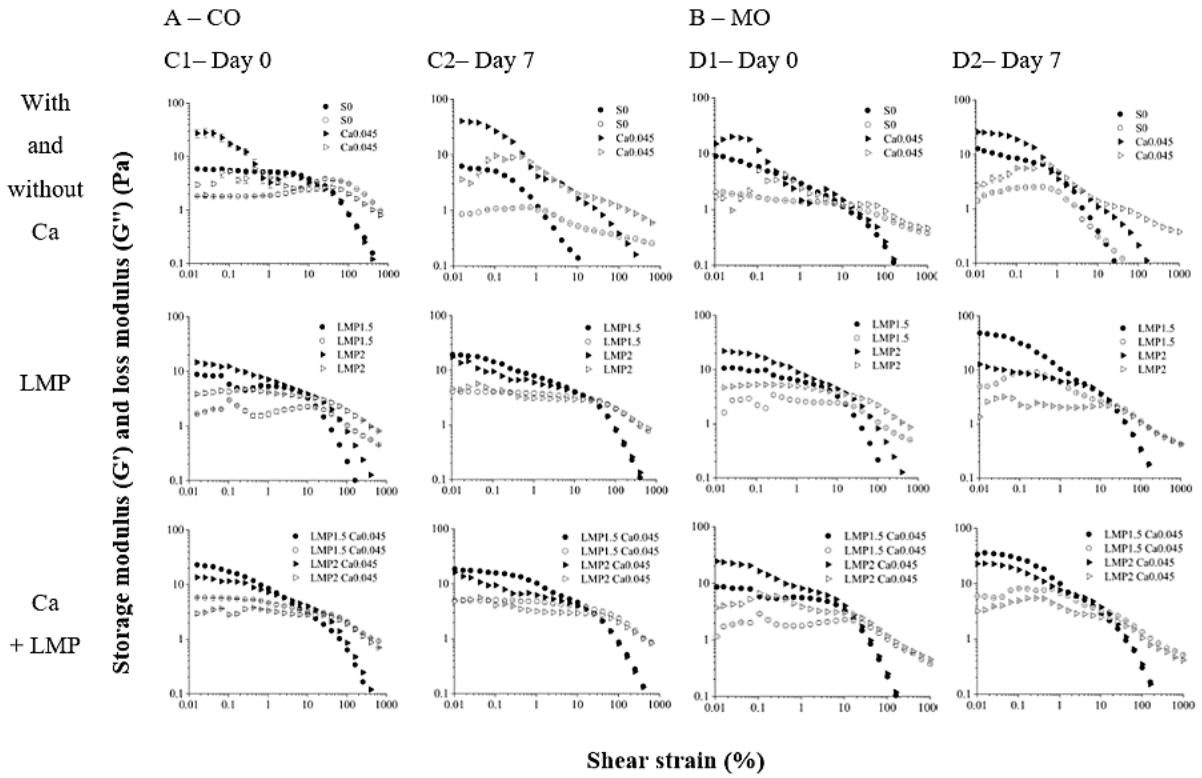

Figure 4.10 Effect of additives on the storage (G', closed) and loss (G", open) modulus with a variation of shear strain (0.01 – 1000%) at a constant frequency of 1 Hz. (A) Emulsions prepared with canola oil (CO) - (A1) day zero and (A2) day seven. (B) Emulsions prepared with mineral oil (MO) – (B1) day zero and (B2) day seven. The aqueous phases were prepared without salt (S), with calcium chloride (Ca), with low methoxyl pectin (LMP) with or without Ca. The concentration of ingredients is mentioned in the figure legends.

4.4.7.2 Tan δ

Tan δ was calculated from the ratio of G" to G'. A tan δ lower than one indicates that G' is superior to G", and the sample showed more elasticity (Figure 4.11). The tan δ calculations performed with the values of G' and G" at 0.01% strain. All emulsions showed tan δ lower than one (< 0.36), which indicates that all emulsions were more elastic than viscous.

For fresh CO-emulsions, lower tan δ, hence more elasticity was observed for S0.125 and AA0.5 (Figure 4.11A). However, a more viscous character was identified in AA0.125 and CA0.125. Fresh MO-emulsions with S-CA0.125 showed the lowest tan δ, indicating most elastic behaviour. In contrast, MO-emulsions with S0.125 exhibited the highest increase in tan δ, suggesting more viscous properties.

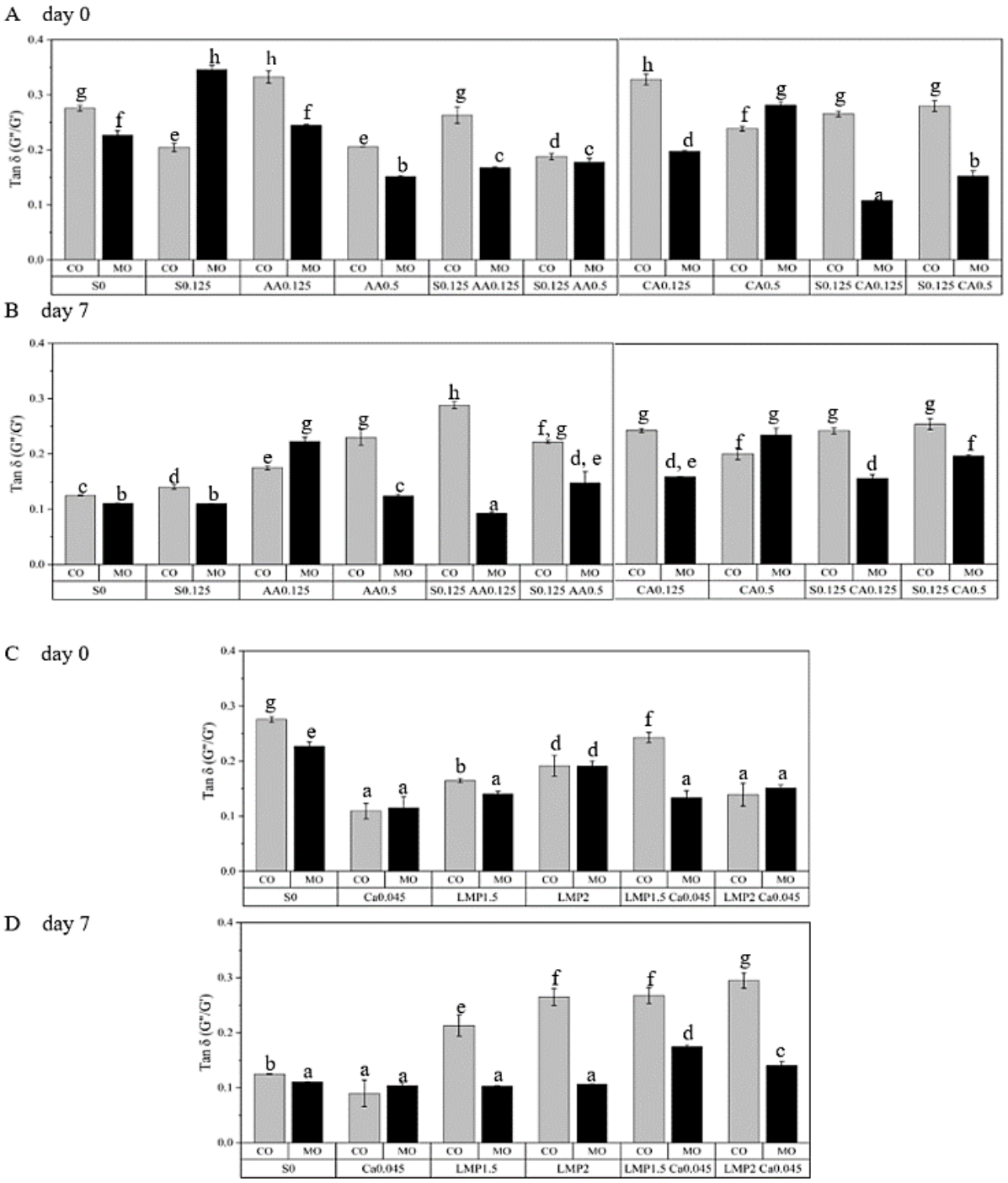

Figure 4.11 Tan δ (G"/G') of emulsions with canola (CO, grey bars) and mineral (MO, black bars) oil at 0.01% of strain. (A) Day 0 and (B) day 7 are for emulsions without any additive (S0) with salt (S), ascorbic acid (AA), citric acid (CA) and S with AA and CA. (C) Day zero and (D) day seven are for emulsions without any additive (S0), with calcium chloride (Ca), low methoxyl pectin (LMP) and Ca with LMP. Different letters represent significant differences at $p \leq 0.05$ (Tukey's test).

After 7 days, a similar trend was performed for all emulsions as day 0, with an even lower tan δ (< 0.31). Most CO and MO-emulsions reduced or remained the same after storage, except S-AA0.125 in CO and S-CA (both concentrations) in MO.

All fresh CO and MO-emulsions with Ca and LMP reported a lower tan δ (< 0.28) than the emulsions without additive (S0) (Figure 4.11C). After 7 days of storage, most CO and MO-emulsions showed an increase in elastic behaviour. Overall, most additives added in the aqueous phase influenced the increment of elastic characteristics in both the CO and MO emulsions, indicating a stronger water droplet network formation.

4.4.8 The interfacial tension between oil and aqueous phases

To understand the emulsifier's surface activity in the presence of various aqueous phase additives, the interfacial tension between the oils and aqueous phases was determined using a Wilhelmy plate force tensiometer. CO without GMO against water without any additive reported an interfacial tension of 21.23 ± 0.05 mN/m, while for MO, interfacial tension was 46.03 ± 0.73 mN/m (data not shown). According to Tuntiwiwattanapun, Tongcumpou, Haagenson, and Wiesenborn (2013), vegetable oils with water displayed interfacial tension between 20 – 30 mN/m. With MO-water, Xaxa (2014) reported an interfacial tension of 45.65 ± 0.57 mN/m. Both values from the present work are within the range found in the literature. Commercial vegetable oils were found to reduce the interfacial tension due to certain minor components' presence, such as free fatty acids, monoacylglycerols or diacylglycerols (Gaonkar, 1989) acting as surface-active molecules at the interface.

For interfacial tension experiments, the bulk oil phases contained 4 wt% GMO, similar to emulsions' concentration. The aqueous solutions were prepared with or without additives related to their emulsion counterparts. The interfacial tension measurement relied on the emulsifier diffusion and adsorption to the oil-water interface. A higher concentration of surface-active molecules should lower interfacial tension unless the critical micelle concentration has reached, where no further decrease in interfacial tension would be observed. Figure 4.12 presents the interfacial tension with CO and MO against the various aqueous phases. All interfacial tension values for CO-aqueous phases showed a non-significant difference among them (1.2 to 1.7 mN/m), and they were lower than all MO-aqueous phases interfacial tension (1.4 to 2.5 mN/m), except for S0, S0.125 (Figure 4.12A), and Ca0.045 (Figure 4.12B). Ghosh and Rousseau (2012) reported the interfacial tension between CO-water 1.6 ± 0.1 mN/m using 4 wt% GMO in CO, which is associated to our data (1.2 ± 0.05 mN/m). MO-S0 system displayed very low interfacial tension, which can be associated with GMO's surface-activity and ability to pack much better in MO, consisting of hydrocarbon

chain without potential groups to bond with GMO. Lower interfacial tension of MO interface is also responsible for the much smaller water droplet size in W/MO emulsion than W/CO emulsions, as reposted in Figure 4.6. Conversely, when CO was the bulk phase in CO-S0 system, GMO can interact with the glycerol polar head of oleic acids and other fatty acids that contains CO, diminishing the alignment at the interface and increasing the interfacial tension.

With the addition of salt (S0.125), a slight increase in the interfacial tension was observed for MO emulsions. Amar-Yuli & Garti (2005) reported that S creates a "salting-out" effect, reducing the emulsifier polar head group hydrophilicity and promoting aggregation. The salting-out outcome may be favourable in oils with an excess of surface-active molecules, as in vegetable oils. However, in MO, the increase of GMO local packing might promote some bare patches at the interface. Besides, Amar-Yuli et al. (2007) addressed that the hydration layer of GMO polar heads decreased in size due to dehydration when GMOs compete with other molecules for binding water, leading to an increase in interfacial tension. MO-aqueous phase system also observed a significant increase in interfacial tension with AA and CA (2.3 and 2.1 mN/m) compared to the aqueous phase without any additive. Therefore, increase in emulsion stability against phase separation with AA and CA was not due to interfacial tension, rather water droplet aggregation and network formation.

CO-water systems with Ca showed slightly lower interfacial tension (1.0 ± 0.00 mN/m) compared to the aqueous phase without additive (S0) (1.2 ± 0.05 mN/m) (Figure 4.12B). It might be correlated with the Ca^{2+} enhancement of GMOs' packing at the interface. CO-water with LMP also demonstrated a low interfacial tension at both concentrations (1.5 – 1.9 ± 0.1 mN/m), similar to the aqueous phase without additive (S0), which can be associated with GMO-LMP interfacial interaction. Lutz, Aserin, Wicker, and Garti (2009) investigated the interfacial tension of limonene-water with 0.5 wt% pectin and attributed the enhancement of GMO orientation at the interface due to its interaction with pectin carboxylic groups. However, the addition of Ca^{2+} to LMP in the aqueous solutions interfered extensively at the CO-water interface leading to a steep rise in interfacial tension. Calcium ions can promote gelation in LMP molecules due to their ionic binding with pectin carboxylic groups (Capel, Nicolai, Durand, Boulenguer, & Langendorff, 2006). LMP formed weak gels at room temperature with Ca^{2+}, which might reduce the GMO adsorption at the interface leading to an increase in interfacial tension. Higher interfacial tension of LMP-Ca systems can also be related to their reduced emulsion stability (61 – 67%) compared to only LMP-added systems (72%) (Figure 4.2). Interfacial tension of the MO-aqueous phase with Ca and LMP followed the similar trend of the CO-aqueous phase (Figure 4.12B). Schmidt et al. (2015) investigated five different pectins at pH 3. The interfacial tension measurements were performed with Tween 20, sucrose, and canola

oil. The pectin solutions showed interfacial tension values from ~45 to 62 mN/m significantly higher than those presented for LMP in this study. It indicates that LMP has surface-active properties. Overall, the interfacial tension was influenced by the oil type, GMO and additive's molecular structure added in the aqueous phase, interacting at the interface.

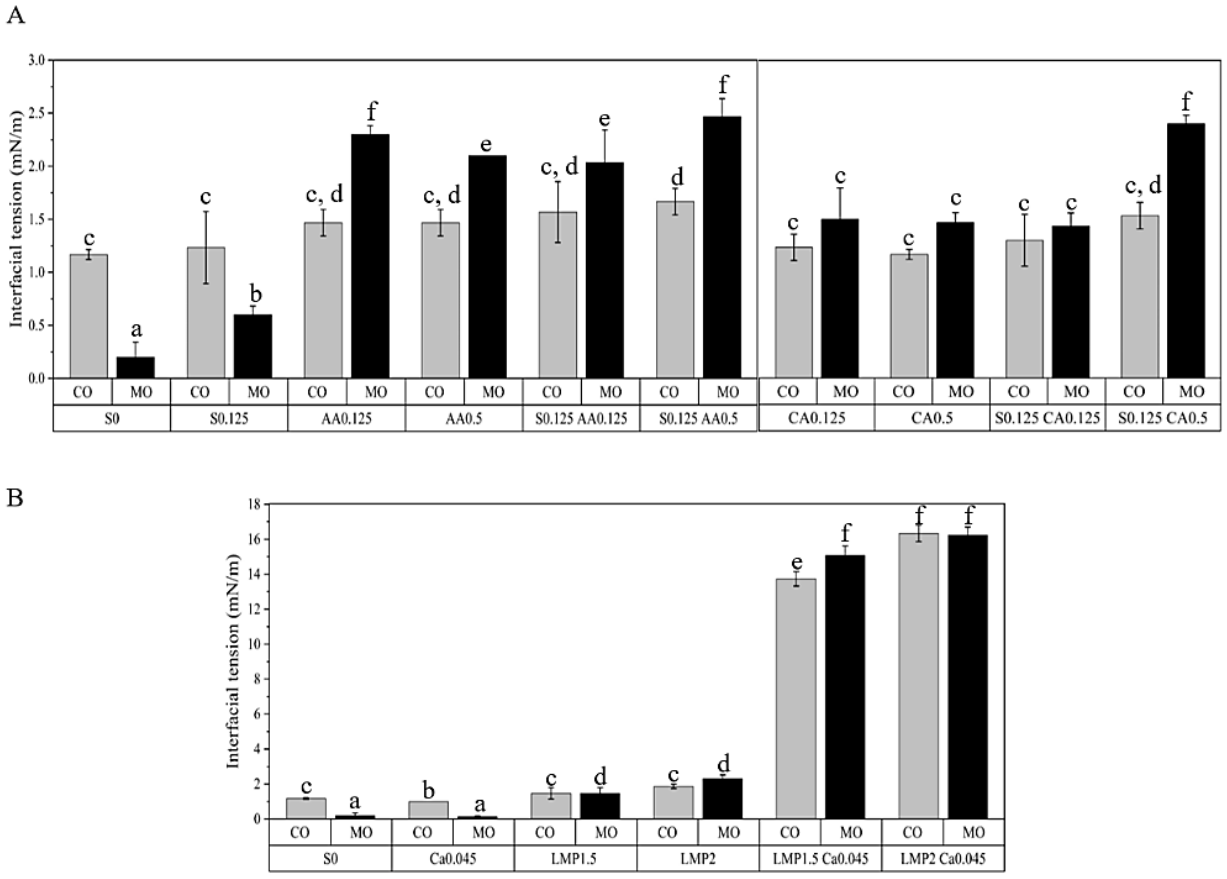

Figure 4.12 Interfacial tension of 4 wt% GMO in CO and MO with different aqueous phase compositions (A) Aqueous phase without any additive (S0) with salt (S), ascorbic acid (AA), citric acid (CA) and S with AA and CA. (B) Aqueous phase without any additive (S0), with calcium chloride (Ca), low methoxyl pectin (LMP), and Ca with LMP. The concentration of ingredients is mentioned in the figure. Different letters represent significant differences at $p \leq 0.05$ (Tukey's test). Note the difference in the Y-axis range between (A) and (B).

4.4.9 Emulsion thermal analysis

DSC thermograms of cooling and heating cycles were obtained for CO and MO-emulsions with and without various aqueous phase additives. All emulsions reported two endothermic peaks in the heating cycle

(Figure 13). The first peak, associated with ice melting, started at –1.5 °C and the second peak, due to GMO melting, started at around 7.5 °C (Bitan-Cherbakovsky, Yuli-Amar, Aserin, & Garti, 2009). Some factors have been identified to influence the melting point, such as intermolecular forces, molecular conformational degrees of freedom, molecular symmetry, and molecular motion, which also rely on the size, and shape of molecules and their orientation as crystals (Katritzky et al., 2001). CO-emulsions without additives (S0) illustrated a broad and pronounced endothermic peak, which reveals hydrogen bonding between water molecules and GMO polar head groups (Figure 4.13A1). The effect of salt was observed with a small peak for S0.125 in CO-emulsion, which indicates that ionic interaction with S diminished the strong hydrogen bond between the water molecules. Emulsions with AA and CA (both concentrations) presented peaks with narrow areas but more prominent than S0.125. It indicates that water molecules hydrogen-bonded to the four hydroxyl groups and one C=O in AA, and four hydroxyl groups with three carbonyl groups in CA. Bitan-Cherbakovsky et al. (2009) reported similar ice melting behaviour in AA (both concentrations) presence associated with water-AA hydrogen bonding. The S addition to AA in CO-emulsions resembled the ice melting peaks to S0.125 emulsions, related to the S-water interaction. In contrast, S addition to CA in CO-emulsions illustrated ice melting peaks with a broader curve, which points out more water interaction with GMO polar head or CA polar groups compared to the mixture S-AA. This difference could be due to the two more carbonyl groups in CA, which might compete to bond water with S.

In contrast to CO, all MO-emulsions showed pronounced ice melting peaks (Figure 4.13B1) and a shift to a higher melting temperature. When intramolecular hydrogen bonding is superior to intermolecular hydrogen bonding, the melting point decrease (Katritzky et al., 2001). In MO, the water molecules formed more intermolecular hydrogen bonding due to the lack of any interaction with fatty acids as in CO. It leads to an increase in ice melting temperature. In the presence of salt, the one interacting was mainly GMO.

The CO-emulsions with Ca (Figure 4.13C1) showed a much broader peak compared to S0 and also S0.125, which can be related to the calcium chelation with the oxygen atom in water and oxygen of GMO polar head hydroxyl groups (Flutto, 2003). This bonding type involves two molecules in the sides, with calcium ions in the middle that might show more energy in the peak shape. Bigger peaks were observed with LMP (both concentrations) in the aqueous phase compared to S0, suggesting that more intermolecular hydrogen bonding was presented with LMP carboxylic groups, leading to an increment of ice melting temperature. When Ca was added to the CO-emulsions with LMP, the ice melting peaks increased compared with only LMP molecules due to higher interaction energy with Ca of Ca^{2+} ions with LMP forming weak gelation (Figure 4.5-I E and F). Conversely, in MO-emulsions, the intermolecular hydrogen bonding of water molecules decreased, as can be observed for the peak shape and the shift to the left than CO-emulsions

(Figure 4.13D1). It can indicate that some water intermolecular hydrogen bonding was increased by the oil composition with an excess of surface-active molecules in CO.

The endothermic peaks between 5 to 20 ºC were from a large GMO melting peak at around 8 ºC followed by a shoulder peak at around ~12 ºC (Figure 4.13A2, B2, C2, D2). The shoulder peak could belong to the traces of saturated fatty acids present in GMO molecules.

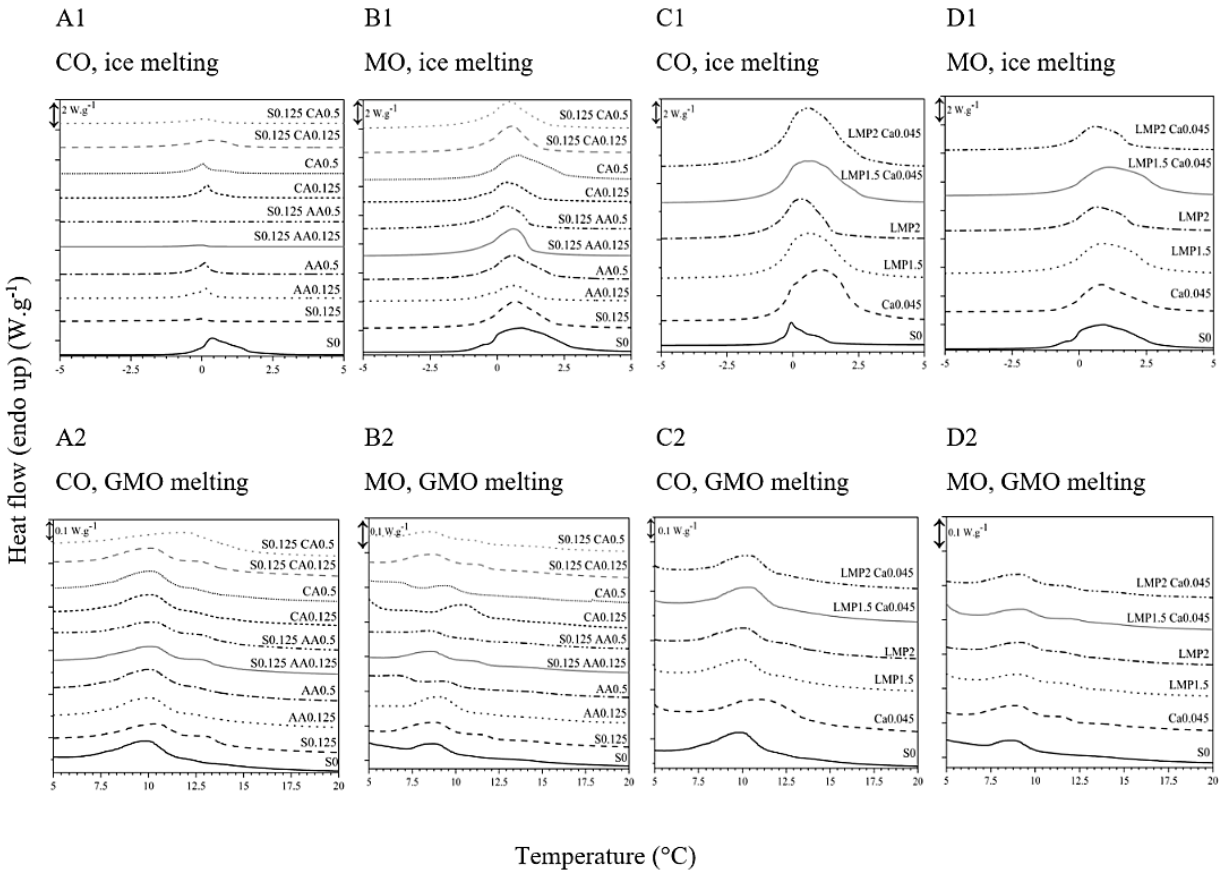

Figure 4.13 DSC thermograms for ice (A1-D1) and GMO melting (A2-D2) peaks of CO and MO-emulsions prepared with 4 wt% GMO and different aqueous phase compositions. (A, B) Aqueous phase without any additive (S0) with salt (S), ascorbic acid (AA), citric acid (CA) and S with AA and CA. (C, D) Aqueous phase without any additive (S0), with calcium chloride (Ca), low methoxyl pectin (LMP) and Ca with LMP. Note the difference in the Y-axis scale between ice melting (A1 – D1) and GMO melting (A2 – D2).

CO-emulsions showed a similar shape in peaks in almost all samples, except S0.125-CA0.5 illustrated a shift to the right (Figure 4.13A2), which could be due to the better packing performed by GMO with CO at the interface. MO-emulsions showed a similar peak shape with CO-emulsions (Figure 4.13B2).

Some decrease in peak can be observed in S0, AA0.5, S-AA0.5, CA0.5, S-CA0.5, in which the absence of fatty acids can influence MO reduced interaction. All CO-emulsions in Figure 4.13C2 showed more prominent peaks than in MO (Figure 4.13D2). It indicates further hydrogen bonding of GMO in CO. Similar to Figure 4.13B2, a shift to the left was observed for MO, which suggests a change from the dominant intermolecular hydrogen bonding to more intramolecular hydrogen bonding in MO.

4.4.9.1 Temperatures of ice melting peaks

To better understand how the interaction of different aqueous phase additives and GMO at the water-oil interface affected ice melting, the peak temperatures were compared in Figure 4.14A, B. A low melting temperature is related to more intramolecular hydrogen bonding and less intermolecular hydrogen bonding. A high melting temperature indicates that intermolecular attraction influences the melting point (Katritzky et al., 2001). CO-emulsions without additive, with S, AA (both concentrations) and CA (both concentrations) showed lower ice melting temperatures compared to MO-emulsions (Figure 4.14A), indicating more intramolecular hydrogen bonding of water molecules controlled the melting point than intermolecular interaction. MO-emulsions without additives report the highest ice melting temperature (0.9 ± 0.1 °C), which could be due to more water molecules hydrogen-bonded with GMO at the interface (Bus et al., 1990). However, S-AA and S-CA emulsions exhibited no difference between the oils in the ice melting point ($p > 0.05$).

Conversely, all CO-emulsions with Ca, LMP and LMP-Ca illustrated a higher water melting point ($p > 0.05$) than MO-emulsions (Figure 4.14B), indicating more intermolecular hydrogen bonding in CO than MO. In LMP, the dissociated carboxylic groups can hydrogen bond with water and GMO, preventing GMO's polar head interaction with CO. With Ca, the chelation is higher in CO than in MO due to more polar groups at the interface to bond with. MO-emulsions with S0 was the only one with higher ice melting point than CO-emulsions, in which, without any additive, the water did not form extra intermolecular hydrogen bond and the carboxyl group in GMO was more attracted to interact with the bulk phase than with water (Ghosh et al., 2011).

4.4.9.2 Enthalpies of ice melting peaks

Similar to ice melting peak temperatures, enthalpies of ice melting peaks can also reveal complementary information on the interfacial interaction of water with GMO and the additive molecules. The enthalpy of melting considers the molecular group interactions in an additive way and constitutive of each group (Zhao & Yalkowsky, 1999). All MO-emulsions showed higher enthalpies (> 30 $J.g^{-1}$) than CO-emulsions (< 20 $J. g^{-1}$), indicating more water intermolecular hydrogen bonding in MO than CO (Figure

4.14C). Once more, the GMO desorption at the interface was demonstrated as the primary influence of high enthalpy in MO-emulsions. Ca chelation interaction was greater in CO than MO-emulsions due to the more surface-active molecules (Figure 4.14D). For LMP, the ice melting enthalpies were higher in both oils (> 50 $J.g^{-1}$), indicating more molecular intermolecular hydrogen bonding due to LMP carbonyl groups. The low concentration in LMP (1.5 wt%) exhibited more interaction than the higher LMP concentration with and without Ca, which suggests that more LMP concentration might form bonds between LMPs' galacturonic acid chains instead of water or GMO.

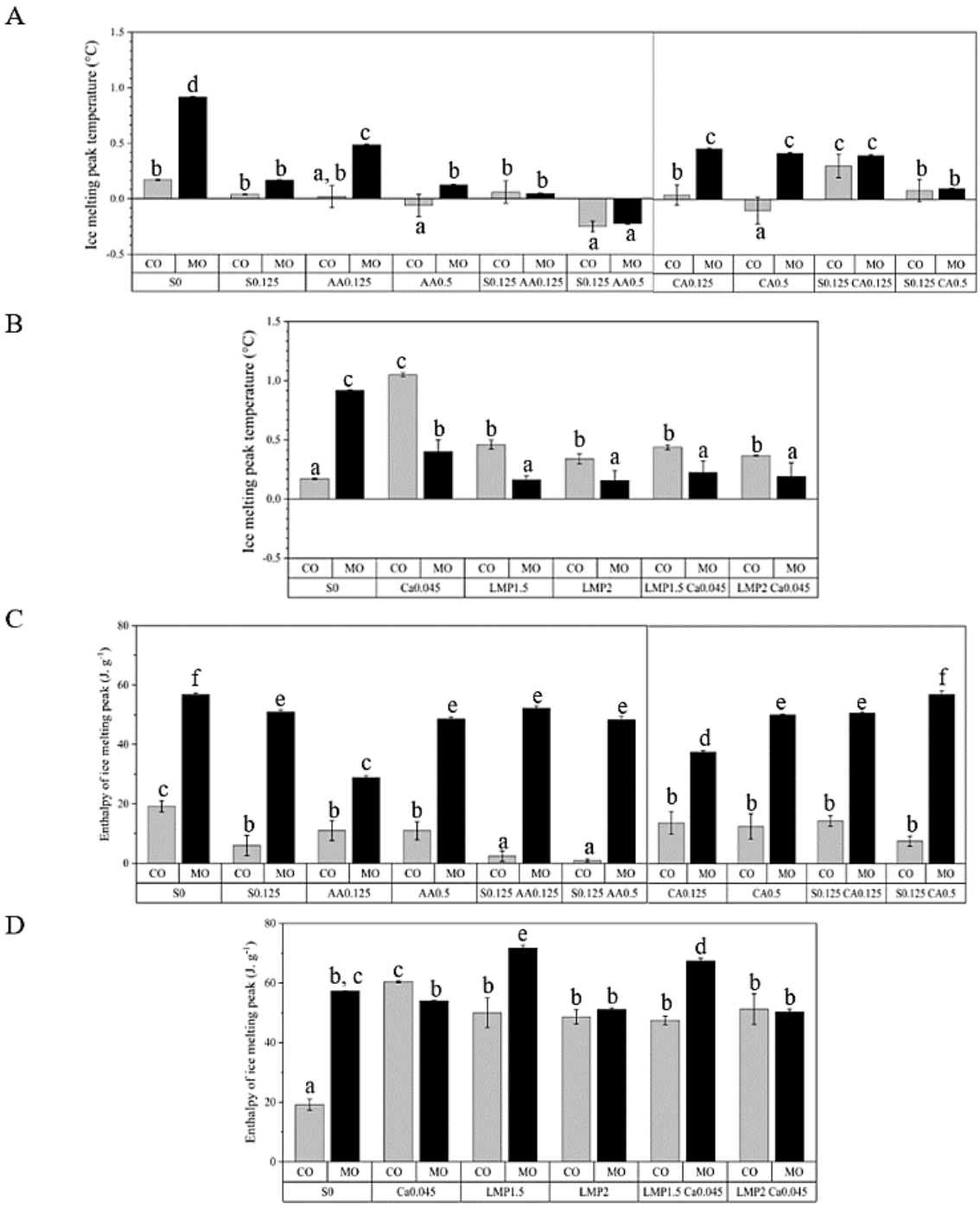

Figure 4.14 (A, B) Ice melting peak temperature (°C) and (C, D) respective ice melting enthalpy ($J.g^{-1}$) of CO and MO-emulsions with different aqueous phases. (A and C) Aqueous phase without any additive (S0) with salt (S), ascorbic acid (AA), citric acid (CA) and S with AA and CA. (B and D) Aqueous phase without any additive (S0), with calcium chloride (Ca), low methoxyl pectin (LMP) and Ca with LMP. The concentration of ingredients is mentioned in the figure. Different letters represent significant differences at $p \leq 0.05$ (Tukey's test).

4.4.9.3 Temperatures and enthalpies of GMO melting peaks

All CO-emulsions reported a GMO peak melting temperature at around 10 °C, which was higher than all MO-emulsions (Figure 4.15A, B). It indicates more GMO intermolecular hydrogen bonding in CO than MO. A similar observation can also be made with peak melting enthalpies (Figure 4.15C, D). Most CO-emulsions showed higher enthalpies (0.9 to 1.1 $J.g^{-1}$) than MO-emulsions (0.2 to 0.8 $J.g^{-1}$) (Figure 4.15C). The same trend was exhibited in CO-emulsions with Ca, LMP and LMP-Ca (Figure 4.15D). In CO, GMO molecules formed more hydrogen bonding, not only at the W-O interface but also in the continuous bulk phase due to the presence of the fatty acids' C=O.

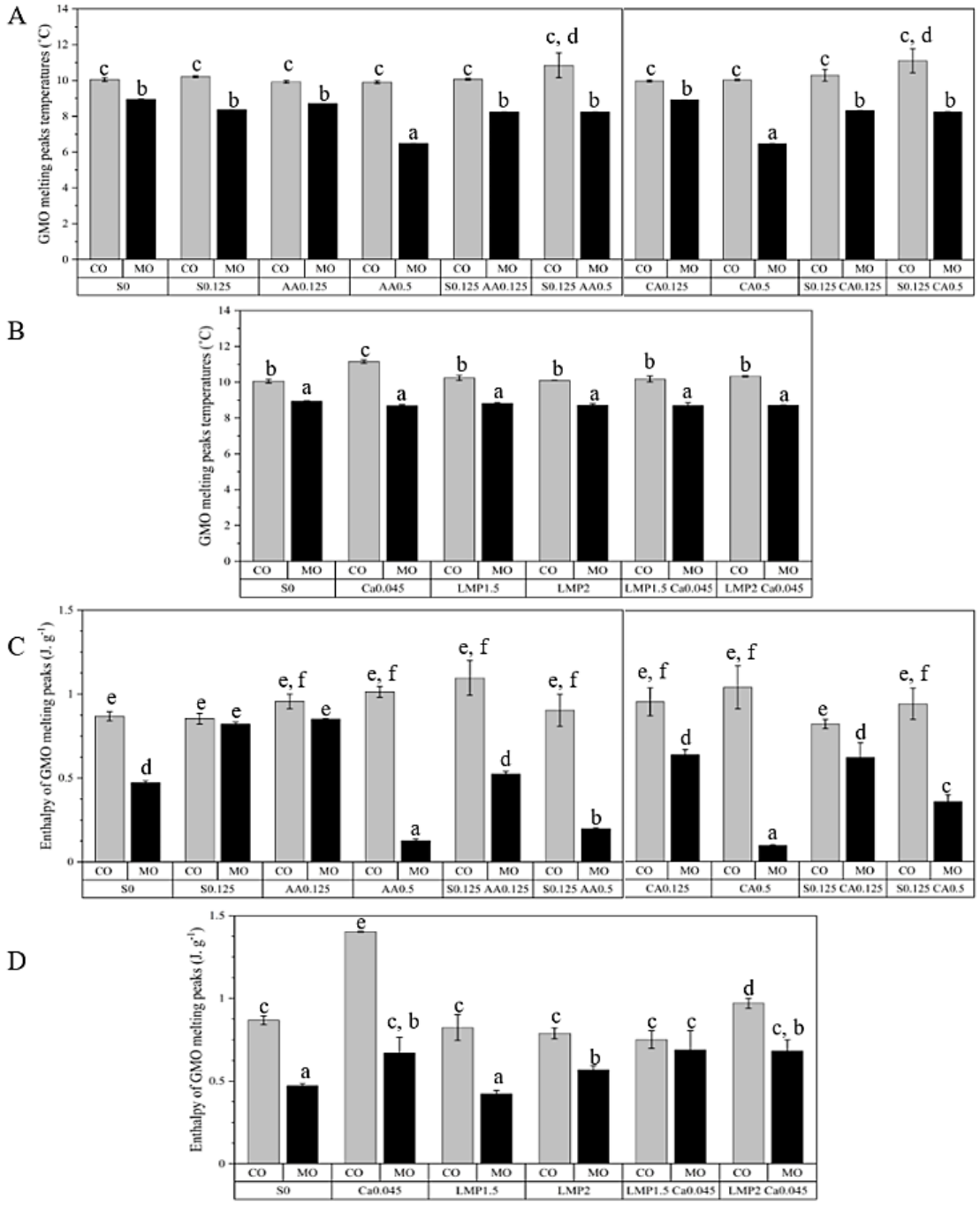

Figure 4.15 (A, B) GMO melting peak temperatures (°C) and (C, D) respective GMO melting enthalpy ($J.g^{-1}$) of CO and MO-emulsions with different aqueous phases. (A and C) Aqueous phase without any additive (S0) with salt (S), ascorbic acid (AA), citric acid (CA) and S with AA and CA. (B and D) Aqueous phase without any additive (S0), with calcium chloride (Ca), low methoxyl pectin (LMP) and Ca with LMP. The concentration of ingredients is mentioned in the figure. CO s was the subpeak found next to the second peak. Different letters represent significant differences at $p \leq 0.05$ (Tukey's test).

4.4.10 Mechanism of interactions among GMO, aqueous phase additives and the continuous oil phase using FTIR spectra

IR spectra of the emulsions were used to identify the mechanism of GMO interactions at the oil-water interface. For this reason, deionized water was replaced with deuterium oxide (D_2O) to avoid the masking of GMO hydroxyl group (OH) hydrogen bond vibrations by water OH stretching vibrations. Bus et al. (1990) studied the hydrogen bonding of GMO molecules in heptane and glycerol trioleate by using FTIR. The absorbance was analyzed based on GMO micelle formation in the bulk oils. Free GMO had an absorption peak at 3630 cm^{-1}. Intramolecular hydrogen bonding in GMO hydroxyl (OH) groups had an absorption peak at 3600 cm^{-1}, while intermolecular hydrogen bonding was at 3400 cm^{-1}. Bus et al. (1990) also reported that carbonyl groups of fatty acids in a glycerol trioleate hydrogen bond with the OH groups of glycerol monooleate (major peak at 3451 cm^{-1}). Besides, Ghosh and Rousseau (2011) analyzed hydrogen bonding interaction between GMO in MO and CO using FTIR (major peak at 3476 cm^{-1} and moderate peaks from ~3510 to 3580 cm^{-1}). They mentioned a mechanism of absorption/desorption performed by GMO at the interface due to the attraction for stronger hydrogen bonding provided by carbonyl groups in CO versus weaker hydrogen bonding with water molecules. In MO, due to non-polar groups' absence, GMO did not H-bond with the oil; instead, extensive intra- and intermolecular GMO hydrogen bonds were detected. In the present case, the IR spectra were analyzed for the emulsions containing no additive (S0), S, AA, S-AA, Ca, LMP, and LMP-Ca to understand the GMO interaction with the aqueous phase additives and the two different types of the continuous oil phase.

4.4.10.1 GMO hydrogen bonding at the oil-water interface (peak at 3400 cm^{-1})

With the replacement of water with deuterium oxide, the hydrogen bond between the GMO polar head and hydroxyl groups of additives at the interface can be clearly seen at around 3400 cm^{-1}. When HOH bending frequency transfers to a higher wavenumber, it indicates an increase in hydrogen bonding strength between GMO and the additives molecules (Kataoka, Kitadai, Hisatomi, & Nakashima, 2011). The spectra for CO and MO-emulsions are presented in Figure 4.16A, B. The peak frequencies of GMO's OH group hydrogen bonding with the molecules were plotted in Figure 4.16C. Almost all MO-emulsions reported a lower frequency than CO-emulsions, except when LMP was present in the aqueous phase. The highest frequency was reported in CO-emulsions with LMP at 3402 ± 2.3 cm^{-1}, indicating more intermolecular hydrogen bonding. More interaction with LMP than AA could be due to more dissociated carboxyl groups to bond with GMO at the interface. The lowest frequency was exhibited in MO-emulsions with AA0.125 of 3355 ± 3.7 cm^{-1} due to less hydrogen bonding between the molecules at the interface related to DSC results

(Figure 4.14A). The area of the peaks is related to the motion of the molecules. A lower area is associated with restricted motion, and a higher area is due to increased motion or disorder in the molecules (Nilsson, Holmgren, & Lindblom, 1994). Figure 4.16D showed the area under the peak at ~3400 cm^{-1}. All CO-emulsions exhibited a bigger area, suggesting more disorder at the interface, which could be to the oil composition and higher variation of fatty acids in CO. All MO-emulsions showed less area compared to CO-emulsions, indicating that GMO molecules could be in a parallel arrangement at the interface. A similar outcome (lower melting enthalpy for GMO in MO than CO) was also found in DSC results, indicating more interaction of GMOs in CO-emulsions than MO-emulsions (Figure 4.15).

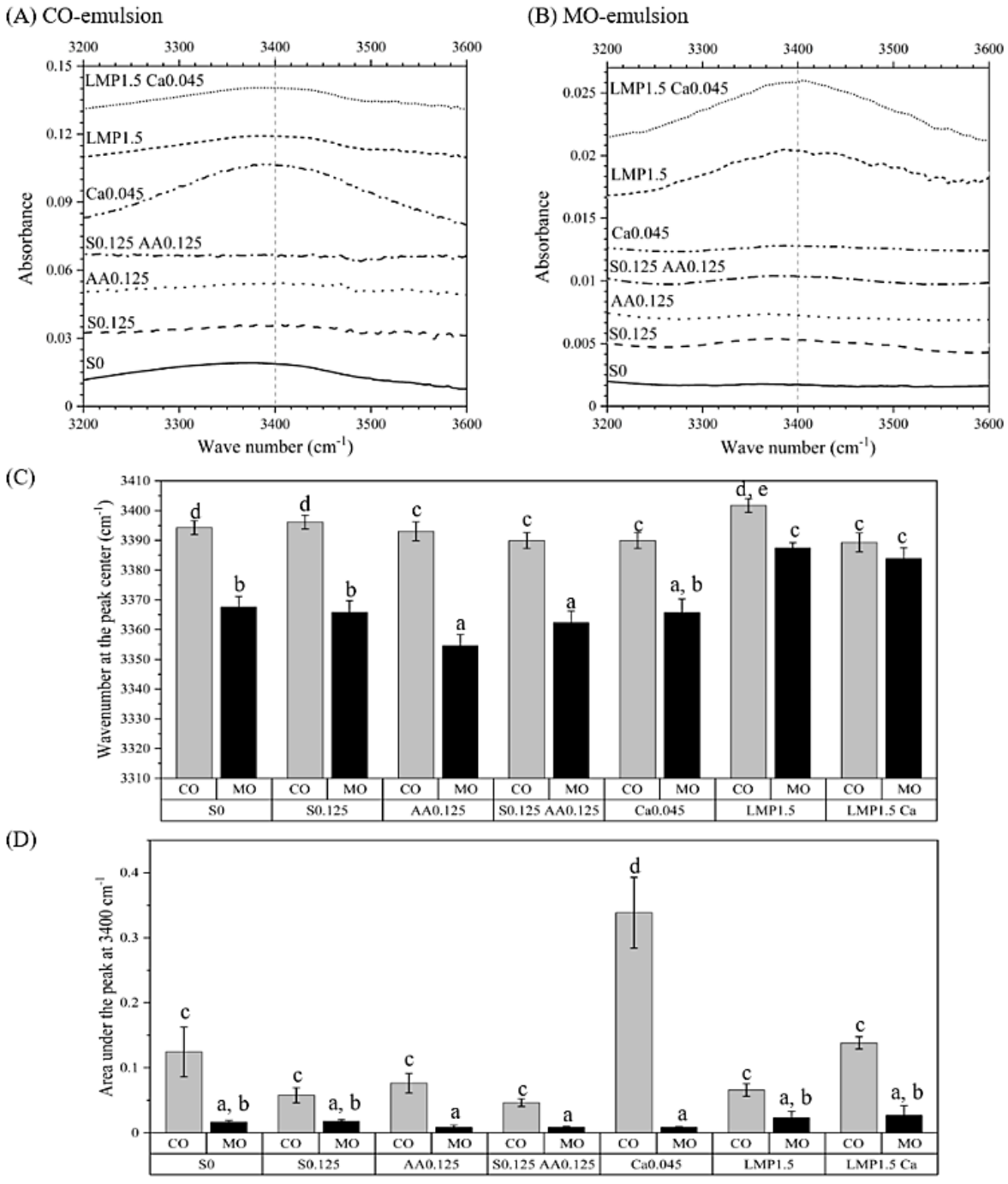

Figure 4.16 ATR-FTIR spectra for intermolecular hydrogen bonding (~3400 cm^{-1}) of GMO hydroxyl (OH) groups in (A) CO and (B) MO-emulsions with aqueous phases containing no additive (S0), salt (S), ascorbic acid (AA), S with AA, calcium chloride (Ca), low methoxyl pectin (LMP) and LMP with Ca. (C) The change in intermolecular hydrogen bonding peak frequency in CO and MO-emulsions. (D) Areas under the peaks in both oil emulsions. The concentration of ingredients is mentioned in the figure. Different letters represent significant differences at $p \leq 0.05$ (Tukey's test).

4.4.10.2 GMO carbonyl group stretching at the oil-water interface (peaks 1735 and 1742 cm^{-1})

A specific vibration mode of GMO, the carbonyl at the α position with a frequency range of 1720 – 1745 cm^{-1}, was analyzed to understand its interaction with water and various aqueous phase additives. The carbonyl band is expressed by a free rotating carbonyl peak at ~1740 cm^{-1} and the intramolecular hydrogen-bonded carbonyl peak at ~1730 cm^{-1} (Bitan-Cherbakovsky et al., 2009). The spectra of all emulsions in the carbonyl (C=O) stretching region are presented for CO (Figure 4.17A) and MO emulsions (Figure 4.17B). The peak areas for the free and bonded carbonyl groups are shown in Figure 4.18C for CO and Figure 4.18D for MO-emulsions. With additives, the peak area for bonded carbonyl (1735 cm^{-1}) significantly decreased in CO-emulsions (Figure 4.17C). A lower peak area indicates less molecular motion (Nilsson et al., 1994), so GMO molecules were more organized at the interface with additives in the aqueous phase, indicating intermolecular interactions. The peak area for free carbonyl groups was significantly higher than the bonded carbonyls, and no significant difference among the various additives could be seen (Figure 4.17C). It can be due to excess acyl groups in bulk CO, which were in high molecular motion. For MO-emulsions, peak areas for both bonded and free carbonyl groups were much lower than CO-emulsions (Figure 4.17D), indicating more GMO molecular order at the interface in MO than CO, due to carbonyl groups absence in MO. Very little difference can also be observed in the peak areas of free and bonded carbonyls in MO-emulsions with various additives, except for higher peak area (more disorder) of free carbonyls in S0.125 and bonded carbonyl in AA0.125 and Ca0.045. The lowest bonded and free carbonyl peak areas were observed for MO-emulsions without additive and LMP-Ca indicating relatively lower GMO molecular motion (more order) at the interface. Overall, more disordered GMO molecules were at the water-CO interface than the water-MO interface supports our initial hypothesis that interfacial packing of GMO could be interrupted by its interaction with CO fatty acids. However, the addition of aqueous phase additives could significantly improve GMO molecular order at the interface, which was responsible for better emulsion stability, as observed in Figures 4.1 and 4.2.

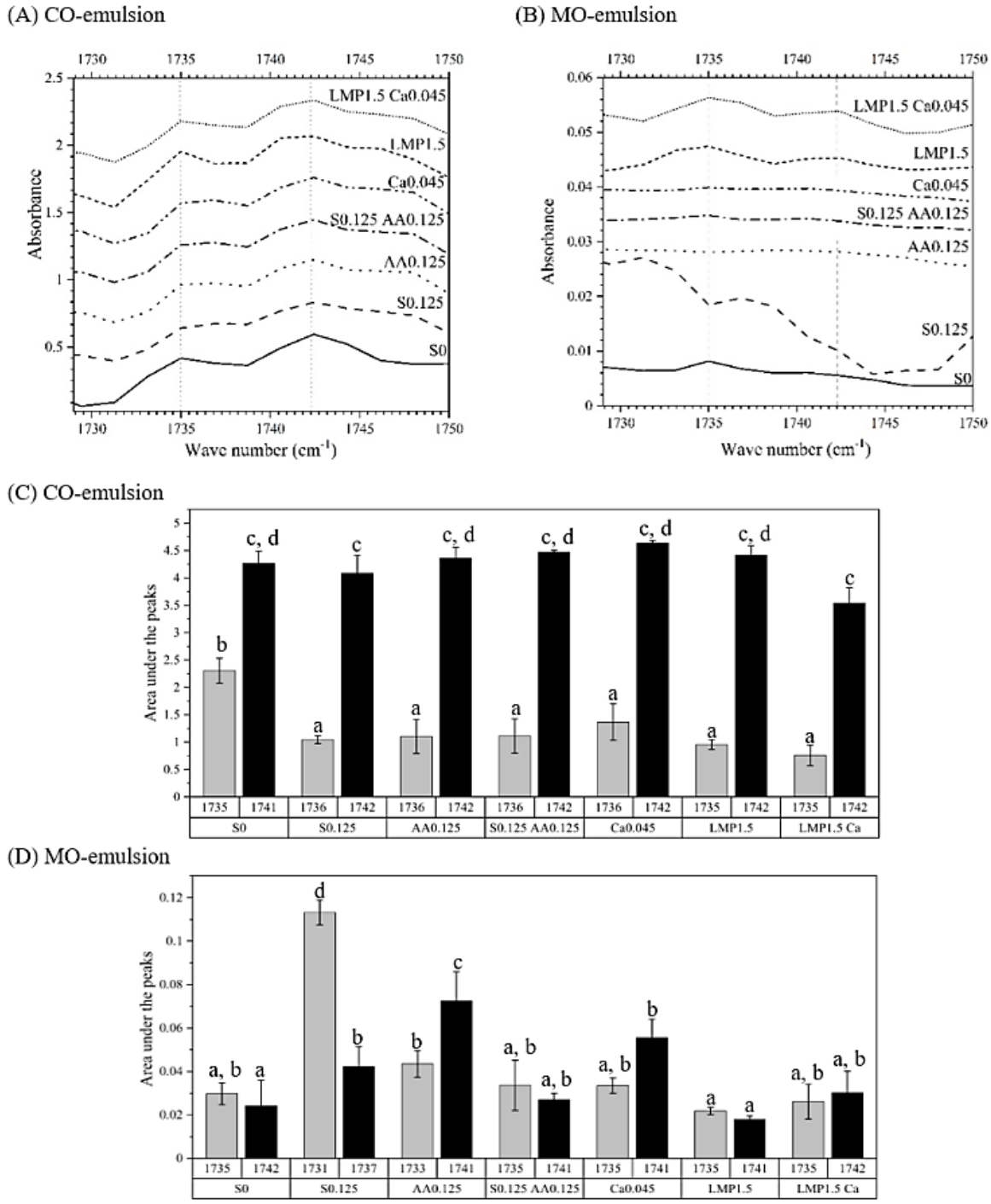

Figure 4.17 ATR-FTIR spectra for free C=O at the α position of GMO's head group (1742 cm^{-1}) and hydrogen-bonded C=O (1735 cm^{-1}) with different aqueous phases containing no additive (S0), salt (S), ascorbic acid (AA), S with AA, calcium chloride (Ca), low methoxyl pectin (LMP), and LMP with Ca in (A) CO, and (B) MO emulsions. (C and D) Areas under the peaks in CO and MO emulsions. The concentration of ingredients is mentioned in the figure. Different letters represent significant differences at $p \leq 0.05$ (Tukey's test).

4.4.10.3 Stretching mode of hydrocarbon chain (CH2 wagging mode from 1330 to 1400 cm^{-1})

The type of oil influences the orientation of the GMO hydrocarbon tail in the interface's hydrophobic side. The CH_2 wagging vibration of GMO could be affected by their interaction with the oil molecules and the vibration of the CH_3 end of GMO involved in non-planner conformations (gauche). The absorption band at ~1341 cm^{-1} for the end gauche CH_2 conformation, ~1354 cm^{-1} for the double-gauche (gg) CH_2 conformation, ~1367 cm^{-1} for the gauche-trans-gauche (gtg) conformation for kinks can be used to identify the disorder in the lipid chain (Bitan-Cherbakovsky et al., 2009). The band at ~1341 cm^{-1} could be influenced by peaks from the D-O-D bending vibration of D_2O (Falk, 1990); hence, it was not considered in our analysis. As the IR adsorption of the terminal CH_3 groups of lipid tail is insensitive to the hydrocarbon chain conformation, researchers have used the CH_3 umbrella band as an internal standard to normalize the neighbouring CH_2 wagging band so that the effect of different additives and oil phase can be compared (Lewis & McElhaney, 2013). The CH_2 wagging IR spectra for CO-emulsions were plotted in Figure 4.18A. The normalized gg and the kink bands area from IR spectra of CO-emulsions were exhibited in Figure 4.18B. In MO, the presence of more conformationally disordered alkanes made impossible identification of subtle changes in the GMO hydrocarbon chain due to various aqueous phase additives (no change in peak area was observed, data not shown). Hence, this approach of chain conformation was not used for MO-emulsion.

An increase in normalized band area of gg and kink conformation indicates higher disorder in the GMO hydrocarbon chain in CO due to its interaction with aqueous phase additives, leading to a looser packing of GMO at the interface. It should be stated that the absorption band of CH_2 groups originated from all lipid molecules, including CO; however, the effect of aqueous phase additive could only affect GMO interfacial packing, which can be noticed from the normalized band intensities. The emulsions without additive and LMP showed the lowest peak area for kink conformation, which indicated that bulky LMP structure gave stability to the GMO lipidic tails. The addition of S, AA, and Ca slightly increased the band area for both peaks, indicating more disorder and looser hydrocarbon chain packing, which was also observed in GMO melting peaks (Figure 4.16C). It is possible that those molecules competed for bonding water with GMO, swelling the GMO polar heads and loosening their fatty acid packing in the oil phase. A similar observation was also made by Bitan-Cherbakovsky et al. (2009) in their study of structural rearrangement of GMO mesophases in the presence of AA (1 to 4 wt%) in water, in which AA increased the space between GMO molecules allowing the incorporation of vitamin E and fatty acids chain from the oil phase.

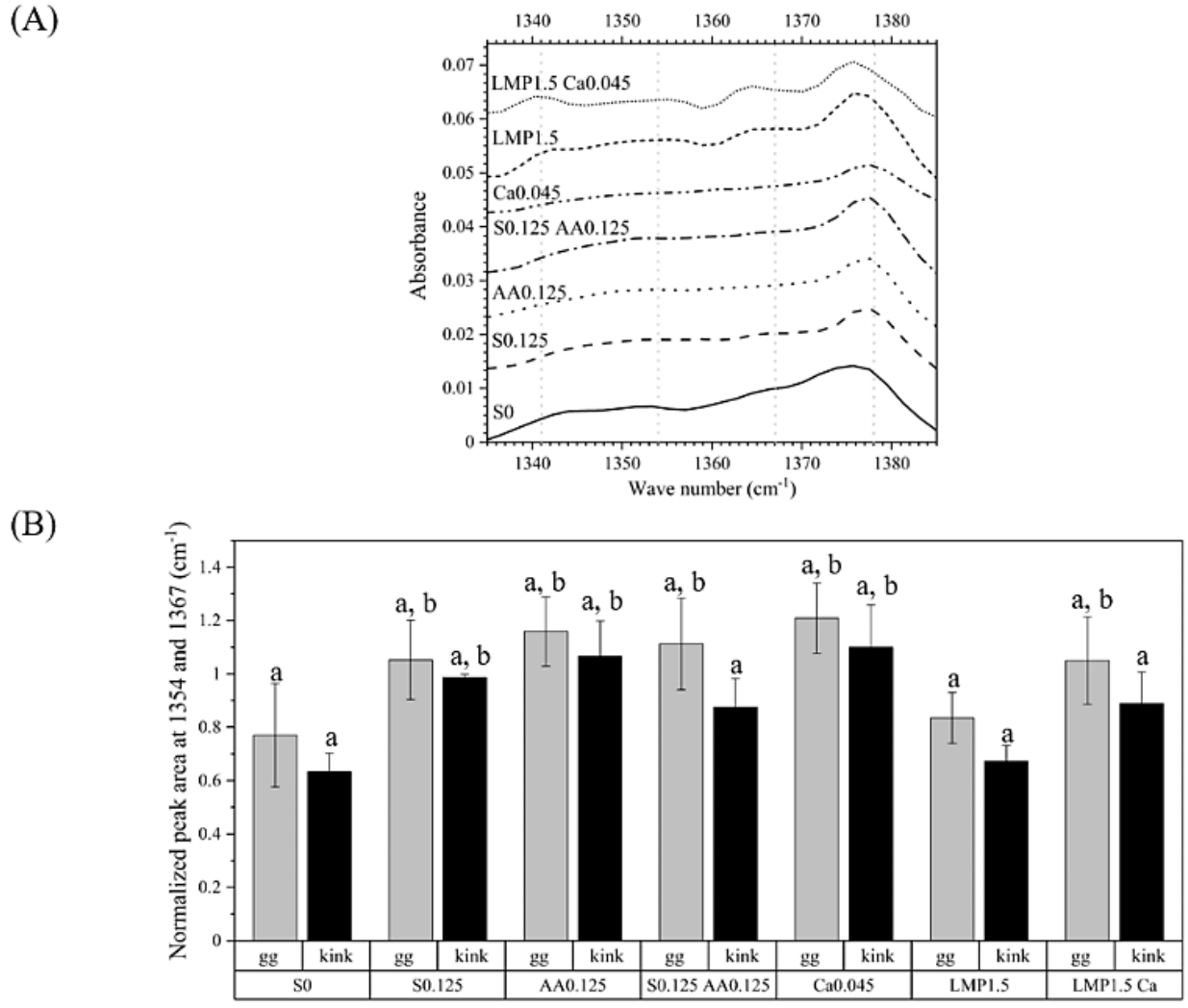

Figure 4.18 ATR-FTIR spectra for hydrocarbon chain CH2 stretching mode from 1300 to 1400 cm^{-1} for CO-emulsions with different aqueous phases containing no additive (S0), salt (S), ascorbic acid (AA), S with AA, calcium chloride (Ca), low methoxyl pectin (LMP), and LMP with Ca. (B) The normalized double-gauche (*gg*) CH_2 band at 1354 cm^{-1} and the normalized gauche-trans-gauche (*kink*) at 1367 cm^{-1} with respect to symmetric bending of the end CH_3 vibration at 1378 cm^{-1}. The ingredients and their concentration is mentioned in the figure. Different letters represent significant differences at $p \leq 0.05$ (Tukey's test).

4.4.11 Discussion

Based on this study's main hypothesis, the incorporation of additives in the aqueous phase interacted at the interface with GMO in a different manner according to the type of bond and structure. The increase of hydrogen bonding was also influenced by the oil type, where CO with GMO had higher interaction found in DSC in GMO melting peak temperatures (Figure 4.16A, B) data and IR spectra in GMO intermolecular

hydrogen bonding (Figure 4.17C). Due to more interaction and molecular motion in CO-GMO, these systems are more complex to understand and establish. However, it was discovered that with hydroxyl donating agents, the interface's GMO desorption mechanism could be prevented. Hydroxyl group donating agents were evaluated, such as AA, CA and LMP molecules as sources of hydroxyl groups to hydrogen bond with GMO at the interface. Still, the polysaccharide showed better performance at the interface, allowing better packing of GMO at the interface due to the molecular size. It indicates that liquid W/O emulsion stability relies on hydrogen bonding interactions and other properties like each phase's viscosity and gelation. CO excess of surface-active molecules influenced in all phenomena. Droplet size was significantly larger in CO than MO, which also influenced more packing of water droplets and higher viscosity. However, gelation showed better characteristics with LMP in CO, exhibiting no yield in G'' after 7 days than all emulsions. It could be related to further interactions of LMP chains between the water droplets with fatty acids, water droplets or LMP.

4.5 Conclusions

Different hydroxyl group donating agents (ascorbic acid, citric acid and low methoxyl pectin) were used to develop stable liquid water-in-oil emulsions. Two different salts (S and Ca) were tested alone and combined with the hydroxyl group donating agents. Emulsions prepared with AA showed higher emulsion stability (43 and 53%) compared to CA (32 and 43%) in CO. However, the combination with salt showed a non-significant difference in emulsion stability (61 – 64%). Besides, CO emulsions with LMP formed the highest emulsion stability after seven days (72%). The addition of Ca did not improve the emulsion stability in either CO or MO. All MO-emulsions reported improved emulsion stability than CO-emulsions. The emulsions with Na^{+} (54%, in CO and 72%, in MO) were more stable than Ca^{+2} (46%, in CO and 60%, in MO) in both oil types. It was found that more intermolecular hydrogen bonding was formed in emulsions with CO, which contains different fatty acids than in MO were mainly alkanes. Thus, more GMO parallel packing was identified in MO-emulsions; however, LMP structure allowed GMO parallel mechanism at the interface in CO. The results in viscosity, gelation, microstructure, DSC and FTIR evidenced the different interactions involved in liquid W/O emulsions. Intermolecular hydrogen bonding between canola oil and GMO controlled the development of gelation, interfacial tension, DSC and FTIR. However, viscosity, droplet size and microstructure exhibited better characteristics in MO emulsions with alkanes with less interaction of fatty acid at the interface, mainly GMO. The combination of those factors allowed higher stability of liquid W/O emulsions with CO and MO.

4.6 Connection to the third study

The second study developed liquid W/O emulsions for cosmetic, skincare and food applications due to the use of two different oils as the continuous phase, light mineral oil and canola oil. The prevention of GMO desorption from the water surface was investigated by the addition of hydroxyl groups donating agents to form stronger interfacial hydrogen bonding. The emulsification was done in a high-pressure homogenizer at a hot temperature (70 °C). Various hydroxyl groups donating molecules – ascorbic acid, citric acid and low methoxyl pectin – were incorporated in the aqueous phase, aiming to form stronger hydrogen bonding with GMO at the interface. Two different salts – S and Ca were utilized. The salts were added to enhance the emulsifier packing at the interface, S was mixed with AA and CA, and Ca with LMP. With these combinations, it was possible to obtain stable water droplets; however, the storage stability against gravitational separation was not significantly increased. LMP was the molecule that showed the least oil phase separation in CO and MO after 7 days at room temperature. All the emulsions showed weak gel behaviour. DSC and IR analysis showed that AA formed intermolecular hydrogen bonding; however, LMP formed even stronger hydrogen bonding. The packing of GMO at the interface was also in parallel order with LMP than in all additive molecules tested, showing more disorder, which influenced the higher emulsion stability with LMP. The type of oil showed its impact; CO with different TAG molecules had high interfacial interaction with GMO than in MO. The hypothesis was validated after all the different analyses were correlated.

Stability of liquid W/O emulsion has not been developed extensively for food application than in the cosmetic or skin-care field. More studies on W/O emulsion stability have been developed with mineral oil containing hydrocarbon chain structure due to the emulsifiers' lack of interaction with this oil type. Thus, the need for developing stable W/O emulsions without any phase separation using vegetable oils with a low percentage of saturated fatty acids guided the interest of the subsequent study. Using the second study's knowledge on W/O emulsion, intermolecular hydrogen bonding between LMP and GMO, the high solubility of GMO in CO, and the visual stability of the emulsion at room temperature were useful in designing the third study. The third study investigated the development of viscoelastic properties from liquid W/O emulsions formed with canola oil. Crystallization of solid fats is the main stabilization mechanism in most food-grade W/O emulsions. Thus, a low concentration of hydrogenated soybean oil was experimented within the emulsion, which crystallized under the storage condition (4 °C). The main objective of the investigation was to increase dispersed water content so that the packing of water droplets would significantly improve their viscoelastic behaviour at a lower fat content.

5. EFFECT OF PECTIN AND WATER CONTENT ON THE VISCOELASTIC IMPROVEMENT OF WATER-IN-CANOLA OIL EMULSIONS FOR FOOD APPLICATIONS[3]

5.1 Abstract

This study aimed to investigate gelation in glycerol monooleate (GMO)-stabilized water-in-canola oil (W/CO) emulsions by increasing water content (20 – 50 wt%) and the addition of LMP in the aqueous phase. A constant ratio of GMO to water was used to keep a similar droplet size in all emulsions. Hydrogenated soybean oil (7 wt%) was used to provide network stabilization in the continuous phase. All fresh emulsions with LMP in the aqueous phase formed a stable and self-supported matrix with higher viscosity and gel strength than emulsions without LMP. Emulsion viscosity and gel strength increased with an increase in water content. All emulsions showed gel-like property (storage moduli (G') > loss moduli (G")) related to the presence of LMP in the aqueous phase and increased water content. Freeze/thaw analysis using a differential scanning calorimeter showed improved stability of the water droplets in the presence of LMP in the aqueous phase. This study demonstrated the presence of LMP in the aqueous phase, its interaction with GMO at the interface, and fat crystals in the continuous phase that could support the water droplets' aggregation to obtain stable elastic W/CO emulsions that can be used as low-fat tablespreads (Figure 5.1).

[3]Published manuscript of an article published in Fluids as part of the Special Issue Fluid Mechanics of Suspensions and Emulsions on June 18, 2021. The present chapter is a modified copy of this publication.
Romero-Peña, M., & Ghosh, S. (2021). Effect of Water Content and Pectin on the Viscoelastic Improvement of Water-in-Canola Oil Emulsions. *Fluids, 6*(6), 228. https://doi.org/10.3390/fluids6060228.
Author role: Romero-Peña, M. carried out the experiments and wrote the first draft. Ghosh, S. conceptualized, supervised, reviewed, and edited.

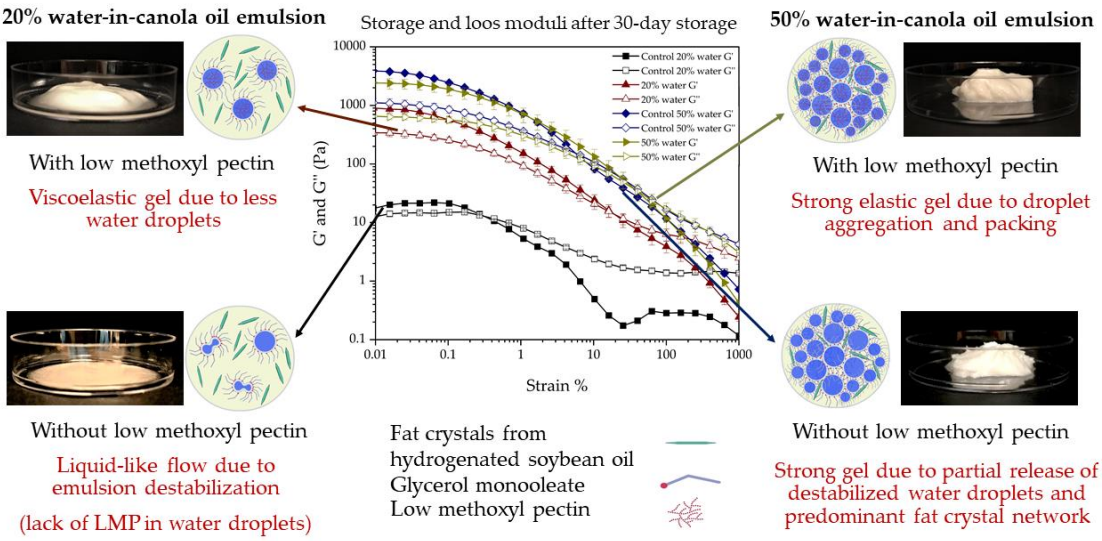

Figure 5.1 Proposed mechanism behind the viscoelastic properties of W/O emulsions with 20 and 50 wt% water content without LMP and with LMO.

5.2 Introduction

Products containing water-in-oil (W/O) emulsions are widely used in the pharmaceutical, cosmetic and food industries. In the cosmetic industry, W/O emulsions have been used to deliver moisture in lipsticks due to the high rigidity provided by excess waxes and pigments (Beri et al., 2013). In food, butter and margarine are W/O emulsions where water droplets are dispersed in a continuous fat phase made of semisolid dairy or vegetable fats, respectively. Recently, interest has shifted to develop stable food-grade W/O with lower fat content, structured with high-quality lipids (low saturated fats) and with the addition of health-beneficial functional molecules in the aqueous phase (Rousseau, 2020). A network of fat or wax crystals or Pickering particles around the water droplets are some of the mechanisms that have been studied to stabilize these emulsions (Ghosh & Rousseau, 2011). The oils have a low dielectric constant; thus, stability cannot be explained purely with the DLVO theory (Scherze et al., 2006). Hence, stabilization due to electrostatic repulsion would be insignificant in W/O emulsion. The emulsifiers most commonly used to emulsify water in a continuous oil phase are non-ionic emulsifiers due to the low hydrophilic-lipophilic balance (HLB) or surface-active Pickering particles (McClements, 2015). Although emulsifiers are essential, most W/VO emulsions are stabilized via fat crystallization, acting as Pickering (surface-active) or 3D network stabilization (surface-inactive) (Ghosh & Rousseau, 2011). It has been shown that in W/O emulsions, fat post-crystallization after emulsification provided more stability than pre-crystallization of fats before emulsification, reducing droplet coalescence and preventing sedimentation (Hodge & Rousseau, 2003).

Due to solid fat, the texture of most W/VO emulsions (e.g., margarine) is solid or semisolid, which also provides desired spreadability or plasticity of the product (Ushikubo & Cunha, 2014). Lately, the water-dispersed phase has been considered an active filler inside a matrix of oil and fat crystals where water droplets have shown to increase the viscosity and viscoelasticity of the whole product (Rousseau, 2020). For instance, Haj-shafiei et al. (2013) developed W/MO emulsions, stabilized by 5% wax of oil phase and 0.025 – 0.125 wt% glycerol monooleate (GMO) of the oil phase. The increase in water content was from 10 – 50 wt%. The researchers reported an increase in viscosity and viscoelasticity of the emulsion at high water content during storage due to grown wax crystals' enmeshing. Iqbal et al. (2012) also investigated the increase of water content from 10 to 40 wt% in W/O emulsions. In this case, thermal denaturation was induced in whey protein isolate solutions at high temperature, salt, and pH neutral to form a gel in the water droplets. The viscoelasticity increased significantly with 30 and 40 wt% water due to the rise in droplet concentration and stronger bonds between the droplets.

With a rise in consumer demand towards low-fat margarine-based tablespread, it is critical to developing W/VO emulsions with a higher water content that would provide improved rheology and structure formation. However, stable W/O emulsions with high water droplet volume fraction and improved viscoelasticity are challenging systems to develop. Vegetable oils are made of triacylglycerols, containing polar carbonyl and hydroxyl groups that interact with surface-active molecules at the interface and pull them out of the water droplet surface, leading to emulsion destabilization (Ghosh et al., 2011). It was found that the only emulsifier that could provide high stability to a liquid W/VO emulsion is a polymeric polyglycerol plyricinoleate (PGPR), which itself provides a strong anchoring at the water-VO interface the thereby preventing their desorption from the water droplet surface (Ushikubo & Cunha, 2014). Conversely, mineral oils made of alkanes have a less complicated hydrocarbon chain structure and do not interact with the emulsifier molecule at the water droplet surface. Hence, many non-polar emulsifiers (e.g., glycerol and sorbitan esters) can be used to stabilize liquid water-in-mineral oil emulsions. However, to stabilize W/VO emulsions with food-grade glycerol monoesters, it is necessary to have fat crystallization at the water droplet surface and in the continuous oil phase. The Pickering crystallization at the water droplet surface could prevent emulsifier desorption to the bulk phase from the water droplet surface. The fat crystal network in the continuous oil phase could also partially immobilize the water droplets, thereby providing stability to the W/VO emulsion. However, how increasing the water droplet volume fraction could enhance the viscoelasticity of the whole W/VO emulsion has not been studied in detail. Rising health concerns over the use of PGPR have also led to a challenge in developing stable W/VO emulsion without the use of PGPR. Therefore, in the present research, our objective was to investigate water content's influence on the structure

formation and rheology of W/VO emulsions. Structuring of W/O emulsions using water droplets could be essential to reduce saturated fats and calories in tablespreads, coatings, bakery goods or ganache.

The W/CO emulsions with 20 – 50 wt% water were developed with GMO as an emulsifier. To prevent GMO's desorption from the water droplet surface, low methoxyl pectin (LMP) was added to the aqueous phase. To provide margarine-like solidity to the emulsions, fully hydrogenated soybean oil (HSO) with high melting point (~50 °C) and high concentration (~85 %) of stearic acid (C18:0) was used as a continuous phase network stabilizer. Fully hydrogenated oils have been used to provide a fat crystal network in the oil phase due to their non-trans fatty acids nature so that fat-products with a healthy balance can be provided (Acevedo & Marangoni, 2014). This study aimed to determine the interaction between water content, the presence of LMP in the aqueous phase, and HSO in the continuous oil phase in order to develop viscoelastic properties of a W/VO emulsion with improved gel strength.

5.3 Materials and methods

5.3.1 Materials

The materials used in this study were the same as mentioned in section 4.3.1 (paragraph 1), except for deuterium oxide, AA, and CA, which were not used in this research. New material, fully hydrogenated soybean oil flakes (HSO), was provided by ADM James R. Randall Research Center (Decatur, IL, USA).

5.3.2 Preparation of aqueous and oil phases

The aqueous phase was prepared with 1.5 wt% LMP, as was presented in section 4.3.2. These solutions were made the same day as emulsions preparation. Bulk oil phases were prepared with HSO and GMO according to Table 5.1. According to preliminary research, it was found that a minimum GMO to aqueous phase ratio of 0.065 was required to stabilize 20 wt% W/CO emulsions. This composition was used as the basis for all emulsions with 20 – 50 wt% water, where the water to GMO ratio was kept constant. We also tried to make emulsions with 60 wt% water. However, due to an extreme increase in viscosity, it was impossible to homogenize the emulsions properly; hence, it was no longer persuaded. It was found that a minimum 7 wt% HSO in the emulsion was required to maintain the water droplets stable. All the oil solutions were kept under stirring (400 rpm) at 80 ± 0.5 °C for 20 min until complete melting of HSO and GMO. These solutions were prepared the same day as the emulsions.

Table 5.1 W/O emulsion composition for all water content in 100 g. The last two rows show the composition of control W/O emulsion without LMP in the aqueous phase. LMP: low methoxyl pectin, CO: canola oil, HSO: fully hydrogenated soybean oil, GMO: glycerol monooleate.

Water (g)	LMP in water (g)	CO (g)	HSO in CO (g)	GMO in CO (g)	GMO: aqueous phase ratio
20	0.30	71.40	7.0	1.30	0.065
30	0.45	60.60	7.0	1.95	0.065
40	0.60	49.80	7.0	2.60	0.065
50	0.75	39.00	7.0	3.25	0.065
20	0	71.70	7.0	1.30	0.065
50	0	39.75	7.0	3.25	0.065

5.3.3 Preparation of W/O emulsions

The aqueous and oil solutions were held warm at 75 ± 0.5 °C in order to keep all the components molten. The oil phase was weighed in a glass beaker and stirred at 400 rpm with a magnetic stirrer (VWR International, Edmonton, AB, Canada). The aqueous phase was weighted in a separate glass beaker and added dropwise into the hot oil solutions while stirring. Final emulsions were developed in two steps. First, coarse emulsification was done with a rotor-stator blender (Polytron, Brinkman, ON, Canada) at level 10 for 1 minute. Secondly, the hot coarse emulsions were further homogenized in a high-pressure homogenizer (Emulsiflex C3, Avestin Inc., Ottawa, ON, Canada) at 5,000 psi for three cycles. The homogenizer was preheated by passing CO (50 ± 2 ℃) at 5,000 psi. The final emulsions at around 50 ºC were collected in 250 mL beakers and cooled down at room temperature for 20 minutes. Each sample weight was then divided into two beakers (40 mL) and stored in a refrigerator at 4 °C.

5.3.4 Emulsion storage stability

Fresh emulsions (15 mL) were transferred into clear glass vials (40 mL) with a top cap (VWR International, Edmonton, AB, Canada) and stored at 4 °C. On day 30, the tube was flipped 90 degrees parallel with the table, and the photos were captured. On day 1, one scoop of W/O emulsion was also placed in a plastic Petri dish (VWR International, Edmonton, AB, Canada) in order to record flow behaviour and covered with aluminum foil for undisturbed storage for 30 days at 4 °C. The images of the samples were taken with an iPhone 8's camera (12 MP).

5.3.5 Microstructure analysis

The fat crystal network and water droplet network were analyzed with brightfield and polarized light. All emulsions were examined with a polarized light microscope on days 1 and 30 with a (Motic BA380 Pol microscope, Richmond, BC, Canada) and a Nikon camera DS-Fi1 (Nikon Corporation, Tokyo, Japan) using a 100x oil immersion objective lens. A small drop of the emulsion was placed over a glass slide (VWR, Edmonton, AB, Canada), and a coverslip was positioned above the sample. Nis-Elements F3.0 software (Nikon Canada Inc., Mississauga, ON, Canada) was utilized to record the images. ImageJ image analysis software (v1.5 2i – Fiji project) was employed in order to enhance images' quality with the brightness and contrast of the 8-bit images (Schindelin et al., 2012).

5.3.6 Rheology of W/O emulsions

Rheology analyses were performed as in section 4.3.8 with a steel crosshatched plate (40 mm diameter, 992478).

5.3.7 Thermal analysis of emulsions

Fresh (day 1) and stored (day 30) samples (<10 mg) were sealed in aluminum T- Zero hermetic lids and pans (TA Instruments, New Castle, DE, USA) and temperature-cycled in a differential scanning calorimeter (DSC) Q2000 (TA Instruments, Montreal, QC, Canada). An empty T-zero pan was utilized as a reference. The samples were heated from 25 °C to –70 °C, heated to 70 °C, followed by a second cooling cycle to –70 °C at 5 °C/min. A temperature hold of 1 min was kept between the thermal cycles. The presence of bulk water crystallization peaks during the first and third cooling cycles was used as an indicator of emulsion instability. Universal Analysis 2000 software (TA Instruments, New Castle, DE, USA) was used to integrate the peaks to obtain crystallization and melting temperatures (°C) along with the enthalpy of phase transition (J/g).

5.3.8 Determination of solid fat content analysis

Mixtures of CO with 3 – 8 wt% HSO were prepared to develop a calibration curve for HSO melting using the DSC. The oil phases were completed melted at 70 °C. Then, a sample was placed in the pan to be hermetically sealed. The procedure used was the same as section 4.3.10. A linear trendline was identified with $R^2 = 0.9972$. The refrigerated emulsions (4 ºC) were thermally analyzed on day 1 and day 30 by heating to 70 °C at 5 °C/min to predict the percentage of solid HSO in the emulsion after the homogenization and storage process using the enthalpy calibration curve.

5.3.9 Statistics

All of the emulsions were prepared in triplicate with the respective analysis on day 1 and day 30. The three means were used to analyze variance with one-way analysis of variance (ANOVA), and the p-value was set with the α value of 0.05%, using the IBM SPSS Statistics 20 software (IBM, Armonk, NY, USA) for this purpose.

5.4 Results

5.4.1 Emulsion appearance and storage stability

The Petri dish test showed visual observation of emulsion flow behaviour during storage on day 1 and day 30 (Figure 5.2A, B). Almost all of the W/O emulsions were highly viscous liquids without any flow, except for the control emulsion (without LMP) with 20 wt% water, which visually flowed on day 1 (Figure 5.2A). However, the control emulsion with 50 wt% water showed no flow due to close packing of excess water droplets, although its surface looked not smooth and without any gloss (Figure 5.2A).

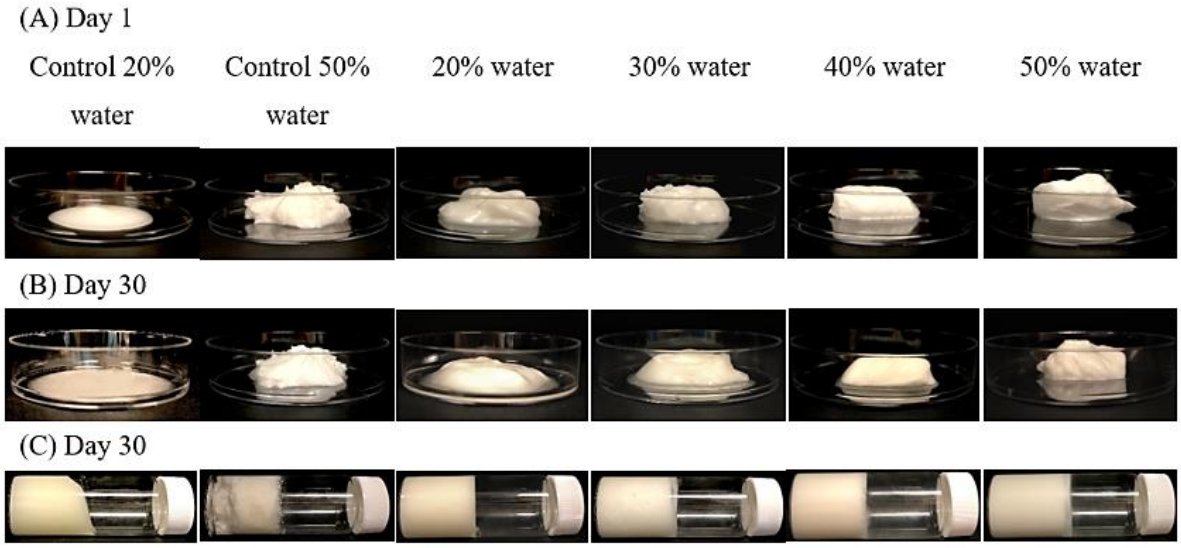

Figure 5.2 Stability of water-in-oil emulsions with different water volume fractions (20, 30, 40 and 50 wt%) prepared with 1.5 wt% LMP or without LMP for control emulsions, GMO and 7 wt% HSO. Petri dish on day 1 (A) and day 30 (B). Glass tube test flipped 90 degrees in parallel with the plane surface on day 30 (C).

Emulsions with aqueous phase LMP and 20, 30, 40, and 50 wt% water self-retained their shape on day 1. On day 30, control emulsion with 20 wt% water content spread over the Petri dish, indicating a

change in emulsions' structure (Figure 5.2B). However, the control emulsions with 50 wt% water showed a similar emulsion shape on day 30 as on day 1. LMP emulsions with 20 wt% water showed a certain degree of spreading compared to day 1, although lower than that of the control emulsions. LMP emulsions with 30 wt% water demonstrated some spreading, but it was less than that of the 20 wt% water emulsions. The LMP-emulsions with 40 and 50 wt% water retained their form without any spreading on day 30, comparable to day 1. Recently Rafanan and Rousseau (2019) reported that W/VO emulsions with 20 wt% water with HSO and PGPR phase separated after 14 days; however, monoacylglycerol-stabilized emulsions exhibited soft, paste-like solids retaining their shape without separation after 28 days of storage. In the present work, shape retention was observed with more water content and at lower GMO and HSO concentrations. Perhaps the presence of LMP in the aqueous phase provided improved stability to the water droplets, leading to improved structure retention.

The flipped glass tubes were also used to detect emulsion stability and gelation after 30 days of storage (Figure 5.2C). Control emulsions with 20 wt% water content showed a partial flow. A similar emulsion with no separation evidence was also found after 28 days of storage with 14.4 wt% HSO and 1.6 wt% GMO by Rafanan and Rousseau (2019). Though control emulsions with 50 wt% water exhibited no flow, aqueous phase separation was observed at the bottom of the glass tube, indicating some emulsion destabilization. All LMP-emulsions reported no phase separation or flow on day 30, suggesting that the emulsions were self-supporting, and a strong gel structure was developed. Similarly, Rafanan and Rousseau (2017) described considerable textural variations with water increment in GMO emulsions. From 5 to 10 wt% water, the emulsions were liquid, and from 15 to 20 wt% water, self-supporting soft solids emulsions were observed for 7 days storage.

5.4.2 Emulsion viscosity

The viscosity graphs exhibited a decreasing trend with the increase in shear rate (Figure 5.3A). The solution of 1.5 wt% LMP began with 4.3 ± 0.7 Pa.s at 0.01 s^{-1}, and after that, the viscosity decreased due to the LMP molecules' de-tangling, and more flow was dominant in the system. The mixture of 7 wt% HSO in CO showed an apparent viscosity of 8.8 ± 1.1 Pa.s at 0.01 s^{-1}, which also decreased with an increase in shear rate due to the rupture of the fat crystals network, and nearly reached nearly a plateau beyond 20 s^{-1} (evidence of liquid-like Newtonian flow behaviour). All emulsions showed a shear-thinning behaviour where viscosity decreased with an increase in shear rate on day 1 and day 30 (Figure 5.3B, C). Control emulsions with 20 wt% water showed the lowest viscosity trend with shear, which began with a low-shear

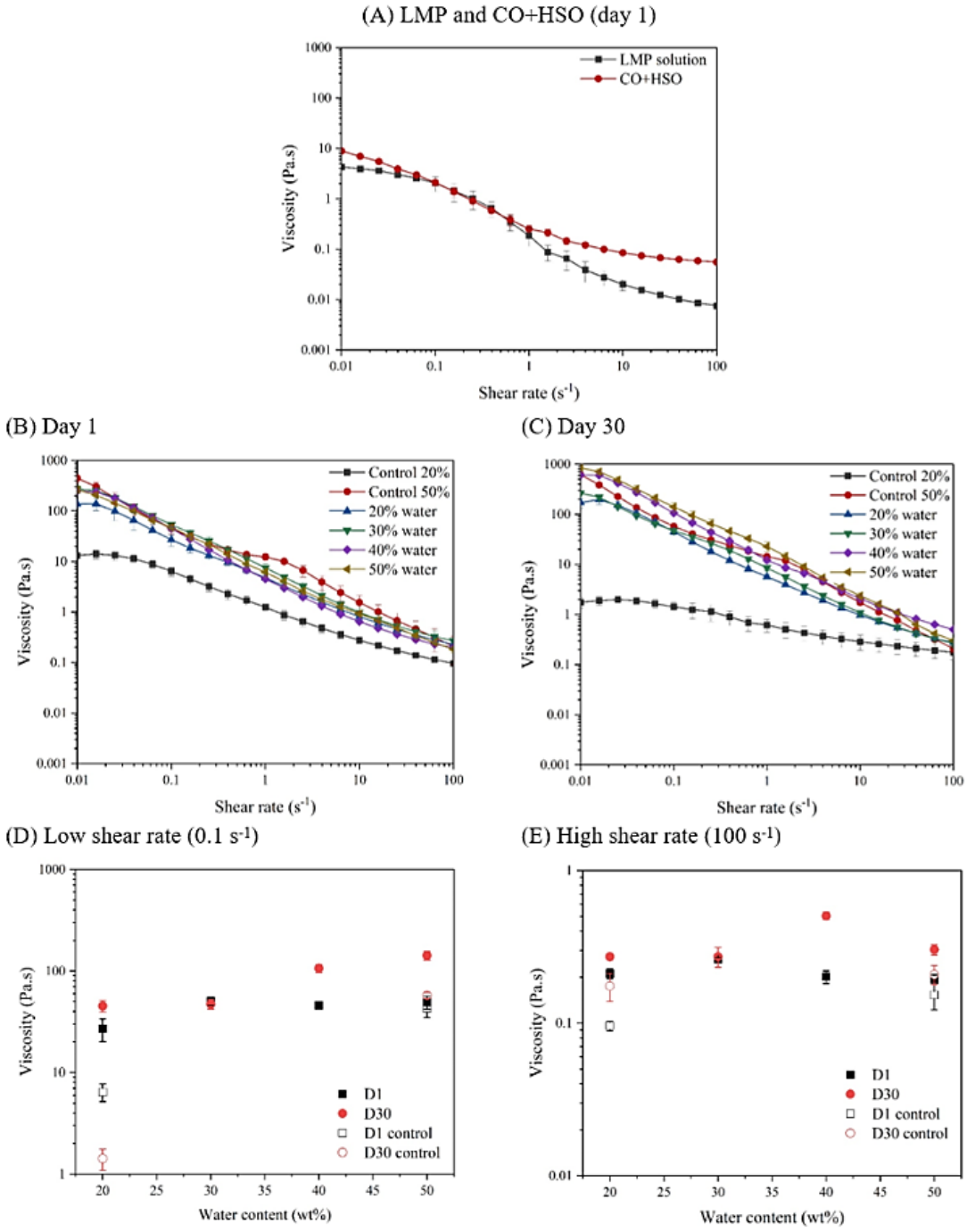

Figure 5.3 Apparent viscosity of 1.5 wt% LMP solution and 7 wt% HSO in canola oil on day 1 (A). (B and C) Viscosity as a function of shear rate for water-in-oil emulsions with different water content 20, 30, 40 and 50 wt%, prepared without and with LMP, GMO and HSO on day 1 (B) and day 30 (C). (D and E) Apparent viscosity of water-in-oil emulsions with different water content 20, 30, 40 and 50 wt%, prepared without and with LMP, GMO and HSO on day 1 and day 30 at a low (0.1 s^{-1}) shear rate and at high (100 s^{-1}) shear rate (E). Note the difference in y-axis scales due to variation in shear rates.

plateau at 13.2 ± 1.7 Pa.s at 0.01 s^{-1} and decreased to at 0.1 ± 0.01 Pa.s at the end of the run at 100 s^{-1} (Figure 5.3B). However, control emulsions with 50 wt% water showed an initial viscosity higher than all emulsions at 0.01 s^{-1}, which showed a slightly irregular viscosity curve as a function of shear than all other emulsions. Such behaviour could be related to their uneven texture observed in the Petri dish (Figure 5.2A). LMP emulsions with 20 wt% water exhibited an initial viscosity significantly higher (137.05 ± 25.02 Pa.s) compared to control 20 wt% water emulsions. There was not much difference in the viscosity trend of other LMP emulsions. In contrast, to control emulsions with 50 wt% water, all of the LMP emulsions showed a brief low-shear viscosity plateau, which indicates their Newtonian fluid-like behaviour at a very low shear rate.

After ageing, control emulsions with 20 wt% water exhibited a significant viscosity drop (Figure 5.3C), which was expected based on their visual observation of its flow behaviour (Figure 5.2B). Control emulsion with 50 wt% water had a similar irregular viscosity curve but, in less magnitude, than on day 1. For all LMP emulsions, the viscosity curves shifted to higher values after 30 days of storage. The viscosity profiles of LMP emulsions with 50 and 40 wt% water were even higher than the 50 wt% water control emulsion after 30 days of storage. Similarly, emulsions with 50 wt% water content reported substantially higher viscosity than 40, 30 and 20 wt% water for W/MO emulsions stabilized with wax and GMO after 28 days storage (Haj-shafiei et al., 2013).

5.4.2.1 Apparent viscosity at a low shear rate

For direct comparison, emulsions' apparent viscosities at two different shear rates were plotted in Figure 5.2 D, E. Apparent viscosity at 0.1 s^{-1} shear rate (Figure 5.3D) would represent emulsion viscosity when the structure was not completely broken down due to shear, while apparent viscosity at 100 s^{-1} of shear rate (Figure 5.3E) would be an indication of free-flowing emulsion where the original structures were largely broken down. On day 1, at 0.1 s^{-1} shear rate, the control emulsion with 20 wt% water showed the lowest viscosity (6.4 ± 1.3 Pa.s), which increased to 42.9 ± 8.0 Pa.s for the control emulsions with 50 wt% water. Such an increase in viscosity is related to the rise in the amount of dispersed water droplets in emulsion (Figure 5.3D). LMP emulsions with 20 wt% water reported a significant rise in viscosity (27 ± 6.7 Pa.s) compared to the control emulsions with 20 wt% water ($p < 0.05$), which must be related to the improved stability of the water droplets in the presence of LMP in the aqueous phase. Upon increasing the water content, a significant increase in LMP emulsion viscosity at 0.1 s^{-1} was observed at 30% water, which did not change with further increase in water content to 50 wt% (on average, 48.5 Pa.s) ($p > 0.05$). In contrast, Haj-shafiei et al. (2013) showed that apparent viscosity of fresh W/MO emulsion stabilized with paraffin

wax and GMO at 10 s^{-1} shear rate increased proportionally to the increment of water content (20 – 50 wt%). In the present case, perhaps the emulsions' structure was broken even at 0.1 s^{-1} shear rate, and a proper indication of their gelation behaviour could be obtained from small-deformation oscillatory rheological measurement (discussed below). The low-shear viscosity of 50 wt% water control emulsions was not significantly different compared to 50 wt% LMP emulsions ($p > 0.05$), which indicates that under fresh conditions, the predominant interaction influencing the viscosity of concentrated emulsions was the active filler property of the water droplets.

On day 30, control emulsions with 20 wt% water demonstrated a decrease in viscosity (1.4 ± 0.3 Pa.s) from day 1 (Figure 5.3D), which could be associated with the visual observation of their flow behaviour under the quiescent condition shown in Figure 5.1B. Nevertheless, control emulsions with 50 wt% water content revealed a viscosity increase after storage (57.5 ± 4.2 Pa.s.), related to further HSO crystallization in the continuous emulsion phase. A slight increase in viscosity was also observed after 30 days for 20 wt% water emulsions with LMP, which did not change for 30 wt% of water ($p > 0.05$). Nevertheless, a significant viscosity rise (~2x) was observed for aged LMP emulsions with 40 and 50 wt% water (106 ± 9.8 and 142 ± 14.2 Pa.s, respectively), suggesting the synergistic effect of HSO crystallization along with water droplet packing during storage. On day 30, the viscosity of the LMP emulsions was significantly higher than the control emulsions, which could be due to the improved stability of the aged droplet network in the presence of LMP in the aqueous phase.

5.4.2.2 Apparent viscosity at a high shear rate

The apparent viscosity decreased for all emulsions at a high shear rate (100 s^{-1}) due to the breakdown of fat crystal networks and water droplet packing. On day 1, control emulsions reported a viscosity range of 0.1 – 0.15 Pa.s, while the LMP emulsions showed a range from 0.2 to 0.26 Pa.s (Figure 5.3E). This indicates that, even at a higher shear rate, the LMP's presence in the water droplets was better against the shear force than its absence. Interestingly, on day 1, high shear viscosity decreased for 40 and 50 wt% water emulsions, compared to 20 and 30 wt% water, which could be associated with water droplets' destabilization from tight packing under high shear force. After ageing, all emulsions reported an increase in apparent viscosity even at higher shear, which could be due to HSO crystallization, as discussed above. Control emulsions with only water showed a viscosity of 0.18 ± 0.04 and 0.21 ± 0.03 for 20 and 50 wt% water, respectively. LMP emulsions presented higher viscosity compared to controls emulsions. Emulsions with 20 and 30 wt% water exhibited an average viscosity of 0.27 Pa.s ($p > 0.05$). However, the highest viscosity was reported by 40 wt% water content followed by 50 wt% water content. The decrease in high-

shear viscosity of 50 wt% water LMP emulsions after storage could be due to higher droplet destabilization under high shear force when they were closely packed. An increase in viscosity from 10 to 40% water followed the trends observed by Iqbal et al. (2012) for PGPR-stabilized water-in-soybean oil emulsions containing whey protein isolate (WPI) and S in the aqueous phase. Heating the emulsions to denature WPI in the aqueous phase, and subsequent cooling, led to a steep increase in apparent viscosity at 10 s^{-1} for 30 and 40 wt% water (~38 and 54 Pa.s, respectively) compared to 10 and 20% water (Iqbal et al., 2012). The authors reported that the viscosity increase was due to the 3D network of the high aggregated water droplets content containing protein network after heating– leading to an increase in effective dispersed phase volume fraction–and due to the shift in their shape from spherical to non-spherical under shear.

5.4.3 Emulsion viscoelasticity

5.4.3.1 Strain-sweep viscoelasticity

As a function of oscillatory strain, all emulsions showed higher storage (G') than loss moduli (G") in the low-strain regime before crossover of G' and G" (Figure 5.4). Interestingly, a very brief linear viscoelastic region (LVR) was observed below 0.1% strain, and G' dropped almost continuously as a function of strain. On day 1, for the control emulsions (without LMP in the water droplets) with 20 wt% water, two distinct inflection points in G' and G" were observed – one during the initial yielding and another at a higher strain (arrow in Figure 5.4A) – indicating a two-step yielding behaviour. After 30 days (Figure 5.4B), the control 20% water emulsions exhibited a significant lowering of G' and G", with more than an order of magnitude lowering in crossover strain; however, the second peak in G' at high strain (arrow in Figure 5.4B) become much more prominent than in the 1-day-old emulsion. Two-step yielding in emulsion rheology is a well-known phenomenon; however, its origin and the associated structural transformation are still unclear (Ahuja, Potanin, & Joshi, 2020). It is commonly believed that the first yielding is associated with network rupture, while the second yielding is due to a breakdown of clusters. Using this theory, Vargas et al. (2018) proposed that the two-step yielding in their water-in-waxy-crude-oil emulsions could be due to the breakdown of the wax crystal network, followed by rupture of attractive water droplet clusters. In the present case, it can be proposed that the first yielding of the emulsion could be due to the breakdown of the HSO crystal network, which was followed by a second yielding due to the rupture of the water droplet aggregates. Previously it has been shown that the presence of GMO at the water droplet interface promotes a shift in the surface activity of HSO crystals, leading to the formation of Pickering crystals on individual droplets and crystal bridges between the droplets (Ghosh & Rousseau, 2011). Such crystal bridges could lead to water droplet aggregates and, hence, a two-step yielding.

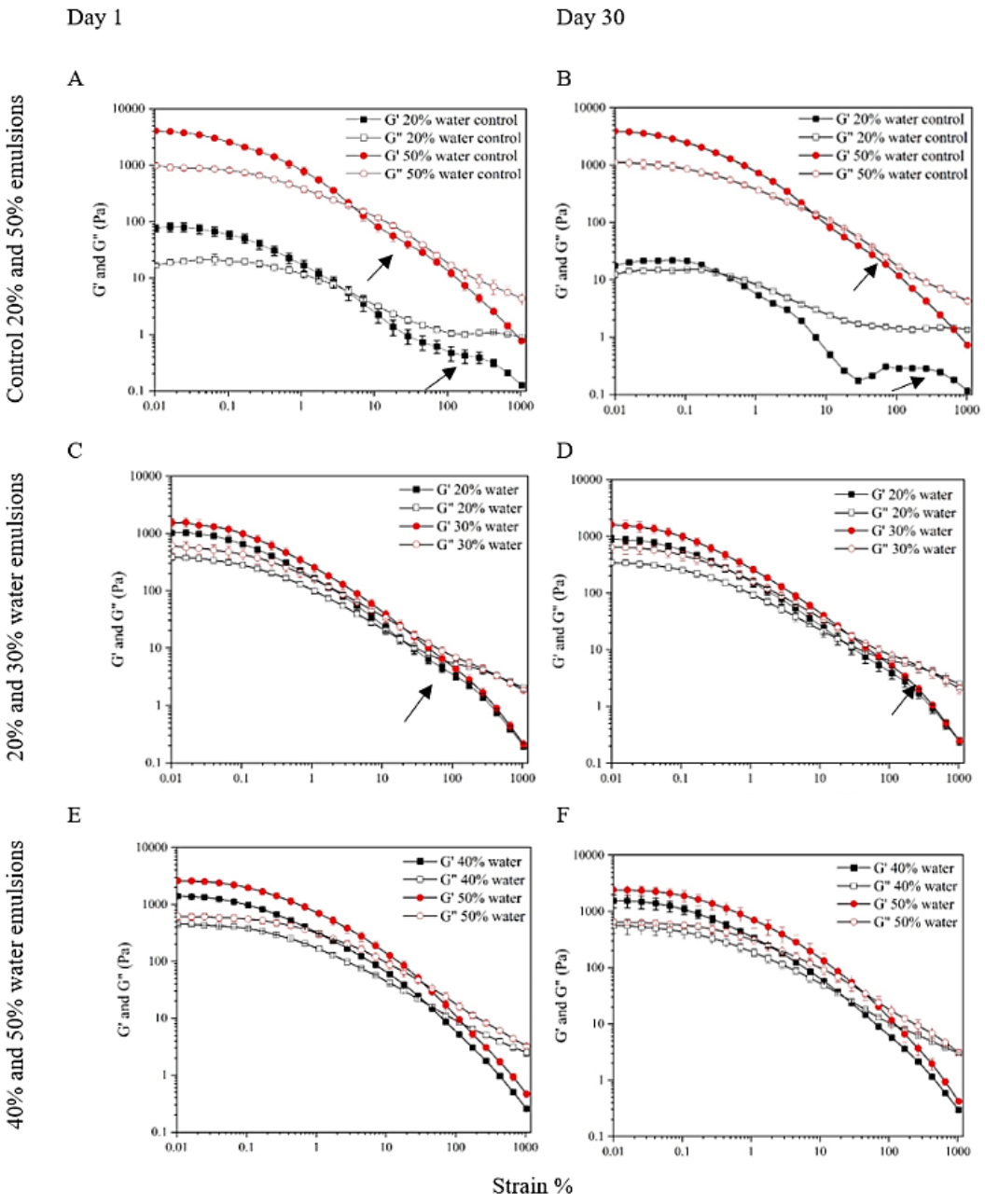

Figure 5.4. Storage (G') and loss moduli (G") as a function of oscillation strain for W/O emulsions with water content from 20 to 50 wt% and 1.5 wt% LMP in the aqueous phase. Control emulsions were made without LMP in the aqueous phase. Data collected on day 1 (A, C, E) and day 30 (B, D, F) are shown for control emulsions (A, B), 20 and 30% water emulsion (C, D) and 40 and 50% water containing emulsions (E, F). The arrow in some figures indicates a peak in G'.

After 30 days, the sharp drop in the first yielding and a prominent peak in the second for 20 wt% water control emulsions could be associated with destabilization of water droplets, leading to a release of free water during cluster rupture. The control 50 wt% water emulsions showed a significant increase in both G' and G" (Figure 5.4A) compared to the control 20 wt% water emulsions; however, the two-step yielding behaviour was almost absent. Although a faint peak could be observed in the G' of the control 50 wt% water emulsions at a lower strain than the 20wt% emulsions (shown by arrows in Figure 5.4A), this did not change after 30 days (Figure 5.4B). The disappearance of two-step yielding upon the increase in gel strength in dense suspension was also reported by Kramb and Zukoski (2010) for hard-sphere suspensions, and by Tang and Ghosh (2021) for oil-in-water emulsions. It was proposed that if a gel is too hard due to attractive interactions among the droplets, it may break apart in a single step. In the present case, the interaction of 50 wt% water and fat crystals created a close-pack structure, forming a highly concentrated system vulnerable to shear force and breaking the crystal network and associated water droplet aggregates.

All emulsions with LMP in the water droplets showed similar viscoelastic behaviour (Figure 5.4C–F), where G' was higher than G" in the low-strain regime, and both of the moduli dropped with an increase in strain with a narrow LVR below 0.1% strain. For 20 and 30 wt% water emulsions (Figure 5.4C, D), a small peak in G' and G" was observed just above 100% strain; however, for 40 and 50 wt% water emulsions, no peak in G' and G" beyond crossover was observed, indicating a stronger droplet-crystal interaction, which broke down in one step. The most striking difference in viscoelastic behaviour was observed for 20 wt% water emulsions with or without LMP in the aqueous phase, which can be related to more mobility of droplets and weaker network, or less aggregated water droplets without LMP in the aqueous phase. The incorporation of LMP significantly increased the gel strength of the emulsions; however, the two-step yielding behaviour was significantly reduced, suggesting that LMP promotes better or firmer water droplet packing, strengthening the 3D network.

5.4.3.2 Comparison of emulsions G' values

Although oscillatory rheology did not show a strong LVR, to compare the gel strength of the various emulsions, their G' at 0.01% strain was re-plotted as a function of water content and LMP's addition to the water droplets on day 1 and day 30 (Figure 5.5A). On day 1, the lowest G' was identified with control emulsions with 20 wt% water, which could be related to partial water droplet destabilization without LMP and lower water content (Figure 5.5A). Water droplet destabilization was also responsible for a significant gel strength drop for control 20 wt% water emulsions after 30 days. Control emulsions with 50 wt% water showed the highest G', associated with the highest water content and packing of water droplets and fat

crystals, which remained similar on day 1 and after storage ($p > 0.05$). This may be associated with the phase separation in the sample (Figure 5.2C), presenting a strongly aggregated fat phase with high gel strength.

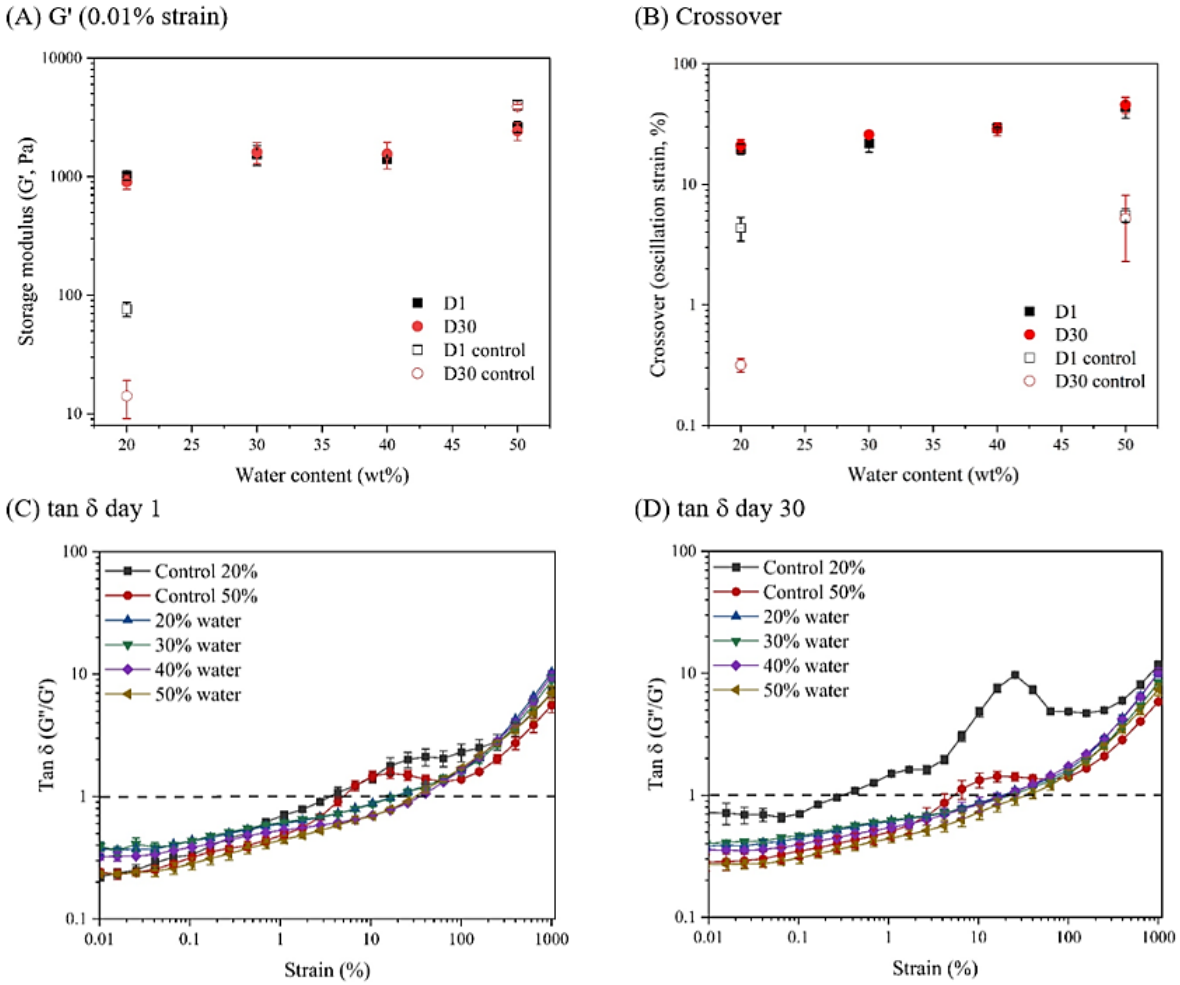

Figure 5.5 (A) Storage modulus (G') at 10% of oscillation strain, (B) crossover (% strain) and (C and D) tan δ of water-in-oil emulsions as a function of oscillation strain with different water volume fractions prepared with LMP, GMO and HSO on day 1 (D1) and day 30 (D30). Note difference in y-axis scales due to variation of analysis.

All emulsions with LMP demonstrated a progressive increase in G' (1023 – 1404 Pa) with the rise of water content from 20 to 40 wt%, although no significant change was observed from 30 and 40 wt% water ($p > 0.05$), which could be related to reaching a steady-state in the water droplet structure. However, 50 wt% water emulsions showed a significant increase in G' (2619.2 ± 271.4 Pa) compared to the other emulsions ($p < 0.05$). Close packing of LMP-added water droplets and their aggregation could be related to

the increase in gel strength. The water droplets essentially acted as an active filler in the continuous fat crystal network (Rafanan & Rousseau, 2017). At 50 wt% water, the aggregated water droplets formed a near close-packing structure in the fat crystal network, leading to a superior gel strength to that of all other water contents. Emulsion gel strength did not change much after storage. Iqbal et al. (2012) reported an increase in gel strength of W/O emulsion with a rise in water content from 10 to 30 wt%, implying that gels become more rigid with greater droplet concentration, as would be projected for a network of aggregated droplets. Based on the theoretical rheological analysis of gels, the shear modulus is proportional to the dispersed phase volume fraction (ϕ), droplet diameter, and the attractive forces among the droplets, relying on the strength and the number of the bond between the droplets. However, similar to our observation, from 30 to 40 wt% water, the gel strength remained the same, which was not fully explained by the authors. They also observed an increase in gel strength after heating the emulsions containing WPI in the aqueous phase. As WPI undergoes heat-induced denaturation and subsequent aggregation, the authors suggested that droplet-droplet interactions were promoted by gelation of the internal aqueous phase, where proteins from one droplet interact with proteins in the other water droplets.

5.4.3.3 Comparison of emulsion crossover strains

The crossover strain in rheology is defined as the strain required for gel breakdown, where G' = G" (Figure 5.5B). Control emulsions with 20 and 50 wt% water showed the lowest crossover on day 1 ($p > 0.05$), which can be due to the absence of LMP, leading to a droplet destabilization. After 30 days, the crossover of 20 wt% water control emulsions further decreased, while no change was observed for 50 wt% water. Such drop in crossover strain for control 20 wt% water emulsions could be due to water droplet destabilization-induced flow (visual observation in Figure 5.2B, C). LMP emulsions' crossover strain increased with an increase in water content and was higher than the control emulsions' crossover strain. Higher water content led to more droplet aggregation and packing, which in turn required higher force in order to break down the gel structure. The presence of LMP also led to LMP-GMO interaction at the interface, which further enhanced the droplet-droplet interaction and, hence, the force required to break the gel strength. After 30 days, no significant change in crossover strain was observed, indicating an unchanged emulsion structure.

5.4.3.4 Emulsion tan δ as a function of strain

The tan δ (G" /G') values as a function of strain at a constant frequency on day 1 and day 30 are shown in Figures 5.5C, D. When tan $\delta < 1$, the emulsion showed an elastic behaviour. Tan $\delta = 1$ reveals a gel breakdown point under strain, whereas higher than 1 indicates a viscous behaviour. On day 1, all

emulsions showed tan δ < 1 below 1% strain, indicating dominant elastic behaviour. Control emulsions with 20 and 50 wt% water exhibited a tan δ = 1 at a lower strain (~3%) compared to the LMP emulsions, indicating an early transformation into more viscous behaviour under the applied strain (Figure 5.5C). LMP emulsions with 20 and 30 wt% water exhibited a transition from elastic to viscous at ~18%. In contrast, for the emulsions with 40 and 50 wt% water, this transition was observed at ~35%, indicating stronger gels that break down at higher stress. After ageing, the gel transition point moved to a lower strain (Figure 5.5D). Control emulsions with 20 wt% water showed the largest drop (10 times) in strain required for gel breakdown (tan δ = 1) at ~0.3%. Control emulsions with 50 wt% water reported a slight rise in tan δ = 1 at 5% strain than day 1, indicating possible gel hardening. LMP emulsions with 20 wt% showed no significant change with the strain-induced transition from elastic into viscous behaviour. An increase in strain required for the transition was exhibited with 30 wt% water (~28% strain). In contrast, a slight decrease was observed for 40 wt% water, with the transition at ~29% strain, and for 50 wt% water was at ~32% strain. Overall, upon storage, LMP emulsions exhibited more elastic behaviour than the control emulsions under higher strain.

5.4.4 Microstructure of emulsions

All of the emulsion microstructures are illustrated in Figure 5.6. All of the images showed HSO fat crystals absorbed at the oil-water interface via the Pickering stabilization mechanism, which is observed as small crystals covering the droplets (arrows in Figure 5.6). Moreover, accumulated crystal structures of different sizes can be observed in the continuous phase. Rousseau's group also found similar observations in 15 and 20 wt% W/O emulsions using 10 wt% HSO, noticing water droplets aggregated or covered with fat crystals as shells (Rafanan & Rousseau, 2017). They also reported that 14.4 wt% HSO in 20 wt% W/O emulsions exhibited large crystal aggregates measuring from 10 to 40 μm without any change over time (Rafanan & Rousseau, 2019). The images of control emulsions with 20 wt% water revealed both aggregated and free water droplets in the continuous phase, and a few evidence of coalescence-induced large droplets. The water droplets' shape was deformed in a few positions at the interface in all emulsions images as a sign of crystallization at the interface. The increase in water content (30, 40, and 50 wt%) in all emulsions led to more packing and compactness of water droplets, which could be related to increased viscosity and viscoelasticity as a function of water content. Not much change in emulsion microstructure can be observed on day 30, except a sign of a brighter crystal network related to crystal growth during storage.

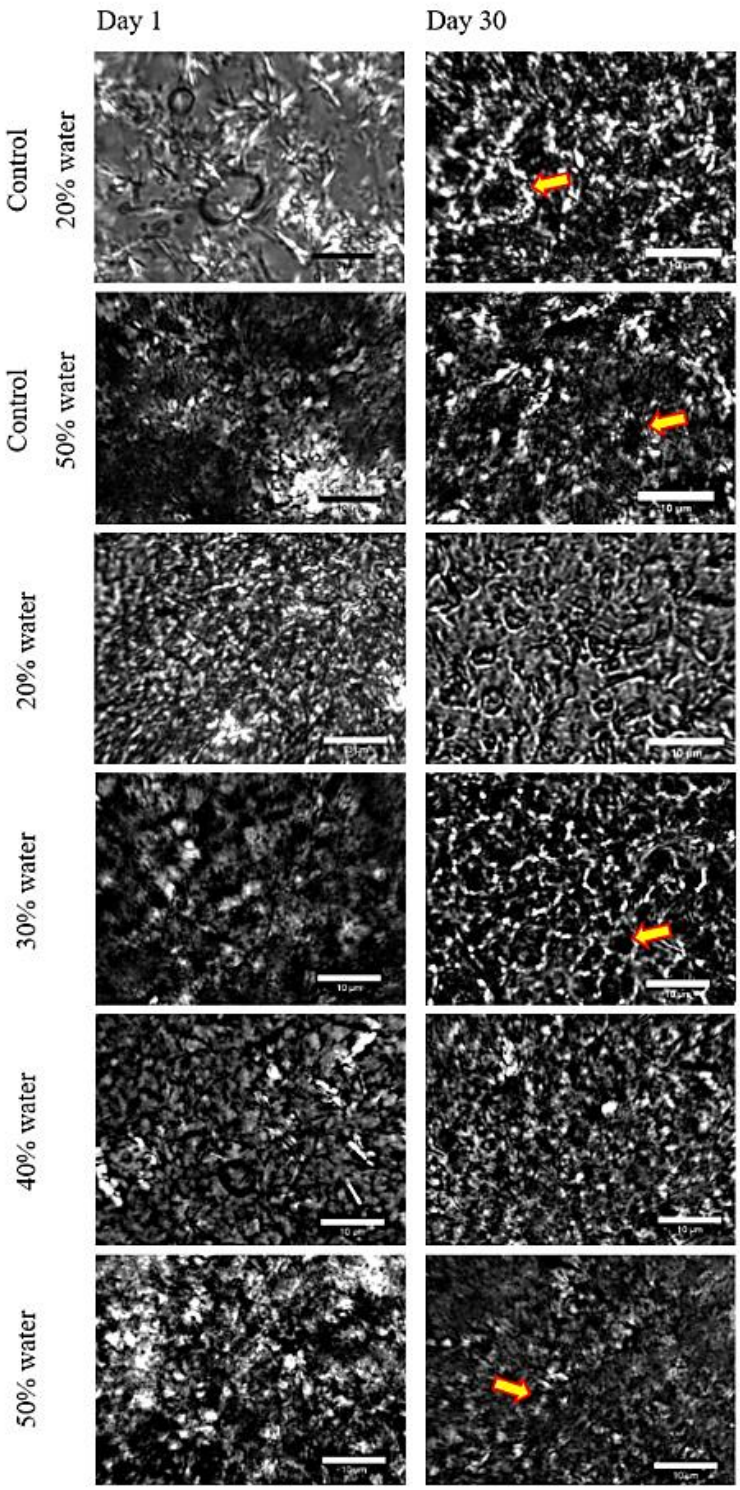

Figure 5.6 Polarized light with bright-field micrographs of water-in-canola oil emulsions on day 1 and day 30 for control emulsions without LMP with 20 and 50 wt% water and for LMP emulsions with 20 to 50 wt% water. Scale bar 10 μm. Arrows indicate interfacial fat crystals around the water droplets.

5.4.5 Emulsion stability analysis from their thermal behaviour

All emulsions were subjected to freeze/thaw cycles in DSC to understand their dispersed phase stability better. Thermal cycles included a cooling from 25 °C to –70 °C, heating to 70 °C, and a second cooling to –70 °C at 5 ºC/min (Figure 5.7). On day 1, control emulsions with 20 wt% water (Figure 5.7A) showed small peaks at around -18 °C due to partially destabilized large water droplets, and again between -27 and –37 °C (peak 1), attributed to the crystallization of smaller water droplets, indicating stable emulsion. After the dispersed phase crystallization, the continuous phase CO crystallized at –50 °C (peak 2). During heating, CO melted from –35 to –8 °C (peak 3), the ice melted between –2 to 5 °C (peak 4), GMO melted between 10 and 16 °C (peak 5), and HSO melted between 50 and 60 °C (peak 6). The second cooling scan exhibited HSO crystallization at 30 °C (peak 7). A large water bulk crystallization peak and several small, dispersed water droplets crystallization peaks between –16 to –36 °C (peak 8) were related to a partial emulsion destabilization. The dispersed droplets' crystallization peaks appeared at a higher temperature in the second cooling cycle than the first cooling cycle were due to the increase in water droplet size due to the melting of stabilizing HSO crystals. The second cooling cycle also showed CO crystallization at –50 °C (peak 9). Control emulsion with 50 wt% water (Figure 5.7A) demonstrated a large water crystallization peak from –15 to –20 °C in the first cooling cycle (peak 10), responsible for destabilized bulk water crystallization, followed by CO crystallization (peak 11). During the heating cycle, CO melted at peak 12, followed by ice melting (peak 13), GMO melting (peak 14), and HSO melting (peak 15). The ice melting peak for the control 50 wt% water emulsions (peak 13) was more significant than that for the control 20 wt% water emulsions (peak 4), due to the presence of more water in the former. The second cooling scan showed HSO crystallization at 30 ºC (peak 16) followed by a large bulk water crystallization peak ranging from –13 to –20 °C (peak 17), which was even larger than the first cooling water crystallization peak (peak 10), indicating extensive water droplet instability, followed by CO crystallization in peak 18.

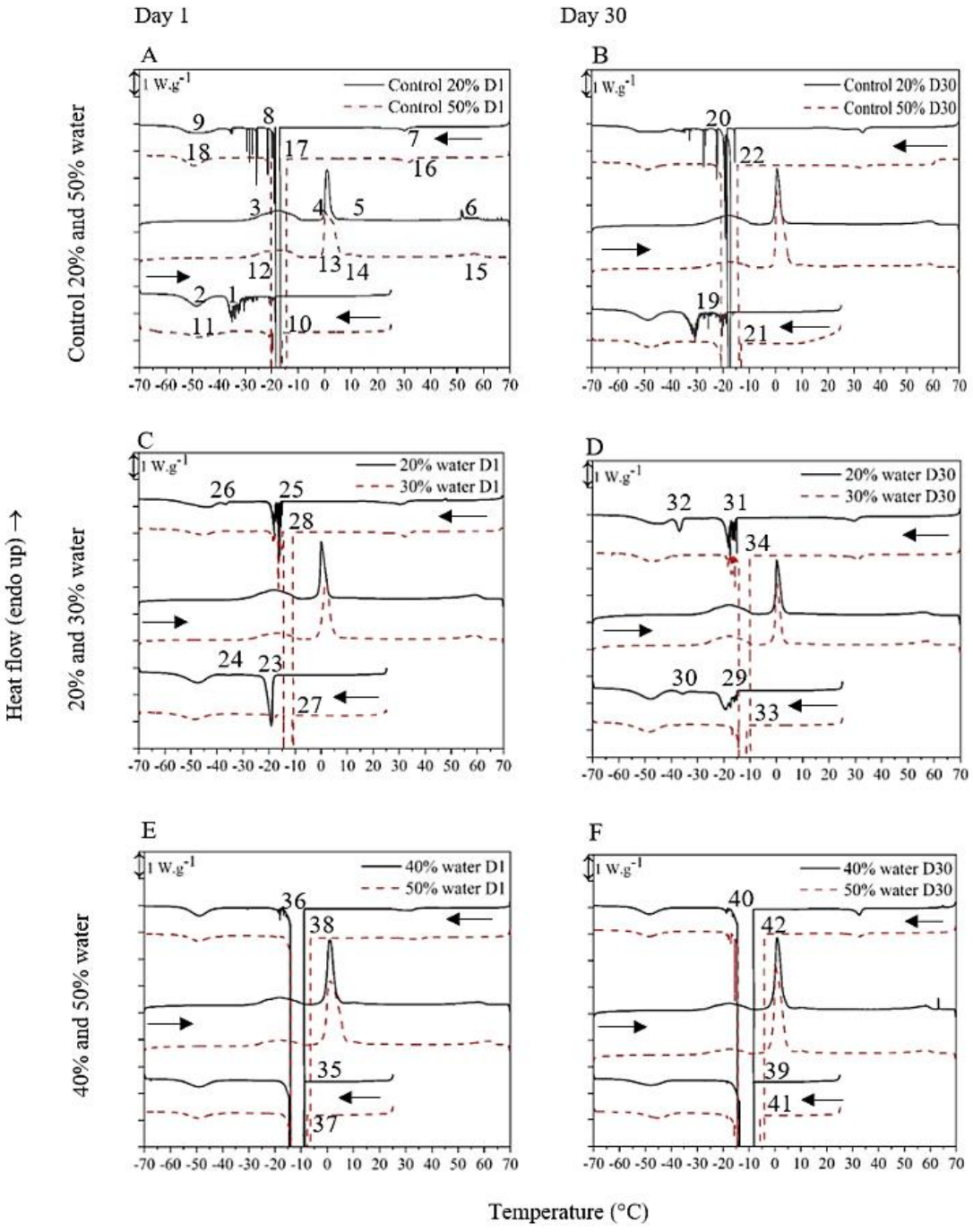

Figure 5.7 DSC freeze/thaw thermograms of water-in-oil emulsions under ageing (on day 1 and day 30) for control emulsions with 20 and 50 wt% water without LMP (A and B) and 20, 30, (C, D) 40 and 50 wt% (E, F) water emulsions with LMP. Samples were cooled from 25 °C to –70 °C, and heated to 70 °C, followed by a second cooling to –70 °C, at a rate 5 °C/min. Arrows indicate the direction of the temperature cycle. Important peaks were identified with numbers and discussed in the text.

From the above discussion of DSC freeze/thaw cycles, emulsion stability can be predicted from water crystallization peaks analysis. The appearance of multiple emulsified water droplet crystallization peaks in the first cooling cycle could be ascribed to homogeneous nucleation of water where the impurities are divided among the numerous water droplets, indicating emulsion stability (Ghosh & Rousseau, 2009). In contrast, the appearance of a bulk water crystallization peak in the first cooling cycle around –20 ºC is a sign of extensive water droplet coalescence and emulsion destabilization. The effect of water droplet size on water crystallization temperature has been studied by Clausse et al. (2005) via thermogranulometry, where the authors showed that the crystallization temperature increased with an increase in droplet size. Therefore, a water droplet crystallization peak at a higher temperature indicates larger coalesced water droplets.

Using a similar DSC methodology, Ghosh et al. (2011) reported a full water droplet destabilization upon heating a 20 wt% W/O emulsion (4 wt% GMO and 10 wt% hydrogenated canola oil), showing a large bulk water crystallization peak during the second cooling cycle at –19 °C. Suppose that a stable emulsion, with droplet crystallization at between –30 and –40 ºC, shows a bulk water crystallization peak (at around –20 ºC) in the second cooling cycle. In that case, it indicates that the melting of fat crystals during the heating cycle was the emulsion's main stabilization mechanism. On the other hand, if an emulsion shows stable water droplet crystallization in the second cooling cycle, its stabilization mechanism must be dependent on fat crystals, but on the emulsifier's interfacial stability. Such insights from using DSC freeze/thaw cycles make them a powerful technique for predicting the emulsion stabilization mechanism.

For the rest of the DSC thermograms, only the water droplet crystallization peak was identified as the key to understand emulsion stability. Aged control emulsions (Figure 5.7B) with 20 wt% water showed similar water crystallization peaks (peak 19) in the first cooling cycle as in the fresh emulsions, indicating unchanged stability. The second cooling also exhibited a large bulk water peak surrounded by a few smaller peaks (peak 20), indicating partial destabilization related to the day 1 emulsions. Aged control emulsions with 50 wt% water showed similar large bulk water crystallization peaks in the first and second cooling cycles (peaks 21 and 22, respectively) to the day 1 emulsion, which illustrated extensive emulsion destabilization. Therefore, between the two controls, 20 wt% water emulsions showed better stability than the 50 wt% water emulsions.

The thermograms of day 1 and day 30 LMP emulsions are shown in Figure 5.7C–F. On day 1, LMP emulsions with 20 wt% water showed water crystallization in a small peak (peak 23) at –18 °C during the first cooling due to crystallization of large water droplets, and a tiny peak at –35 ºC (peak 24) due to very

small water droplets, indicating stable emulsions (Figure 5.7C). The second cooling scan illustrated water crystallization at –14 °C (peak 25) with multiple tiny peaks, related to water droplets, followed by another small stable water droplet crystallization peak at –35 ºC (peak 26), indicating that the emulsion was able to prevent complete destabilization even by complete melting of the stabilizing HSO crystals. Khudyakov et al. (2019) found that pectins can modify the ice morphology during the transition of liquid water to ice. Even a small pectin concentration (0.2 and 0.4 wt%) exhibited cryoprotective properties in frozen cells' integrity. In the present case, utilizing water droplet crystallization enthalpy, we calculated that LMP emulsions with 20 wt% water presented a 65% reduction in the crystallization enthalpy of water droplets in the second cooling cycle (Figure 5.7A), indicating 65% destabilization due to freeze/thaw, which was much lower than the 93% destabilization for 20 wt% control emulsions (figure 5.7C). This indicates a similar cryoprotective effect associated with LMP incorporation in the emulsion.

LMP emulsions with 30 wt% water illustrated a large bulk water crystallization peak at –10 °C (peak 27), followed by two small spikes at around –19 °C during the first cooling cycle. The second cooling exhibited destabilized bulk water crystallization at –10 °C, with a large peak and subsequent small peaks until –20 °C (peak 28). This indicates that most water droplets were unstable, but the emulsions did not completely destabilize, even after melting the stabilizing HSO crystals. Aged LMP emulsions with 20 and 30 wt% water (Figure 5.7D) showed similar peaks to those observed on day 1 (peaks 29 – 34), which indicates that the emulsion stability remained unchanged after 30 days of storage.

LMP emulsions with 40 wt% water (Figure 5.7E) exhibited water crystallization at around –10 °C during the first cooling scan on day 1 (peak 35). In the second cooling, water crystallized with a similar large peak at around –10 °C, followed by a few tiny peaks related to some very large water droplets (peak 36). LMP emulsions with 50 wt% water (day 1, Figure 5.7E) also illustrated a long sharp peak of water crystallization at –10 °C during first cooling (peak 37), and a similar peak during second cooling (peak 38), which suggested entirely unstable water droplets. Aged emulsions with 40 wt% water (Figure 5.7F) reported similar water crystallization peaks (peak 39) as on day 1, showing that some droplets were still present in the second cooling (peak 40).

Moreover, LMP emulsions with 50 wt% water reported similar water crystallization peaks as on day 1, but with few spikes and peaks that followed the large peaks (peaks 41 and 42), indicating only a few stable water droplets. From the DSC freeze/thaw cycles of emulsions, it is clear that as the water content increased, more water crystallized at a higher temperature, similar to bulk water instead of emulsified water droplets. In highly concentrated emulsions, impurities would be distributed in many droplets, leading to

faster heterogeneous nucleation in many droplets. Moreover, as the water droplets were close-packed, crystallization in one droplet could lead to ice crystals rupturing other surrounding droplets' membranes, leading to inter-droplet heterogeneous nucleation and crystallization of all droplets at a higher temperature (Ghosh & Rousseau, 2009). Upon melting, the ice crystal bridge between the droplet would lead to collision-mediated coalescence and destabilization of emulsions. Therefore, the ability of the DSC to predict emulsion stability is not quite applicable to concentrated emulsions.

Similar freeze/thaw-induced emulsion destabilization via ice-crystal-induced water droplet collision was also observed by Lin et al. (2008). Aronson and Petko (1993) also reported freeze/thaw experiments of 92 wt% water-in-paraffin oil emulsion (10 wt% GMO in the oil phase and magnesium sulfate in the aqueous phase). The emulsion without the salt in the aqueous phase consisted of 90% ice when frozen and could not resist destabilization via the freeze/thaw cycle. During freezing, the water droplets progressively distorted to create ice blocks, breaking the interdroplet oil film and puncturing other water droplets. During thawing, the ice melted, leading to the coalescence of water droplets and emulsion destabilization. In the emulsion with magnesium sulfate in the aqueous phase, 83% ice was formed, while 9% water remained liquid due to salt-induced depression of freezing point. This emulsion was stable to the freeze/thaw cycle. The authors proposed that the presence of liquid water wetted the ice crystals and provided protection against fusion among the ice crystals from adjacent water droplets.

5.4.6 Solid fat content of emulsions

The viscoelastic property of the W/O emulsions originate from the presence of water droplets and the fat crystal network in the continuous phase and around the water droplets. To investigate the effect of water content on emulsion viscoelasticity, we kept the amount of HSO constant in all emulsions (7 wt%). However, depending on the water content, the amount of GMO was varied. The amount of total solid fat in the emulsions at 4 ºC also varied based on the solubility of HSO in CO (Ghosh et al. 2011). Therefore, the emulsions' solid fat content at 4 ºC was determined by measuring the solid fat enthalpies using a DSC (Figure 5.8).

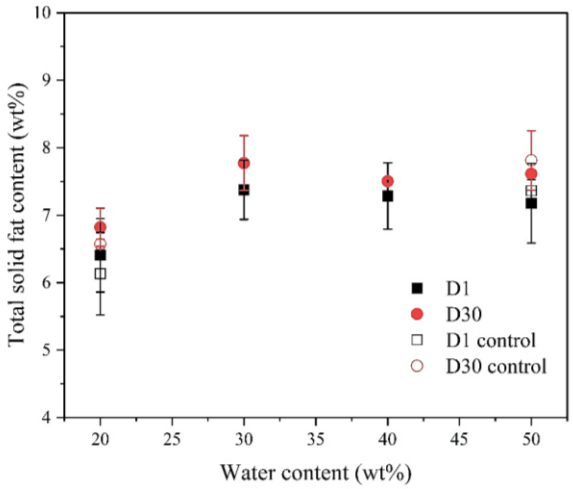

Figure 5.8 The solid fat content of water-in-oil emulsions on day 1 (D1) and day 30 (D30). Control emulsions were prepared without any LMP in the aqueous phase.

On day 1, all emulsions showed solid fat content ranging from 6.4 ± 0.5 wt% to 7.4 ± 0.4 wt% ($p > 0.05$). After 30 days, solid fat content increased in all emulsions (6.8 ± 0.3 wt% to 7.8 ± 0.4 wt%), although it was not significant ($p > 0.05$). Such an increase over time could be due to crystal growth. Similar results have been reported by Ghosh and Rousseau (2012) using hydrogenated canola oil with an initial solid fat content of ~6 wt% in fresh emulsions. After 4 weeks, the solid fat content increased to 7 wt%. The authors implied that in fresh emulsions, GMO's presence might hinder the packing of saturated fatty acids into crystal lattices (Ghosh & Rousseau, 2012). In this study, the increase in solid fat content of more than 7 wt% could be due to partial GMO crystallization at the water droplet surface. The DSC thermograms of all emulsions showed a GMO melting peak at around 10 ºC; we also observed GMO crystallization at around 13 ºC from CO in the bulk oil phase (data not shown). The minor increase in solid fat content could also be due to water evaporation during storage. Emulsions slowly destabilize over time due to water droplet coalescence, and the free water is more accessible to evaporate during storage leading to a slight increase in solid fat content. However, such a minor increase in solid fat content would not significantly influence emulsion viscoelasticity for various emulsions; therefore, the change in the water volume fraction is the most important factor for the variation in emulsions' viscoelasticity.

5.5 Discussion

It should be mentioned that the presence of a continuous phase fat crystal network is critical for W/O emulsion elasticity, as emulsions made without HSO in the oil phase were liquid and destabilized with

extensive water droplet sedimentation (data not shown). However, in the present system, rather than the fat crystal network in the continuous phase (the amount of HSO was constant in all emulsions), the amount of water and the water droplets' stability were more critical in providing a stable elastic system that did not flow under gravity. Such a highly concentrated water-in-vegetable-oil emulsion stabilized with GMO, with high stability and gel strength at a lower saturated fat concentration, is a difficult system to stabilize. The role of aqueous phase LMP in stabilizing the GMO-coated water droplets was one of the most critical aspects in developing such systems with close-packed water droplets, which could be used in the development of low-fat tablespreads.

5.6 Conclusions

GMO-stabilized water-in-canola-oil emulsions with self-supporting structure and highly elastic properties were developed with water content increments from 20 to 50 wt%, LMP addition in the aqueous phase, and the presence of a minimum amount of saturated fat crystals (HSO) in the continuous phase. The appearance of fresh and 30-day-aged emulsions showed no spreading on Petri dishes, and complete stability without any flow or phase separation in glass vials. The emulsions' apparent viscosity at a low shear rate ($0.1\ s^{-1}$) increased with water content. Emulsion gel strength and crossover strain for gel break down also increased with water content. Control emulsions without LMP in the water droplets showed lower gel strength than the LMP emulsions at 20% water, though their gel strength was comparable at 50 wt% water. However, both the control emulsions' crossover strain was significantly lower than the LMP-added emulsions, indicating that the less stable control emulsion gels could break down at a lower strain. The DSC freeze/thaw cycle was used for an improved understanding of water droplet stability. The control emulsions were stable on day 1, but water droplet destabilization increased significantly during ageing. LMP emulsions with 20 wt% water showed stable water droplets during freeze/thaw cycles even after melting HSO, indicating a lesser role of fat crystals in providing emulsion stability at a lower water content when the water droplets were stabilized by LMP. However, with the increase in water, DSC showed partial destabilization of water droplets in LMP emulsions, although the emulsions were stable, indicating that the DSC method was not suitable for high water contents. Overall, it was possible to develop GMO-stabilized, non-flowable, elastic W/VO emulsions with high gel strength using a close-packed structure of water droplets, where the LMP in the aqueous phase acted as an essential interfacial stabilizing agent of GMO. Such elastic W/VO emulsion could be utilized to reduce the fat content in margarine-type tablespreads.

6. GENERAL DISCUSSION

6.1 Overview

This thesis was divided into three sections that proposed the various stabilization mechanisms and structure formation in W/O emulsions for various applications. The first study focused on developing liquid W/MO as bioreactors for PCR, exposed to vortex homogenization and multiple thermal cycles. The second section of the work investigated the mechanism of stability of liquid W/VO emulsions compared with W/MO emulsions, with the addition of hydroxyl group donating agents to enhance interfacial bonding of the emulsifier GMO. The knowledge of the molecular interactions at the interface was deepened with the help of FTIR spectroscopy. The last section of the work investigated how to increase the elasticity of a model W/VO emulsion with the increment of water content, the addition of solid fat and a hydroxyl donating agent in the aqueous phase.

6.2 Emulsion model

This work started with a model emulsion to investigate the intermolecular interactions. The model compromised 20 wt% water and 80 wt% mineral oil. The emulsifier type and concentration were varied to obtain stable emulsions. This model has been used in many studies for liquid W/O emulsions to identify emulsifiers' performance at the interface to increase the overall emulsion stability (Opawale & Burgess, 1998; Ushikubo & Cunha, 2014). In the first piece of work, the aqueous phase was adapted according to the composition used in PCR buffers to mimic the same conditions, so the results obtained were closer to the polymerization reaction but without any DNA (Baier et al., 2011). The oil phase was initially investigated with light mineral oil (LMO) (viscosity 44.8 ± 0.73 mPa.s). Later, heavy mineral oil (HMO) (viscosity 143.8 ± 0.83 mPa.s) was considered with mixtures for testing five different viscosity levels to enhance the emulsions' stability exposed to vortex mixer emulsification and multiple thermal cycles. Three emulsifiers were tested to identify their thermal resistance abilities in a large range of concentrations. The emulsifiers selected were Span 80 (2 – 10 %) with a smaller molecular size, PGPR (0.2 – 10%) and AOT (0.3 – 10%) with a larger molecular size, all with low HLB. Only the emulsion showed no separation after the vortex mixer homogenization was selected for the thermal cycle exposure. After the multiple thermal cycles, the stable emulsions were identified based on no aqueous phase separation in the emulsion. While separation

of oil layer at the top was deemed acceptable, the emulsions were determined as unstable for the aqueous phase separation at the bottom.

In the second body of work, the percentages of water and oil were kept at 20 wt% and 80 wt%, respectively. For the oil phase, both canola oil and light mineral oil were used because the main objective was to identify the influence of oil type over the emulsifier, GMO, the oil phase, and the additives in the aqueous phase. The hydroxyl group donating agents, AA, CA, and LMP, were added to the aqueous phase to interact with GMOs at the interface. Initially, the two small molecules, AA, and CA were tested with four concentration levels (0.125, 0.5, 2 and 4 wt%). LMP was included for being a macromolecule with more carboxyl groups in the galacturonic acid chain (Flutto, 2003) in two levels (1.5 and 2 wt%). Two types of salt were experimented with to identify if they promote emulsion stability. For AA and CA, sodium chloride was used in two different concentration levels (0.125 and 0.5 wt%). For LMP, calcium chloride was applied in two concentration levels (0.03 and 0.045 wt%). The emulsifier selected for food applications was GMO because one of the most effective emulsifiers for W/O emulsion, PGPR, has been permitted just for chocolate products since 2017 (Health Canada, 2017). The critical micelle concentration of GMO in CO was 4 wt%, and in LMO was 0.15 wt%, a higher value was in CO due to the interaction of GMO with fatty acids in CO (Ghosh & Rousseau, 2011). However, for comparison, GMO concentration (4 wt%) was kept the same in both oils to obtain clear identification of hydrogen bonding with the additives. After all the analyses, LMP was the molecule that performed stronger intermolecular hydrogen bonding, the highest emulsion stability and gelation characteristics after storage in both oils. Thus, the concentration 1.5 wt% LMP in the aqueous phase was selected for the subsequent study.

In the last piece of research, the main application was for low-fat tablespreads due to the high demand for healthy products. Thus, CO was used as one of the most nutritional vegetable oil on the market (Eskin et al., 2020). The emulsion model concentrations were modified as part of the objective was to induce higher viscoelastic properties. The water content was tested from 20 to 60 wt%; however, it was impossible to homogenize the emulsion with 60 wt% water for the desired three cycles due to the excessively high viscosity of the material. The ratio between GMO and water was kept constant to obtain a similar droplet size in all emulsions. The ratio (0.065) is the grams of GMO to the grams of water per emulsion. Fully hydrogenated soybean oil (HSO) was selected as the solid fat to create a fat crystal network in the oil phase and tested in different levels (7 to 10%) to optimize the concentration over stability. It was found that a minimum of 7 wt% HSO was needed for emulsion stability. The LMP concentration (1.5 wt% of the aqueous phase) was taken from the previous study. Visual observation of the emulsions was key to identify phase separation or flow in two tests: 1) perpendicular to the surface and 2) 90° flipped in parallel to the surface

after day 30 of storage. Rheological analyses were vital to identify the improvement or modification in emulsion viscoelasticity.

6.3 Determination of thermal stability by modifying emulsifier and continuous phase composition

The development of thermally stable liquid W/O emulsions for biotechnological applications was assessed in the first study (Chapter 3). This work was of interest due to the lack of studies in liquid W/O emulsions (Colucci et al., 2020) and even more for emulsion-based PCR quantification without breaking the water droplets. Most of the studies for ddPCR force a rupture of water droplets after DNA polymerization by centrifugation or ultrasonification (Baier et al., 2011; Musyanovych et al., 2005). To obtain water droplet stability, Span 80, PGPR and AOT were tested as an emulsifier. For instance, Span 80 has been used for PCR formulations at 4.5% with cosurfactants (Tween 80 and Triton X-100) at 0.45% under stirring (Williams et al., 2006). However, in this work, the emulsifiers were exposed to vortex mixer emulsification for a short time (2 min), and fast mobility was required. It was expected that Span 80 would show high stability with BSA in the aqueous phase (Gaiti et al., 1994). Still, the packing at the interface has been reported not to be ordered due to the unsaturated lipidic branch of Span 80 (Yoshioka et al., 1994). Even though BSA supported the interface during emulsification, during the thermal cycles, BSA unfolded, reducing the possible hydrogen bonding with the emulsifier at the interface (Holm et al., 2007). At that point, the thermal stability was mainly governed by the emulsifier, which was poor for Span 80, and the emulsion destabilized. PGPR is an effective emulsifier for W/O emulsions. It is highly surface-active, has a bulky structure, high viscosity and thermally stable (Ciriminna et al., 2015). All the emulsions made with PGPR were stable, showing their high efficacy at the interface. However, the PGPR concentration in the emulsions had to be reduced to allow the formation of larger water droplets suitable for ddPCR. At this point, to provide the large droplets, an additional stabilization effect was hypothesized that an optimum viscosity of the continuous oil phase would be required, which must be higher than LMO. Therefore, five different viscosities were investigated with the incorporation of HMO. PGPR demonstrated stable emulsions with large droplets with 50% LMO + 50% HMO and 25% LMO + 75% HMO at very low concentrations of 0.3 wt% and 0.4 wt% in the oil phase. The instability of the emulsions with the other three viscosity levels (100% LMO, 75% LMO + 25% HMO and 100% HMO) was conferred to emulsifiers' mobility at the interface. When the emulsifiers were exposed to multiple thermal cycles, it was induced an interfacial flow performing an adsorption-desorption mechanism due to the temperature (Sengupta et al., 2018). It indicates a low viscosity might not reduce the desorption and too high viscosity might significantly reduce the reabsorption movement of the emulsifier to the interface.

AOT is an anionic oil-soluble emulsifier with a bulky structure and thermally stable and known to have high efficacy for W/O emulsions (Nave, Eastoe, Heenan, et al., 2000). AOT was initially analyzed with one level of viscosity (50% LMO + 50% HMO) with a range of concentrations (0.3 to 10%). Only two concentrations showed thermal stability (8 and 10 %) with desired water droplet size. The CMC of both PGPR and AOT with BSA increased with the oil phase viscosity up to 50% LMO + 50% HMO, which indicates that more emulsifier was accommodated at the interface. However, when the viscosity further increased to 25% LMO + 75% HMO, both emulsifiers showed a lower CMC, indicating that higher viscosity of the oil phase limited the mobility and more stretched organization of individual emulsifier molecules at the interface, thereby reaching the surface saturation with lower concentration. The interfacial tension had a similar trend for both emulsifiers, being higher for the lower viscosity (50% LMO + 50% HMO) and lower for the higher viscosity (25% LMO + 75% HMO) oil phase. However, the values of interfacial tension for AOT were significantly lower than PPGR, which was ascribed to the formation of a double layer structure at the interface.

6.4 Effect of high energy homogenization and mixing processes

Emulsification can be performed by high or low energy processes, aiming to reduce the droplet size as small as possible. Low-energy emulsification depends on spontaneous droplet formation and phase-inversion under favourable requirements. However, it has several limitations like a high emulsifier or cosurfactants concentration and can be produced by selected oils and emulsifiers (McClements & Rao, 2011). In the first study, emulsions were made using a vortex mixer due to the need for large water droplets (80 – 100 µm) and a fast and straightforward process to generate microvolume emulsions. Understanding the dynamics of the oil and water during the vortex mixing process is very complex. Recently, Tiribocchi et al. (2021) presented the non-equilibrium states during vortex homogenization of water droplets in oil, which depended on hydrodynamic interactions and the continuous periodic motion distributed in various parts in the vortex, the top and medium-half region. The vortex mixer parameters were optimized with several tests to obtain stable emulsions with variations in speed (2000 to 3200 rpm) and time (1 to 2 min) in the vortex mixer. The vortex speed is not easy to measure, as is in arbitrary units in the equipment and varies slightly with each vortex (Flies & Chen, 2003). However, the methodology worked well for the objective persuaded of forming thermally stable coarse W/O emulsions.

One of the most common ways to make highly stable emulsions with sub-micron droplets is to use high-pressure homogenization. Many factors can affect the droplet size during homogenization, such as homogenizer type, pressure, duration, emulsifier type and concentration, and both phases' viscosity (Jafari,

Assadpoor, He, & Bhandari, 2008). The high-pressure homogenization method was used in second and third research studies (Chapters 4 and 5) to obtain a highly stable emulsion. The most efficient way to produce an emulsion is in two steps (Jafari et al., 2008), as applied in both the studies. First, coarse emulsions were made using high-speed mixing followed by high-pressure homogenization. Scherze et al. (2006) reported that high-pressure homogenizers' superior efficiency is due to droplet reduction by elongation of laminar flow. In a high-pressure homogenizer, the energy is given by the high-pressure plunger pump, which determines the force acting on the valve plug and the gap size (Jahnke, 1998). However, a rotor-stator mixer possesses a narrow gap designed by a rotating disk around a static rod where the liquids flow through the gap at high speed (Jafari et al., 2008). The combination of both pieces of equipment reduces the droplet size progressively. However, a common issue of high-energy emulsification is over-processing when the emulsions are passed through the homogenizer for many cycles. An initial decrease in droplet size due to an increase in number cycle can also produce the opposite effect and the droplet size could increase (Jafari et al., 2008). Thus, multiple tests in both oils, CO, and MO, were performed with the model concentrations (20 wt% water and 80 wt% oil) to define the number of cycles required to get an optimum reduction in the water droplet size. It was found that three cycles were needed to decrease the droplet size in a stable range (150 to 320 nm) for both oils.

6.5 Preventing desorption of glycerol monooleate from water-in-canola oil emulsions

The second research study (Chapter 4) focused on the prevention of the emulsifier, GMO's desorption from the water droplets' surface in liquid CO and MO emulsions. Quick separation of liquid W/O emulsions has been reported in many research (Opawale & Burgess, 1998; Ushikubo & Cunha, 2014). Mainly, the investigations have been done in alkane oils, acting as model oils, and PGPR as the most effective emulsifier in W/O emulsions. However, PGPR has been under investigation since 1952 for its negative effect on the liver and kidney using *in vivo* studies (Bastida-Rodríguez, 2013). For this reason, in Canada, since 2017, PGPR use is permitted just in chocolate products in the amount of 0.25 to 0.5 wt% (Health Canada, 2017). In the present work, GMO, a substitution for PGPR, was investigated to obtain similar effective stability in W/O emulsions. The main intention was to find the mechanism of interfacial interaction to enhance the efficiency of a small-molecule emulsifier, GMO, with high mobility at the interface.

The stability of liquid water-in-CO emulsions represented a challenge due to phase separation and droplet destabilization. However, these oleic linoleic acid-rich vegetable oils have a richer fatty acid profile, and canola oil is one of the healthiest edible oils (Eskin et al., 2020). Therefore, there is a greater need to

understand the mechanism of destabilization of liquid W/CO emulsions. The lipophilic small-molecule emulsifier (e.g., GMO) interacts with the fatty acid carboxylic groups in the TAG molecules of CO, leading to their desorption from the interface (Ghosh et al., 2011). GMO is a small emulsifier with high surface activity, with two free hydroxyl groups in the glycerol backbone that can establish hydrogen bonds with water molecules (Milak & Zimmer, 2015). However, the GMO-water hydrogen bonding is weaker than GMO-TAG bonding, leading to their desorption from the interface. Chapter 4 of the present research investigated hydroxyl group donating agents' effect in the aqueous phase, which could form intermolecular hydrogen bonding with GMO polar head at the W-O interface, thereby improving emulsion stability. The molecules selected to interact with GMO were AA, CA and LMP with or without S and Ca. The stability was monitored by observing the emulsions in glass vials at room temperature. On day 1, no separation was observed in all emulsions; however, after 7 days of storage, all the emulsions with the hydroxyl group donating agents exhibited moderate emulsions stability with oil separation but no water separation. Emulsions without any hydroxyl group donating agents in the aqueous phase showed water and oil separation. To interpret those results and to understand the interfacial interactions, DSC and FTIR were used. The melting point of ice and GMO behaviour can give insight into the type of bonding. When the melting point decreased, more intramolecular hydrogen bonding was predicted than intermolecular hydrogen bonding (Katritzky et al., 2001). More competition for bonding with water was observed with S and its mixture with AA and CA. Ionic interaction also distorted the water molecules reducing intermolecular hydrogen bonding and melting temperature. AA, CA and LMP formed intermolecular hydrogen bonding with water. However, LMP exhibited a higher ice melting enthalpy than AA and CA. Ca showed high enthalpy energy and peak shape, which was attributed to the Ca^{+2} chelation between the two molecules, water, and GMO. With the small molecules (AA and CA), W/MO emulsions showed higher ice-melting temperature, while with the polymeric molecules (LMP) W/MO emulsions exhibited decreased ice-melting temperature compared to W/CO emulsions. It indicates that LMP-GMO formed more intermolecular hydrogen bonding in CO with an excess of fatty acids, so water molecules bonded with LMP, GMO and fatty acids of CO.

Water was replaced by deuterium oxide to identify hydrogen bonding between GMO and the additives using FTIR spectroscopy. The wavenumber at ~3400 cm^{-1} is the frequency for GMO intermolecular hydrogen bond (Bus et al., 1990). A shift towards a higher wavenumber indicates increased hydrogen bonding between the molecules (Kataoka et al., 2011). All CO-emulsions showed higher wavenumber than MO-emulsions, and LMP was the molecule that showed the highest wavenumber in both oils. This work validated the initial hypothesis, showing stronger intermolecular hydrogen bonding of

GMO-LMP at the interface, the higher the stability of liquid W/O emulsions. A difficulty in the second study was the complex hydrogen bonding analysis, it was challenging to understand that level of research in structure and interaction. The initial experiment design was significantly large, with two hydroxyl group molecules with and without salts in 4 different concentration levels per molecule. As droplet size analyses were complicated because of the extensive floc formation by the dispersed water droplets, commonly reported in W/O emulsions (Colucci et al., 2020), image analysis was used to calculate the volume average droplet size. The limitations were in the interpretations of DSC results and experimental analysis and interpretation of FTIR data, being new methods to understand.

6.6 Improvement of viscoelasticity by increasing water content and modifying the interfacial composition

In the third research study (Chapter 5), the formation of elastic W/VO emulsion based on the liquid emulsion developed in the previous research was investigated. CO was selected as a source of liquid vegetable oil, rich in unsaturated fatty acids, with the aim of reducing saturated fat in tablespreads. Nevertheless, a certain amount of continuous phase fat crystal network was necessary to provide plasticity and spreadability to the emulsion. It was found that a minimum amount of 7 wt% fully hydrogenated soybean oil in the emulsion was enough to give stability to the water droplets. Emulsion viscoelasticity was improved by increasing the water content (20 to 60 wt%) in the emulsion, thereby lowering the total fat content. Based on the second research study's findings, 1.5 wt% LMP was added into the aqueous phase to provide stability to the dispersed water droplets. The water increment was only possible until 50 wt% of the emulsion weight due to the extremely high viscosity of the 60 wt% W/O emulsion, which made it impossible to pass through the homogenizer. The ratio of GMO to water was identified in preliminary research as the minimum concentration to stabilize 20 wt% W/CO emulsions. It was expected that the increase of water content would increase the viscosity of the emulsions. As the water droplet volume fraction surpasses the level required for close packing, it would lead to a strong elastic gel (Lee, Tan, Ravanfar, & Abbaspourrad, 2019). This work's innovation was applying intermolecular hydrogen bonding between LMP and GMO, which allowed higher stability of liquid W/CO emulsions in the second research study and proportionally increased water content. It was hypothesized that the addition of LMP in the aqueous phase would significantly enhance emulsion stability and gelation.

All emulsions with LMP in the aqueous phase did not show any flow against gravity even after 30 days. Conversely, emulsions without LMP and 20 wt% water showed significant flow under gravity and lowest G'. The viscosity of the emulsions increased with the rise of water content during ageing. All

emulsions with LMP showed a progressive increase in G' with the increase of water content from 20 to 40 wt% water; however, a significant increase was not observed from 30 to 40 wt% water. However, 50 wt% water exhibited a considerable increase in G', similarly for control emulsions 50 wt% water. A similar outcome was also observed for highly concentrated W/O emulsion, where the researchers found no change of storage modulus between 30 and 40 wt% water (Iqbal et al., 2012). It could be possible that the droplet size did not diminish with the increase in water content, representing no significant increase in the storage moduli. Besides, it is unknown if the intermolecular hydrogen bonding increased because those interactions also depend on the arrangement and special packing at the interface. The increase in crossover strain of G' and G" was proportional to the water content increment in LMP emulsions and without change after storage. Still, for both control emulsions without LMP, the values were significantly lower and diminished for 20 wt% water. It indicates that LMP influenced the gel point (G' = G") of emulsions, related to the pectin-pectin interaction between the water droplets, which enhanced the droplet aggregation and close packing.

The challenge in the third study was the interpretation of the viscoelastic behaviour, representing the interaction of CO, water, HSO, GMO and LMP. Control emulsions with 20 wt% water exhibited two-step yielding in G' and G" during oscillatory strain sweep on day 1 and day 30. This type of behaviour has been reported in many studies; however, the origin and structural transformation are still not clear (Ahuja et al., 2020; Kramb & Zukoski, 2010). The first yield point has been related to the breakdown of more robust structures like droplet flocs, and the second yield point after the gel point to droplets' dispersion in a liquid system (Tang & Ghosh, 2021). In the present case, the first yield was influenced by dissociating the structure formed with water droplet flocs and fat crystal network, while the second yield by the separation of water droplets. Understanding the molecular dynamics in these systems opens the application of more water in liquid vegetable oil to form viscoelastic W/O emulsion with low solid fat content.

6.7 Summary

This investigation contributes to the development of W/O emulsions with a wide range of applications in different fields. The modification of additives concentration produces the research of new mechanisms in the system, which open more options for development. The first and second studies impart innovation in developing liquid W/O emulsions, which have not been deeply studied before. The knowledge generated in this research will significantly impact the subsequent development of products for the biotechnology, cosmetics, skincare, and food industry for liquid. All the hypotheses were successfully tested; however, further work needs to be done in the first and second studies to enhance liquid emulsions' stability. Even though the second study was the one with the highest stability of aged liquid W/O emulsion,

complete stability without phase separation will be a significant achievement in the future. The third study is a subsequent development of gel-like W/O emulsions from the second study. The scaling up of the third study needs more work by adding colour and flavour additives and a more extended analysis of emulsion stability for 6, 8, 10 and 12 months. The Canadian government's regulations dictated that monoglycerides and diglycerides can be used in margarine at 0.5% and in shortenings at 10%; however, pectin is not regulated yet for tablespreads, which drops in the section of the Good Manufacturing Practice (Health Canada, 2012). The development in the third study fits with the requirements in shortenings; however, the further reduction should be investigated to match for margarine.

7. GENERAL CONCLUSIONS

The global goal of the thesis was to investigate three objectives: (1) to develop coarse W/O emulsions stable to multiple thermal cycles by modifying ingredient formulation and implementing vortex mixing processing, (2) to stabilize food-grade W/VO emulsions by modifying emulsifiers' interactions at the water-vegetable oil interface and finally, (3) to improve viscoelastic behaviour of W/O emulsions by modifying water droplet size, volume fraction and optimizing ingredient interactions. Interfacial tension, rheology, droplet size and emulsion visual observation were based on stability analyses in all studies. The model 20 wt% of an aqueous phase and 80 wt% of continuous oil phase was the initial formulation in the first and second study. The third study included the increment of water content and reduction of the oil phase. Some conclusions can be extracted from the individual studies and the whole thesis.

Chapter 3 contains the first study that produced thermally stable liquid coarse W/O emulsions with two different bulk viscosities using PGPR and AOT as emulsifiers at two concentration levels for biotechnology or medical applications. This study represents an innovation to conventional PCR and brings a new droplet digital PCR, where the water droplets act as micro-reactor for DNA polymerization and remain stable without breakups during DNA detection. It was obtained partially thermal stable liquid coarse W/O emulsions, with oil separation ~40% from the emulsion phase after the thermal cycles. BSA being part of the aqueous phase, also interacted with PGPR or AOT at the interface. At the interface, PGPR and AOT behaved differently. Without BSA, PGPR showed more interfacial tension than AOT. However, the main difference with BSA was the emulsifier concentration. PGPR required less concentration with BSA to reach the critical micelle concentration (CMC) in the oil phase. Conversely, in AOT, the concentration increased with BSA to attain the CMC. The shape of AOT could cause this, with two open branches having more trouble to pack at the interface with BSA. For this reason, the concentration required for AOT was significantly higher than in PGPR to stabilize the liquid emulsions. BSA supported the interfacial strength with both emulsifiers, which endorsed the emulsion stability under vortex homogenization; even though BSA was denatured during the thermal cycles, its interfacial activity supported emulsion stability. The viscosity of the continuous oil phase was essential to obtain a stable fresh emulsion and thermal stability. The range of viscosity was created with the combination of light and heavy mineral oil, which controlled the mobility and cover of the emulsifier at the interface during homogenization and thermal exposure.

Overall, the outcomes of this investigation suggest some significant points. PGPR and AOT interactions were subjected to structure, size, and shape. The mineral oil containing various alkanes facilitated the interactions at the interface without bonding with the emulsifiers. Even with this advantage, multiple thermal cycles were extreme conditions, interfering with the emulsifiers' mobility towards and at the interface.

Chapter 4 presented the second study, which extended the research on liquid W/O emulsions in CO and MO and stabilized by food-grade GMO. The stability was analyzed with and without the addition of hydroxyl group donating agents and salts. Partially stable liquid W/O emulsions were formed with AA, CA, LMP and their mixtures with or without S and Ca in the aqueous phase that can be used in cosmetics, skincare, and food formulations. Visual observation, microstructure, droplet size, accelerated stability, rheology, interfacial tension, thermal analysis, and FTIR spectroscopy were evaluated to understand the emulsion stability and the underlying mechanism. Without the additives, liquid emulsions showed 17 to 39% emulsion height after phase separation after 7 days for CO and MO-emulsions. A significant increase in emulsion stability against phase separation was obtained with the inclusion of additives, reporting a range of emulsion height from 45 to 79%. Droplet size in CO was significantly larger compared to MO; however, the microstructure of most emulsions exhibited a wide range of droplet aggregation. Sedimentation velocity on day 0 was low for all CO-emulsions with additives, which was similar in MO-emulsions except with Ca, AA, CA, and their salt combination that showed higher sedimentation velocity. Almost all additives increased the viscosity of MO-emulsions after 7 days; nevertheless, the CO-emulsions trend was a decrease in viscosity after 7 days. All emulsions showed a weak to medium gel with a slight tendency to increase in gel strength after 7 days. All emulsions showed a tan δ below 0.37, indicating more elastic gels than viscous. The interfacial tension with 4 wt% GMO showed a similar range for all CO-aqueous phases. In the presence of MO, the interfacial tension was much lower than CO without any aqueous phase additives, which was associated with GMO's ability for better interfacial packing in MO than CO. With the additives in the aqueous phase, all MO-aqueous phase showed a significant increase in interfacial tension.

To understand the mechanism of GMO's interfacial interactions, DSC thermal analysis of water and GMO melting and FTIR spectroscopy were performed. The ice melting analyses indicated more intermolecular hydrogen bonding between water molecules and GMO or additives in MO-emulsions than CO-emulsion, except for LMP and their mixtures with Ca. The GMO melting peaks exhibited higher temperatures for all CO-emulsions than MO-emulsions related to higher interaction between GMO and CO. From FTIR analysis, the intermolecular hydrogen bonding at 3400 cm^{-1} reported higher bonding between GMO and additives in CO-emulsions than MO-emulsions, associated with the excess of fatty acids in CO that can also interact at the interface. The area under the peaks was significantly higher in CO-emulsions,

indicating greater GMO molecular motion at the interface in CO than MO. The α-carbonyl group intramolecular hydrogen bond showed less GMO molecular motion at the interface than the free C=O in CO-emulsions. In MO-emulsions, both wavenumbers showed a significant reduction in area, indicating less GMO oscillation at the interface. The hydrocarbon chain conformation was analyzed only for CO because for MO, alkanes' disorder masks the small changes in GMO conformation. A slight decrease of the gg and kink conformation was exhibited in emulsions without any additive and LMP, indicating that LMP provided stability to the GMO tails. A slight increase in area was observed for S, AA and Ca associated with a loose packing of the GMO chains. The progress of analysis in molecular interactions was necessary to understand the complete role of additives in the aqueous phase and their effects on conformation. It was possible to improve the stability of liquid W/O emulsions with the incorporation of hydroxyl donating agents; however, LMP was the molecule that showed better interaction with GMO at the interface. This research was proved the hypothesis that emulsifiers performed desorption from the interface due to the bonding with the carbonyl groups of liquid VO.

The last body of work was presented in Chapter 5. It evaluated the increase of water content with and without LMP in the aqueous phase to enhance the viscoelasticity of CO-emulsions developed in the previous study. Five levels of water content were tested to increase and reach a close packing of water droplets. The inclusion of GMO was to reduce the interfacial tension, and HSO collaborated with the crystal formation in the continuous phase, providing network stabilization. Emulsion stability, microstructure, rheology, thermal analysis, and fat content were assessed. Over 30 days, all emulsions with LMP in the aqueous phase retained their shape, and no phase separation was observed. However, control emulsions without LMP in the aqueous showed evidence of flow (20 wt% water) or phase separation (50 wt% water). LMP-emulsions with all levels of water content exhibited higher viscosity after 30 days, except the control emulsion with 20 wt% water. All emulsions showed a G' higher than G", with a short LVR. The presence of LMP increased emulsion gelation, enhancing the packing of water droplets. The gel point as a function of strain indicated a proportional increase with the increment of water content for LMP-emulsions on day 1 and day 30. For control emulsions, the crossover strain was significantly lower than LMP-emulsions, indicating weaker gels. The microstructure images showed HSO crystals at the interface and accumulated in the continuous oil phase. Close contact of water droplets was observed after 30 wt% water content. Freeze/thaw cycles in a DSC were used to identify emulsion stabilization mechanism, where the emulsions with 20 wt% water content with and without LMP appeared most stable; however, with LMP, lower water destabilization was calculated. With higher water content, it was not possible to detect further thermal stability using the DSC due to the close contact of water droplets leading to destabilization. The total solid fat content slightly increased in all emulsions from day 1 to day 30, associated with the crystal growth or

evaporation of free water during storage; however, that tiny increase could not significantly influence the rise in viscosity observed with the increase of water content. Overall, this work enhanced the viscoelasticity of W/O emulsions with the essential role of LMP inside the aqueous phase incremented, HSO and GMO in the aqueous phase to induce gelation in the whole system, which proved our hypothesis in the diverse interaction at the interface and continuous phase.

Overall, this thesis has shown different conditions for developing liquid W/O emulsions, such as homogenization, emulsifier type and concentration, the inclusion of additives in the aqueous phase, and a subsequent approach to viscoelastic improvement. All the studies had their impact according to the application and objective of development on biotechnology, cosmetics, skincare, or the food industry. The final research concluded with a viable methodology for the development of low-fat tablespreads.

8. FUTURE STUDIES

W/O emulsions are complex systems developed by different homogenization conditions and compositions in the oil and aqueous phases. Different directions could be implemented in each study to optimize the conditions utilized to accomplish the objectives or modify the applications.

Regarding the first study for ddPCR application, the creation of water droplets can be tested with microfluidic channels, using hydrophobic porous membranes with equal size perforations to develop monodisperse W/O emulsions (Kawakatsu et al., 2001). The hydrophobic materials of these membranes can be poly (dimethylsiloxane), poly(methylmethacrylate), urethane, stainless steel, or nickel; the design can vary the location where the dispersed phase encounter the continuous phase, presenting two options (1) with a straight vertical flow from bottom or (2) horizontal flow encountering both phases at the same level (Kobayashi & Nakajima, 2006). For W/O emulsions, the contact angle of the water droplet should be more than 120° (Kawakatsu et al., 2001). A downside is the maximum capacity of the microfluidic channel plate varying from 0.1 to 6 mL/hour, which formed faster the water droplet when the dispersed phase goes from the bottom. It can represent a bottleneck for the reaction because the multiple thermal cycles complete in ~ 1 hour 30 min. However, it is an effective way to obtain monodisperse droplets with very low standard deviation. The concentration of PGPR and AOT should be re-evaluated as well as the viscosity of the oil phase. Kawakatsu et al. (2001) reported that average water droplet size increased as the continuous phase viscosity increased and decreased as the dispersed phase viscosity increased. It is possible that light mineral oil should be used for microfluidic channel emulsification. Another direction would be the testing of the combination of emulsifiers. Musyanovych et al. (2005) used Span 80 (4.5 % v/v), Tween 80 (0.4 % v/v) and Triton X-100 (0.05 % v/v); however, the droplet size obtained has been 15 μm. The reduction in concentration could form coarse water droplets, and the packing with multiple emulsifiers might enhance the stability of the emulsions. A solution to remain the water droplets size after the thermal cycles could be the addition of a polymer in the oil phase.

In the second study, desorption of GMO from the interface was prevented using aqueous phase ingredients. However, that knowledge can also be enhanced by trying other ingredients (e.g., low-acyl gellan) or homogenization methodologies (e.g., just rotor-stator). The aqueous phase concentration of AA or CA reduced the pH to ~3. Thus, to compare the agents' ability to form hydrogen bonding with GMO at the interface, the LMP solution was also modified to pH 3. It is known that LMP formed a weak gel in pH

conditions (Yuliarti & Othman, 2018). However, modifying the pH a bit higher can enhance the stability of LMP with fewer hydrogen ions in the aqueous phase (Flutto, 2003). This modification in pH could increase the hydrogen bonding interaction with GMO during emulsification. Further research should also be done to identify if LMP (LM-101 AS) can create similar interactions in other types of liquid oils to know if similar GMO-fatty acids close packing could be developed. LMP possesses features due to its structure, like the side chains preventing aggregation in the aqueous phase, and the commercial amidation gives flexibility to the molecule (Flutto, 2003). Thus, the selection of other LMP can show other the interaction at the interface due to the differences in structure. In pectin, even the source can change the molecular behaviour. For instance, apple pectin tends to have a random ester distribution; instead, citrus pectin tends to show blockwise distribution (Flutto, 2003). In this research, citrus pectin was the origin of the LMP used, which could be associated with the ordered packing promoted in GMO at the interface. To corroborate the H-bonding mechanism at the interface, another sophisticated technique that can be considered is the synchrotron in the Canadian Light Source with also IR spectra. In that equipment, the path length is from 100 - 500 μm. Wavenumber shifts will be possible to identify related to each bond as was discussed in Chapter 5; however, due to the small path length the collection of data will take longer. For the analysis in droplet size and solid fat content, it can be implemented NMR and PFG-NMR, which is less time consuming compared to image analysis to calculate the droplet size. The emulsions developed for non-food applications may required GMO substitution with PEGs emulsifiers that are commonly used in cosmetic or skincare products. Investigation of other molecules that can combine its action with LMP in the aqueous phase should be done like k-carrageenan, locust bean gum, xanthan gum in low percentage. Nasirpour-Tabrizi, Azadmard-Damirchi, Hesari, Khakbaz Heshmati, and Savage (2020) used 0.09% locust bean gum, 1.95% carrageenan, 0.8% xanthan gum and 10% maltodextrin with PGPG and MAGs. Synergism between LMP and those molecules can be formed without competing for binding GMO. Special attention should be focused on the concentration of materials according to the regulations. Thus, I consider a combination between MAGs as a better fit; for instance, between GMO and GMS will give better stability. It is well reported that GMS has higher stability abilities than GMO due to its rapid transition to solid-state after emulsification (Ghosh et al., 2011). GMS can provide more gel-strength and thermal stability to the system.

In the third study, further investigation can focus on controlling HSO crystals size during cooling, which could influence network structure and emulsion rheology (Rousseau, 2020). High crystallization speeds develop soft products due to small crystals; however, crystals growing together are responsible for the hardness (Juriaanse & Heertje, 1988). The composition of the polar lipids is also important; MAGs had a higher melting point than MAG; however, some percentage of MAGs present in the composition can also crystallize (Rousseau, 2000). Further research should be done on the mixture composition of the polar lipids, more reduction of solid fat content, and how to approach margarine characteristics. Another effective option

is the partial substitution of GMO by Pickering particles (e.g., polyphenol organic crystals) to improve the freeze/thaw stability and fit in the regulation of MAG and DAG at 0.5% in margarine. Polyphenol crystals are surface-active materials that can form stable W/O emulsions. Zembyla et al. (2018) investigated the stability of W/O emulsions with quercetin and curcumin. The crystal's shape and size influenced their interfacial abilities, and quercetin was superior to curcumin, forming a stronger interface. More research can be done mixing GMO with quercetin to identify a possible synergistic effect, including LMP in the aqueous phase. Modifying this ingredient would reduce the solid fat content, which some consumers look for. The increment of water in formula could be possible with the use of rotor-stator instead of the homogenizer, in which time and temperature factor should be controlled. It is important to consider the increase of water related to microbiology risk so further analysis should be with an antimicrobial preservative. Droplet size is also important in tablespreads, preferable < 5 μm (Juriaanse & Heertje, 1988). Further research should give emphasis in the analysis of droplet size with PFG-NMR, due to the relevance of its impact on gel strength (Erramreddy et al., 2017) and thermal stability. Tablespreads' spreadability is essential to test at room temperature and refrigeration temperature, which was not assessed in this study. A cone penetrometer test is a standardized method (AOCS Method Cc 16-60) to identify index hardness and force required to obtain deformation (Deman, 1983). However, other groups have migrated to sensory evaluation to test the same parameters with panellists, which is very complicated to achieved in comparative studies. Some studies have observed better fit comparing the sensorial analysis and the texture analyzer with the conical probe (Nasirpour-Tabrizi et al., 2020; Rohm et al., 1997).

9. REFERENCES

Acevedo, N. C., & Marangoni, A. G. (2014). Functionalization of non-interesterified mixtures of fully hydrogenated fats using shear processing. *Food and Bioprocess Technology, 7*(2), 575-587.

Aguilera, J. M. (2005). Why food microstructure?. *Journal of Food Engineering, 67*(1-2), 3-11.

Ahuja, A., Potanin, A., & Joshi, Y. M. (2020). Two step yielding in soft materials. *Advances in Colloid and Interface Science*, 102179.

Alexa, R. I., Mounsey, J. S., O'Kennedy, B. T., & Jacquier, J. C. (2010). Effect of κ-carrageenan on rheological properties, microstructure, texture and oxidative stability of water-in-oil spreads. *LWT - Food Science and Technology, 43*(6), 843-848.

Alexander, M., & Dalgleish, D. G. (2006). Dynamic light scattering techniques and their applications in food science. *Food Biophysics, 1*(1), 2-13.

Amar-Yuli, I., & Garti, N. (2005). Transitions induced by solubilized fat into reverse hexagonal mesophases. *Colloids and Surfaces B: Biointerfaces, 43*(2), 72-82.

Amar-Yuli, I., Wachtel, E., Shoshan, E. B., Danino, D., Aserin, A., & Garti, N. (2007). Hexosome and hexagonal phases mediated by hydration and polymeric stabilizer. *Langmuir, 23*(7), 3637-3645.

Amer, V. (1981). *Low fat butter-like spread*. USA Patent No. 4307125.

Andersen, F. A. (1998). Amended final report on the safety assessment of dioctyl sodium sulfosuccinate. *International Journal of Toxicology, 17*, 1-20.

Anton, N., Mojzisova, H., Porcher, E., Benoit, J.-P., & Saulnier, P. (2010). Reverse micelle-loaded lipid nano-emulsions: New technology for nano-encapsulation of hydrophilic materials. *International Journal of Pharmaceutics, 398*(1-2), 204-209.

Aronson, M. P., & Petko, M. F. (1993). Highly concentrated water-in-oil emulsions: Influence of electrolyte on their properties and stability. *Journal of Colloid and Interface Science, 159*(1), 134-149.

Ash, M., & Ash, I. (2004). *Handbook of Preservatives*. New York, NY: Synapse Information Resources. Inc.

Baier, G., Musyanovych, A., Landfester, K., Best, A., Lorenz, S., & Mailänder, V. (2011). DNA amplification via polymerase chain reaction inside miniemulsion droplets with subsequent poly (n-butylcyanoacrylate) shell formation and delivery of polymeric capsules into mammalian cells. *Macromolecular Bioscience, 11*(8), 1099-1109.

Balinov, B., Mariette, F., & Söderman, O. (2004). NMR studies of emulsions with particular emphasis on food emulsions. In S. E. Friberg, K. Larsson, & J. Sjöblom (Eds.), *Food Emulsions Fourth Edition, Revised and Expanded* (pp. 593-632). New York, NY: Marcel Dekker.

Balinov, B., Söderman, O., & Wärnheim, T. (1994). Determination of water droplet size in margarines and low-calorie spreads by nuclear magnetic resonance self-diffusion. *Journal of the American Oil Chemists' Society, 71*(5), 513-518.

Bancroft, W. D. (1912). The theory of emulsification, v. *The Journal of Physical Chemistry, 17*(6), 501-519.

Bastida-Rodríguez, J. (2013). The food additive polyglycerol polyricinoleate (e-476): Structure, applications, and production methods. *ISRN Chemical Engineering, 2013*, 21.

Belitz, H.-D., Grosch, W., & Schieberle, P. (2009). Food additives. *Food Chemistry*, 429-466.

Benichou, A., Aserin, A., & Garti, N. (2001). Polyols, high pressure, and refractive indices equalization for improved stability of w/o emulsions for food applications. *Journal of Dispersion Science and Technology, 22*(2-3), 269-280.

Bergenståhl, B. (2008). Physicochemical aspects of an emulsifier functionality. In G. L. Hasenhuettl & R. W. Hartel (Eds.). *Food Emulsifiers and Their Applications Second Edition* (pp. 173-194). New York, NY: Springer.

Beri, A., Norton, J., & Norton, I. (2013). Effect of emulsifier type and concentration, aqueous phase volume and wax ratio on physical, material and mechanical properties of water in oil lipsticks. *International Journal of Cosmetic Science, 35*(6), 613-621.

Bi, J., Yang, F., Harbottle, D., Pensini, E., Tchoukov, P., Simon, S., Sjöblom, J., Dabros, T., Czarnecki, J., Liu, Q. & Xu, Z. (2015). Interfacial layer properties of a polyaromatic compound and its role in stabilizing water-in-oil emulsions. *Langmuir, 31*(38), 10382-10391.

Binks, B. (1993). Relationship between microemulsion phase behavior and macroemulsion type in systems containing nonionic surfactant. *Langmuir, 9*(1), 25-28.

Binks, B., & Lumsdon, S. (2000). Catastrophic phase inversion of water-in-oil emulsions stabilized by hydrophobic silica. *Langmuir, 16*(6), 2539-2547.

Binks, B. P., Clint, J. H., & Whitby, C. P. (2005). Rheological behavior of water-in-oil emulsions stabilized by hydrophobic bentonite particles. *Langmuir, 21*(12), 5307-5316.

Bitan-Cherbakovsky, L., Yuli-Amar, I., Aserin, A., & Garti, N. (2009). Structural rearrangements and interaction within hii mesophase induced by cosolubilization of vitamin e and ascorbic acid. *Langmuir, 25*(22), 13106-13113.

Blochowicz, T., Gögelein, C., Spehr, T., Müller, M., & Stühn, B. (2007). Polymer-induced transient networks in water-in-oil microemulsions studied by small-angle x-ray and dynamic light scattering. *Physical Review E, 76*(4), 041505.

Bouchama, F., van Aken, G. A., Autin, A. J. E., & Koper, G. J. M. (2003). On the mechanism of catastrophic phase inversion in emulsions. *Colloids and Surfaces A: Physicochemical and Engineering Aspects, 231*(1), 11-17.

Bourne, M. (2002). *Food Texture and Viscosity: Concept and Measurement Second Edition* (pp. 1 – 416). London, UK: Academic Press.

Boyle, E., German, J. B., & Whelan, J. (1996). Monoglycerides in membrane systems. *Critical Reviews in Food Science and Nutrition, 36*(8), 785-805.

Brooker, B. E. (1993). The stabilization of air in foods containing fat - a review. *Food Structure, 12*(1), 115-122.

Brooks, C. F., Fuller, G. G., Frank, C. W., & Robertson, C. R. (1999). An interfacial stress rheometer to study rheological transitions in monolayers at the air−water interface. *Langmuir, 15*(7), 2450-2459.

Buján-Núñez, M. C., & Dickinson, E. (1994). Brownian dynamics simulation of a multi-subunit deformable particle in simple shear flow. *Journal of the Chemical Society, Faraday Transactions, 90*(18), 2737-2742.

Burdock, G. A., Carabin, I. G., & Griffiths, J. C. (2006). Toxicology and pharmacology of sodium ricinoleate. *Food and Chemical Toxicology, 44*(10), 1689-1698.

Bus, J., Groeneweg, F., & van Voorst Vader, F. (1990). Effect of hydrogen bonding on water in oil emulsion properties. *Surfactants and Macromolecules: Self-Assembly at Interfaces and in Bulk*, 122-130.

Capel, F., Nicolai, T., Durand, D., Boulenguer, P., & Langendorff, V. (2006). Calcium and acid induced gelation of (amidated) low methoxyl pectin. *Food Hydrocolloids, 20*(6), 901-907.

Carlton, R. A. (2011). Polarized light microscopy. In R.A. Carlton (Ed.), *Pharmaceutical Microscopy* (pp. 7-64). New York, NY: Springer.

Carretero, M. I., & Pozo, M. (2010). Clay and non-clay minerals in the pharmaceutical and cosmetic industries part ii. Active ingredients. *Applied Clay Science, 47*(3), 171-181.

Chatzidaki, M. D., Mateos-Diaz, E., Leal-Calderon, F., Xenakis, A., & Carriere, F. (2016). Water-in-oil microemulsions versus emulsions as carriers of hydroxytyrosol: An in vitro gastrointestinal lipolysis study using the phstat technique. *Food & Function, 7*(5), 2258-2269.

Chevalier, Y., & Bolzinger, M. A. (2013). Emulsions stabilized with solid nanoparticles: Pickering emulsions. *Colloids and Surfaces A: Physicochemical and Engineering Aspects, 439*, 23-34.

Choudhary, U., Sabikhi, L., Abdul Hussain, S., Khamrui, K., Sharma, V., & Vij, S. (2018). Stabilizing the primary emulsion with hydrophobic emulsifiers and salt for encapsulating herbal extracts in a double emulsion. *Journal of Food Processing and Preservation, 42*(8), e13699.

Christiansen, K. (2014). PGPR, polyglycerolpolyricinoleate, E476 209. In V. Norn (Ed.), *Emulsifiers in Food Technology Second Edition* (pp. 209-230). West Sussex, UK: John Wiley & Sons, Ltd.

Chrysan, M. M., & Hwang, H. S. (2020). Margarines and spreads. In F. Shahidi (Ed.), *Bailey's Industrial Oil and Fat Products Seventh Edition* (pp. 31-72). Hoboken, NJ: John Wiley & Sons, Ltd.

Ciriminna, R., Katryniok, B., Paul, S., Dumeignil, F., & Pagliaro, M. (2015). Glycerol-derived renewable polyglycerols: A class of versatile chemicals of wide potential application. *Organic Process Research & Development, 19*(7), 748-754.

Clausse, D., Gomez, F., Dalmazzone, C., & Noik, C. (2005). A method for the characterization of emulsions, thermogranulometry: Application to water-in-crude oil emulsion. *Journal of Colloid and Interface Science, 287*(2), 694-703.

Colucci, G., Santamaria-Echart, A., Silva, S. C., Fernandes, I. P., Sipoli, C. C., & Barreiro, M. F. (2020). Development of water-in-oil emulsions as delivery vehicles and testing with a natural antimicrobial extract. *Molecules, 25*(9), 2105.

Constantinides, P. P., Lancaster, C. M., Marcello, J., Chiossone, D. C., Orner, D., Hidalgo, I., Owen, A. J. (1995). Enhanced intestinal absorption of an RGD peptide from water-in-oil microemulsions of different composition and particle size. *Journal of Controlled Release, 34*(2), 109-116.

Council Regulation EC. 1996. No. 2291/94. *Laying down standards for spreadable fats.* Retrieved May 17, 2021 from http://www.fao.org/faolex/results/details/en/c/LEX-FAOC018589.

Coupland, J. N. (2014). *An Introduction to the Physical Chemistry of Food*. New York, NY: Springer.

Coupland, J. N., & McClements, D. J. (2001). Droplet size determination in food emulsions: Comparison of ultrasonic and light scattering methods. *Journal of Food Engineering, 50*(2), 117-120.

Cox, M. F., & Weerasooriya, U. (1997). Methyl ester ethoxylates. *Journal of the American Oil Chemists' Society, 74*(7), 847-859.

Croda. (2018). Spans. Retrieved from https://www.crodacropcare.com/es-mx/technical-library/datasheets-and-msds

Dalgleish, D., & Hallett, F. (1995). Dynamic light scattering: Applications to food systems. *Food Research International, 28*(3), 181-193.

Dalgleish, D. G. (2004). Food emulsions: Their structures and properties. In S. E. Friberg, K. Larsson, & J. Sjöblom (Eds.), *Food Emulsions Fourth Edition, Revised and Expanded* (pp. 1-44). New York, NY: Marcel Dekker.

Dalgleish, D. G. (2006). Food emulsions—their structures and structure-forming properties. *Food Hydrocolloids, 20*(4), 415-422.

Davies, J. T. (1957). *A Quantitative Kinetic Theory of Emulsion Type I Physical Ehemistry of the Emulsifying Agent.* Paper presented at the 2nd International Congress Surface Activity, Butterworths, London.

de Guertechin, L. O. (2009). Surfactants: Classification. In A. O. Barel, M. Paye & H. I. Maibach (Eds.), *Cosmetic Science and Technology Third Edition* (pp. 769-786). New York, NY: Informa Healthcare USA, Inc.

Deman, J. (1983). Consistency of fats: A review. *Journal of the American Oil Chemists' Society, 60*(1), 82-87.

Dickinson, E. (1992). *An Introduction to Food Colloids*. New York, NY: Oxford University Press.

Dressman, D., Yan, H., Traverso, G., Kinzler, K. W., & Vogelstein, B. (2003). Transforming single DNA molecules into fluorescent magnetic particles for detection and enumeration of genetic variations. *Proceedings of the National Academy of Sciences, 100*(15), 8817-8822.

Duffus, L. J., Norton, J. E., Smith, P., Norton, I. T., & Spyropoulos, F. (2016). A comparative study on the capacity of a range of food-grade particles to form stable o/w and w/o Pickering emulsions. *Journal of Colloid and Interface Science, 473*, 9-21.

Dukhin, S. S., Kretzschmar, G., & Miller, R. (1995). *Dynamics of Adsorption at Liquid Interfaces, Theory, Experiment, Application*. Amsterdam, The Netherlands: Elsevier Science B.V.

Dunphy, P. J., Meyers, Alan J., Rigg, Richard T. (1992). *Cosmetic water-in-oil emulsion lipstick comprising a phospholipid and glycerol fatty acid esters emulsifying system*. United States Patent No. 5085856.

Eastoe, J., Young, W. K., Robinson, B. H., & Steytler, D. C. (1990). Scattering studies of microemulsions in low-density alkanes. *Journal of the Chemical Society, Faraday Transactions, 86*(16), 2883-2889.

EFSA Panel on Food Additives and Nutrient Sources added to Food (ANS), Mortensen, A., Aguilar, F., Crebelli, R., Di Domenico, A., Dusemund, B., Frutos, M.J., Galtier, P., Gott, D., Gundert-Remy, U., Leblanc, J., Lindtner, O., Moldeus, P., Mosesso, P., Parent-Massin, D., Oskarsson, A., Stankovic, I., Waalkens-Berendsen, I., Woutersen, R. A., Wright, M., Younes, M., Boon, P., Chrysafidis, D., Gürtler, R., Tobback, P., Rincon, A. M., Tard, A. & Lambre, C. (2017). Re-evaluation of polyglycerol polyricinoleate (E 476) as a food additive. *EFSA Journal, 15*(3), e04743.

Engel, R., & Riggi, S. (1969). Intestinal absorption of heparin facilitated by sulfated or sulfonated surfactants. *Journal of Pharmaceutical Sciences, 58*(6), 706-710.

Erramreddy, V. V., Tu, S., & Ghosh, S. (2017). Rheological reversibility and long-term stability of repulsive and attractive nanoemulsion gels. *RSC Advances, 7*(75), 47818-47832.

Eskin, M. N. A., Aladedunye, F., Unger, E. H., Shah, S., Chen, G., & Jones, P. J. (2020). Canola oil. In F. Shahidi (Ed.), *Bailey's Industrial Oil and Fat Products Seventh Edition* (pp. 57-158). Hoboken, NJ: John Wiley & Sons, Ltd.

Etchepare, R., Oliveira, H., Azevedo, A., & Rubio, J. (2017). Separation of emulsified crude oil in saline water by dissolved air flotation with micro and nanobubbles. *Separation and Purification Technology, 186*, 326-332.

European Parliamnet and Council Directive (1995). 95/2/EC on food additives other than colours and sweeteners. *OJ L, 61*(18.3).

Evans, D. F., & Wennerström H. (1994). *The colloidal domain: Where Physics, Chemistry, Biology and Technology Meet*. New York, NY: VCH.

Falk, M. (1990). Frequencies of h–o–h, h–o–d and d–o–d bending fundamentals in liquid water. *Journal of Raman Spectroscopy, 21*(9), 563-567.

Farell, E. M., & Alexandre, G. (2012). Bovine serum albumin further enhances the effects of organic solvents on increased yield of polymerase chain reaction of GC-rich templates. *BMC Research Notes, 5*(1), 257.

Fischer, K., & Schmidt, M. (2016). Pitfalls and novel applications of particle sizing by dynamic light scattering. *Biomaterials, 98*, 79-91.

Flies, D. B., & Chen, L. (2003). A simple and rapid vortex method for preparing antigen/adjuvant emulsions for immunization. *Journal of immunological methods, 276*(1-2), 239-242.

Flutto, L. (2003). Pectin: Properties and determination. In B. Caballero, P. Finglas & F. Toldrá (Eds.), *Encyclopedia of Food Sciences and Nutrition Second Edition* (pp. 4449-4456). San Diego, California: Academic Press.

Ford, R. E., & Furmidge, C. G. L. (1966). Studies at phase interfaces: II. The stabilization of water-in-oil emulsions using oil-soluble emulsifiers. *Journal of Colloid and Interface Science, 22*(4), 331-341.

Forgiarini, A., Esquena, J., González, C., & Solans, C. (2001). Formation of nano-emulsions by low-energy emulsification methods at constant temperature. *Langmuir, 17*(7), 2076-2083.

Frasch-Melnik, S., Norton, I. T., & Spyropoulos, F. (2010). Fat-crystal stabilised w/o emulsions for controlled salt release. *Journal of Food Engineering, 98*(4), 437-442.

Freer, E. M., Svitova, T., & Radke, C. J. (2003). The role of interfacial rheology in reservoir mixed wettability. *Journal of Petroleum Science and Engineering, 39*(1), 137-158.

Freer, E. M., Yim, K. S., Fuller, G. G., & Radke, C. J. (2004). Interfacial rheology of globular and flexible proteins at the hexadecane/water interface: Comparison of shear and dilatation deformation. *The Journal of Physical Chemistry B, 108*(12), 3835-3844.

Friberg, S., Larsson, K., & Sjoblom, J. (2004). *Food Emulsions Fourth Edition, Revised and Expanded*. New York, NY: Marcel Dekker.

Fruijtier-Pölloth, C. (2005). Safety assessment on polyethylene glycols (PEGs) and their derivatives as used in cosmetic products. *Toxicology, 214*(1-2), 1-38.

Gaiti, N., Aserin, A., & Cohen, Y. (1994). Mechanistic considerations on the release of electrolytes from multiple emulsions stabilized by BSA and nonionic surfactants. *Journal of Controlled Release, 29*(1-2), 41-51.

Gaonkar, A. G. (1989). Interfacial tensions of vegetable oil/water systems: effect of oil purification. *Journal of the American Oil Chemists' Society, 66*(8), 1090-1092.

Garti, N., & Remon, G. F. (1984). Relationship between nature of vegetable oil, emulsifier and the stability of w/o emulsion. *International Journal of Food Science & Technology, 19*(6), 711-717.

Garti, N., Schlichter, J., & Sarig, S. (1986). Effect of food emulsifiers on polymorphic transitions of cocoa butter. *Journal of the American Oil Chemists' Society, 63*(2), 230-236.

Garti, N., Wellner, E., Aserin, A., & Sarig, S. (1983). Analysis of sorbitan fatty acid esters by HPLC. *Journal of the American Oil Chemists' Society, 60*(6), 1151-1154.

Ghosh, S., Pradhan, M., Patel, T., Haj-shafiei, S., & Rousseau, D. (2015). Long-term stability of crystal-stabilized water-in-oil emulsions. *Journal of Colloid and Interface Science, 460*, 247-257.

Ghosh, S., & Rousseau, D. (2009). Freeze–thaw stability of water-in-oil emulsions. *Journal of Colloid and Interface Science, 339*(1), 91-102.

Ghosh, S., & Rousseau, D. (2010). Emulsion breakdown in foods and beverages. In L. Skibsted, J. Risbo & M. Andersen (Eds.), *Chemical Deterioration and Physical Instability of Food and Beverages* (pp. 260-295). Boca Raton, US: CRC Press LLC.

Ghosh, S., & Rousseau, D. (2011). Fat crystals and water-in-oil emulsion stability. *Current Opinion in Colloid & Interface Science, 16*(5), 421-431.

Ghosh, S., & Rousseau, D. (2012). Triacylglycerol interfacial crystallization and shear structuring in water-in-oil emulsions. *Crystal Growth & Design, 12*(10), 4944-4954.

Ghosh, S., Tran, T., & Rousseau, D. (2011). Comparison of pickering and network stabilization in water-in-oil emulsions. *Langmuir, 27*(11), 6589-6597.

Goff, H. D. (1997). Review. Colloidal aspects of ice cream. *International Dairy Journal, 7*, 363-373.

Goldburg, W. I. (1999). Dynamic light scattering. *American Journal of Physics, 67*(12), 1152-1160.

Green, R., Hopkinson, I., & Jones, R. (1999). Unfolding and intermolecular association in globular proteins adsorbed at interfaces. *Langmuir, 15*(15), 5102-5110.

Grenha, A. (2012). Chitosan nanoparticles: A survey of preparation methods. *Journal of Drug Targeting, 20*(4), 291-300.

Griffin, W. C. (1949). Classification of surface-active agents by "HLB". *Journal of the Society of Cosmetic Chemists, 1*, 311-326.

Gross-Rother, J., Herrmann, N., Blech, M., Pinnapireddy, S., Garidel, P., & Bakowsky, U. (2018). The application of STEP-technology® for particle and protein dispersion detection studies in biopharmaceutical research. *International Journal of Pharmaceutics, 543*(1-2), 257-268.

Gülseren, İ., & Corredig, M. (2012). Interactions at the interface between hydrophobic and hydrophilic emulsifiers: Polyglycerol polyricinoleate (PGPR) and milk proteins, studied by drop shape tensiometry. *Food Hydrocolloids, 29*(1), 193-198.

Haj-shafiei, S., Ghosh, S., & Rousseau, D. (2013). Kinetic stability and rheology of wax-stabilized water-in-oil emulsions at different water cuts. *Journal of Colloid and Interface Science, 410*, 11-20.

Hasenhuettl, G. L. (2008). Synthesis and commercial preparation of food emulsifiers. In G. L. Hasenhuettl & R. W. Hartel (Eds.), *Food Emulsifiers and Their Applications: Second Edition* (pp. 11-37). New York, NY: Springer New York.

Health Canada. (2012). *List of permitted emulsifying, gelling, stabilizing or thickening agents (lists of permitted food additives)*. Retrieved April 19, 2021, from https://www.canada.ca/en/health-canada/services/food-nutrition/food-safety/food-additives/lists-permitted/4-emulsifying-gelling-stabilizing-thickening-agents.html

Health Canada. (2017). *Notice of modification to the list of permitted emulsifying, gelling, stabilizing or thickening agents to enable the use of polyglycerol esters of interesterified castor oil fatty acids in unstandardized chocolate confectionery NOM/ADM-0088 C.F.R.* Retrieved April 10, 2021, from https://www.canada.ca/en/health-canada/services/food-nutrition/public-involvement-partnerships/modification-list-permitted-use-polyglycerol-esters-interesterified-castor-oil-fatty-acids-unstandardized-chocolate.html

Hiemenz, P. C., & Rajagopalan, R. (1997). *Principles of Colloid and Surface Chemistry Third Edition, Revised and Expanded*. New York, NY: Marcel Dekker, Inc.

Higuchi, R., Fockler, C., Dollinger, G., & Watson, R. (1993). Kinetic PCR analysis: Real-time monitoring of DNA amplification reactions. *Bio/technology, 11*(9), 1026-1030.

Hodge, S., & Rousseau, D. (2003). Flocculation and coalescence in water-in-oil emulsions stabilized by paraffin wax crystals. *Food Research International, 36*(7), 695-702.

Hodge, S., & Rousseau, D. (2005). Continuous-phase fat crystals strongly influence water-in-oil emulsion stability. *Journal of the American Oil Chemists' Society, 82*(3), 159-164.

Höhne, G., Hemminger, W. F., & Flammersheim, H.-J. (2003). *Differential Scanning Calorimetry Second Edition*. Berlin, Germany: Springer-Verlag.

Holm, N. K., Jespersen, S. K., Thomassen, L. V., Wolff, T. Y., Sehgal, P., Thomsen, L. A., Christiansen, G., Andersen, C. B., Knudsen, A. D. & Otzen, D. E. (2007). Aggregation and fibrillation of bovine serum albumin. *Biochimica et Biophysica Acta (BBA)-Proteins and Proteomics, 1774*(9), 1128-1138.

Holmberg, K., Jönsson, B., Kronberg, B., & Lindman, B. (2002). Emulsions and emulsifiers. In K. Holmberg, B. Jönsson, B. Kronberg, & B. Lindman (Eds.), *Surfactants and Polymers in Aqueous Solution Second Edition* (pp. 451-472). Hoboken, NJ: John Wiley & Sons, Ltd.

Holstborg, J., Pedersen, B. V., Krog, N., & Olesen, S. K. (1999). Physical properties of diglycerol esters in relation to rheology and stability of protein-stabilised emulsions. *Colloids and Surfaces B: Biointerfaces, 12*(3), 383-390.

Hoque, M. A., Mitu, A., Patoary, M.-O., & Islam, D. M. S. (2016). Physicochemical studies on effect of additives on clouding behavior and thermodynamics of polyoxyethylene (20) sorbitan monooleate. *Indian Journal of Chemistry, 55A*, 793-802.

Hori, M., Fukano, H., & Suzuki, Y. (2007). Uniform amplification of multiple DNAs by emulsion PCR. *Biochemical and Biophysical Research Communications, 352*(2), 323-328.

Hunter, R. J. (1989). *Foundations of Colloid Science Volume II*. Oxford, UK: Oxford University Press.

Huston, K. J., & Larson, R. G. (2015). Reversible and irreversible adsorption energetics of poly(ethylene glycol) and sorbitan poly(ethoxylate) at a water/alkane interface. *Langmuir, 31*(27), 7503-7511.

Ioannou, K., Nydal, O. J., & Angeli, P. (2005). Phase inversion in dispersed liquid–liquid flows. *Experimental Thermal and Fluid Science, 29*(3), 331-339.

Iqbal, S., Hameed, G., Baloch, M. K., & McClements, D. J. (2012). Formation of semi-solid lipid phases by aggregation of protein microspheres in water-in-oil emulsions. *Food Research International, 48*(2), 544-550.

Iqbal, S., Hameed, G., Baloch, M. K., & McClements, D. J. (2013a). Structuring lipids by aggregation of acidic protein microspheres in w/o emulsions. *LWT - Food Science and Technology, 51*(1), 16-22.

Iqbal, S., Hameed, G., Baloch, M. K., & McClements, D. J. (2013b). Structuring of lipid phases using controlled heteroaggregation of protein microspheres in water-in-oil emulsions. *Journal of Food Engineering, 115*(3), 314-321.

Iqbal, S., Xu, Z., Huang, H., & Chen, X. D. (2019). Structuring of water-in-oil emulsions using controlled aggregation of polysaccharide in aqueous phases. *Journal of Food Engineering, 258*, 34-44.

Israelachvili, J. N. (2011). *Intermolecular and Surface Forces Third Edition*. Waltham, MA: Elsevier Inc.

Ito, M., Uehara, M., Wakui, R., Shiota, M., & Kuroiwa, T. (2017). Preparation characteristics of water-in-oil emulsion using olive oil as a continuous phase in microchannel emulsification. *Japan Journal of Food Engineering, 18*(2), 103-111.

Izquierdo, P., Esquena, J., Tadros, T. F., Dederen, C., Garcia, M. J., Azemar, N., & Solans, C. (2002). Formation and stability of nano-emulsions prepared using the phase inversion temperature method. *Langmuir, 18*(1), 26-30.

Jafari, S. M., Assadpoor, E., He, Y., & Bhandari, B. (2008). Re-coalescence of emulsion droplets during high-energy emulsification. *Food Hydrocolloids, 22*(7), 1191-1202.

Jahnke, D.-I. S. (1998). The theory of high-pressure homogenization. *Emulsions and Nanosuspensions for the Formulation of Poorly Soluble Drugs*, 177.

Jiao, J., & Burgess, D. J. (2003). Ostwald Ripening of water-in-hydrocarbon emulsions. *Journal of Colloid and Interface Science, 264*(2), 509-516.

Johansson, D., Bergenståhl, B., & Lundgren, E. (1995). Water-in-triglyceride oil emulsions. Effect of fat crystals on stability. *Journal of the American Oil Chemists' Society, 72*(8), 939-950.

John-Innes-Center. (2007). *What is Light Microscopy?* Retrieved January 12, 2018, from https://www.jic.ac.uk/microscopy/intro_LM.html

Jorgensen, L., Van De Weert, M., Vermehren, C., Bjerregaard, S., & Frokjaer, S. (2004). Probing structural changes of proteins incorporated into water-in-oil emulsions. *Journal of Pharmaceutical Sciences, 93*(7), 1847-1859.

Juriaanse, A., & Heertje, I. (1988). Microstructure of shortenings, margarine and butter-a review. *Food Structure, 7*(2), 8.

Kanagawa, T. (2003). Bias and artifacts in multitemplate polymerase chain reactions (PCR). *Journal of Bioscience and Bioengineering, 96*(4), 317-323.

Kataoka, Y., Kitadai, N., Hisatomi, O., & Nakashima, S. (2011). Nature of hydrogen bonding of water molecules in aqueous solutions of glycerol by attenuated total reflection (ATR) infrared spectroscopy. *Applied Spectroscopy, 65*(4), 436-441.

Katritzky, A. R., Jain, R., Lomaka, A., Petrukhin, R., Maran, U., & Karelson, M. (2001). Perspective on the relationship between melting points and chemical structure. *Crystal Growth & Design, 1*(4), 261-265.

Kawakatsu, T., Trägårdh, G., Trägårdh, C., Nakajima, M., Oda, N., & Yonemoto, T. (2001). The effect of the hydrophobicity of microchannels and components in water and oil phases on droplet formation in microchannel water-in-oil emulsification. *Colloids and Surfaces A: Physicochemical and Engineering Aspects, 179*(1), 29-37.

Khudyakov, A. N., Kuleshova, L. G., Zaitseva, O. O., Sergushkina, M. I., Vetoshkin, K. A., & Polezhaeva, T. V. (2019). Effect of pectins on water crystallization pattern and integrity of cells during freezing. *Biopreservation and Biobanking, 17*(1), 52-57.

Kiefer, J., Frank, K., & Schuchmann, H. P. (2011). Attenuated total reflection infrared (ATR-IR) spectroscopy of a water-in-oil emulsion. *Applied Spectroscopy, 65*(9), 1024-1028.

Kim, W.-H., Lee, K.-S., & Lee, K.-K. (2012). An experimental study on the property and stability of w/o emulsion by various structures of emulsifier. *Journal of the Society of Cosmetic Scientists of Korea, 38*(2), 119-131.

Kizling, J., & Kronberg, B. (1990). On the formation and stability of concentrated water-in-oil emulsions, aphrons. *Colloids and Surfaces, 50*, 131-140.

Kobayashi, I., & Nakajima, M. (2006). Generation and multiphase flow of emulsions in microchannels. In N. Kockmann (Ed.), *Micro Process Engineering: Fundamnetals, Devices, Fabrication, and Applications* (pp. 149-171). Weinheim, Germany: Wiley-VCH Verlag GmbH.

Komaiko, J. S., & McClements, D. J. (2016). Formation of food-grade nanoemulsions using low-energy preparation methods: A review of available methods. *Comprehensive Reviews in Food Science and Food Safety, 15*(2), 331-352.

Koneva, A., Safonova, E., Kondrakhina, P., Vovk, M., Lezov, A., Chernyshev, Y. S., & Smirnova, N. (2017). Effect of water content on structural and phase behavior of water-in-oil (n-decane) microemulsion system stabilized by mixed nonionic surfactants SPAN 80/TWEEN 80. *Colloids and Surfaces A: Physicochemical and Engineering Aspects, 518*, 273-282.

Korhonen, M., Lehtonen, J., Hellen, L., Hirvonen, J., & Yliruusi, J. (2002a). Rheological properties of three component creams containing sorbitan monoesters as surfactants. *International Journal of Pharmaceutics, 247*(1-2), 103-114.

Korhonen, M., Lehtonen, J., Hellen, L., Hirvonen, J., & Yliruusi, J. (2002b). Rheological properties of three component creams containing sorbitan monoesters as surfactants. *International Journal of Pharmaceutics, 247*(1), 103-114.

Koroleva, M., Tokarev, A., & Yurtov, E. (2015). Simulation of flocculation in w/o emulsions and experimental study. *Colloids and Surfaces A: Physicochemical and Engineering Aspects, 481*, 237-243.

Koroleva, M. Y., & Yurtov, E. (2003). Effect of ionic strength of dispersed phase on Ostwald Ripening in water-in-oil emulsions. *Colloid Journal, 65*(1), 40-43.

Kovalchuk, K., & Masalova, I. (2012). Factors influencing the crystallisation of highly concentrated water-in-oil emulsions: A DSC study. *South African Journal of Science, 108*(3-4), 00-00.

Kovárová, M., & Dráber, P. (2000). New specificity and yield enhancer of polymerase chain reactions. *Nucleic Acids Research, 28*(13), e70-e70.

Kralova, I., & Sjöblom, J. (2009). Surfactants used in food industry: A review. *Journal of Dispersion Science and Technology, 30*(9), 1363-1383.

Kramb, R. C., & Zukoski, C. F. (2010). Yielding in dense suspensions: Cage, bond, and rotational confinements. *Journal of Physics: Condensed Matter, 23*(3), 035102.

Krog, N. J., & Vang Sparsø, F. (2004). Food emulsifiers: their chemical and physical properties. In S. Friberg, J. Sjoblom, & K. Larsson (Eds.), *Food Emulsions Fourth Edition, Revised and Expanded* (pp. 45-92). New York, NY: Marcel Dekker.

Kumar, A., Li, S., Cheng, C.-M., & Lee, D. (2015). Recent developments in phase inversion emulsification. *Industrial & Engineering Chemistry Research, 54*(34), 8375-8396.

Larkin, P. (2017). *Infrared and Raman Spectroscopy: Principles and Spectral Interpretation*. Waltham, USA: Elsevier.

Le Révérend, B. J. D., Taylor, M. S., & Norton, I. T. (2011). Design and application of water-in-oil emulsions for use in lipstick formulations. *International Journal of Cosmetic Science, 33*(3), 263-268.

Lee, M. C., Tan, C., Ravanfar, R., & Abbaspourrad, A. (2019). Ultrastable water-in-oil high internal phase emulsions featuring interfacial and biphasic network stabilization. *ACS Applied Materials & Interfaces, 11*(29), 26433-26441.

Lewis, R. N., & McElhaney, R. N. (2013). Membrane lipid phase transitions and phase organization studied by Fourier transform infrared spectroscopy. *Biochimica et Biophysica Acta (BBA)-Biomembranes, 1828*(10), 2347-2358.

Lifshitz, I. M., & Slyozov, V. V. (1961). The kinetics of precipitation from supersaturated solid solutions. *Journal of Physics and Chemistry of Solids, 19*(1-2), 35-50.

Lin, C., He, G., Dong, C., Liu, H., Xiao, G., & Liu, Y. (2008). Effect of oil phase transition on freeze/thaw-induced demulsification of water-in-oil emulsions. *Langmuir, 24*(10), 5291-5298.

Lindenstruth, K., & Muller, B. W. (2004). Parameters with influence on the droplet size of w/o emulsions. *Pharmazie, 59*(3), 187-190.

Lowry, G. V., Hill, R. J., Harper, S., Rawle, A. F., Hendren, C. O., Klaessig, F., Nobbmann, U., Sayre, P. & Rumble, J. (2016). Guidance to improve the scientific value of zeta-potential measurements in nanoEHS. *Environmental Science: Nano, 3*(5), 953-965.

Lutz, R., Aserin, A., Wicker, L., & Garti, N. (2009). Structure and physical properties of pectins with block-wise distribution of carboxylic acid groups. *Food Hydrocolloids, 23*(3), 786-794.

Maag, H. (1984). Fatty acid derivatives: Important surfactants for household, cosmetic and industrial purposes. *Journal of the American Oil Chemists' Society, 61*(2), 259-267.

Malkin, A. Y., Masalova, I., Slatter, P., & Wilson, K. (2004). Effect of droplet size on the rheological properties of highly-concentrated w/o emulsions. *Rheologica Acta, 43*(6), 584-591.

Malvern. (2012). *A Basic Guide to Particle Characterization*. Retrived May 10, 2020, from https://www.malvernpanalytical.com/en/learn/knowledge-center/whitepapers/WP120620BasicGuidePartChar

Marques, D. S., Sørland, G., Less, S., & Vilagines, R. (2018). The application of pulse field gradient (PFG) NMR methods to characterize the efficiency of separation of water-in-crude oil emulsions. *Journal of Colloid and Interface Science, 512*, 361-368.

Márquez, A. L., Medrano, A., Panizzolo, L. A., & Wagner, J. R. (2010). Effect of calcium salts and surfactant concentration on the stability of water-in-oil (w/o) emulsions prepared with polyglycerol polyricinoleate. *Journal of Colloid and Interface Science, 341*(1), 101-108.

Martin, A., Bos, M., & Van Vliet, T. (2002). Interfacial rheological properties and conformational aspects of soy glycinin at the air/water interface. *Food Hydrocolloids, 16*(1), 63-71.

Masalova, I., & Malkin, A. Y. (2007). Rheology of highly concentrated emulsions–concentration and droplet size dependencies. *Applied Rheology, 17*(4), 42250-42251-42250-42259.

Mason, T. G. (1999). New fundamental concepts in emulsion rheology. *Current Opinion in Colloid & Interface Science, 4*(3), 231-238.

Maxon, B. D. (1988). *Dimethicone copolyol sulfosuccinates*. USA Patent No. 4849127A.

McClements, D. J. (2005). *Food Emulsions: Principles, Practice, and Techniques Second Edition*. Boca Raton, FL: CRC Press.

McClements, D. J. (2010). Emulsion design to improve the delivery of functional lipophilic components. *Annual Review of Food Science and Technology, 1*, 241-269.

McClements, D. J. (2012). Nanoemulsions versus microemulsions: Terminology, differences, and similarities. *Soft Matter, 8*(6), 1719-1729.

McClements, D. J. (2015). *Food Emulsions: Principles, Practices, and Techniques Third Edition.* Boca Raton, FL: CRC Press.

McClements, D. J., & Rao, J. (2011). Food-grade nanoemulsions: Formulation, fabrication, properties, performance, biological fate, and potential toxicity. *Critical Reviews in Food Science and Nutrition, 51*(4), 285-330.

McIntyre, R. (1979). Polyglycerol esters. *Journal of the American Oil Chemists' Society, 56*(11), 835A-840A.

Meng-Juguang, C. Y. (2014). *Preparation method of dioctyl sodium sulfosuccinate*. China Patent No. CN103709078A.

Merianos, J. J. (2001). Surface-active agents. In S. S. Block (Ed.), *Desinfection, Sterilization and Preservation Fifth Edition* (pp. 283-320). Philadelphia, USA: Lippincott Williams & Wilkins.

Mettu, S., Wu, C., & Dagastine, R. R. (2018). Dynamic forces between emulsified water drops coated with poly-glycerol-poly-ricinoleate (PGPR) in canola oil. *Journal of Colloid and Interface Science, 517*, 166-175.

Milak, S., & Zimmer, A. (2015). Glycerol monooleate liquid crystalline phases used in drug delivery systems. *International Journal of Pharmaceutics, 478*(2), 569-587.

Mohanan, A., Tang, Y. R., Nickerson, M. T., & Ghosh, S. (2020). Oleogelation using pulse protein-stabilized foams and their potential as a baking ingredient. *RSC Advances, 10*(25), 14892-14905.

Mullis, K., Faloona, F., Scharf, S., Saiki, R., Horn, G., & Erlich, H. (1986). Specific enzymatic amplification of DNA in vitro: The polymerase chain reaction. *Cold Spring Harbor Symposia on Quantitative Biology, 51*(1), 263-273.

Murray, B. S. (2002). Interfacial rheology of food emulsifiers and proteins. *Current Opinion in Colloid & Interface Science, 7*(5-6), 426-431.

Murray, B. S. (2019). Pickering emulsions for food and drinks. *Current Opinion in Food Science, 27*, 57-63.

Murray, B. S., & Dickinson, E. (1996). Interfacial rheology and the dynamic properties of adsorbed films of food proteins and surfactants. *Food Science and Technology International, Tokyo, 2*(3), 131-145.

Musyanovych, A., Mailänder, V., & Landfester, K. (2005). Miniemulsion droplets as single molecule nanoreactors for polymerase chain reaction. *Biomacromolecules, 6*(4), 1824-1828.

Nadin, M., Rousseau, D., & Ghosh, S. (2014). Fat crystal-stabilized water-in-oil emulsions as controlled release systems. *LWT - Food Science and Technology, 56*(2), 248-255.

Naiim, M., Boualem, A., Ferre, C., Jabloun, M., Jalocha, A., & Ravier, P. (2015). Multiangle dynamic light scattering for the improvement of multimodal particle size distribution measurements. *Soft Matter, 11*(1), 28-32.

Nakano, M., Komatsu, J., Matsuura, S.-i., Takashima, K., Katsura, S., & Mizuno, A. (2003). Single-molecule PCR using water-in-oil emulsion. *Journal of Biotechnology, 102*(2), 117-124.

Nasirpour-Tabrizi, P., Azadmard-Damirchi, S., Hesari, J., Khakbaz Heshmati, M., & Savage, G. P. (2020). Production of a spreadable emulsion gel using flaxseed oil in a matrix of hydrocolloids. *Journal of Food Processing and Preservation, 44*(8), e14588.

National Organic Standards Board Technical Advisory Panel. (2001). *Glycerol Monooleate processing*. Retrieved January 15, 2019, from https://www.ams.usda.gov/sites/default/files/media/Glycerin%20Oleate%20TR.pdf

Nave, S., Eastoe, J., Heenan, R. K., Steytler, D., & Grillo, I. (2000). What is so special about aerosol-ot? 2. Microemulsion systems. *Langmuir, 16*(23), 8741-8748.

Nave, S., Eastoe, J., & Penfold, J. (2000). What is so special about aerosol-ot? 1. Aqueous systems. *Langmuir, 16*(23), 8733-8740.

Nicholson, R. A., & Marangoni, A. G. (2020). Enzymatic glycerolysis converts vegetable oils into structural fats with the potential to replace palm oil in food products. *Nature Food, 1*(11), 684-692.

Nilsson, A., Holmgren, A., & Lindblom, G. (1994). An FTIR study of the hydration and molecular ordering at phase transitions in the monooleoylglycerol/water system. *Chemistry and Physics of Lipids, 71*(2), 119-131.

Nishimi, T., & Miller, C. A. (2001). Spontaneous emulsification produced by chemical reactions. *Journal of Colloid and Interface Science, 237*(2), 259-266.

Norn, V. (2014). Polyglycerol esters. In V. Norn (Ed.), *Emulsifiers in Food Technology Second Edition* (pp. 181-208). Hoboken, NJ: John Wiley & Sons, Ltd.

Norton, J., Fryer, P., Parkinson, J., & Cox, P. (2009). Development and characterisation of tempered cocoa butter emulsions containing up to 60% water. *Journal of Food Engineering, 95*(1), 172-178.

Nwaneshiudu, A., Kuschal, C., Sakamoto, F. H., Anderson, R. R., Schwarzenberger, K., & Young, R. C. (2012). Introduction to confocal microscopy. *Journal of Investigative Dermatology, 132*(12), 1-5.

Oldenbourg, R. (2013). Polarized light microscopy: Principles and practice. *Cold Spring Harbor Protocols, 2013*(11).

Oldenbourg, R., & Mei, G. (1994). *Polarized light microscopy*. USA Patent No. 5521705A.

Opawale, F. O., & Burgess, D. J. (1998). Influence of interfacial properties of lipophilic surfactants on water-in-oil emulsion stability. *Journal of Colloid and Interface Science, 197*(1), 142-150.

Paddock, S. W. (1999). Confocal laser scanning microscopy. *Biotechniques, 27*(5), 992-1004.

Pagliaro, M. (2017). Esters, ethers, polyglycerols, and polyesters. In M. Pagliaro (Ed.), *Glycerol: The Renewable Platform Chemical* (pp. 59-90). Cambridge, MA: Elsevier.

Pal, R. (2000). Shear viscosity behavior of emulsions of two immiscible liquids. *Journal of Colloid and Interface Science, 225*(2), 359-366.

Panchal, K., Desai, A., & Nagar, T. (2006). Physicochemical behavior of mixed nonionic-ionic surfactants in water and aqueous salt solutions. *Journal of Dispersion Science and Technology, 27*(1), 33-38.

Peltonen, L., Hirvonen, J., & Yliruusi, J. (2001). The behavior of sorbitan surfactants at the water–oil interface: straight-chained hydrocarbons from pentane to dodecane as an oil phase. *Journal of Colloid and Interface Science, 240*(1), 272-276.

Peng, L.-C., Liu, C.-H., Kwan, C.-C., & Huang, K.-F. (2010). Optimization of water-in-oil nanoemulsions by mixed surfactants. *Colloids and Surfaces A: Physicochemical and Engineering Aspects, 370*(1), 136-142.

Pérez, M. P., Wagner, J. R., & Márquez, A. L. (2016). Influence of different factors on the particle size distribution and solid fat content of water-in-oil emulsions. *Journal of the American Oil Chemists' Society, 93*(6), 793-801.

Perkins, G., Lu, H., Garlan, F., & Taly, V. (2017). Droplet-based digital PCR: application in cancer research. *Advances in Clinical Chemistry, 79*, 43-91.

Pickering, S. U. (1907). Cxcvi.—emulsions. *Journal of the Chemical Society, Transactions, 91*, 2001-2021.

Pinnamaneni, S., Das, N. G., & Das, S. K. (2003). Comparison of oil-in-water emulsions manufactured by microfluidization and homogenization. *Pharmazie, 58*(8), 554-558.

Poghosyan, A. H., Adamyan, M. P., & Shahinyan, A. A. (2019). A rippled defective phase of AOT lamella: a molecular dynamics study. *Colloids and Surfaces A: Physicochemical and Engineering Aspects, 578*, 123578.

Politova, N. I., Tcholakova, S., Tsibranska, S., Denkov, N. D., & Muelheims, K. (2017). Coalescence stability of water-in-oil drops: effects of drop size and surfactant concentration. *Colloids and Surfaces A: Physicochemical and Engineering Aspects, 531*, 32-39.

Ponton, A., Clément, P., & Grossiord, J. (2001). Corroboration of Princen's theory to cosmetic concentrated water-in-oil emulsions. *Journal of Rheology, 45*(2), 521-526.

Porras, M., Solans, C., Gonzalez, C., & Gutierrez, J. (2008). Properties of water-in-oil (w/o) nano-emulsions prepared by a low-energy emulsification method. *Colloids and Surfaces A: Physicochemical and Engineering Aspects, 324*(1-3), 181-188.

Prichapan, N., McClements, D. J., & Klinkesom, U. (2017). Influence of rice bran stearin on stability, properties and encapsulation efficiency of polyglycerol polyricinoleate (PGPR)-stabilized water-in-rice bran oil emulsions. *Food Research International, 93*, 26-32.

Princen, H. (1986). Osmotic pressure of foams and highly concentrated emulsions. I. Theoretical considerations. *Langmuir, 2*(4), 519-524.

Princen, H., & Kiss, A. (1986). Rheology of foams and highly concentrated emulsions: III. Static shear modulus. *Journal of Colloid and Interface Science, 112*(2), 427-437.

Qiu, H., & Caffrey, M. (2000). The phase diagram of the monoolein/water system: metastability and equilibrium aspects. *Biomaterials, 21*(3), 223-234.

Quemada, D., & Berli, C. (2002). Energy of interaction in colloids and its implications in rheological modeling. *Advances in Colloid and Interface Science, 98*(1), 51-85.

Rafanan, R., & Rousseau, D. (2017). Dispersed droplets as active fillers in fat-crystal network-stabilized water-in-oil emulsions. *Food Research International, 99*, 355-362.

Rafanan, R., & Rousseau, D. (2019). Dispersed droplets as tunable fillers in water-in-oil emulsions stabilized with fat crystals. *Journal of Food Engineering, 244*, 192-201.

Raith, K., Schmelzer, C. E. H., & Neubert, R. H. H. (2006). Towards a molecular characterization of pharmaceutical excipients: Mass spectrometric studies of ethoxylated surfactants. *International Journal of Pharmaceutics, 319*(1), 1-12.

Rajagopal, K. R. (1993). Mechanics of non-Newtonian fluids. *Pitman Research Notes in Mathematics Series*, 129-129.

Ray, M., Gupta, R., & Rousseau, D. (2015). Properties and applications of multilayer and nanoscale emulsions. In C. M. Sabliov, H. Chen & R. Y. Yada (Eds.), *Nanotechnology and Functional Foods: Effective Delivery of Bioactive Ingredients* (pp. 175-190). Hoboken, NJ: John Wiley & Sons, Ltd.

Robinson, B. H., Toprakcioglu, C., Dore, J. C., & Chieux, P. (1984). Small-angle neutron-scattering study of microemulsions stabilised by aerosol-ot. Part 1.—Solvent and concentration variation. *Journal of the Chemical Society, Faraday Transactions 1: Physical Chemistry in Condensed Phases, 80*(1), 13-27.

Rohm, H., Strobl, M., & Jaros, D. (1997). Butter colour affects sensory perception of spreadability. *Zeitschrift für Lebensmitteluntersuchung und-Forschung A, 205*(2), 108-110.

Romero-Peña, M., Ng, E. K., & Ghosh, S. (2020). Development of thermally stable coarse water-in-oil emulsions as potential DNA bioreactors. *Journal of Dispersion Science and Technology*, 1-10.

Rosen, M. J. (2004). Emulsification by Surfactants. In M. J. Rosen & J. T. Kunjappu (Eds.), *Surfactants and Interfacial Phenomena Fourth Edition* (pp. 303-331). Hoboken, NJ: John Wiley & Sons, Inc.

Rousseau, D. (2000). Fat crystals and emulsion stability—a review. *Food Research International, 33*(1), 3-14.

Rousseau, D. (2020). Aqueous droplets as active fillers in oil-continuous emulsions. *Current Opinion in Food Science, 33*, 173-186.

Rousseau, D., & Hodge, S. M. (2005). Stabilization of water-in-oil emulsions with continuous phase crystals. *Colloids and Surfaces A: Physicochemical and Engineering Aspects, 260*(1-3), 229-237.

Salzer, R., & Siesler, H. W. (2014). *Infrared and Raman Spectroscopic Imaging: Second, Completely Revised and Updated Edition*. Weinheim, Germany: Wiley-VCH Verlag & Co. KGaA.

Sarkar, A., & Dickinson, E. (2020). Sustainable food-grade Pickering emulsions stabilized by plant-based particles. *Current Opinion in Colloid & Interface Science, 49*, 69-81.

Scherze, I., Knoth, A., & Muschiolik, G. (2006). Effect of emulsification method on the properties of lecithin- and pgpr-stabilized water-in-oil-emulsions. *Journal of Dispersion Science and Technology, 27*(4), 427-434.

Schindelin, J., Arganda-Carreras, I., Frise, E., Kaynig, V., Longair, M., Pietzsch, T., Preibisch, S., Rueden, C., Saalfeld, S., Schmid, B., Tinevez, J-Y., White, D. J., Hartenstein, V., Eliceiri, K., Tomancak, P. & Cardona, A. (2012). Fiji: an open-source platform for biological-image analysis. *Nature Methods, 9*(7), 676-682.

Schmidt, U., Schmidt, K., Kurz, T., Endreß, H.-U., & Schuchmann, H. (2015). Pectins of different origin and their performance in forming and stabilizing oil-in-water-emulsions. *Food Hydrocolloids, 46*, 59-66.

Schramm, G. (1994). *A Practical Approach to Rheology and Rheometry Second Edition*. Retrieved March 5, 2021, from http://www.asi-team.com/asi%20team/haake/haake%20data/A%20practical%20approach%20to%20rheology%20and%20rhometry.pdf

Sengupta, R., Walker, L. M., & Khair, A. S. (2018). Effective viscosity of a dilute emulsion of spherical drops containing soluble surfactant. *Rheologica Acta, 57*(6-7), 481-491.

Shakeel, F., & Ramadan, W. (2010). Transdermal delivery of anticancer drug caffeine from water-in-oil nanoemulsions. *Colloids and Surfaces B: Biointerfaces, 75*(1), 356-362.

Shendure, J., Porreca, G. J., Reppas, N. B., Lin, X., McCutcheon, J. P., Rosenbaum, A. M., Wang, M. D., Zhang, K., Mitra, R. D. & Church, G. M. (2005). Accurate multiplex polony sequencing of an evolved bacterial genome. *Science, 309*(5741), 1728-1732.

Shinoda, K., & Saito, H. (1968). The effect of temperature on the phase equilibria and the types of dispersions of the ternary system composed of water, cyclohexane, and nonionic surfactant. *Journal of Colloid and Interface Science, 26*(1), 70-74.

Shishu, Rajan, S., & Kamalpreet. (2009). Development of novel microemulsion-based topical formulations of acyclovir for the treatment of cutaneous herpetic infections. *AAPS PharmSciTech, 10*(2), 559-565.

Sigma-Aldrich. (2018). *Spans*. Retrieved February 10, 2019, from https://www.sigmaaldrich.com/canada-english.html

Smith, M., Wilson, R., & Hepburn, P. (1998). Assessment of the carcinogenic potential of polyglycerol polyricinoleate (PGPR) in rats and mice. *Food and Chemical Toxicology, 36*(9-10), 747-754.

Solans, C., Izquierdo, P., Nolla, J., Azemar, N., & Garcia-Celma, M. J. (2005). Nano-emulsions. *Current Opinion in Colloid & Interface Science, 10*(3), 102-110.

Spink, C. H. (2008). Differential scanning calorimetry. *Methods in Cell Biology, 84*, 115-141.

Stocker, I. N., Miller, K. L., Welbourn, R. J., Clarke, S. M., Collins, I. R., Kinane, C., & Gutfreund, P. (2014). Adsorption of aerosol-ot at the calcite/water interface–comparison of the sodium and calcium salts. *Journal of Colloid and Interface Science, 418*, 140-146.

Surh, J., Vladisavljevic, G. T., Mun, S., & McClements, D. J. (2007). Preparation and characterization of water/oil and water/oil/water emulsions containing biopolymer-gelled water droplets. *Journal of Agricultural and Food Chemistry, 55*(1), 175-184.

TA-Instruments. (2018). ARES-G2 Rheometer. Retrieved April 9, 2019, from http://www.tainstruments.com/wp-content/uploads/BROCH-ARES-G2-2017-EN.pdf

Tadros, T. F. (2013). *Emulsion Formation and Stability*. Weinheim, Germany: Wiley-VCH Verlag GmbH & Co. KGaA.

Tadros, T. F. (2014). Adsorption at the air/liquid, liquid/liquid, and solid/liquid Interfaces. In T. F. Tadros (Ed), *Formulation of Disperse Systems: Science and Technology* (pp. 55-76). Weinheim, Germany: Wiley-VCH Verlag GmbH & Co. KGaA.

Takemori, T., Tsurumi, T., & Takagi, M. (1992). *Heat-resistant chocolate and a method for producing it*. USA Patent 5160760.

Tang, Y. R., & Ghosh, S. (2021). Stability and rheology of canola protein isolate-stabilized concentrated oil-in-water emulsions. *Food Hydrocolloids, 113*, 106399.

Tawfik, D. S., & Griffiths, A. D. (1998). Man-made cell-like compartments for molecular evolution. *Nature Biotechnology, 16*(7), 652.

Taylor, G. I. (1932). The viscosity of a fluid containing small drops of another fluid. *Proceedings of the Royal Society of London. Series A, Containing Papers of a Mathematical and Physical Character, 138*(834), 41-48.

Tcholakova, S., Mitrinova, Z., Golemanov, K., Denkov, N. D., Vethamuthu, M., & Ananthapadmanabhan, K. P. (2011). Control of Ostwald Ripening by using surfactants with high surface modulus. *Langmuir, 27*(24), 14807-14819.

Thakur, R. K., Villette, C., Aubry, J. M., & Delaplace, G. (2008). Dynamic emulsification and catastrophic phase inversion of lecithin-based emulsions. *Colloids and Surfaces A: Physicochemical and Engineering Aspects, 315*(1), 285-293.

Tian, H., Xiang, D., Wang, B., Zhang, W., & Li, C. (2021). Using hydrogels in dispersed phase of water-in-oil emulsion for encapsulating tea polyphenols to sustain their release. *Colloids and Surfaces A: Physicochemical and Engineering Aspects, 612*, 125999.

Tiribocchi, A., Montessori, A., Lauricella, M., Bonaccorso, F., Succi, S., Aime, S., Milani, M. & Weitz, D. (2021). The vortex-driven dynamics of droplets within droplets. *Nature Communications, 12*(1), 1-10.

Tuntiwiwattanapun, N., Tongcumpou, C., Haagenson, D., & Wiesenborn, D. (2013). Development and scale-up of aqueous surfactant-assisted extraction of canola oil for use as biodiesel feedstock. *Journal of the American Oil Chemists' Society, 90*(7), 1089-1099.

Tyagi, V. (2006). Sulfosuccinates as mild surfactants. *Journal of Oleo Science, 55*(9), 429-439.

Unilever. (2008). *Edible emulsions with PGPR*. Netherlands Patent No. WO 2008/058893A1.

U.S. Food and Drug Administration (2021). *Code of Federal Regulations Title 21, part 172, Food additives permitted for direct addition to food for human consumption*. Retrieved May 14, 2021, from https://www.ecfr.gov/cgi-bin/text-idx?SID=7bc3b7743d572ccf70c9b36204e31882&mc=true&tpl=/ecfrbrowse/Title21/21cfr172_main_02.tpl.

Ushikubo, F. Y., & Cunha, R. L. (2014). Stability mechanisms of liquid water-in-oil emulsions. *Food Hydrocolloids, 34*, 145-153.

Usón, N., Garcia, M. J., & Solans, C. (2004). Formation of water-in-oil (w/o) nano-emulsions in a water/mixed non-ionic surfactant/oil systems prepared by a low-energy emulsification method. *Colloids and Surfaces A: Physicochemical and Engineering Aspects, 250*(1), 415-421.

van Aken, G. A. (2004). Coalescence mechanisms in protein-stabilized emulsions. In S. E. Friberg, K. Larsson, & J. Sjoblom (Eds.), *Food Emulsions*: *Fourth Edition, Revised and Expanded* (pp. 299-326). New York: Marcel Dekker, Inc.

van Os, N. M. (1998). *Nonionic Surfactants.* New York, NJ: Marcle Dekker, Inc.

Vargas, G. G., Soares, E. J., Thompson, R. L., Sandoval, G. A., Andrade, R. M., Campos, F. B., & Teixeira, A. (2018). Emulsion effects on the yield stress of gelled waxy crude oils. *Fuel, 222*, 444-456.

Verstringe, S., Danthine, S., Blecker, C., & Dewettinck, K. (2014). Influence of a commercial monoacylglycerol on the crystallization mechanism of palm oil as compared to its pure constituents. *Food Research International, 62*, 694-700.

Wagner, C. (1961). Theory of precipitate change by redissolution. *Z. Elektrochem, 65*, 581-591.

Walstra, P. (1996). *Emulsion stability*. In P. Becher (Ed.), *Encyclopedia of Emulsion Technology Volume 4* (pp. 1-62). New York, NY: Marcel Dekker Inc.

Walstra, P. (2003). *Physical Chemistry of Foods.* New York, NJ: Marcel Dekker, Inc.

Walstra, P. (2005). Emulsions. In J. Lyklema (Ed.), *Fundamentals of Interface and Colloid Science Volume V Soft Colloids*, pp. 8.1-8.94). San Diego, CA: Elsevier Ltd.

Wang, F. C., Peyronel, F., & Marangoni, A. G. (2016). Phase diagram of glycerol monostearate and sodium stearoyl lactylate. *Crystal Growth & Design, 16*(1), 297-306.

Weder, H. G., & Mütsch, M. (1992). *Process for the production of a nanoemulsion of oil particles in an aqueous phase*. USA Patent No. 5152923A.

Willenbacher, N., & Georgieva, K. (2013). Rheology of disperse systems. *Product Design and Engineering*, 7-49.

Williams, R., Peisajovich, S. G., Miller, O. J., Magdassi, S., Tawfik, D. S., & Griffiths, A. D. (2006). Amplification of complex gene libraries by emulsion PCR. *Nature Methods, 3*(7), 545-550.

Wilson, R., & Smith, M. (1998). Human studies on polyglycerol polyricinoleate (PGPR). *Food and Chemical Toxicology, 36*(9-10), 743-745.

Wilson, R., van Schie, B. J., & Howes, D. (1998). Overview of the preparation, use and biological studies on polyglycerol polyricinoleate (PGPR). *Food and Chemical Toxicology, 36*(9), 711-718.

Wilson, T. (1994). Confocal microscopy. In B. G. Yacobi, D. B. Holt & L. L. Kazmerski (Eds.), *Microanalysis of Solids* (pp. 219-232). Boston, MA: Springer.

Wu, H., Ramachandran, C., Weiner, N. D., & Roessler, B. J. (2001). Topical transport of hydrophilic compounds using water-in-oil nanoemulsions. *International Journal of Pharmaceutics, 220*(1), 63-75.

Wu, Y., Iglauer, S., Shuler, P., Tang, Y., & Goddard, W. A. (2010). Alkyl polyglycoside-sorbitan ester formulations for improved oil recovery. *Tenside Surfactants Detergents, 47*(5), 280-287.

Xaxa, R. K. (2014). *Spreading behavior of oil-in-water emulsion on model solid substrates* (Master dissertation). Indian Institute of Science Eduaction and Research, Pune, India. http://dr.iiserpune.ac.in:8080/xmlui/handle/123456789/351

Xu, J.-y., Li, D.-h., Guo, J., & Wu, Y.-x. (2010). Investigations of phase inversion and frictional pressure gradients in upward and downward oil–water flow in vertical pipes. *International Journal of Multiphase Flow, 36*(11), 930-939.

Yang, F., Tchoukov, P., Pensini, E., Dabros, T., Czarnecki, J., Masliyah, J., & Xu, Z. (2014). Asphaltene subfractions responsible for stabilizing water-in-crude oil emulsions. Part 1: Interfacial behaviors. *Energy & Fuels, 28*(11), 6897-6904.

Yi, J., Zhu, Z., McClements, D. J., & Decker, E. A. (2014). Influence of aqueous phase emulsifiers on lipid oxidation in water-in-walnut oil emulsions. *Journal of Agricultural and Food Chemistry, 62*(9), 2104-2111.

Yoshioka, T., Sternberg, B., & Florence, A. T. (1994). Preparation and properties of vesicles (niosomes) of sorbitan monoesters (Span 20, 40, 60 and 80) and a sorbitan triester (Span 85). *International Journal of Pharmaceutics, 105*(1), 1-6.

Young, N. W., & Wassell, P. (2019). Margarines and spreads. In G. L. Hasenhuettl & R. W. Hartel (Eds.), *Food Emulsifiers and their Applications Third Edition* (pp. 379-405). Cham, Switzerland: Springer Nature Switzerland AG.

Yuliarti, O., & Othman, R. M. B. (2018). Temperature dependence of acid and calcium-induced low-methoxyl pectin gel extracted from cyclea barbata miers. *Food Hydrocolloids, 81*, 300-311.

Zaidel, D. N. A., Sahat, N. S., Jusoh, Y. M. M., & Muhamad, I. I. (2014). Encapsulation of anthocyanin from roselle and red cabbage for stabilization of water-in-oil emulsion. *Agriculture and Agricultural Science Procedia, 2*, 82-89.

Zembyla, M., Murray, B. S., & Sarkar, A. (2018). Water-in-oil pickering emulsions stabilized by water-insoluble polyphenol crystals. *Langmuir, 34*(34), 10001-10011.

Zhao, L., & Yalkowsky, S. H. (1999). A combined group contribution and molecular geometry approach for predicting melting points of aliphatic compounds. *Industrial & Engineering Chemistry Research, 38*(9), 3581-3584.

Zhao, Y., Xia, Q., Yin, Y., & Wang, Z. (2016). Comparison of droplet digital PCR and quantitative PCR assays for quantitative detection of Xanthomonas citri Subsp. citri. *PloS ONE, 11*(7), e0159004.

10. APPENDICES

10.1 Copyright permission for the use of Garti et al. (1983) work in Table 2.1.

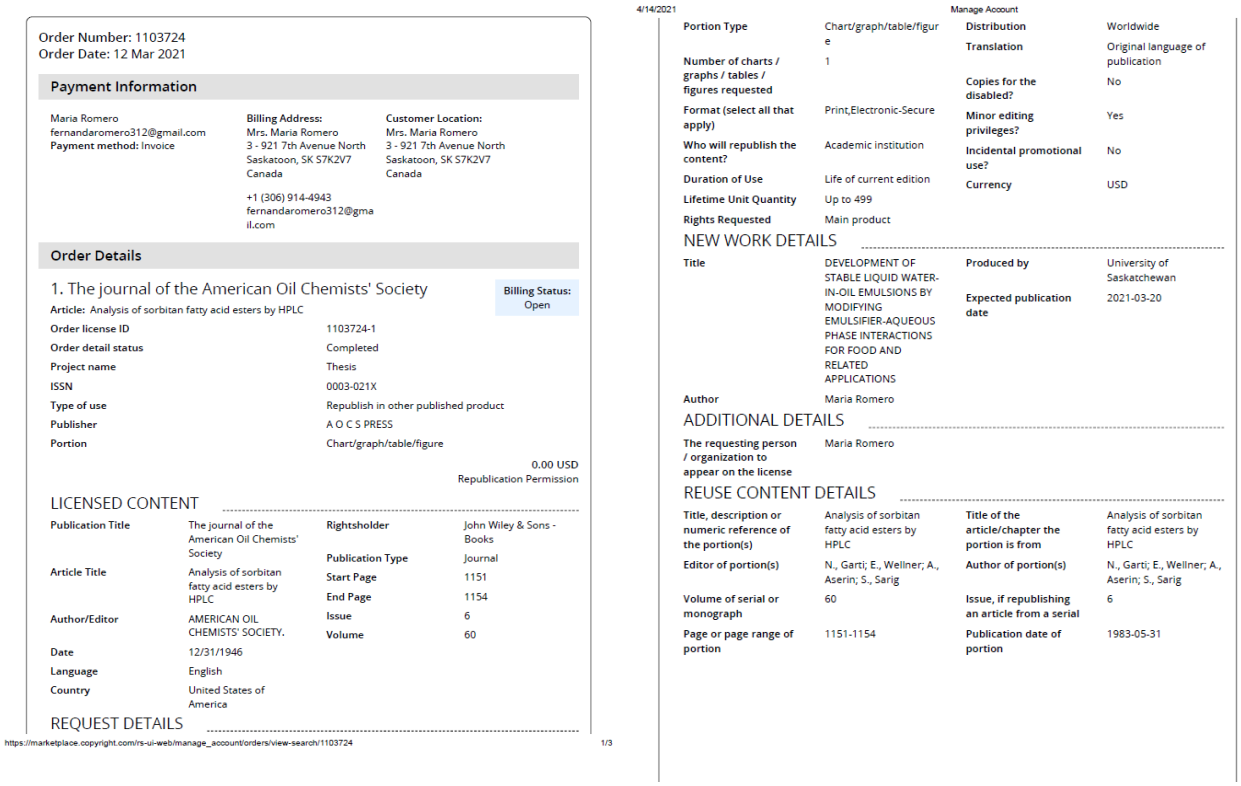

Order Number: 1103724
Order Date: 12 Mar 2021

Payment Information

Maria Romero
fernandaromero312@gmail.com
Payment method: Invoice

Billing Address:
Mrs. Maria Romero
3 - 921 7th Avenue North
Saskatoon, SK S7K2V7
Canada

+1 (306) 914-4943
fernandaromero312@gmail.com

Customer Location:
Mrs. Maria Romero
3 - 921 7th Avenue North
Saskatoon, SK S7K2V7
Canada

Order Details

1. The journal of the American Oil Chemists' Society — **Billing Status:** Open

Article: Analysis of sorbitan fatty acid esters by HPLC

Order license ID	1103724-1
Order detail status	Completed
Project name	Thesis
ISSN	0003-021X
Type of use	Republish in other published product
Publisher	A O C S PRESS
Portion	Chart/graph/table/figure

0.00 USD
Republication Permission

LICENSED CONTENT

Publication Title	The journal of the American Oil Chemists' Society	**Rightsholder**	John Wiley & Sons - Books
Article Title	Analysis of sorbitan fatty acid esters by HPLC	**Publication Type**	Journal
		Start Page	1151
		End Page	1154
Author/Editor	AMERICAN OIL CHEMISTS' SOCIETY.	**Issue**	6
		Volume	60
Date	12/31/1946		
Language	English		
Country	United States of America		

REQUEST DETAILS

https://marketplace.copyright.com/rs-ui-web/manage_account/orders/view-search/1103724 1/3

4/14/2021 Manage Account

Portion Type	Chart/graph/table/figure	**Distribution**	Worldwide
		Translation	Original language of publication
Number of charts / graphs / tables / figures requested	1	**Copies for the disabled?**	No
Format (select all that apply)	Print,Electronic-Secure	**Minor editing privileges?**	Yes
Who will republish the content?	Academic institution	**Incidental promotional use?**	No
Duration of Use	Life of current edition	**Currency**	USD
Lifetime Unit Quantity	Up to 499		
Rights Requested	Main product		

NEW WORK DETAILS

Title	DEVELOPMENT OF STABLE LIQUID WATER-IN-OIL EMULSIONS BY MODIFYING EMULSIFIER-AQUEOUS PHASE INTERACTIONS FOR FOOD AND RELATED APPLICATIONS	**Produced by**	University of Saskatchewan
		Expected publication date	2021-03-20
Author	Maria Romero		

ADDITIONAL DETAILS

The requesting person / organization to appear on the license	Maria Romero

REUSE CONTENT DETAILS

Title, description or numeric reference of the portion(s)	Analysis of sorbitan fatty acid esters by HPLC	**Title of the article/chapter the portion is from**	Analysis of sorbitan fatty acid esters by HPLC
Editor of portion(s)	N., Garti; E., Wellner; A., Aserin; S., Sarig	**Author of portion(s)**	N., Garti; E., Wellner; A., Aserin; S., Sarig
Volume of serial or monograph	60	**Issue, if republishing an article from a serial**	6
Page or page range of portion	1151-1154	**Publication date of portion**	1983-05-31

10.2 Copyright permission for the use of Hasenhuettl (2008) work in Figures 2.3 and 2.4.

SPRINGER NATURE LICENSE
TERMS AND CONDITIONS

Feb 21, 2021

This Agreement between University of Saskatchewan -- Maria Romero ("You") and Springer Nature ("Springer Nature") consists of your license details and the terms and conditions provided by Springer Nature and Copyright Clearance Center.

License Number	5013910717374
License date	Feb 21, 2021
Licensed Content Publisher	Springer Nature
Licensed Content Publication	Springer eBook
Licensed Content Title	Synthesis and Commercial Preparation of Food Emulsifiers
Licensed Content Author	Gerard L. Hasenhuettl
Licensed Content Date	Jan 1, 2019
Type of Use	Thesis/Dissertation

Requestor type	academic/university or research institute
Format	print and electronic
Portion	figures/tables/illustrations
Number of figures/tables/illustrations	2
Will you be translating?	no
Circulation/distribution	1 - 29
Author of this Springer Nature content	no
Title	PhD. Candidate
Institution name	University of Saskatchewan
Expected presentation date	Apr 2021
Portions	Chapter 2, Figures 2.3 and 2.7
Requestor Location	University of Saskatchewan 3 - 921 7th Avenue North 3 (side door) Saskatoon, SK S7K 2V7

10.3 Copyright permission for the use of Robison et al. (1984) work in Figure 2.7.

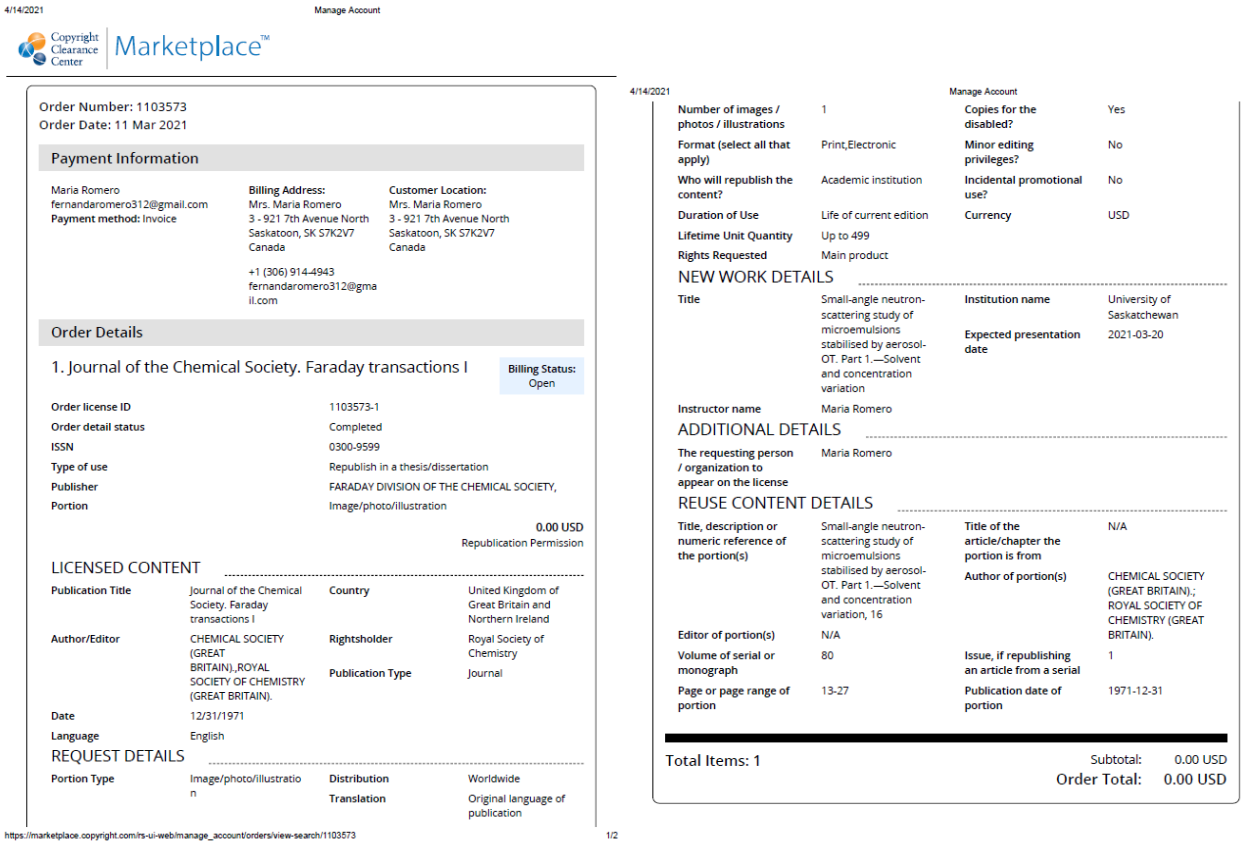

4/14/2021 Manage Account

Copyright Clearance Center | Marketplace™

Order Number: 1103573
Order Date: 11 Mar 2021

Payment Information

Maria Romero
fernandaromero312@gmail.com
Payment method: Invoice

Billing Address:
Mrs. Maria Romero
3 - 921 7th Avenue North
Saskatoon, SK S7K2V7
Canada

+1 (306) 914-4943
fernandaromero312@gmail.com

Customer Location:
Mrs. Maria Romero
3 - 921 7th Avenue North
Saskatoon, SK S7K2V7
Canada

Order Details

1. Journal of the Chemical Society. Faraday transactions I — **Billing Status:** Open

Order license ID	1103573-1
Order detail status	Completed
ISSN	0300-9599
Type of use	Republish in a thesis/dissertation
Publisher	FARADAY DIVISION OF THE CHEMICAL SOCIETY,
Portion	Image/photo/illustration

0.00 USD
Republication Permission

LICENSED CONTENT

Publication Title	Journal of the Chemical Society. Faraday transactions I	**Country**	United Kingdom of Great Britain and Northern Ireland
Author/Editor	CHEMICAL SOCIETY (GREAT BRITAIN).,ROYAL SOCIETY OF CHEMISTRY (GREAT BRITAIN).	**Rightsholder**	Royal Society of Chemistry
		Publication Type	Journal
Date	12/31/1971		
Language	English		

REQUEST DETAILS

Portion Type	Image/photo/illustration	**Distribution**	Worldwide
		Translation	Original language of publication

https://marketplace.copyright.com/rs-ui-web/manage_account/orders/view-search/1103573 1/2

4/14/2021 Manage Account

Number of images / photos / illustrations	1	**Copies for the disabled?**	Yes
Format (select all that apply)	Print,Electronic	**Minor editing privileges?**	No
Who will republish the content?	Academic institution	**Incidental promotional use?**	No
Duration of Use	Life of current edition	**Currency**	USD
Lifetime Unit Quantity	Up to 499		
Rights Requested	Main product		

NEW WORK DETAILS

Title	Small-angle neutron-scattering study of microemulsions stabilised by aerosol-OT. Part 1.—Solvent and concentration variation	**Institution name**	University of Saskatchewan
		Expected presentation date	2021-03-20
Instructor name	Maria Romero		

ADDITIONAL DETAILS

The requesting person / organization to appear on the license	Maria Romero		

REUSE CONTENT DETAILS

Title, description or numeric reference of the portion(s)	Small-angle neutron-scattering study of microemulsions stabilised by aerosol-OT. Part 1.—Solvent and concentration variation, 16	**Title of the article/chapter the portion is from**	N/A
		Author of portion(s)	CHEMICAL SOCIETY (GREAT BRITAIN).; ROYAL SOCIETY OF CHEMISTRY (GREAT BRITAIN).
Editor of portion(s)	N/A		
Volume of serial or monograph	80	**Issue, if republishing an article from a serial**	1
Page or page range of portion	13-27	**Publication date of portion**	1971-12-31

Total Items: 1

Subtotal: 0.00 USD
Order Total: 0.00 USD

10.4 Copyright permission for the use of Nave, Eastoe, and Penfold (2000) work in Figure 2.8.

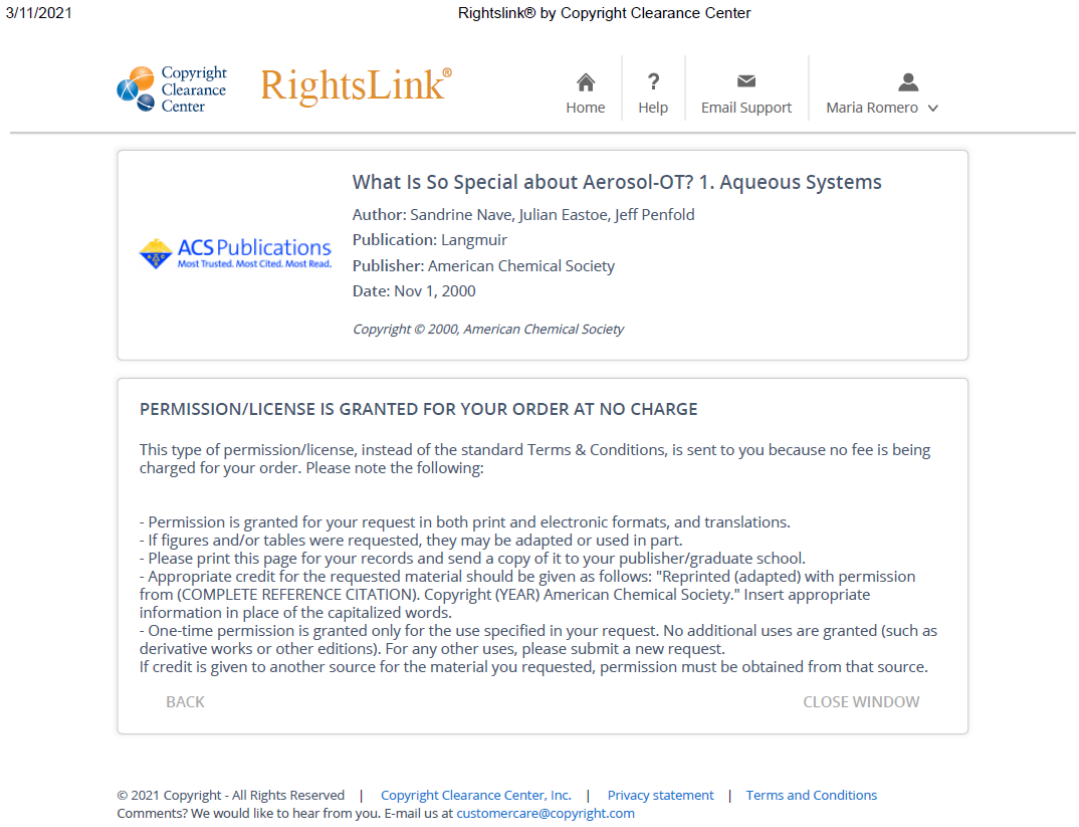

3/11/2021 Rightslink® by Copyright Clearance Center

Copyright Clearance Center RightsLink®

Home | Help | Email Support | Maria Romero

ACS Publications
Most Trusted. Most Cited. Most Read.

What Is So Special about Aerosol-OT? 1. Aqueous Systems

Author: Sandrine Nave, Julian Eastoe, Jeff Penfold
Publication: Langmuir
Publisher: American Chemical Society
Date: Nov 1, 2000

Copyright © 2000, American Chemical Society

PERMISSION/LICENSE IS GRANTED FOR YOUR ORDER AT NO CHARGE

This type of permission/license, instead of the standard Terms & Conditions, is sent to you because no fee is being charged for your order. Please note the following:

- Permission is granted for your request in both print and electronic formats, and translations.
- If figures and/or tables were requested, they may be adapted or used in part.
- Please print this page for your records and send a copy of it to your publisher/graduate school.
- Appropriate credit for the requested material should be given as follows: "Reprinted (adapted) with permission from (COMPLETE REFERENCE CITATION). Copyright (YEAR) American Chemical Society." Insert appropriate information in place of the capitalized words.
- One-time permission is granted only for the use specified in your request. No additional uses are granted (such as derivative works or other editions). For any other uses, please submit a new request.

If credit is given to another source for the material you requested, permission must be obtained from that source.

BACK CLOSE WINDOW

10.5 Copyright permission for the use of Rousseau and Hodge (2005) work in Figures 2.9 and 2.11.

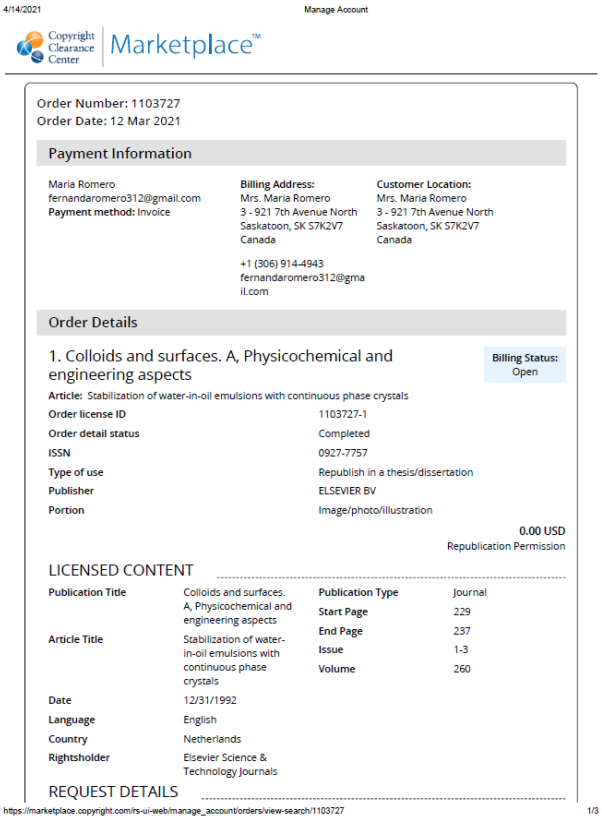

4/14/2021 Manage Account

Copyright Clearance Center | Marketplace™

Order Number: 1103727
Order Date: 12 Mar 2021

Payment Information

Maria Romero
fernandaromero312@gmail.com
Payment method: Invoice

Billing Address:
Mrs. Maria Romero
3 - 921 7th Avenue North
Saskatoon, SK S7K2V7
Canada

+1 (306) 914-4943
fernandaromero312@gmail.com

Customer Location:
Mrs. Maria Romero
3 - 921 7th Avenue North
Saskatoon, SK S7K2V7
Canada

Order Details

1. Colloids and surfaces. A, Physicochemical and engineering aspects

Billing Status: Open

Article: Stabilization of water-in-oil emulsions with continuous phase crystals

Order license ID	1103727-1
Order detail status	Completed
ISSN	0927-7757
Type of use	Republish in a thesis/dissertation
Publisher	ELSEVIER BV
Portion	Image/photo/illustration

0.00 USD
Republication Permission

LICENSED CONTENT

Publication Title	Colloids and surfaces. A, Physicochemical and engineering aspects	**Publication Type**	Journal
Article Title	Stabilization of water-in-oil emulsions with continuous phase crystals	**Start Page**	229
		End Page	237
		Issue	1-3
		Volume	260
Date	12/31/1992		
Language	English		
Country	Netherlands		
Rightsholder	Elsevier Science & Technology Journals		

REQUEST DETAILS

https://marketplace.copyright.com/rs-ui-web/manage_account/orders/view-search/1103727 1/3

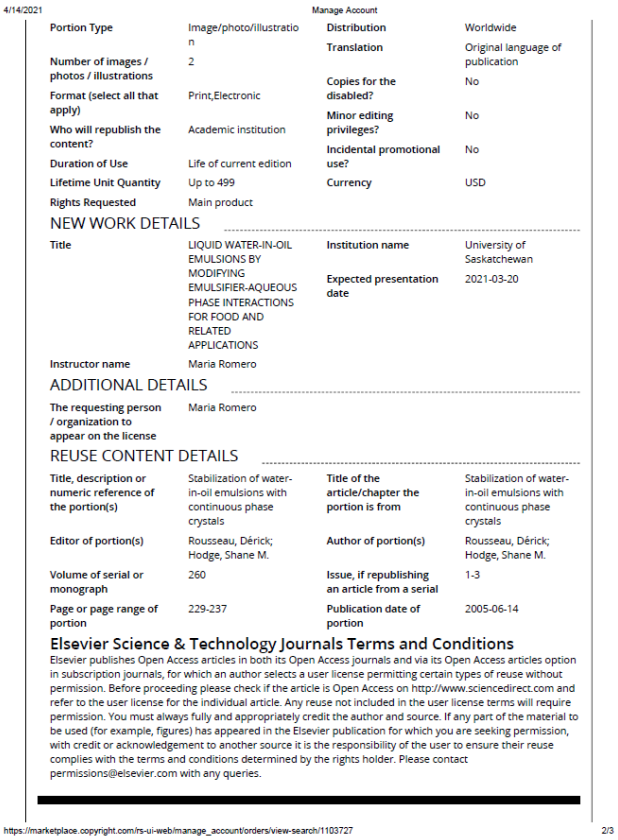

4/14/2021 Manage Account

Portion Type	Image/photo/illustration	**Distribution**	Worldwide
Number of images / photos / illustrations	2	**Translation**	Original language of publication
Format (select all that apply)	Print,Electronic	**Copies for the disabled?**	No
Who will republish the content?	Academic institution	**Minor editing privileges?**	No
Duration of Use	Life of current edition	**Incidental promotional use?**	No
Lifetime Unit Quantity	Up to 499	**Currency**	USD
Rights Requested	Main product		

NEW WORK DETAILS

Title	LIQUID WATER-IN-OIL EMULSIONS BY MODIFYING EMULSIFIER-AQUEOUS PHASE INTERACTIONS FOR FOOD AND RELATED APPLICATIONS	**Institution name**	University of Saskatchewan
		Expected presentation date	2021-03-20
Instructor name	Maria Romero		

ADDITIONAL DETAILS

The requesting person / organization to appear on the license	Maria Romero

REUSE CONTENT DETAILS

Title, description or numeric reference of the portion(s)	Stabilization of water-in-oil emulsions with continuous phase crystals	**Title of the article/chapter the portion is from**	Stabilization of water-in-oil emulsions with continuous phase crystals
Editor of portion(s)	Rousseau, Dérick; Hodge, Shane M.	**Author of portion(s)**	Rousseau, Dérick; Hodge, Shane M.
Volume of serial or monograph	260	**Issue, if republishing an article from a serial**	1-3
Page or page range of portion	229-237	**Publication date of portion**	2005-06-14

Elsevier Science & Technology Journals Terms and Conditions

Elsevier publishes Open Access articles in both its Open Access journals and via its Open Access articles option in subscription journals, for which an author selects a user license permitting certain types of reuse without permission. Before proceeding please check if the article is Open Access on http://www.sciencedirect.com and refer to the user license for the individual article. Any reuse not included in the user license terms will require permission. You must always fully and appropriately credit the author and source. If any part of the material to be used (for example, figures) has appeared in the Elsevier publication for which you are seeking permission, with credit or acknowledgement to another source it is the responsibility of the user to ensure their reuse complies with the terms and conditions determined by the rights holder. Please contact permissions@elsevier.com with any queries.

https://marketplace.copyright.com/rs-ui-web/manage_account/orders/view-search/1103727 2/3

10.6 Copyright permission for the use of Rousseau (2000) work in Figure 2.10.

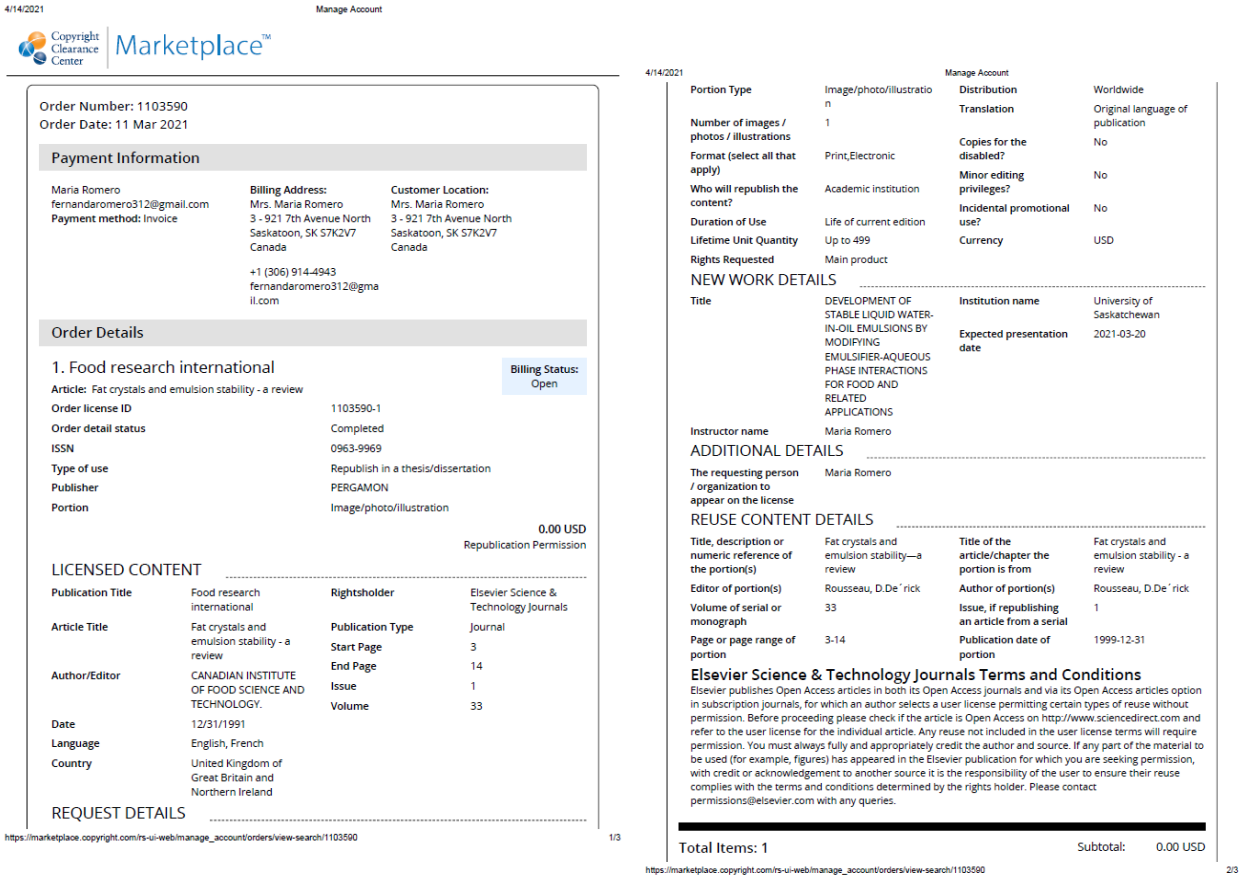

4/14/2021 Manage Account

Copyright Clearance Center | Marketplace™

Order Number: 1103590
Order Date: 11 Mar 2021

Payment Information

Maria Romero
fernandaromero312@gmail.com
Payment method: Invoice

Billing Address:
Mrs. Maria Romero
3 - 921 7th Avenue North
Saskatoon, SK S7K2V7
Canada

+1 (306) 914-4943
fernandaromero312@gmail.com

Customer Location:
Mrs. Maria Romero
3 - 921 7th Avenue North
Saskatoon, SK S7K2V7
Canada

Order Details

1. Food research international

Billing Status: Open

Article: Fat crystals and emulsion stability - a review

Order license ID	1103590-1
Order detail status	Completed
ISSN	0963-9969
Type of use	Republish in a thesis/dissertation
Publisher	PERGAMON
Portion	Image/photo/illustration

0.00 USD
Republication Permission

LICENSED CONTENT

Publication Title	Food research international	**Rightsholder**	Elsevier Science & Technology Journals
Article Title	Fat crystals and emulsion stability - a review	**Publication Type**	Journal
Author/Editor	CANADIAN INSTITUTE OF FOOD SCIENCE AND TECHNOLOGY.	**Start Page**	3
		End Page	14
		Issue	1
		Volume	33
Date	12/31/1991		
Language	English, French		
Country	United Kingdom of Great Britain and Northern Ireland		

REQUEST DETAILS

https://marketplace.copyright.com/rs-ui-web/manage_account/orders/view-search/1103590 1/3

4/14/2021 Manage Account

Portion Type	Image/photo/illustration	**Distribution**	Worldwide
Number of images / photos / illustrations	1	**Translation**	Original language of publication
Format (select all that apply)	Print,Electronic	**Copies for the disabled?**	No
Who will republish the content?	Academic institution	**Minor editing privileges?**	No
Duration of Use	Life of current edition	**Incidental promotional use?**	No
Lifetime Unit Quantity	Up to 499	**Currency**	USD
Rights Requested	Main product		

NEW WORK DETAILS

Title	DEVELOPMENT OF STABLE LIQUID WATER-IN-OIL EMULSIONS BY MODIFYING EMULSIFIER-AQUEOUS PHASE INTERACTIONS FOR FOOD AND RELATED APPLICATIONS	**Institution name**	University of Saskatchewan
		Expected presentation date	2021-03-20
Instructor name	Maria Romero		

ADDITIONAL DETAILS

The requesting person / organization to appear on the license	Maria Romero

REUSE CONTENT DETAILS

Title, description or numeric reference of the portion(s)	Fat crystals and emulsion stability—a review	**Title of the article/chapter the portion is from**	Fat crystals and emulsion stability - a review
Editor of portion(s)	Rousseau, D.De´rick	**Author of portion(s)**	Rousseau, D.De´rick
Volume of serial or monograph	33	**Issue, if republishing an article from a serial**	1
Page or page range of portion	3-14	**Publication date of portion**	1999-12-31

Elsevier Science & Technology Journals Terms and Conditions

Elsevier publishes Open Access articles in both its Open Access journals and via its Open Access articles option in subscription journals, for which an author selects a user license permitting certain types of reuse without permission. Before proceeding please check if the article is Open Access on http://www.sciencedirect.com and refer to the user license for the individual article. Any reuse not included in the user license terms will require permission. You must always fully and appropriately credit the author and source. If any part of the material to be used (for example, figures) has appeared in the Elsevier publication for which you are seeking permission, with credit or acknowledgement to another source it is the responsibility of the user to ensure their reuse complies with the terms and conditions determined by the rights holder. Please contact permissions@elsevier.com with any queries.

Total Items: 1 Subtotal: 0.00 USD

https://marketplace.copyright.com/rs-ui-web/manage_account/orders/view-search/1103590 2/3

10.7 Copyright permission for the use of Zembyla et al. (2005) work in Figure 2.12.

Regarding Incident 4207029 Permission to reuse

support@services.acs.org <support@services.acs.org>
Fri 2021-03-12 8:05 AM
To: Romero Pena, Maria <mfr513@mail.usask.ca>

ACS Chemistry for Life®

Dear Dr. Romero,

Thank you for contacting ACS Publications Support.

Your permission request is granted and there is no fee for this reuse.
In your planned reuse, you must cite the ACS article as the source, add this direct link: https://pubs.acs.org/doi/abs/10.1021/acs.langmuir.8b01438, and include a notice to readers that further permissions related to the material excerpted should be directed to the ACS.

Please do not hesitate to contact us if you need any further assistance.

Sincerely,

Vojin Vucic
ACS Publications
Customer Services & Information
Website: https://help.acs.org
Incident Information:

Incident #: 4207029
Date Created: 2021-03-12T14:40:31
Priority: 3
Customer: Maria Romero Pena
Title: Permission to reuse

10.8 Copyright permission for the use of McClements (2005) work in Figure 2.14.

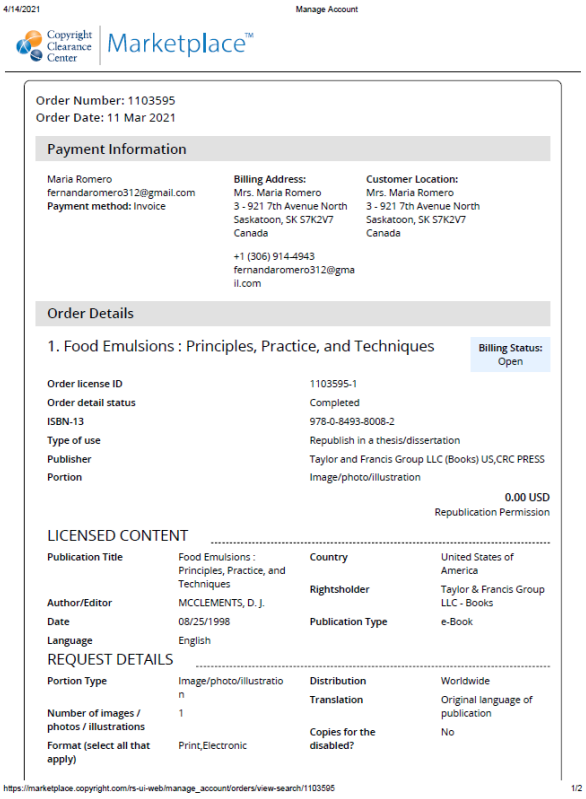

4/14/2021 Manage Account

Copyright Clearance Center | Marketplace™

Order Number: 1103595
Order Date: 11 Mar 2021

Payment Information

Maria Romero
fernandaromero312@gmail.com
Payment method: Invoice

Billing Address:
Mrs. Maria Romero
3 - 921 7th Avenue North
Saskatoon, SK S7K2V7
Canada

+1 (306) 914-4943
fernandaromero312@gmail.com

Customer Location:
Mrs. Maria Romero
3 - 921 7th Avenue North
Saskatoon, SK S7K2V7
Canada

Order Details

1. Food Emulsions : Principles, Practice, and Techniques

Billing Status: Open

Order license ID	1103595-1
Order detail status	Completed
ISBN-13	978-0-8493-8008-2
Type of use	Republish in a thesis/dissertation
Publisher	Taylor and Francis Group LLC (Books) US,CRC PRESS
Portion	Image/photo/illustration

0.00 USD
Republication Permission

LICENSED CONTENT

Publication Title	Food Emulsions : Principles, Practice, and Techniques	**Country**	United States of America
Author/Editor	MCCLEMENTS, D. J.	**Rightsholder**	Taylor & Francis Group LLC - Books
Date	08/25/1998	**Publication Type**	e-Book
Language	English		

REQUEST DETAILS

Portion Type	Image/photo/illustration	**Distribution**	Worldwide
Number of images / photos / illustrations	1	**Translation**	Original language of publication
Format (select all that apply)	Print,Electronic	**Copies for the disabled?**	No

https://marketplace.copyright.com/rs-ui-web/manage_account/orders/view-search/1103595 1/2

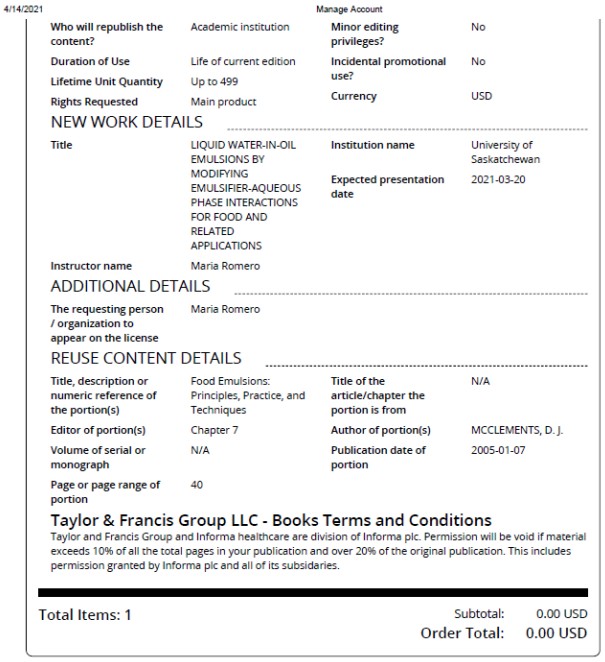

4/14/2021 Manage Account

Who will republish the content?	Academic institution	**Minor editing privileges?**	No
Duration of Use	Life of current edition	**Incidental promotional use?**	No
Lifetime Unit Quantity	Up to 499	**Currency**	USD
Rights Requested	Main product		

NEW WORK DETAILS

Title	LIQUID WATER-IN-OIL EMULSIONS BY MODIFYING EMULSIFIER-AQUEOUS PHASE INTERACTIONS FOR FOOD AND RELATED APPLICATIONS	**Institution name**	University of Saskatchewan
		Expected presentation date	2021-03-20
Instructor name	Maria Romero		

ADDITIONAL DETAILS

The requesting person / organization to appear on the license	Maria Romero

REUSE CONTENT DETAILS

Title, description or numeric reference of the portion(s)	Food Emulsions: Principles, Practice, and Techniques	**Title of the article/chapter the portion is from**	N/A
Editor of portion(s)	Chapter 7	**Author of portion(s)**	MCCLEMENTS, D. J.
Volume of serial or monograph	N/A	**Publication date of portion**	2005-01-07
Page or page range of portion	40		

Taylor & Francis Group LLC - Books Terms and Conditions

Taylor and Francis Group and Informa healthcare are division of Informa plc. Permission will be void if material exceeds 10% of all the total pages in your publication and over 20% of the original publication. This includes permission granted by Informa plc and all of its subsidaries.

Total Items: 1

Subtotal: 0.00 USD
Order Total: 0.00 USD

10.9 Peak deconvolution example for IR spectra analysis in Origin 2020b software – Original IR spectra: blue line, second derivative curve: red line and peaks deconvolution: red lines.